

© 2021

Ahmad (Benjamin) Soraghi

ALL RIGHTS RESERVED

PROBABILISTIC CHARACTERIZATION OF BOND BEHAVIOR AT REBAR-
CONCRETE INTERFACE IN CORRODED RC STRUCTURES: EXPERIMENT,
MODELING, AND IMPLEMENTATION

A Dissertation

Presented to

The Graduate Faculty of the University of Akron

In Partial Fulfillment

of the Requirements for the Degree

Doctor of Philosophy in Civil Engineering

Ahmad Soraghi

December, 2021

PROBABILISTIC CHARACTERIZATION OF BOND BEHAVIOR AT REBAR-
CONCRETE INTERFACE IN CORRODED RC STRUCTURES: EXPERIMENT,
MODELING, AND IMPLEMENTATION

Ahmad Soraghi

Dissertation

Approved:

Accepted:

Advisor
Dr. Qindan Huang

Department Chair
Dr. Wieslaw Binienda

Committee Member
Dr. David Roke

Dean of the College
Dr. Craig Menzemer

Committee Member
Dr. Craig Menzemer

Interim Director, Graduate School
Dr. Marnie Saunders

Committee Member
Dr. Ping Yi

Date

Committee Member
Dr. Richard Einsporn

ABSTRACT

Adequate rebar-concrete bonding is crucial to ensure the reliable performance of reinforced concrete (RC) structures. Many factors (such as the concrete properties, concrete cover depth, transverse reinforcement, and the presence of corrosion) affect the bond behavior, and consequently the structural performance. This bond behavior is typically described by a bond stress-slip relationship, where there are two critical quantities: bond strength – the maximum shear stress that bond can withstand, and peak slip – the slippage at the interface when the bond strength is reached. It is understood that the bond deteriorates when corrosion is present and behaves differently under two distinct bond failure modes (i.e., splitting and pull-out). While many prior studies have focused on the influence of the aforementioned factors on the bond strength, the impact of the failure mode coupled with corrosion on the bond stress-slip relationship and structural performance have not been thoroughly investigated. This study is aimed to address this issue.

In this study, first a probabilistic bond failure mode prediction model that considers various influencing factors including loading type and corrosion is developed in this study. This study uses the bond testing results of 132 beam-end specimens subjected to monotonic and cyclic loading and adopts classification methods to develop the prediction model, which is then used to evaluate the impact of bond behavior on the reliability of a RC beam with a lap splice. Then, multivariate nonlinear regression with all-possible subset model

selection and symbolic multi-gene regression are adopted for probabilistic model development for bond strength and peak slip under the two bond failure modes considering corrosion. In particular, a comprehensive bond dataset collected from bond tests on the beam and beam-end specimens in the literature and from the experimental testing conducted in this study, and a criterion to specify the bond failure mode is also proposed.

Next, incorporating bond in the structural analysis is investigated. Since in reality, perfect bonding does not exist, especially in beam and column or column and footing connections, reinforcement slip occurs as a result of imperfect bonding. Reinforcement slip in the footing of a RC column can significantly influence the lateral displacement of the column, a critical structural response under lateral loads such as seismic loading. Many past researchers studied and developed models to capture the anchorage slip of rebar; however, a model that can reflect the actual bond-slip relationship (especially in the presence of corrosion) and yet be simple-to-use for structural analysis is not well developed. In this study, a new simple bar stress-slip macromodel is developed to predict reinforcement anchorage slip given a rebar stress. The proposed rebar anchorage slip model is derived by implementing a macromodel solution based on a simple bond stress distribution function that captures the bond stress distribution numerically obtained from a real bond-slip relationship. Available experimental bond stress-slip data collected from literature are used to optimize the model parameter in the proposed bond stress distribution function, which reflects the impact of the structural parameters on the rebar slippage such as concrete strength and corrosion level. The proposed rebar slip model is then incorporated into a fiber beam-column model for numerical analysis, and is further validated by

comparing flexural behavior of several RC columns (with and without corrosion) based on the numerical model with the experimental data. The results demonstrate the importance of incorporating rebar slippage and corrosion effect on bond. Using this fiber beam-column model, seismic performance of an example RC bridge column is evaluated, and one can conclude the rebar slip plays a critical role in the seismic evaluation. As the proposed rebar slip macromodel provides simple formulation and it is explicitly expressed with a model parameter that can be updated easily to incorporate new information, it is practical for application in the structural analysis.

DEDICATION

I dedicate this manuscript to my beautiful sister, Nazanin, as she was my source of motivation, inspiration, and energy to pursue my degree with all the hardships I encountered. Also, to my mother and father who were greatly supportive all these years of my education, and to all my good friends who were incredibly generous with sharing their knowledge with me.

ACKNOWLEDGEMENT

The research presented in this dissertation was conducted at the Department of Civil Engineering, University of Akron, Akron, Ohio. During the study, the chairmanship of the department was held by Dr. Wieslaw K. Binienda. The author takes this opportunity to acknowledge the excellent academic guidance, supports, and advices in the past five years offered by his advisor and chair of his dissertation committee, Dr. Qindan Huang. Without her guidance, this dissertation would not have become a reality. The author also thank other committee members Dr. Craig Menzemer and Dr. David Roke form Civil Engineering Department, Dr. Ping Yi from Transportation Engineering Department, and Dr. Richard Einsporn from Department of Mathematics for their attendance and their useful comments. Thanks also go to my friends and colleagues, and the department faculty and staff, particularly Ms. Kimberly Stone for their support, and making my time at The University of Akron a great experience. Finally, my special thanks go to my family for their encouragements, patience, and supports.

This material is based upon work supported by the National Science Foundation under Grant No. CMMI 1635507. Any opinions, findings, and conclusions, or recommendations expressed in this material are those of the authors and do not necessarily reflect the views of the National Science Foundation.

TABLE OF CONTENTS

	Page
LIST OF TABLES	11
LIST OF FIGURES	13
CHAPTER	
I. INTRODUCTION	
Research goal and objectives	16
Background and motivations	18
Corrosion effect	18
Local bond stress-slip relationship.....	20
Bond deterioration	22
Deterioration on monotonic bond behavior	23
Deterioration on cyclic bond behavior.....	24
Structural Analysis Considering Deterioration on Bond	26
Dissertation Organization	27
II. PROBABILISTIC PREDICTION MODEL FOR RC BOND FAILURE	
MODE	29
Experimental program	31
Specimen design and details	31
Corrosion process.....	34
Test setup	36
Experimental results and discussion	39
Probabilistic prediction model for bond failure mode	41
Existing deterministic models.....	42
Classification algorithms	43
Model development	45
Model comparison	52
Case study	57
Flexural behavior	60
Reliability analysis.....	63

III. PROBABILISTIC MODELING OF RC BOND BEHAVIOR CONSIDERING FAILURE MODE AND CORROSION.....	68
Background.....	71
Bond Strength	71
Peak slip	74
Failure mode identification	77
Experimental Data	79
Various types of bond test setups.....	80
Proposed criteria for bond failure mode	80
Data collection	83
Average bond strength and peak slip model development	88
Probabilistic model for average bond strength, τ_{avg}	90
Probabilistic model for the bond peak slip s_1	96
Model evaluation	103
Prediction comparison of the proposed model with existing models ..	103
IV. SIMPLE REBAR ANCHORAGE SLIP MACROMODEL CONSIDERING CORROSION DETERIORATION EFFECT.....	112
Background.....	116
Conventional macromodel method.....	117
Pan et al. method.....	120
Proposed macromodel	123
Bar slip comparison	126
Application of bar slip macromodel into the structural analysis	129
Modified rebar constitutive model.....	129
Flexural behavior of RC columns	130
Seismic performance of a RC bridge column	138
Deterioration on cyclic bond behavior	144
Probabilistic development of bond stress-slip constitutive law considering corrosion effect.....	146
Preliminary findings.....	147
V. SUMMARY AND CONCLUSIONS	155
BIBLIOGRAPHY.....	161
APPENDICES	197
APPENDIX A.....	198
APPENDIX B	201

APPENDIX C	205
APPENDIX D	206
APPENDIX E	208
APPENDIX F.....	210

LIST OF TABLES

Table	Page
2.1 Summary of design parameters of testing specimens.....	29
2.2 Potential variables used for model development.....	42
2.3. Four possible prediction outcomes.....	44
2.4. Statistics summary for the top three logistic classification models for each model size.....	46
2.5. Logistic model coefficients.....	46
2.6. Lasso model coefficients.....	47
2.7. Predictive accuracy of various prediction methods.....	52
2.8. Beam flexural behavior comparison for different scenarios.....	56
2.9. Probability information of the basic random variables.....	56
3.1. Summary of existing studies for peak slip, s_1	71
3.2. Summary of the collected data for model development.....	82
3.3. Details of experimental RC beams studied by Abdel-Kareem.....	85
3.4. Explanatory functions for multivariate nonlinear regression analysis.....	89
3.5. Model coefficients for pull-out and splitting bond strength model.....	90
3.6. GPTIPS run settings.....	95
3.8. Statistics of model coefficients for pull-out bond peak slip model.....	96
3.9. Model parameters for bond peak slip in splitting.....	98
3.10. Existing prediction models for bond strength.....	100

3.11. Comparison of proposed models and existing models for bond strength prediction.....	102
3.12. Comparison of proposed models and existing models for peak slip.....	105
4.1. Specimen properties for collected testing results for rebar stress – slip..... relationship.....	122
4.2. Properties of the test columns.....	128
4.3. Calculated and actual capacity of the experiment columns tested under..... monotonic loading.....	133
4.4. Design parameters of the example bridge with one single-column bent.....	136
4.5. Ground motion records used in the time-history analysis.....	138

LIST OF FIGURES

Figure	Page
1.1	Illustration of general bond behavior under monotonic loading.....11
1.3	Force-displacement curves considering different slippage values.....20
2.1	Beam-end specimens: (a) schematic design and (b) as-casted beam-end specimen.....28
2.2	Schematic view of (a) humidity tents and (b) corrosion setup.....30
2.3	(a) Boundary conditions of testing specimen; (b) 3D rendering view of test setup, (c) testing frame, (d) laboratory test setup.....31
2.4	(a) Actuator force and displacement diagram32
2.5	Typical actuator force-displacement34
2.6	A typical cracking pattern for (a) splitting and (b) pull-out failure mode.....35
2.7	Schematic view of crack patterns formed on the test specimens after failure: (a) splitting failure mode and (b) pull-out failure mode.....35
2.8	Example of a scatter plot of failure mode for terms (a) c/d , (b) K_{tr} , and (c) logistic curve for their interaction term ($K_{tr} \cdot c/d$).....41
2.9	Sensitivity comparison between logistic and lasso logistic model.....48
2.10	Prediction plot for (a) pull-out failure and (b) splitting failure.....50
2.11	Cross-section and longitudinal detailing of the beam53

2.12	Adopted bond-slip curve based on CEB	53
2.13	Comparison of pull-out and splitting failure.....	53
2.14	Fragility curves under different corrosion levels.....	60
2.15	Reliability index curves under various corrosion levels	61
3.1	Bond failure mode stress-slip curves for different levels of confinement.....	63
3.2	Bond-slip model based on CEB.....	64
3.3	Longitudinal cracking observed by (a) Lin et al. and (b) Tang.....	66
3.4	Different failure modes observed by Hanjari et al.	66
3.5	Specimens fail in splitting	73
3.6	Schematic view of crack patterns formed on the test specimens after failure.....	73
3.7	Typical bond stress-slip behavior from the study by the authors.....	76
3.8	Monotonic test results of Lin et al. with corrected failure mode	77
3.9	Histogram comparison.....	79
3.10	Cross-section of RC beams studied by Abdel-Kareem et al.....	82
3.11	The impact of the variations in τ_{avg} and s_1 on load-deflection of RC beams.....	84
3.12	Bond strength prediction, $\ln(\tau_{avg}/\sqrt{f'_c})$, using Sajedi and Huang model.....	86
3.13	Bond strength prediction, $\ln(\tau_{avg}/\sqrt{f'_c})$	91
3.14	An example of the formulation of SMGR.....	93
3.15	Histogram and the fitted PDF for peak slip under splitting bond failure.....	97
3.16	Scatter plot of developed s_1 models (in mm).....	98
3.17	Comparison of bond strength predictions.....	101
3.18	Sensitivity to proposed bond strength (τ_{avg}) prediction.....	102
3.19	Comparison of the proposed models for s_1 and existing models	104
3.20	Comparison of predicted load-deflection of RC beams	106
4.1	Four bond distribution fields and their relationships in rebar anchorage region.	108

4.2	Bond stress distributions conventional, Pan et al., and proposed models.....	112
4.3	Uniaxial stress-strain constitutive model of rebar ($\sigma - \varepsilon$ relationship).....	114
4.4	Normalized bond stress vs. normalized development length.....	116
4.5	Predicted and measured stress-slip relationship for the experimental data.....	124
4.6	Geometry and configuration of the column specimens	107
4.7	Configuration of Opensees model of an RC column.....	129
4.8	Measured and estimated lateral force-displacement response	130
4.9	Calculated and measured cyclic response of the columns.....	135
4.10	Configuration of the example RC highway bridge with single-column bent.....	135
4.12	Pushover results for the bridge column under various cases	137
4.13	Time-history response of three selected ground motions.....	140
4.14	Seismic deformation fragilities of the bridge column.....	141
4.15	Local bond behavior model by (a) Eligehausen et al., and (b) Hawkins.....	148
4.16	Analytical bond stress-slip relationship for monotonic loading.....	149
4.17	General schematic of proposed cyclic bond model.....	150
4.18	(a) Schematic and (b) a typical cyclic behavior.....	151
4.19	Cycles number 1, 4, and 7 used for the comparison purposes.....	152
4.20	Comparison of τ_{\max} , τ_f , and S_{\max} with the number of cycles.....	153
4.21	Comparison of τ_{\max} , τ_f , and S_{\max} with the structural parameters.....	155
4.22	Comparison of τ_{\max} , τ_f , and S_{\max} with the structural parameter's interactions.....	156

CHAPTER I

INTRODUCTION

1.1. Research goal and objectives

Civil infrastructure, which includes buildings, transportation network systems, energy systems, and water systems, is a critical functional component of any modern society. The American Society of Civil Engineers (Herrmann, 2015) report card indicates that our infrastructure is failing and that it would take an estimated \$3.6 trillion to upgrade the existing aging infrastructure (Herrmann, 2015). Although aging itself is not a structural failure mechanism, it decreases the robustness and sustainability of the infrastructure against natural or man-made hazards. However, in engineering practice, the typical design of reinforced concrete (RC) structures does not consider aging deterioration and in the quantitative performance evaluation of aging RC structures subjected to extreme hazards, the deterioration in bond behavior at rebar-concrete interface is normally ignored/disregarded. This is in large part because *i*) there remains a significant knowledge gap on the effects of corrosion on bond behavior, particularly for cyclic behavior; and *ii*) there remains a lack of necessary tools/software for non-linear time history analysis incorporating a bond stress-slip constitutive relationship that considers corrosion effects.

The goal of the proposed research is to advance and facilitate the implementation of the quantitative tools available for risk assessment and management of aging civil

infrastructure particularly when considering resilience and sustainability against extreme hazards. To address the aforementioned shortcomings in the quantitative risk management of aging reinforced concrete structures subjected to extreme hazards in terms of knowledge and implementation, one needs to fill the knowledge gap regarding the deterioration in bond behavior using a novel probabilistic approach, and to facilitate the implementation of the new knowledge obtained in the first objective into the structural design practice by enhancing and augmenting the available standards and into the structural numerical modeling under extreme hazards for the benefit of the research community. Accordingly, three objectives are proposed. Objective 1: to obtain bond behavior under various corrosion levels; Objective 2: to probabilistically model bond failure mode and bond strength and conduct structural analysis with the bond deterioration; and Objective 3: to probabilistically characterize bond behavior and implement the bond deterioration into numerical analysis.

To achieve the stated objectives, three tasks are developed. Task 1: Beam specimens based on all possible influence factors will be designed and subjected to various corrosion levels for bond tests under monotonic and cyclic loading, which will provide a more complete understanding of corrosion mechanism on RC structures. Task 2: The bond failure mode and bond strength are then probabilistically predicted and implemented. In particular, probabilistic models are developed for the prediction of the bond failure mode and the bond strength (Task 2-1). Then a reliability-based life-cycle analysis is performed to RC beams considering bond behavior (Task 2-2). Task 3: The bond behavior obtained from Task 1 is probabilistically characterized and implemented. In this task, the bond

stress-slip constitutive law under cyclic loading is developed first (Task 3-1) and subsequently, the developed constitutive law will be implemented into the finite element modeling software OpenSees, providing a numerical simulation tool with the incorporation of corrosion effect for more accurate and realistic analysis of aging structures (Task 3-2), and finally the corrosion impact on reliability and fragility estimation of RC structures will be investigated (Task 3-3).

1.2. Background and motivations

The dangers are posed by aging infrastructure to our nation's economic health are as great as those posed by the current financial crisis (Betti, 2010). Safety evaluation or prediction of critical infrastructure should be based on rigorous and quantitative models that can provide reliable measures of the remaining capacity and the reliability of the asset that accounts for deterioration due to aging. In particular, appropriate quantification of large uncertainties becomes crucial when assessing infrastructure's environmental, social, economic and cost-benefit impacts. Stochastic modeling of the load and the capacity of infrastructure (including probabilistic aging models) is required.

1.3.1. Corrosion effect

Corrosion is a leading factor in the deterioration of RC infrastructure, and prevention and remediation of corrosion is costly. As one example, the annual direct cost of corrosion for highway bridges is estimated to be \$13.6 billion. Corrosion of the steel reinforcement embedded in concrete is an electrochemical process, where the oxidation of

iron (rust) forms on the surface of the rebar, causing cracking near the rebar-concrete interface. Such cracking can become extensive, with rust accumulation that can be up to six times the original volume of the rebar (Liu & Weyers, 1999; Mehr et al., n.d.), and can cause the concrete to spall from the rebar. Corrosion can be particularly severe in areas with high humidity (e.g., close to the sea) or in the presence of saline water. As corrosion initiates cracking and spalling of the concrete cover and affects material properties and bond behavior between concrete and rebar, it could reduce structural stiffness and structural load carrying capacity and even change the ductile failure mode that the design intends to achieve to a brittle failure mode, increasing the risk of a catastrophic failure of a structure that occurs without warning (Al-Sulaimani et al., 1990; Bilcik & Holly, 2013; A. Castel et al., 2000; C. Fang et al., 2004). Furthermore, corrosion can be even more problematic when the corroded structure is subjected to cyclic loading (such as seismic loading). Experimental studies have been shown that under cyclic loads, the energy dissipation capacity and ductility of the structure decrease with the increase of the corrosion level (Di Carlo et al., 2017; A. Guo et al., 2015; Ma et al., 2012; Ou et al., 2012).

To quantify the effect of corrosion, empirical models are typically used that are expressed in terms of a damage rate and an elapsed time since corrosion initiation. These empirical models are not mechanics-based and are heavily reliant on experimental data (Biondini et al., 2006; Corr et al., 2001). On the other hand, probabilistic corrosion models are developed from mechanics-based analysis combined with model assessment in which model parameters are calibrated empirically using measured data. Although not completely random in nature, the resulting probabilistic corrosion models are more reliable than the

empirical ones and can capture the dominant uncertainties within a certain range for a given application. In addition, because deterioration is stochastic in nature, using the probabilistic approach is more appropriate for capturing all the relevant uncertainties.

1.3. Local bond stress-slip relationship

Adequate bonding between rebar and concrete is the key to ensuring the reliable performance of RC structures. Bond behavior has been treated as a material property, and it is found empirically that many factors affect bond, including concrete cover, bar spacing, bar size, transverse reinforcement, bar geometry, concrete properties, steel stress and yield strength, bar surface condition, bar casting position, development and splice length, distance between spliced bars, and concrete consolidation (Bond, 2003). To accurately evaluate structural performance, the bond constitutive law including monotonic and cyclic behavior should be developed. In particular, for structures under dynamic loading (such as seismic excitations), the bond cyclic behavior becomes essential for determining the absorbed hysteretic energy and fatigue damage (degradation in stiffness, strength, and pinching) as well as ductility capacity.

In studying bond behavior, the majority of research has focused on developing the constitutive relation of bond stress-slip under monotonic loading. The general bond behavior is illustrated in [Figure 1-1](#). For design and analysis purposes, analytical models are developed to describe such behavior. Back in 1957, Rehm (Rehm, 1957) developed the first bond law under monotonic loading using nonlinear regression. Later, Muguruma and Morita (MUGURUMA & MORITA, 1967) developed a model utilizing an exponential

function. Nilson (Tong et al., 2007) and Mirza and Houde (Mirza & Houde, 1978) fitted their experimental data using a high degree of polynomial regression. Other complicated mathematical expressions were subsequently developed (e.g., (Sung-nam Hong, 2008; Sungnam Hong & Park, 2012; Ikki & Kiyomiya, 1996; Shima et al., 1987b; Yang & Chen, 1988)). Yet, bilinear models are well accepted due to their simplicity (e.g., three-segment model by Nilson (Nilson, 1972), five-segment model by Guo and Shi (Z.-H. Guo & Shi, 2003), and a six-segment model by Tassios (Tassios, 1979). The CEB-FIB model (fib, 2013) is one of the most popular models, and it considers pullout and splitting failure modes. However, in the CEB-FIB model, the transition from an unconfined condition to a fully confined condition is not clear at all.

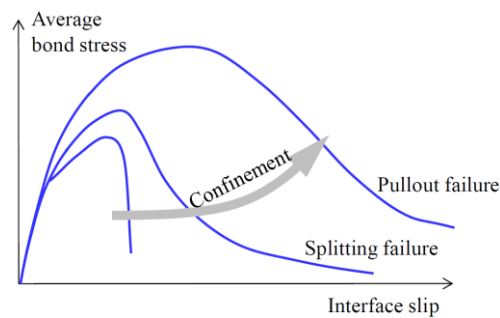


Figure 1.1 Illustration of general bond behavior under monotonic loading

While cyclic bond behavior can be critical, very few models have been developed to characterize it. One of the most accepted hysteretic models is the one developed by Eligehausen et al. (Eligehausen et al., 1982) based on pullout tests under monotonic and cyclic loadings, and it uses the dissipated energy from each cycle to determine the reduced

monotonic envelope. However, pullout specimens are the least realistic, when compared with beam-end or beam specimen in terms of studying bond behavior, as the stress field within the specimen matches few cases in actual construction (ACI, 2003).

1.4. Bond deterioration

Since a bond provides the load path between the concrete and rebar, deterioration on the bond could significantly impact the integrity of RC structures. Most of studies on bond deterioration, however, have focused solely on bond strength. In this regard, researchers predict corroded bond strength by multiplying an empirical reduction factor by the bond strength of intact rebar, and the reduction factor is usually evaluated based on a regression analysis using the experimental results of corroded specimens (Bhargava et al., 2007; Chung et al., 2004; Maaddawy & Topper, 2005; Jesus Rodriguez et al., 1994). The main shortcoming of such models is that the intact bond strength needs to be estimated first, whereas the model error in estimating the intact bond strength should also be considered. Instead of assessing the bond deterioration through intact bond strength, probabilistic predictive model of intact and corroded average bond strength as a function of the corrosion level and parameters that influence bond strength (such as concrete compressive strength, stirrups, development length, etc.) is developed based on a comprehensive database collected from the literature. This model considers uncertainties in structural properties, statistical uncertainties, and model error.

1.4.1. Deterioration on monotonic bond behavior

Numerous studies have investigated the corrosion effect on bond experimentally under monotonic loading. Currently, there are two typical ways to consider corrosion on the bond behavior by assessing the effect on bond strength only (e.g., (Maaddawy & Topper, 2005)) or by evaluating bond strength and bond stiffness (e.g., (Lee et al., 2002)). In either case, the corrosion on the interface slip is ignored. For illustration purposes, [Figure 1.2](#) shows force–displacement of a RC beam with the consideration of bond behavior based on the CEB-FIB splitting failure model (fib, 2013). Three different values of slippage corresponding to the bond strength, s_1 , are used. The impact of s_1 value on stiffness, strength, and ductility is significant as shown in [Figure 1.2](#). Note that in the old version of CEB-FIB (fib, 2013), s_1 is 0.6 mm for an un-confined condition and 1.0 mm for a well-confined condition, and when the deterioration occurs on rebar, s_1 should theoretically have a value in-between. Kivell et al. (Kivell et al., 2011) developed modification factors for stress and slip quantities. As the modification factors are dependent on corrosion levels only, they are not applicable for other structural members as the material and geometric quantities are different from the experimental specimens used in Kivell et al. (Kivell et al., 2011). Hence, *the monotonic bond constitutive law (both stress and slip) needs to be developed considering both corrosion effect and structural and geometric properties.*

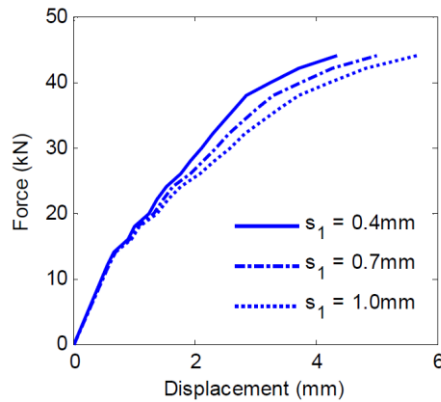


Figure 1.3 Force-displacement curves considering different slippage values

1.4.2. Deterioration on cyclic bond behavior

Cyclic bond behavior is critical to determine hysteretic energy dissipation of RC structures where reversals in the inelastic displacement cause increased damage and degradation of strength and stiffness in the structure. Therefore, the degradation on cyclic bond could result in significant changes in the structural performance. Filippou et al. (Filippou et al., 1983) found that a reduction in bond strength of as little as 15% may result in a 30% reduction in total energy dissipation of a beam column joint. In particular, the loss of bond can cause the penetration of yielding into the anchorage zone, degrading the available development length and reducing the anchorage capacity.

However, regarding understanding the corrosion effect on the structural behavior under cyclic loading, the majority of the work has been focused on the cyclic behavior of corroded rebars (e.g. (Apostolopoulos, 2007; Hawileh et al., 2011; Kashani et al., 2013)), and some experimental studies can be found on the cyclic responses of structures with

corroded reinforcement (e.g.(A. Guo et al., 2015; Ma et al., 2012; Meda et al., 2014; Ou et al., 2012)) only found in the past decade. Extremely limited studies have been performed on studying cyclic bond deterioration due to corrosion. Among those studies, Fang et al. (C. Fang et al., 2006; C. Q. Fang, 2006), Zhao et al. (Zhou, Lu, Xv, Dong, et al., 2015; Zhou, Lu, Xv, Zhou, et al., 2015), Kivell et al. (Kivell et al., 2011) conducted experimental studies on corrosion effect on bond-slip relation. In particular, Kivell et al. is the only study that developed analytical cyclic bond models considering corrosion. Nevertheless, there are major limitations in the models proposed by Kivell et al.: *i*) the models are developed based on pullout testing that is not suggested for use in studying the true bond response; *ii*) the modification factors used in the models only consider the confinement content and corrosion level, and these two factors are considered separately not interactively; *iii*) other key factors such as compressive strength and the ratio of cover depth to rebar diameter are not considered in model, limiting the application of the models and restraining the models to be updated by possible future experiments; and *iv*) the prevailing uncertainties, such as statistical uncertainties and model errors are not considered.

In summary, to develop a reliable constitutive bond stress-slip relationship, a large database of test results of beam-end or beam specimens is needed. Therefore, all possible important factors (namely, the size of steel bars, the ratio of concrete cover to bar diameter, the concrete compressive strength, content of confining reinforcement, and type of confinement) and all relevant uncertainties should be incorporated in the constitutive law based on a probabilistic approach such that the probabilistic models can be easily updated whenever any future experimental data becomes available.

1.4.3. Structural Analysis Considering Deterioration on Bond

Bond deterioration will have a great impact in the recently developed design and performance evaluation aspects that are dependent on the bond development. Although reliability assessment of corroded RC structures (particularly bridges) using probabilistic corrosion models has been the subject of numerous studies in the last decade (Akgül & Frangopol, 2003; Enright & Frangopol, 1998a, 1998b; Frangopol & Liu, 2007; Petcherdchoo et al., 2008; Stewart & Rosowsky, 1998), few studies have attempted to evaluate the structural performance of corroded RC bridges subject to extreme hazards (Alipour et al., 2011; Choe et al., 2008; Ghosh & Padgett, 2010; Simon et al., 2010). Among these studies, the corrosion deterioration on bond has been either ignored or assumed to be inconsequential for members with sufficient reinforcement confinement based on a study by Fang et al. (C. Fang et al., 2004).

However, the findings by Fang et al. (C. Fang et al., 2004) were based on a very limited number of specimens tested under monotonic loading, considering a corrosion level only up to 6% and with no corrosion on the stirrups. Studies have shown that corrosion on stirrups should be considered on the bond strength degradation and the performance of the corroded structure (X. H. Wang & Liu, 2008), even though stirrups can control the bond deterioration up to a certain corrosion level (Valente, 2012). Bond deterioration can become a more serious issue for older structures that are not designed based on current seismic code provisions, which require high transverse steel ratios in columns. Moreover, under cyclic loadings, experimental results have demonstrated a large reduction in the bond capacity for corroded confined rebars (C. Fang et al., 2006; C. Q. Fang, 2006; Kivell et al.,

2011; Lee et al., 2003). Lastly but most importantly, one of the reasons that the majority of structural analyses do not include corrosion on the cyclic bond is simply because no software is available for non-linear time histories analysis that incorporates the effect of corrosion on bond. *Therefore, to incorporate the aging effect into resilience design or evaluate structural performance of corroded structures, in addition to the material properties, it is necessary to incorporate the corrosion effect on the bond behavior in the structural analysis.*

1.3. Dissertation Organization

This dissertation is prepared in five chapters. In Chapter I, the introduction and research significance are elaborated. In Chapter II, a probabilistic prediction model for RC bond failure is developed based on the experimental program performed in this research. The proposed model can be used to predict the probability that a specimen, or even a structural member, could fail in pull-out or splitting bond failure. In chapter III, probabilistic models are developed for the two important bond behavior parameters that are the bond strength and peak slip. Extensive experimental testing results gathered from previous literature to develop a comprehensive model using nonlinear multivariable and genetic programming techniques. In chapter IV, a simple rebar slip model is developed using macromodel approach that can be implemented into finite element modeling of structures, such as columns and bridges. Lastly, Chapter V represents the summary and conclusions of this dissertation.

From this dissertation, one conference and one journal paper is published in ASCE Structures Congress and Journal of Engineering Structures (Elsevier) (A. Soraghi et al., 2019; Ahmad Soraghi & Huang, 2021) based on the materials in Chapter II, one journal paper is under review in the Journal of Structures and Infrastructures Engineering (Taylor and Francis) based on the materials in Chapter III, and one Journal paper under review in the Journal of Engineering Structures (Elsevier) based on the materials in Chapter IV.

CHAPTER II

PROBABILISTIC PREDICTION MODEL FOR RC BOND FAILURE MODE

Reinforced concrete (RC) is a widely used construction material for civil structures like bridges (Huang et al., 2010a), buildings (Zaker Esteghamati et al., 2018), and dams (Hariri-Ardebili & Saouma, 2016). As the bond between rebar and concrete (i.e., rebar–concrete interaction) is meant to ensure the transformation of force between the rebar and concrete, bond behavior directly impacts the structure load-carrying capacity and failure mode. This bond is known to be influenced by many factors such as the concrete properties, transverse reinforcement, the ratio of concrete cover to rebar size, loading type, and rebar corrosion. Many researchers have studied how those influencing factors affect the bond strength, through which impact structural performance (Almusallam et al., 1996; Fu & Chung, 1997; M. H. Harajli, 2004; Hussain et al., 1995; Kivell et al., 2011; Sajedi & Huang, 2015; A. Soraghi et al., 2019; Stanish et al., 1999; H. Wang, 2009).

Another aspect of bond behavior that is also crucial for determining the performance of RC structures is the bond failure mode. Based on ACI [13], there are two distinguished bond failure mode: pull-out and splitting failure. Pull-out bond failure occurs when there is sufficient confinement and/or concrete cover to prevent concrete splitting and restrain crack growth, resulting in the shearing of concrete between ribs. Splitting failure occurs when confinement or cover is not provided adequately to achieve the

complete pull-out strength. In splitting failure, the deformation-bearing forces cause splitting that spreads through the sides of the member and makes the concrete to lose its bonding and cover.

In contrast to bond strength, the bond failure mode has not been well studied, especially in the presence of corrosion and/or under cyclic loading. Both ACI (ACI, 2012) criteria and CEB (fib, 2013) use bar size, concrete cover, and confinement of transverse stirrups to determine the bond failure mode. Cucchiara et al. (Cucchiara et al., 2004) and Zandi Hanjari et al. (Hanjari et al., 2011) examined the impact of the existence of the stirrups on the failure mode. Kivell (Kivell et al., 2011) observed that specimens with high levels of corrosion (more than 12%) or under cyclic loading have more tendency to fail in pull-out. Soraghi and Huang (A. Soraghi et al., 2019) developed models for predicting the bond failure mode using logistic and lasso classification algorithms to consider various influence factors including the presence of transverse stirrups, cover to rebar diameter ratio, the level of corrosion, and the loading type.

This study develops probabilistic prediction models of bond failure mode based on classification methods and examines the importance of bond failure mode prediction in the structure performance evaluation. The model development uses the results from a comprehensive experimental testing where various influencing factors are considered, including compressive strength of concrete, ratio of concrete cover to rebar diameter ratio, confinement of transverse stirrups, corrosion level, and loading type.

In this paper, the bond tests conducted on a set of beam-end specimens are described first, next the probabilistic models based on various classification methods are

developed, and then the prediction accuracy of the models is compared. Lastly, a case study is presented using the developed bond failure mode prediction model to examine how the bond impacts the flexural performance of an RC beam with a lap splice under various corrosion levels based on the reliability analysis.

2.1. Experimental program

2.1.1. Specimen design and details

A set of beam-end specimens are designed to investigate the intact and corroded rebar bond behavior under monotonic and cyclic loading. The design of the specimens are based on four parameters that found to be influencing bond behavior according to the findings of previous studies (e.g., (Mohamed H. Harajli et al., 2004; Maaddawy & Topper, 2005; Sajedi & Huang, 2015; A. Soraghi et al., 2019)) and they are: concrete compressive strength (f'_c), cover size to rebar diameter ratio (c/d), corrosion level (Q), and transverse rebar confinement that can be quantified by an index value, K_{tr} (Orangun et al., 1977), as shown below:

$$K_{tr} = \frac{f_{y,tr} \cdot A_{tr}}{4136.85 \cdot d_b \cdot s} \quad (1.1)$$

where $f_{y,tr}$ is the yield strength of transverse reinforcement (kN/m²), A_{tr} is the transverse reinforcement area (m²), d_b is the diameter of intact rebar (m), and s is the spacing of the transverse reinforcement (m). The detailed specification for each specimen is provided in [Tables A.1–A.3](#) in [Appendix A](#). [Table 2.1](#) summarizes the ranges of the design parameters. The specimens are classified into three groups (as shown in [Table 2.1](#))

based on the three designated concrete compressive strength levels: 25 MPa, 35 MPa, and 45 MPa (corresponding to measured averages of 27 MPa, 36 MPa, and 43 MPa, respectively, obtained in the cylinder tests). Each of the three groups consists of 44 beam-end specimens; thus, 132 specimens are tested. The level of corrosion, Q , is the percentage of mass reduction of the reinforcement in the bonded region. Group 1 consists of 22 corroded specimens with the designed Q ranging from 5% to 20% (corresponding to measured Q of 3.2% to 15.6% after load testing was completed) and 12 intact specimens ($Q = 0\%$). Group 2 consists of 38 corroded specimens with the designed Q ranging from 5% to 15% (corresponding to measured Q of 4.93% to 19.08% after testing was completed) and 6 intact specimens. Group 3 also consists of 38 corroded specimens with designed Q ranging from 5% to 15% (corresponding to measured Q of 3.74% to 16.85% after load testing was completed) and 6 intact specimens.

Table 2.1 Summary of design parameters of testing specimens.

Group	f'_c (MPa)		No. of specimens (Imperial rebar size)		No. of specimens (Loading type*)			No. of intact specimens	Corroded specimens w/ corrosion, Q (%)	
	Target	Actual							Target	Actual
1	25	27	16 (#5)	16 (#6)	12 (#8)	18 (M)	26 (C)	12	5 ~ 20	3.2 ~ 15.6
2	35	36	16 (#5)	16 (#6)	12 (#8)	22 (M)	22 (C)	6	5 ~ 15	4.93 ~ 19.0
3	45	43	16 (#5)	16 (#6)	12 (#8)	22 (M)	22 (C)	6	5 ~ 15	3.74 ~ 16.8

Specimens in each group use three sizes of reinforcement bars: #5 bars ($d_b = 15.875$ mm), #6 bars ($d_b = 19.05$ mm), and #8 bars ($d_b = 25.4$ mm). Among the 44 specimens in Group 1, 22 have transverse stirrups with K_{tr} values ranging from 3.68 to 5.89, and the remaining 22 specimens have no transverse stirrups (i.e., $K_{tr} = 0$). All specimens in Groups 2 and 3 have transverse stirrups to increase the chance of pull-out failure, with K_{tr} values ranging from 7.3 to 11.7. For loading type, in Group 1, 18 of the specimens are tested under monotonic loading, while 26 specimens are tested under cyclic loading; in groups 2 and 3, 22 specimens in each group have monotonic loading and the other 22 specimens have cyclic loading.

Dimensions and reinforcement detailing for the designed beam-end specimens are shown in [Figure 2.1 \(a\)](#), and [Figure 2.1 \(b\)](#) shows an actual casted beam-end specimen. All specimens are 508 mm \times 381 mm \times 190.5 mm. All transverse, parallel, and longitudinal reinforcements are #3 rebar with a diameter of 76.2 mm. All the reinforcements are coated with epoxy to prevent corrosion except for the test bar. The test bar is covered by PVC pipes at the two ends within the concrete. The middle bonded region of the test bar that is not covered by PVC pipe has a bonded length, l_b , as shown in [Figure 2.1 \(a\)](#), and $l_b = 88.9$ mm, 114.3 mm, and 152.4 mm are adopted for the specimens with rebar sizes of #5, #6, and #8, respectively. These bonded lengths are chosen to prevent rebar tensile yielding prior to bond failure, to ensure a relatively uniform distribution of bond stress (Sajedi & Huang, 2015), and prevent conical failure of the specimens (Darwin & Graham, 1993). The yield strength, F_y , and ultimate strength, F_u , of rebar are 420 MPa and 600 MPa, respectively, regardless of the rebar size.

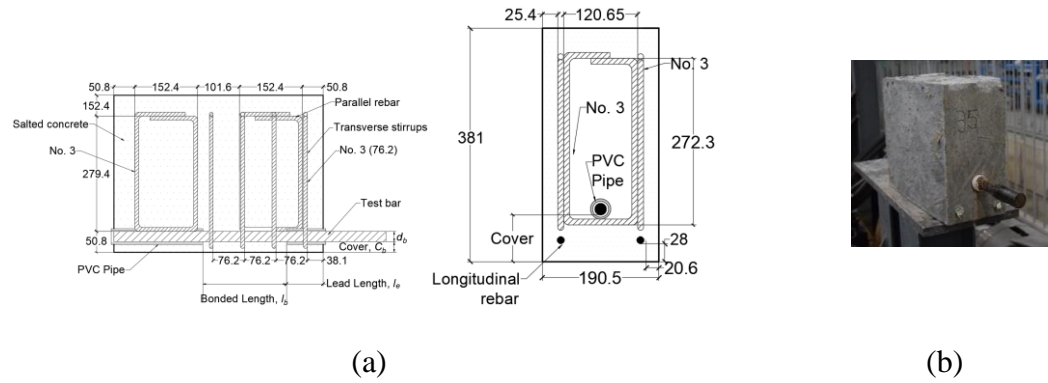


Figure 2.1 Beam-end specimens: (a) schematic design and (b) as-casted beam-end specimen.

To accelerate corrosion on the test bar, sodium chloride (NaCl) was added to the concrete before it was poured into the specimen molds. The amount of salt (NaCl) in the concrete is calculated based on 3.75% weight of cement as is suggested by previous researchers (Abosrra et al., 2011; Yalciner et al., 2012) to achieve accelerated corrosion.

2.1.2. Corrosion process

Accelerated corrosion is achieved by applying current to the test bar. The designed corrosion level can be calculated as:

$$Q = \frac{\Delta M}{\gamma \cdot l_b \cdot A_{b0}} \times 100\% \quad (1.2)$$

where ΔM (grams) is the change in mass of the rebar due to corrosion; $\gamma = 7.86 \text{ gr/cm}^3$ is the density of iron, l_b is the corroded length (or bond length), and A_{b0} refers to the intact cross-sectional area of rebar. With a desired level of Q , ΔM can be estimated based on Equation (1.2). Then the accelerated corrosion time, T , during which the current needs to

be applied can be calculated to achieve the desired corrosion level based on Faraday's law (Ahmed et al., 2007):

$$T = \frac{\Delta M \cdot Z \cdot F}{A \cdot I} \quad (1.3)$$

where $A = 56$ grams referring to the atomic weight of iron; I is current (Amp); $Z = 2$ is the valency number of ions of the substance, Fe, and $F = 96500$ (Amp·sec), which is referred to as Faraday's constant.

After casting, the specimens are cured with sufficient humidity (ACI Committee 308, 2001). In this study, all specimens are kept in the designed humidity tents (schematically shown in [Figure 2.2 \(a\)](#)) for curing as well as corroding. The corrosion setup (schematically shown in [Figure 2.2 \(b\)](#)) is designed to allow power supplies to be connected to the specimens to supply the required current for accelerating corrosion while keeping the specimens in the humidity tents. The corrosion setup uses a parallel circuit system where the rebar serves as the anode, while a stainless steel plate that was located underneath the specimen (mostly underneath the bonded region) acts as the cathode (C. Fang et al., 2006). The parallel system allows specimen(s) to be removed without stopping the current that runs through the other specimens, and such a setup is necessary, as each specimen is designed for different corrosion levels and requires a different corrosion time. In addition, the parallel system allows the use of power supplies with lower voltage compared to a setup using a series circuit system.

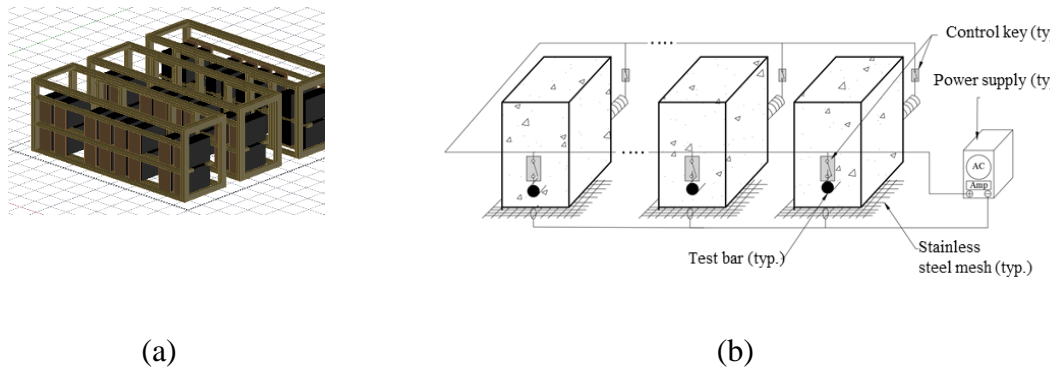
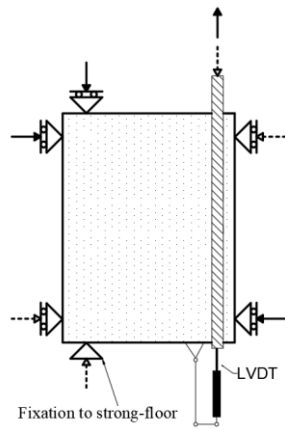


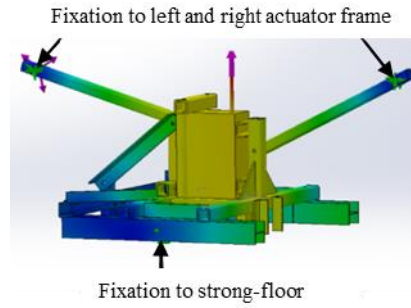
Figure 2.2 Schematic view of (a) humidity tents and (b) corrosion setup.

2.1.3. Test setup

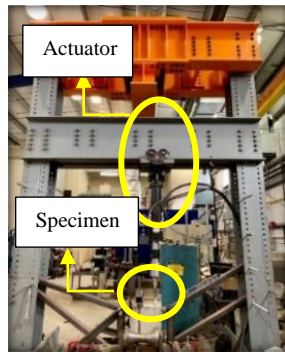
Monotonic and cyclic testing are performed to study the corrosion impact on bond behavior. Utilizing the testing frame that is securely mounted on a rigid floor in the testing lab, a vertical test setup is designed for this study based on ASTM A944-10 and a previous study by Bandelt and Billington (Bandelt & Billington, 2016) where the applied loading on beam-end specimens is in a vertical direction as well. Figure 2.3 (a) and (b) are a schematic of the setup that shows the boundary conditions and a 3D-rendering view of the setup, respectively. It should be noted that the roller/pin supports were provided at six locations, where three supports react (shown in solid arrows) when the rebar is under tension and the other three supports react (shown in dashed arrows) when the rebar is under compression, as shown in Figure 2.3 (a). Figure 2.3 (c) and (d) show the testing frame and the laboratory test setup, respectively.



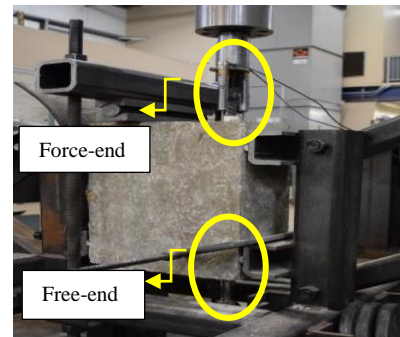
(a)



(b)



(c)



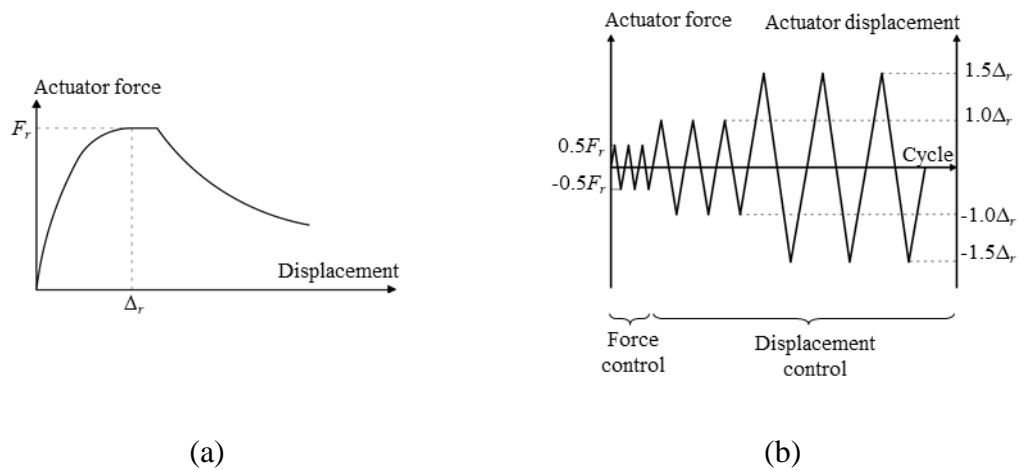
(d)

Figure 2.3 (a) Boundary conditions of testing specimen; (b) 3D rendering view of test setup; (c) testing frame, (d) laboratory test setup.

A 245-kN actuator is secured to the testing frame in a vertical position; a threaded rod is welded to the test bar and the specimen connects to the actuator through a special connection designed particularly for this test. Rebar slippage is measured according to ASTM standard A944-10 (ASTM A944-10, 2015) using linear variable differential transducers (LVDTs) at the free-end of the specimen. The LVDTs are mounted on the

bottom of the concrete as shown in [Figure 2.3 \(a\)](#) such that the slippage of the rebar relative to the bottom of the concrete could be measured.

To accomplish the testing, it is necessary to first determine the loading procedure and loading rate. ASTM standard 944-10 (ASTM A944-10, 2015) specifies that a loading rate between 10% and 33% of the predicted rupture force be reached within one minute. However, this rate is too fast to allow recording the critical points during the failure process, particularly the point at which the rupture force occurs (i.e., the bond strength is achieved). Thus, the loading rate is recalculated in such a way that the rupture force will not occur in less than three minutes. Accordingly, all monotonic specimens are tested in displacement-control with a rate equal to 0.005 mm/sec (that is, 1.3 mm per 3 minutes). [Figure 2.4 \(a\)](#) shows an actuator force-displacement diagram under monotonic loading, where F_r is the rupture force and Δ_r is the displacement of the actuator at rupture.



[Figure 2.4](#) (a) Actuator force and displacement diagram under monotonic loading and (b) cyclic loading protocol.

As ASTM standard 944-10 does not specify the cyclic loading procedure for bond testing, the procedure used in Kivell (Kivell et al., 2011) is adopted in this study. [Figure](#)

2.4 (b) shows the adopted cyclic loading protocol consists of three sets of cycles, where F_r and Δ_r are extracted from the corresponding monotonic curve (Figure 2.4 (a)).

In the cyclic loading, the first set of cycles are force-controlled with a maximum force of $0.5F_r$; the other two sets of cycles are displacement-controlled with maximum displacements of $1.0\Delta_r$ and $1.5\Delta_r$, respectively. The first set is mainly used for weakening the bond, while the second and third sets of cycles are designed to break the bond and capture the behavior after exceeding the bond strength. For the force-controlled cycles, the loading rate is $10\%F_r \sim 33\%F_r$ per minute; for the displacement-controlled cycles, the displacement rate is $10\%\Delta_r \sim 33\%\Delta_r$ per minute.

2.1.4. Experimental results and discussion

After testing is complete, the monotonic and cyclic bond behaviors of all specimens are obtained. The work presented in this paper focuses on the prediction of the failure modes; the study on the other bond characteristics (e.g., bond strength) will be presented in future papers. Two distinct failure modes, pull-out and splitting failure are observed, and the failure modes for each specimen are summarized in Table A.1-A.3 in Appendix A, where failure mode “P” refers to the pull-out failure and “S” is the splitting failure. However, there were 12 specimens whose failure modes were not distinguishable due to various reasons (e.g., the actuator reached its force capacity before the bond failure occurred); these specimens are marked as “NA” in failure mode. Figure 2-5 shows the typical actuator force-displacement diagrams under monotonic or cyclic loading with splitting or pull-out failure modes. A common feature of splitting failure under either

monotonic or cyclic loading is the sudden drop in force when the specimen reaches its rupture force, followed by observing large surface and/or sides cracks on the specimen.

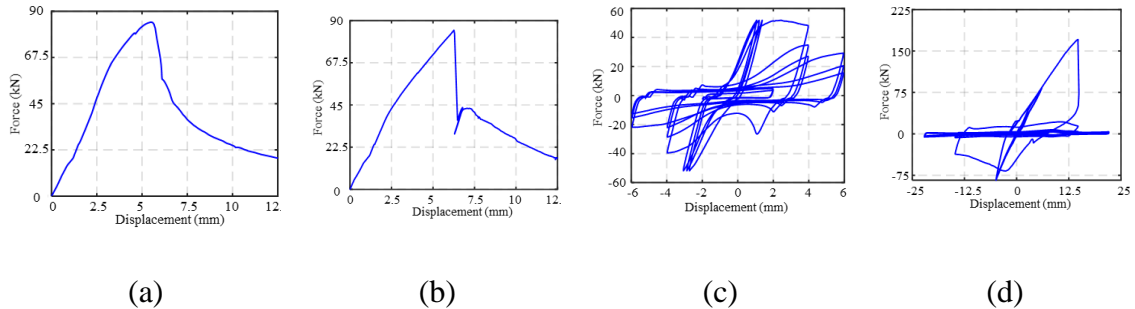


Figure 2.5 Typical actuator force-displacement (a) under monotonic loading with pull-out failure, (b) under monotonic loading with splitting failure, (c) under cyclic loading with pull-out failure, and (d) under cyclic loading with splitting failure.

In addition, different crack patterns are observed for the two failure modes. Figure 2.6 shows typical crack patterns for pull-out and splitting failure modes, and Figure 2.7 presents a schematic view of crack patterns for each mode of failure. Generally, with splitting failure, not only the surface of the specimen is crushed, but at least one crack is initiated from the testing rebar as shown in Figure 2.7 (a). This is because such surface cracks are propagated from the radial splitting of the concrete due to the wedge action of the test bar ribs when the bond fails in splitting. However, with pull-out failure, the cracks do not initiate from the testing rebar (as shown in Figure 2.7 (b)), as there is sufficient confinement to restrain the concrete surrounding the rebar from splitting. Darwin and Graham (Darwin & Graham, 1993) also found that splitting failure (which was the only failure mode observed in their specimens) have some crack patterns based on the presence of transverse stirrups as well as on the cover size, which is consistent with the splitting mode cracking patterns observed in this study. Thus, identifying the cracking pattern could help to determine the failure mode.



Figure 2.6 A typical cracking pattern for (a) splitting failure mode and (b) pull-out failure mode.

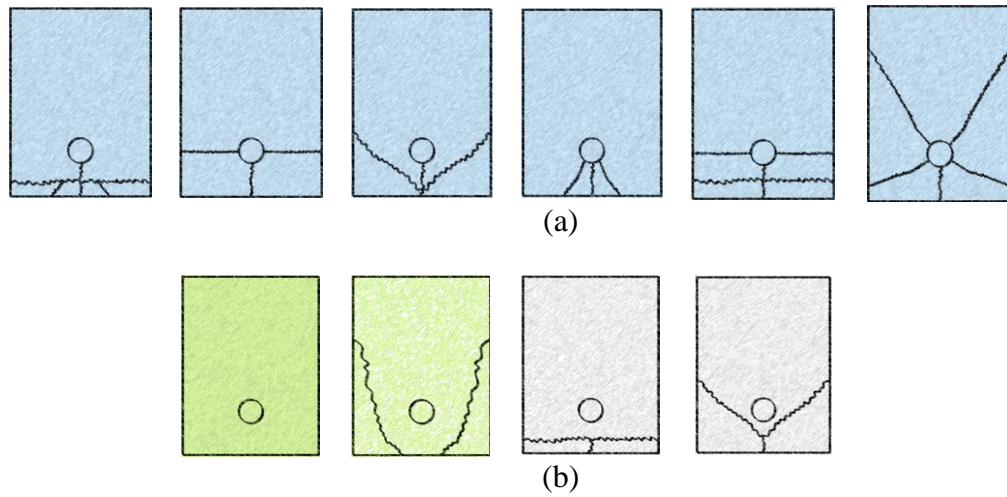


Figure 2.7 Schematic view of crack patterns formed on the test specimens after failure: (a) splitting failure mode and (b) pull-out failure mode.

2.2. Probabilistic prediction model for bond failure mode

In this section, existing deterministic models for bond failure mode and various classification algorithms are reviewed. The logistic and lasso classification algorithms used

in the model development are described, and the performances of the various prediction models are compared based on the experimental data.

2.2.1. Existing deterministic models

In the literature, very few models are available for predicting RC bond failure modes. If let $Y = 1$ and $Y = 0$ represent pull-out and splitting bond failure, respectively, the prediction by CEB criteria can be written as (fib, 2013).

$$Y = \begin{cases} 1 & c \geq 5d_b \\ 0 & c_{\max} / c_{\min} = 2.0 \& c_{\min} = d_b \& d_b \leq 20\text{mm} \& K_{tr,CEB} = 2\% \end{cases} \quad (2.4a)$$

where $c_{\max} = \max\{c_x, c_{si}\}$ and $c_{\min} = \min\{c_x, c_y, c_{si}\}$, in which c_x and c_y are the concrete cover toward the horizontal and vertical edges, respectively, and c_{si} is the half of the center-to-center test bar spacing (if more than one test bar is implemented); $K_{tr,CEB} = A_{tr}/(n_b \cdot d_b \cdot s)$, in which n_b is the number of anchored test bars. However, it is obvious that conditions for splitting failure (i.e., $c_{\max}/c_{\min} = 2.0$, $c_{\min} = d_b$ and $K_{tr,CEB} = 2\%$) are very strict, which makes these CEB criteria almost inapplicable. Thus, instead of using the CEB criteria literally, the “equal” sign in the expressions may be interpreted to be “no larger than”, and the logical operator between the expressions be interpreted to be “or”, rather than “and”. Also, for the cases that do not satisfy both pull-out and splitting conditions of the CEB criteria, the prediction can be treated as “unknown”. Thus, the CEB criteria is interpreted as follows in this study:

$$Y = \begin{cases} 1 & c \geq 5d_b \\ 0 & c_{\max} / c_{\min} \leq 2.0 \text{ or } c_{\min} \leq d_b \text{ or } d_b \leq 20\text{mm or } K_{tr,CEB} \leq 2\% \\ \text{unknown} & \text{otherwise} \end{cases} \quad (2.4b)$$

Meanwhile, ACI (ACI, 2003) uses the following criteria for the bond failure mode prediction:

$$Y = \begin{cases} 1 & (c + K_{tr,ACI} / d_b) \geq 2.5 \\ 0 & (c + K_{tr,ACI} / d_b) < 2.5 \end{cases} \quad (2.5)$$

where $K_{tr,ACI} = A_{tr} \cdot f_{y,tr} / (1500 \cdot s \cdot n_b)$.

The two prediction models shown above are deterministic based; thus, uncertainty is not considered. More importantly, these two models do not holistically consider all the parameters that might influence the bond failure mode, such as corrosion and loading types.

2.2.2. Classification algorithms

Supervised machine learning techniques (i.e. regression and classification) are extensively implemented in engineering purposes for response estimation. Whilst the regression algorithm is appropriate for continuous response prediction, the classification algorithm is suitable for categorical responses such as failure modes (Harrington, 2012). In this study, classification methods are used to develop probabilistic models based on all the influencing parameters. In the following, a brief description of the classification algorithms of logistic and lasso classification is described, and other classification algorithms adopted in this research is provided in [Appendix B](#).

2.2.2.1. Logistic classification

The logistic classification algorithm evaluates the relationship between independent variables and dependent variables (i.e., categorical response) using a logistic function. The binary response, Y , refers to the bond failure mode and is defined as the same as before: $Y = 1$ for pull-out and $Y = 0$ for splitting. The formulation for logistic classification to estimate the probability of pull-out failure is shown as:

$$\Pr(Y = 1 | \mathbf{x}) = \frac{\exp(z)}{1 + \exp(z)} = \frac{\exp\left(\beta_0 + \sum_{i=1}^m \beta_i \mathbf{x}_i\right)}{1 + \exp\left(\beta_0 + \sum_{i=1}^m \beta_i \mathbf{x}_i\right)} \quad (2.6)$$

where $\mathbf{x} = \{x_i\}$, in which x_i are the independent variables selected, m is the number of independent variables used, and β_0 and $\{\beta_i\}$ are the coefficients for logistic classification that can be obtained using the maximum likelihood technique (Chang et al., 2019) through a likelihood function as:

$$l(\boldsymbol{\beta}) = \sum_{j=1}^N \left(y_j \boldsymbol{\beta}^T \tilde{\mathbf{x}}_j - \log \left[1 + \exp(\tilde{\mathbf{x}}_j \boldsymbol{\beta}) \right] \right) \quad (2.7)$$

where the subscript j refers to the j^{th} observation data, $\tilde{\mathbf{x}}_j = \{1 \ \mathbf{x}\}^T$, and $\boldsymbol{\beta} = \{\beta_0 \ \beta_1 \ \beta_2 \ \dots \ \beta_m\}^T$. As Y is a binary variable, then $P(Y = 0 | \mathbf{x}) = 1 - P(Y = 1 | \mathbf{x})$. It should be noted that the deviance of the fitted model is proportional to $-\log[l(\boldsymbol{\beta})]$; accordingly, by maximizing $l(\boldsymbol{\beta})$ for the $\boldsymbol{\beta}$ evaluation, the deviance will be minimized.

2.2.2.2. Lasso classification

While the lasso classification uses the same formulation (shown in Equation (2.6)) as the logistic algorithm, the way to evaluate the model parameters is different. Lasso classification requires a constraint on the coefficients in the maximum likelihood evaluation, which can be expressed as:

$$l(\boldsymbol{\beta}) = \sum_{j=1}^N \left(y_j \boldsymbol{\beta}^T \mathbf{x}_j - \ln \left[1 + \exp(\mathbf{x}_j \boldsymbol{\beta}) \right] - \lambda \sum_{i=0}^p |\beta_i| \right) \quad (2.8)$$

where λ is a penalty factor also known as the constraint. Lasso classification stabilizes a system by applying a cost of the sum of absolute values of the coefficients. This is called sparse regularization to constrain over-fitting and is conducted using the *lassoglm* function in MATLAB by which the deviance will be minimized in order to estimate the model parameters in Equation (8). Lasso classification is a more desirable technique when working with a relatively small size of data, or when there is a correlation between independent variables (Tibshirani, 1996), and lasso's strength is to reduce the fitted model deviance without substantially increasing the prediction bias.

2.2.3. Model development

2.2.3.1. Independent variables selected for the models

From an engineering perspective, logistic and lasso classification are capable of providing explicit formulations. For this reason, both methods are used in developing the probabilistic model. Other methods, including the two deterministic models and other

classification algorithms (i.e., decision tree, discriminant analysis, K -nearest neighbors, Naïve-Bayes, random forest, and support vector machine) that are described in Appendix B, will be assessed in terms of their model prediction accuracy.

Independent variables selected for the models

To develop the failure mode prediction models based on Equation (2.6), a preliminary analysis needs to be performed first to select the potential variable x_i . Next, a model selection procedure is used to delete the independent variables that are not contributing significantly to the model prediction.

In this study, the variables showing the potential impacts on the failure mode (Y) are: f_c , c/d , K_{tr} , Q , and MC , where MC is a dummy variable defined as:

$$MC = \begin{cases} 1 & \text{monotonic loading} \\ 2 & \text{cyclic loading} \end{cases} \quad (2.9)$$

In addition, the linear interactions among these five variables are also examined via scatter plots. As an example, Figure 2.8 (a) and (b) show the scatter plots of K_{tr} and c/d versus the actual response y , respectively; and Figure 2.8 (c) shows the interaction term, $K_{tr} \cdot c/d$, versus y with a fitted logistic curve. These three plots in Figure 2.8 show that although the individual variables might not contribute to the failure mode prediction, their interaction might. Table 2.2 lists all the potential variables, x_i , used in Equation (2.6) for the model development using logistic and lasso classification.

Table 2.2 Potential variables used for model development.

Term types	x_i				
Single variable	f_c	c/d	K_{tr}	Q	MC
Interaction of 2 variables	$K_{tr} \cdot c/d$	$K_{tr} \cdot Q$	$K_{tr} \cdot f_c$	$K_{tr} \cdot MC$	$c/d \cdot Q$

	$c/d \cdot MC$	$c/d \cdot f_c$	$Q \cdot MC$	$Q \cdot f_c$	$MC \cdot f_c$
Interaction of 3 variables	$K_{tr} \cdot c/d \cdot Q$ $K_{tr} \cdot MC \cdot f_c$	$K_{tr} \cdot Q \cdot MC$ $c/d \cdot Q \cdot MC$	$K_{tr} \cdot c/d \cdot MC$ $c/d \cdot Q \cdot f_c$	$K_{tr} \cdot c/d \cdot f_c$ $c/d \cdot MC \cdot f_c$	$K_{tr} \cdot Q \cdot f_c$ $Q \cdot MC \cdot f_c$
Interaction of 4 variables	$K_{tr} \cdot c/d \cdot Q \cdot MC$	$K_{tr} \cdot c/d \cdot Q \cdot f_c$	$K_{tr} \cdot c/d \cdot MC \cdot f_c$	$K_{tr} \cdot Q \cdot MC \cdot f_c$	$c/d \cdot Q \cdot MC \cdot f_c$
Interaction of 5 variables	$K_{tr} \cdot c/d \cdot Q \cdot MC \cdot f_c$				

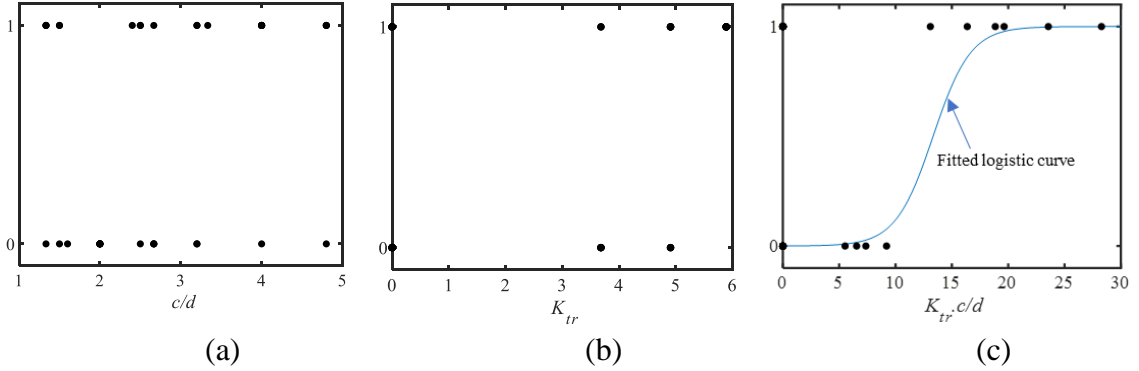


Figure 2.8 Example of a scatter plot of failure mode for terms (a) c/d , (b) K_{tr} , and (c) logistic curve for their interaction term ($K_{tr} \cdot c/d$).

2.2.3.2. Model prediction accuracy

Different quantities are adopted to measure the performance of the developed models, such as the mean absolute error of prediction, *MAE*:

$$MAE = \frac{\sum_{i=1}^n |y_i - \hat{y}_i|}{n} = \frac{\sum_{i=1}^n |e_i|}{n} \quad (2.10)$$

where \hat{y}_i is the prediction, y_i is the true value, and n is the number of data points. Another way to measure prediction accuracy is the hit-or-miss approach. Using the prediction probability formula from Equation (6) and opting a threshold level of α (that is set to be 50% in this study), then $P(Y = 1|\mathbf{x}) \geq \alpha$ indicates a pull-out failure and $P(Y = 1|\mathbf{x}) < \alpha$

indicates a splitting failure. Accordingly, based on the correct or wrong prediction of the failure mode, there are four possible outcomes as shown in [Table 2.3](#): true positive (TP) and true negative (TN) as the correct detections, and false positive (FP) and false negative (FN) as the false detections. Then the probability of correct detection, P_{CD} , as a measure of model prediction accuracy, can be calculated using the number of TP tests (n_{TP}), the number of TN tests (n_{TN}), and the total number of tests (n_{total}):

$$P_{CD} = \frac{n_{TP} + n_{TN}}{n_{total}} \quad (2.11)$$

Similar measurements can be used for pull-out and splitting failure mode, separately, as follows:

$$P_{CD,pull-out} = \frac{n_{TP}}{n_{TP} + n_{FP}} = \frac{n_{TP}}{n_{pull-out}} \quad (2.12)$$

and

$$P_{CD,splitting} = \frac{n_{TN}}{n_{TN} + n_{FN}} = \frac{n_{TN}}{n_{splitting}} \quad (2.13)$$

[Table 2.3](#). Four possible prediction outcomes.

Failure mode	Predicted to be pull-out	Predicted to be splitting
Pull-out ($Y = 1$)	True positive (TP)	False negative (FN)
Splitting ($Y = 0$)	False positive (FP)	True negative (TN)

2.2.3.3. Model selection

When using all the 31 variables (listed in [Table 2.2](#)) in [Equation \(2.6\)](#), the model is considered as a full model with a model size of 31. For logistic classification, a model selection is performed to the full model to remove the variables with insignificant contributions to the model prediction. In particular, the all possible subset approach (Lindsey & Sheather, 2010) is adopted in which all potential combinations of x_i are first formulated for every reduced model size (ranging from 1 to 30), which will result in more than two billion possible models. To keep the model practical, the maximum model size is capped at four (i.e., four variables in a model), which also greatly reduces the computational time. Accordingly, all subsets with model size of five and above are excluded.

In addition, the models with any model parameters having p -values greater than 10% and variance inflation factors ($VIFs$) greater than 10 are treated as invalid and are eliminated. Statistical measurements such as R -squared (R -sq), adjusted R -squared (Adj - R -sq), and Akaike information criterion (AIC) are then used for each model size to evaluate the performance of models.

Models with the highest R -sq and Adj - R -sq or the lowest AIC are the most favorable model for a specific model size. The most favorable models from each subset are then compared to determine the final model. It is noted that different statistical measurements (Adj - R -sq, R -sq, and AIC) may result in a different best model.

The most desirable models for various model sizes are shown in [Table 2.4](#). MAE and P_{CD} are also calculated to compare the performance of those models. It can be observed

that the model with a model size of 4 has improved accuracy regarding R -sq and Adj - R -sq; the model with a model size of 3 has the same accuracy in terms of MAE and slightly improved accuracy regarding P_{CD} . Thus, the smaller model size is preferred, and z in Equation (2.6) for logistic regression is written as:

$$z = \beta_0 + \beta_1(c/d \cdot Q) + \beta_2(f'_c \cdot c/d) + \beta_3(Q \cdot MC \cdot f'_c) \quad (2.14)$$

The statistics of the model coefficients in Equation (2.14) are summarized in Table 2.5.

Table 2.4. Statistics summary for the top three logistic classification models for each model size.

Model size	Independent variables				R -sq (%)	Adj - R -sq (%)	AIC	MAE	P_{CD} (%)
1	$c/d \cdot MC \cdot f'_c$				21	20	13.4	0.48	66
2	$c/d \cdot f'_c$	$MC \cdot f'_c$			30	27	124.8	0.42	75
3	$c/d \cdot Q$	$c/d \cdot f'$	$Q \cdot MC \cdot f'_c$		32	30	123.3	0.33	79
4	MC	$c/d \cdot f'_c$	$K_{rr} \cdot Q \cdot MC$	$Q \cdot MC \cdot f'_c$	35.2	32	122.5	0.33	78

Table 2.5. Logistic model coefficients.

Model coefficients	β_0 (Intercept)	β_1 ($c/d \cdot Q$)	β_2 ($c/d \cdot f'_c$)	β_3 ($Q \cdot MC \cdot f'_c$)
Mean	-3.46	-4.00	+0.031	0.65
Standard deviation	0.81	1.62	0.008	0.14
Coefficient of variation	-0.23	-0.40	0.25	0.21

The method of cross-validation is used to train and validate the lasso model. Cross-validation method divides train set into m folds (10 folds is used in this research), then the model parameters are evaluated through a subsequence manner for various penalty factor values (λ), meaning that in the sparse regularization the independent variables having a corresponding coefficient of zero are eliminated for a given penalty factor value. Hence there will be a subsequence of models having different model sizes associated with the

continuance of the penalty factor value. The model with the minimum average deviance plus one standard deviation is suggested to be the final model (Tibshirani, 1996), since this model will balance the prediction that is measured by deviance as opposed to false discovery.

Since the method of cross-validation randomly divides data, there is a possibility that each analysis leads to a different result. Thus, the analyses are performed multiple times on the total dataset (100 times in this study). The variables selected at the end of each analysis that appear most frequently among all the repetition is the one selected as the final term. As the result of the multiple analyses conducted in this study, four terms appear most frequently: three terms (i.e., $c/d \cdot f'_c$, $MC \cdot f'_c$, $Q \cdot MC \cdot f'_c$) appear in all analyses, and one term (i.e., $K_{tr} \cdot c/d \cdot f'_c$) appear in half of the analyses. However, when using all these four terms, the accuracy of the resulting model was found to be lower than that for a model using only three terms (i.e., $c/d \cdot f'_c$, $MC \cdot f'_c$, $Q \cdot MC \cdot f'_c$); thus, $K_{tr} \cdot c/d \cdot f'_c$, is excluded. Accordingly, based on lasso classification, z in Equation (2.6) can be written as:

$$z = \beta_0 + \beta_1 (c / d \cdot f'_c) + \beta_2 (MC \cdot f'_c) + \beta_3 (Q \cdot MC \cdot f'_c) \quad (2.15)$$

The estimated model coefficients in Equation (2.15) are provided in Table 2.6.

Table 2.6. Lasso model coefficients.

Model coefficients	β_0 (Intercept)	β_1 ($MC \cdot f'_c$)	β_2 ($c/d \cdot f'_c$)	β_3 ($Q \cdot MC \cdot f'_c$)
Mean	-4.5	0.049	0.014	0.0194
Standard deviation	0.26	0.003	0.001	0.019
Coefficient of variation	-0.06	0.06	0.08	0.97

2.2.4. Model comparison

Using either logistic or lasso classification, both Equation (2.14) and Equation (2.15) suggest that four independent variables contribute to the failure mode prediction: f'_c , c/d , Q , and MC . It is worthy to understand how these four variables contribute to the bond failure mode. Recall that splitting bond failure involves the radial splitting of the concrete cover by the wedge action of the bar ribs, while pull-out bond failure mainly involves the shearing of the bar against the surrounding concrete. As concrete compressive strength, f'_c , is directly correlated to concrete tensile splitting resistance and shearing cracking resistance, it is not surprising that f'_c is selected in the proposed formulation. Cover to rebar diameter ratio, c/d , was found in many previous literature as an important factor to affect failure mode (M. H. Harajli, 2009; Hongwei Lin, Zhao, Ozbolt, et al., 2019; Hongwei Lin, Zhao, Yang, et al., 2019; Y. F. Wu & Zhao, 2013), as it measures the confinement around the test bars that could help effectively prevent the splitting cracking in concrete.

The impact of corrosion of rebar, Q , on the bond failure mode, on the other hand, changes the failure mode by changing the interactive effect of ribs and concrete. The produced layer of rust (i.e., steel oxidizes) within the gap between rebar and concrete could act as a lubricant and thus alter the failure mode, mostly from splitting to pull-out (Almusallam et al., 1996; Kivell et al., 2011). Lastly, the loading type of the specimen, monotonic and cyclic, MC , was also found to be a contributing factor in the response of the bond behavior. This is because the cycles in cyclic loading can weaken the bond on each cycle before rupture without causing extensive splitting cracks in concrete (M. H. Harajli, 2009), which leads to the bond failing in a pull-out fashion.

In addition, when comparing the selected terms in the logistic and lasso model formulations, it was found that they both include two terms ($c/d \cdot f_c$ and $Q \cdot MC \cdot f_c$) and have a negative intercept β_0 . Note that both models do not select any terms that include K_{tr} . This finding shows that within the ranges of K_{tr} considered in this study, the transverse stirrup does not influence the failure mode prediction. This is consistent with the findings from Lin et al. (Hongwei Lin, Zhao, Ožbolt, & Reinhardt, 2017). In addition, Soraghi and Huang (A. Soraghi et al., 2019) also found that the presence of a higher amount of transverse stirrups will not necessarily lead to pull-out failure.

Figure 2.9 shows the comparison for the sensitivity of the two models to three parameters: Q , f_c , and c/d under monotonic or cyclic loading. For all three parameters, both models show the same trend: the model prediction for the model under cyclic loading is more sensitive to the x -axis quantity than the one under monotonic loading, which is in agreement with the finding of Kivell et al. (Kivell et al., 2011). In addition, Figure 2.9 indicates that with an increase in Q , f_c , or c/d , the probability of the failure being pull-out increases; the result regarding corrosion is also consistent with the previous finding from Kivell et al. (Kivell et al., 2011). However, under cyclic loading, the lasso model is found to be more sensitive than the logistic model with respect to Q (Figure 2.9 (a)) and f_c (Figure 2.9 (b)). Under monotonic loading, the logistic model is found to be more sensitive than the lasso model with respect to f_c (Figure 2.9 (b)) and c/d loading (Figure 2.9 (c)).

— Logistic
 - - - Lasso

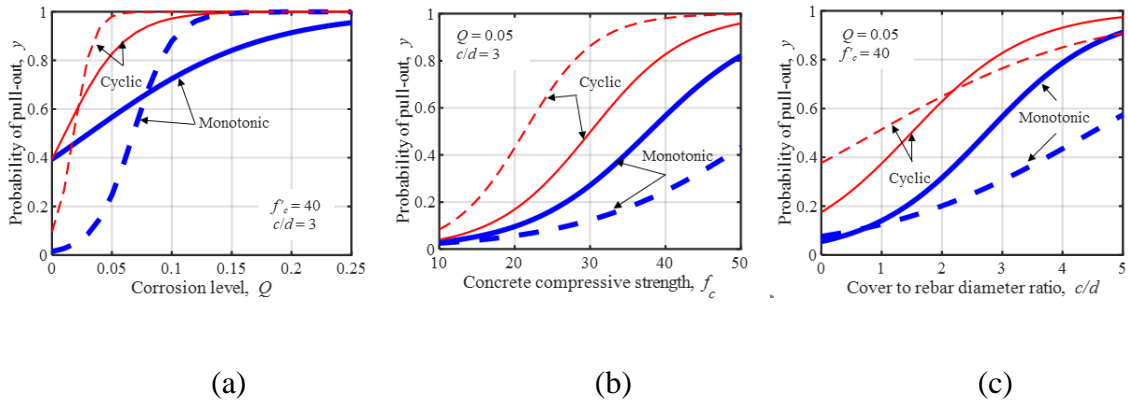


Figure 2.9 Sensitivity comparison between logistic and lasso logistic models for (a) corrosion level, (b) concrete compressive strength, and (c) ratio of cover to rebar diameter.

Figure 2.10 shows a comparison for the predicted probabilities for the specimens based on the developed logistic model (denoted as ‘o’) and the lasso model (denoted as ‘*’). For probability prediction, if pull-out failure and splitting failure (shown in **Figures. 2.10 (a) and (b)**, respectively), the probability value of the y-axis is closer to one, yielding a better prediction. Overall, for most cases, the predictions from both models are fairly close, and both models provide better predictions for the splitting failure specimens. At lower corrosion levels (less than 10%), the prediction discrepancy between the predictions from the two models seems to be smaller, especially for the splitting failure mode.

○ Logistic * Lasso

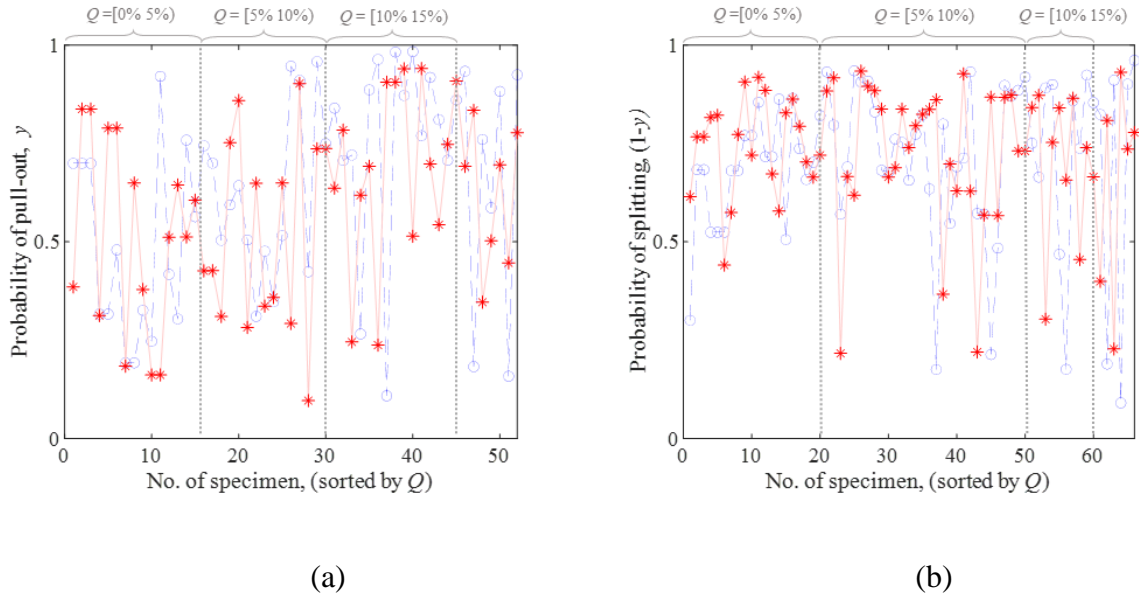


Figure 2.10 Prediction plot for (a) pull-out failure and (b) splitting failure.

Next, the prediction performance of the probabilistic models based on logistic and lasso classification is compared with other methods of classification and the two deterministic models in terms of MAE , P_{CD} , $P_{CD,pull-out}$, and $P_{CD,splitting}$. Note that to calculate P_{CD} for the deterministic criteria of CEB (Equation (2.4)), Equation (2.11) does not consider the cases if the criteria indicate unknown. Thus, to calculate P_{CD} , a 50% of correct detection (i.e. reflecting a random guess) is assigned for the unknown cases. The prediction accuracy comparison is summarized in Table 2.7. It can be seen that the deterministic models (i.e., CEB and ACI-318) have much lower P_{CD} values and higher MAE values compared to the classification methods, indicating a poor prediction capability. On the other hand, the performance of all the classification methods is reasonably close. While the accuracies of the logistic and lasso models are not among the highest in terms of $P_{CD,pull-}$

out, they both perform fairly well in terms of $P_{CD,splitting}$, and P_{CD} . In addition, the lasso classification performs best in terms of MAE .

Table 2.7. Predictive accuracy of various prediction methods.

	Prediction method	$P_{CD,pull-out}$ (%)	$P_{CD,splitting}$ (%)	P_{CD} (%)	MAE
Deterministic methods	CEB (fib, 2013)	35	59	47	0.72
	ACI-318 (ACI Committee 318, 2014)	41	58	49	0.75
Classification methods	Logistic	69	84	78	0.34
	Lasso	65	90	80	0.31
	Decision Tree	81	90	85	0.35
	Discriminant	69	88	79	0.36
	k-nearest	56	91	63	0.4
	Naïve Bayes	77	76	76	0.38
	Random forest	94	75	80	0.33
	Support vector machine	86	74	78	0.4

As mentioned earlier, classification techniques other than logistic and lasso classification do not result in an explicit formulation. Thus, the logistic and lasso models are still preferred, considering their comparable performance to other classification techniques. In addition, as the lasso model shows better accuracy than the logistic model in terms of MAE and P_{CD} , the model based on lasso classification is suggested to be used for the failure mode prediction.

2.3. Case study

Corrosion of steel reinforcement is one of the main deterioration mechanisms in RC structure performance, as it changes the material properties and weakens the bonding between rebar and concrete. Such deterioration can lead to insufficient rebar development length and, thus, can alter the performance and failure mode of the structure (Almusallam et al., 1996; A. Castel et al., 2000; Champiri et al., 2012; Jesus Rodriguez et al., 1994). Since the investigation has shown that corrosion of rebar may change the bond failure mode as shown in the developed probabilistic models, it is worth attempting to evaluate the impact of corrosion on the structural performance.

In the literature, four-point testing is typically adopted by researchers to study rebar-concrete bond behavior. In this study, an RC beam with a lap splice studied by Abdel-Kareem et al. (Abdel-Kareem, 2014) is adopted to investigate how corrosion might impact the reliability of the beam flexural performance under a four-point loading through its impact on the bond failure mode. The geometry and reinforcement detailing of this beam are shown in [Figure 2.11](#). The support-to-support length of the beam is 3000 mm. Transverse stirrups with 100 mm spacing and a diameter of 8 mm are provided along the beam to avoid shear failure. As shown in [Figure 2.11](#), the lap-spliced rebar is distributed along with the constant moment region. The lap splice l_s is calculated using ACI 318 (ACI Committee 318, 2014), resulting in $l_s = 542$ mm. The related equations for calculating l_s are provided in Appendix C. In addition, the concrete compressive strength, f'_c , is assumed to be 40 MPa.

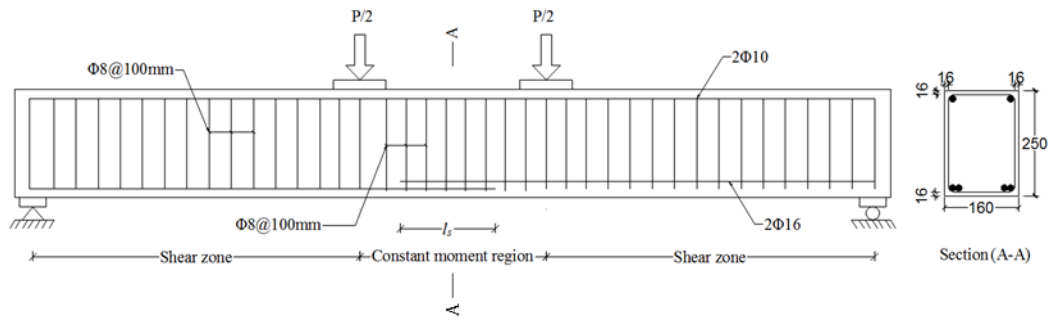


Figure 2.11 Cross-section and longitudinal detailing of the beam (dimensions are in mm) (Abdel-Kareem, 2014).

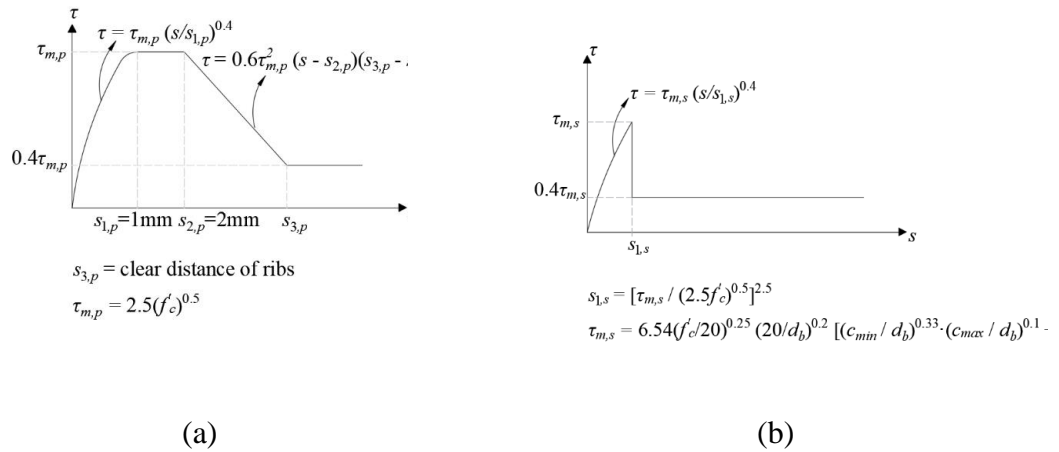


Figure 2.12 Adopted bond-slip curve based on CEB for (a) pull-out failure mode and (b) splitting failure mode (fib, 2013).

In order to incorporate the stress-slip bond behavior, the nonlinear load-deflection behavior of the RC beams is obtained through an analytical procedure proposed by Sajedi and Huang (Sajedi & Huang, 2017). This analytical procedure can be applied to lap-spliced beams or beams without lap splice, taking into account the effects of corrosion on the diameter of the reinforcements, the yield strength of bars, and the stress-slip bond behavior at the rebar-concrete interface. This procedure utilizes the extension of steel reinforcement between flexural cracks that considers the bond-slip behavior at the rebar-concrete

interface to estimate the nonlinear force-displacement of RC beams. The detailed information about this procedure is summarized in Appendix D. Next, the analytical procedure is embedded in the first-order reliability analysis (FORM) to obtain the probability of failure.

The bond behavior under pull-out or splitting failure used in the analytical procedure is based upon the stress-slip curve in the CEB code (fib, 2013), where bond stress, τ , between rebar and concrete is determined as a function of relative slippage, s , as illustrated in Figure 2.12, where τ_m is the maximum bond stress (i.e., bond strength) and s_1 is the slippage when $\tau = \tau_m$. It is worth to note that the prediction performance of the CEB criteria for bond failure mode is not very good at all as shown in Table 2.9, but the CEB bond stress-slip model formula has been widely accepted and validated by many previous literature ((Bamonte & Gambarova, 2007; Coronelli & Gambarova, 2004; H Lin et al., 2017; K. Lundgren, 2005; Nakamura et al., 2006; Z. Wu et al., 2014; Y. Zhang et al., 2020)), and this stress-slip formula shown in Figure 2.12 is consequently adopted in this research.

To consider the effect of corrosion, the bond strength is calculated using a model previously developed by Sajedi and Huang (Sajedi & Huang, 2015), as shown in Equation (D.2) in Appendix D. Since Equation (D.2) is developed based on the specimens that failed in splitting failure modes, it can be used for assessing bond strength under splitting failure, $\tau_{m,s}$, not for bond strength under pull-out failure, $\tau_{m,p}$. By utilizing the ratio of the bond strength for pull-out failure (i.e., $8.0(f'_c/20)^{0.25}$) to the bond strength for splitting failure

(i.e., $2.5f_c^{0.5}$) as suggested by CEB (fib, 2013), $\eta = 8.0(f_c/20)^{0.25}/(2.5f_c^{0.5})$, one can set $\tau_{m,p} = \eta \cdot \tau_{m,s}$.

2.3.1. Flexural behavior

Four levels of corrosion are studied and compared: 0% (intact beam), 5%, 10%, and 15%. First, the flexural behaviors for the intact and corroded RC beams under four-point loading are compared through deterministic analyses that consider the bond pull-out behavior and splitting behavior separately. Three criteria are used to stop the analysis as a flexural failure: the first criterion is when the ultimate bond stress, τ_u , becomes larger than the bond strength, τ_m ($\tau_u > \tau_m$); the second criterion is when the concrete reaches its allowable strain (i.e., $\epsilon_{concrete} > 0.0038$), at which point the concrete is considered to fail by crushing; and the third criterion is when the rebar stress reaches its ultimate tensile strength ($f_s > f_u$). Notice that the third failure criterion never occurred in the case study. Also, note that these failure scenarios (e.g., bond failure and concrete crushing) could occur before or after rebar yielding, and rebar yielding itself does not indicate a beam failure in this study.

Figure 2.13 shows the force-displacement curves for the RC beams and Table 2.8 summarizes the characteristics of the flexural behavior: modulus before yielding (E), yielding force (F_y), yielding displacement (Δ_y), rupture force (F_u), ultimate displacement (Δ_u), ductility (Δ_u/Δ_y), and hardening ratio (F_u/F_y). The results from both Figure 2.13 and Table 2.8 show that the structure performs differently when bond behaviors are in pull-out mode or splitting mode. Such a difference becomes more apparent when the corrosion level is increased.

Table 2.8. Beam flexural behavior comparison for different scenarios.

Corrosion level, Q	Bond behavior	E	F_y	Δ_y	F_u	Δ_u	$\mu = \Delta_u/\Delta_y$	F_u/F_y
Intact beam	Pull-out	5.3	71	13.2	92	46.9	3.5	1.3
	Splitting	4.4	71	15.1	92	60.8	4.0	1.3
$Q = 5\%$	Pull-out	4.9	67	13.5	88	49.1	3.6	1.3
	Splitting	3.8	67	17.6	73	25.7	1.5	1.1
$Q = 10\%$	Pull-out	4.6	64	13.7	84	51.1	3.7	1.3
	Splitting	3.6	-	17.4	64	-	< 1	-
$Q = 15\%$	Pull-out	5	60	13.4	81	55.5	4.1	1.35
	Splitting	3.78	-	17.7	60	-	< 1	-

Table 2.9. Probability information of the basic random variables.

Type	Random variable	Distribution (Mean [*] , std.)	Importance measure ($Q = 5\%$, $D = 60$ kN)	
			Pull-out	Splitting
Geometrical	d_b (mm)	Normal (16, 0.32) (Lu et al., 1994)	0.078	0.031
	h (mm)	Normal (250, 2.5) (Lu et al., 1994)	-0.061	0.078
	b (mm)	Normal (160, 0.32) (Lu et al., 1994)	0	0
	C_x (mm)	Normal (16, 1.92) (Sajedi et al., 2017)	0	0
	C_t (mm)	Normal (16, 1.92) (Sajedi et al., 2017)	0	0
	C_b (mm)	Normal (16, 1.92) (Sajedi et al., 2017)	0	0
	d_{st} (mm)	Normal (8, 0.16) (Lu et al., 1994)	0	0
Mechanical	f_y (MPa)	Normal (440, 22) (Sajedi et al., 2017)	0.121	0.156
	f_c (MPa)	Normal (40, 7.2) (Sajedi et al., 2017)	-0.729	-0.470
	$f_{y,st}$ (MPa)	Normal (280, 14) (Sajedi et al., 2017)	0	0
Model error	$\sigma\epsilon$	Normal (0, 0.169) (Sajedi et al., 2017)	-0.668	-0.861

For the beams with the same level of Q except for $Q = 15\%$, F_y is about the same regardless of the bond behavior. A beam with pull-out bond behavior will have a higher modulus, a higher ductility, and a higher hardening ratio as shown in [Table 2.8](#). As expected, the performance of the beam with pull-out bond behavior is more desirable. In the flexural curves shown in [Figure 2.13](#), the stiffness of the beam initially changes when the load reaches around 11 kN, and this change at the beginning of the curve is due to the

creation of initial cracks in the concrete considered in the analytical formulation. Furthermore, when the beam is under pull-out bond behavior, the flexural failure ends with concrete crushing; however, when the beam is under splitting bond behavior, the beam fails in bond except for the intact case. More importantly, for the beams with corrosion levels of 10% and 15% under splitting bond behavior, the bond failure occurs prior to yielding, which is a brittle failure, not a desirable type of failure.

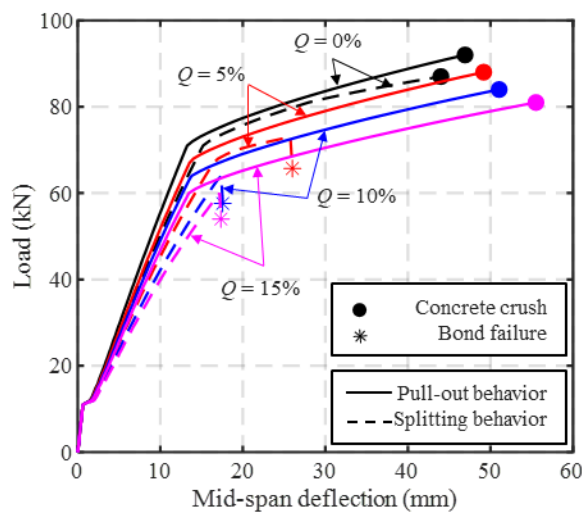


Figure 2.13 Comparison of pull-out and splitting failure for different levels of corrosion.

To avoid such brittle failure, one could increase the splice length as the value suggested by ACI 318 does not appear to be sufficient when corrosion is present (Sajedi et al., 2017) or design the beam so that the bond will exhibit in a pull-out behavior. To ensure pull-out bond behavior, one could utilize the proposed model shown in Equation (2.15) that is determined by four variables f'_c , c/d , Q , and MC . In particular, one could determine the values of the two design parameters, f'_c , and c/d , in order to ensure the desired probability level of achieving pull-out bond, with the consideration of the corrosion and loading scenarios that could happen in the service life.

2.3.2. Reliability analysis

To evaluate the reliability of the beam flexural performance, the probability of failure is calculated as:

$$P_f = P\left(\bigcup_k g_k \leq 0\right) \quad (2.16)$$

where g_k is the limit-state function corresponding to the failure mode k and the subscript k denotes the failure mode of the beam (1 for bond being pull-out and 2 for bond being splitting). The limit state function is defined by:

$$g_k = C_k(\mathbf{x}_r) - D \quad (2.17)$$

where $C_k(\cdot)$ refers to the capacity of the beam; \mathbf{x}_r is a random variable vector that includes all basic random variables such as material properties and geometric dimensions, and D is the force demand applied to the structure. Since bond behavior being pull-out or splitting are two mutually exclusive events, [Equation \(2.16\)](#) can be written as:

$$\begin{aligned} P_f &= P\left[\left(C_1(\mathbf{x}_r) - D \leq 0 \mid Y = 1\right)\right] \cdot P(Y = 1) \\ &+ P\left[\left(C_2(\mathbf{x}_r) - D \leq 0 \mid Y = 0\right)\right] \cdot P(Y = 0) \end{aligned} \quad (2.18)$$

where $P(Y = 1)$ and $P(Y = 0) = 1 - P(Y = 1)$ refer to the probability of the bond being a pull-out behavior or a splitting behavior, respectively, which can be calculated based on the developed model shown in [Equation \(2.6\)](#) and [Equation \(2.14\)](#). The capacity $C(\mathbf{x}_r)$, which is the maximum force the beam can resist before flexural failure is obtained from the analytical procedure in [Appendix D](#). Note that when the failure occurs, it does not

necessarily indicate bond failure. In practice, the reliability index, β , is typically used as the performance measure, and its relationship with P_f is as follows:

$$P_f = \Phi(-\beta) \quad (2.19)$$

The basic random variables, \mathbf{x}_r , are adopted based on the literature (Lu et al., 1994; Sajedi et al., 2017) and their probability information is provided in [Table 2.9](#). Note that the model error, σ_ε , in [Table 2.9](#) refers to the model error in the bond strength model adopted from the literature (Sajedi & Huang, 2015) that is elaborated in [Appendix D](#).

The contribution of each random variable to the variability of the limit state function ([Equation \(2.17\)](#)) is also investigated based on the important measures of the random variables when considering 5% corrosion and a demand of 60 kN, and the results are shown in [Table 2.9](#). A larger absolute value of importance measure indicates a greater contribution of the corresponding random variable on the variability of the limit state function. The detailed information of importance measures in reliability analysis can be found in related literature (Huang et al., 2015). [Table 2.9](#) shows that for both cases (bond behaves in splitting and in pull-out), three variables, model error in bond strength, f_y , and f'_c (namely bond, concrete, and steel properties) dominates the contribution to the variability of the limit state function.

[Figure 2.14](#) shows the fragility curves conditioned on demand values with corrosion levels of 0% (intact beam), 5%, 10%, and 15%. For a given level of corrosion, the fragility curves show the differences in the structural performance due to different bond behaves in pull-out, splitting, or unknown (that is determined by the developed bond failure prediction model), and these differences become more apparent with the increase in corrosion.

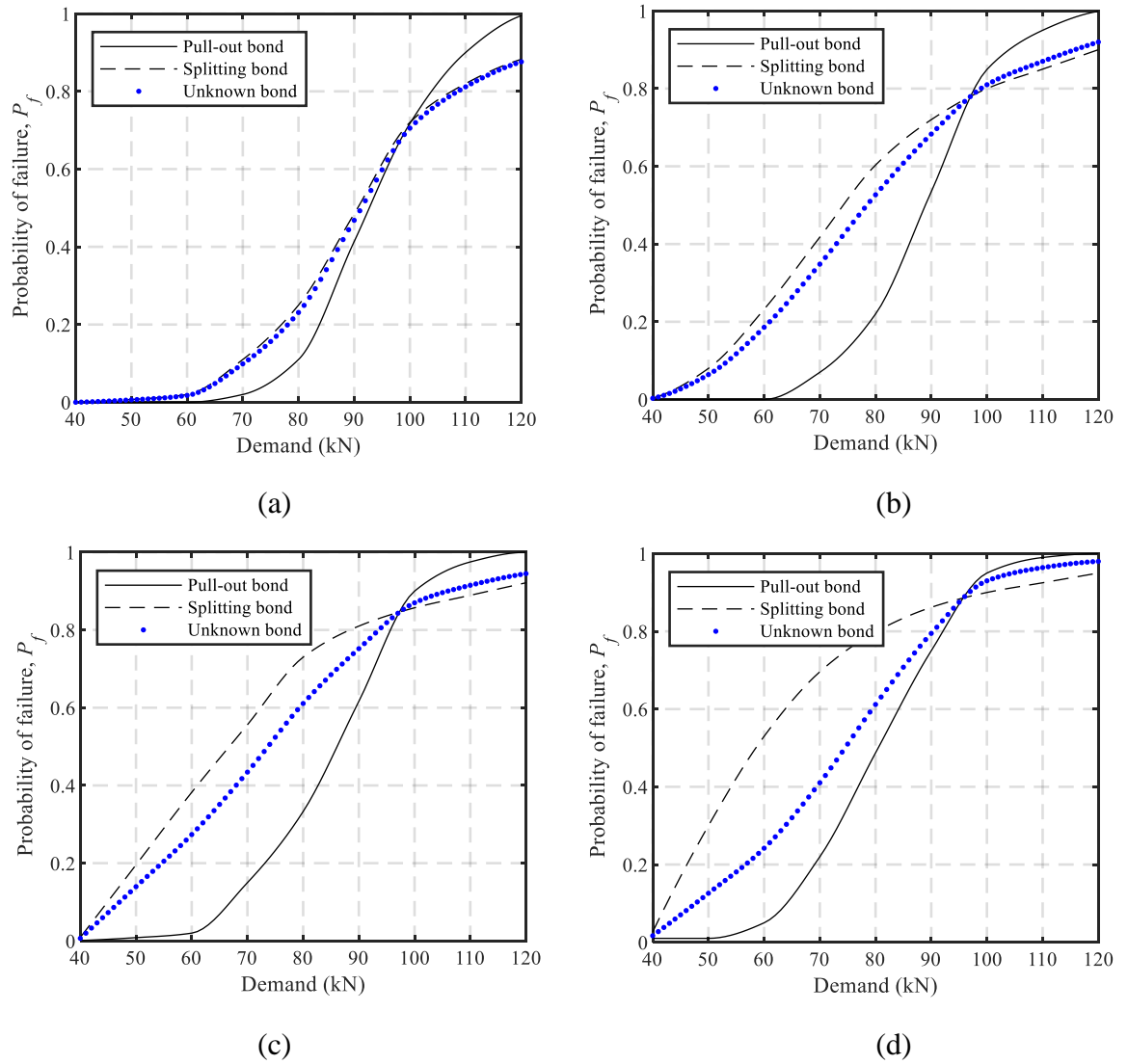


Figure 2.14 Fragility curves under different corrosion levels: (a) $Q = 0\%$ (intact beam), (b) $Q = 5\%$, (c) $Q = 10\%$, and (d) $Q = 15\%$.

For the bond failure modes at each considered probability, the fragility curve for unknown bond failure mode (shown as a dotted line) is between the fragility curves for the bond in pull-out behavior (shown as a solid line) and the bond in splitting behavior (shown as a dashed line), as expected. In particular, the fragility curve with the unknown bond is closer to the curve for splitting bond behavior when the corrosion level Q is low, but it

moves closer to the curve with pull-out bond behavior when Q increases. This is understandable, as the probability of being pull-out increases with the level of corrosion (as shown in [Figure 2.14](#)).

While compares the four plots in [Figure 2.14](#), the fragility curves with a given bond behavior shift to the left as Q increases. This shows the corrosion increases the probability of failure as expected. In particular, the fragility curves for splitting bond behavior are more distant from each other with the increase of Q . For example, at the lowest level of corrosion ($Q = 5\%$) shown in [Figure 2.14 \(b\)](#), the fragility curve for splitting failure is significantly distant from the curve for the intact beam shown in [Figure 2.14 \(a\)](#). However, the fragility curves for pull-out bond behavior do not change dramatically with the change of Q . This indicates that corrosion has more impact on the performance of a structure with a splitting bond than the structure with a pull-out bond. It can also be seen that with the increase of the corrosion level, the fragility curves became steeper, indicating that the probability of failure becomes more sensitive to demand with more corrosion.

[Figure 2.15 \(a\)](#) and [\(b\)](#) show the reliability index curves with respect to the level of corrosion Q by setting the demand D as a deterministic value of 60 kN and as a random variable with mean $\mu_D = 60$ kN and $COV = 0.15$, respectively. The purpose of [Figure 2.15](#) is to examine how the bond behavior impacts the structural performance with a progressing deterioration; thus, the demand used in [Figure 2.15](#) can be arbitrary. Moreover, the reliability index curve with the unknown bond failure mode is between the other two curves. The reliability index curve with splitting bond behavior is much lower than the one with pull-out bond behavior, and its rate of decrease is much greater. From $Q = 0\%$ to $Q =$

5%, β decreases from 3.3 to 1.8 in Figure 2.15 (a) and decreases from 3.1 to 2.1 in Figure 2.15 (b). Consistent with the previous observations in Figures. 2.13 and 2.14, the result from both Figure 2.15 (a) and (b) indicates that the bond behavior plays a critical role in the time-dependent performance evolution, particularly when the specimen is exposed to a high level of corrosion. In addition, the prediction of the bond failure behavior is important, as it determines the actual structural performance.

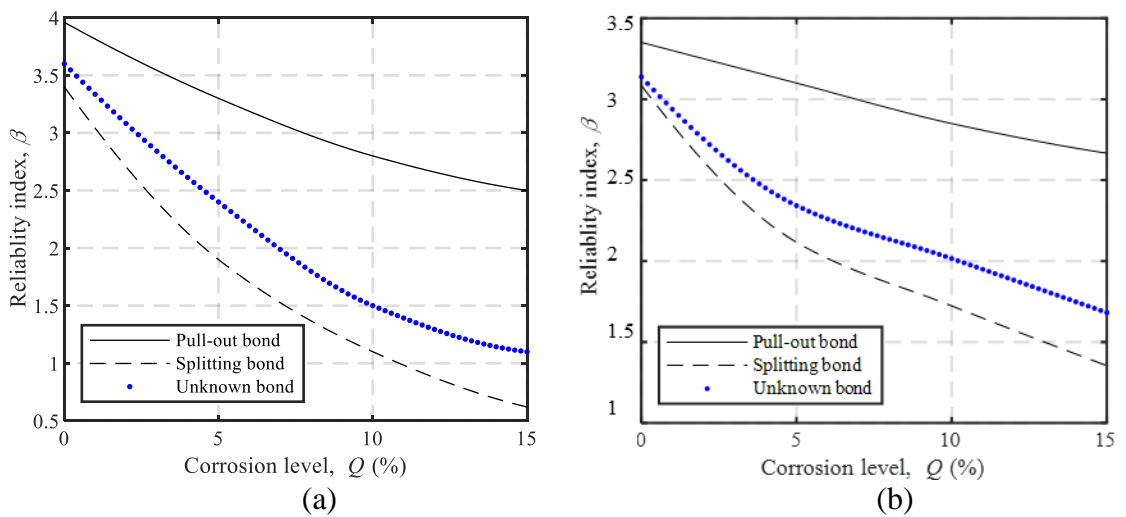


Figure 2.15 Reliability index curves under various corrosion levels conditioned on different bond behaviors under (a) $D = 60$ kN and (b) $\mu_D = 60$ kN and $COV = 0.15$

CHAPTER III

PROBABILISTIC MODELING OF RC BOND BEHAVIOR CONSIDERING FAILURE MODE AND CORROSION

Bond behavior between the rebar and concrete plays a critical role in the structural performance of reinforced concrete (RC) structures in terms of load-carrying capacity, ductility, and failure mode. Previous researchers have shown that the bond at the rebar-concrete interface is influenced by many factors such as concrete cover, rebar size, transverse reinforcement, concrete properties, rebar geometry, loading type, etc. (e.g., Alsiwat & Saatcioglu, 1992; Dolati & Mehrabi, 2021a; Harajli, 2009; Harajli et al., 2004; Murcia-Delso et al., 2013; Rahai & Abasi, 2018; Sabzi et al., 2020; Taslimi & Tehranizadeh, 2021). Moreover, such bond can be adversely affected by corrosion on the rebar, a leading deterioration mechanism for RC structures. The corrosion that initiates at the interface of the rebar and concrete not only deteriorates the material property of rebar and concrete and reduces the rebar diameter, but also generates corrosion products (i.e., rust) that cause a volumetric expansion around the rebar (Balafas & Burgoyne, 2011), resulting in cracking in concrete and weaken the bond between rebar and concrete.

When there is sufficient concrete to prevent splitting and restrain crack growth in concrete, bond fails in shearing of the concrete between ribs, corresponding to a failure mode called pull-out failure; when there is insufficient confinement, the deformation-bearing forces cause splitting cracks that spread through the sides of the RC member and

make the concrete to lose its bonding and cover, corresponding to a bond failure mode called splitting failure (ACI, 2012). The bond behavior is typically described using a bond stress-slip relationship. Figure 1 shows three bond stress-slip curves for different confinement levels (Hongwei Lin, Zhao, Ožbolt, & Hans-Wolf, 2017). As shown in Figure 1, more confinement leads to a more ductile behavior and the bond fails in pull-out, while less confinement makes the curve descending part drop at a much faster rate (a brittle fashion) and the bond fails in a splitting. In other words, the bond behaves differently for each bond failure mode (Tarfan et al., 2019).

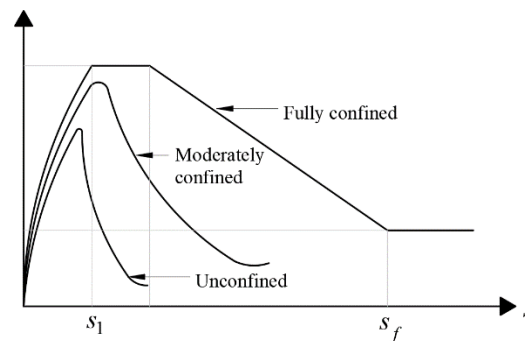


Figure 3.1 Bond failure mode stress-slip curves for different levels of confinement (Hongwei Lin, Zhao, Ožbolt, & Hans-Wolf, 2017)

Meanwhile, CEB (2013) provides two widely used models to describe the bond-slip relationship for the two bond failure modes (i.e., pull-out and splitting failure modes), where bond stress, τ , is modeled as a function of relative slippage, s , as shown in [Figure 3.2](#). In particular, bond strength, τ_{\max} , (referring to the maximum stress that can be transferred through the rebar to concrete) and peak slip, s_1 , (referring to the slip corresponding to bond strength) are the two most determinative quantities in defining the ascending branch of the bond-slip curve, since reaching the bond strength represents the outset of the bond failure. However, no corrosion impact is considered in the CEB models.

Therefore, these two quantities τ_{max} and s_1 need to be re-evaluated considering corrosion for each bond failure mode.

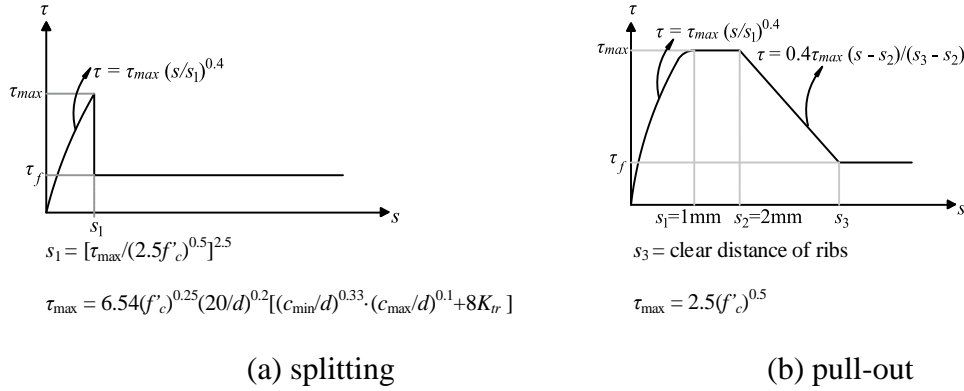


Figure 3.2 Bond-slip model based on CEB (2013)

The experimental testing to study bond is typically conducted through pull-out test (e.g., Kivell et al., 2011), beam-end test (e.g., Darwin & Graham, 1993), and beam tests (e.g., M. Harajli et al., 2002) in laboratories. To study how rebar deterioration impacts bond behavior, accelerated corrosion is the typical practice to introduce the corrosion on rebar (Alsiwat & Saatcioglu, 1992; Lin et al., 2019). Using the experimental data, prediction models for bond behavior can be developed. Based on the literature review of the past studies on bond strength and peak split that is discussed in Section 2, there is a lack of well-accepted prediction models for these two critical quantities considering bond failure mode and corrosion effect. In particular, the bond strength in pull-out has not been studied well previously. The goal of this study is to address this need. The proposed models are developed based on a comprehensive bond dataset collected from bond tests on the beam and beam-end specimens in the literature, and a criterion to specify the bond failure mode is also proposed. Then, probabilistic models to predict the bond strength under pull-out

and splitting are developed based on multivariate nonlinear regression analysis with all-possible subset model selection. These two models, without adopting any reduction factor, can predict either intact or corroded bond strength by treating corrosion level as a continuous parameter. Next, probabilistic models for the peak slip prediction are developed based on a genetic programming algorithm, due to the lack of pre-existing knowledge about the correlation between the peak slip and potential influencing factors. Lastly, the developed probabilistic models for bond strength and peak slip are compared with the existing prediction models and then implemented in structural analysis to evaluate the flexural behavior of RC beams.

3.1. Background

3.1.1. Bond Strength

Note that the maximum bond strength τ_{\max} cannot be measured directly from testing; instead, the average bond strength τ_{avg} is usually calculated based on the maximum applied force divided by the concrete-rebar interface area. Given a distribution of the bond stress along with the rebar, one can calculate τ_{\max} using τ_{avg} . Some discussion on the distribution of bond stress can be found in the literature (Main, 1951; Thompson, 1966; Somayaji & Shah, 1981; Jiang et al., 1984). According to the suggestion by Thompson (1966), one could assume $\tau_{\max} = 1.5 \tau_{\text{avg}}$.

In the past, researchers have examined the quantitative impact of various influential factors on τ_{avg} (Almusallam et al., 1996; Castel et al., 2016; Dolati & Mehrabi, 2021b;

Harajli et al., 2004; Kivell et al., 2015; Murcia-Delso et al., 2013; Murcia-Delso & Benson Shing, 2015; Shekarchi et al., 2019; Torre-Casanova et al., 2013; Wang, 2009). For example, Harajli et al. (2004) recognized that the amount of transverse rebar influences the ductility of bond behavior in non-corroded structures and bond strength. Wang (2009) found that the concrete cover to the main rebar diameter ratio contributes significantly to the bond strength when no confinement reinforcement is provided. Torre-Casanova et al. (2013) and Castel et al. (2016) developed a numerical model to incorporate the effects of stirrups confinement on rebar-concrete bond strength. In addition, studies also showed that the bond strength is a function of tensile strength or compressive concrete strength (Arnaud Castel et al., 2016; A. Soraghi et al., 2019; Torre-Casanova et al., 2013). Furthermore, many studies found corrosion on the rebar has a significant impact on the bond strength and consequently on the RC structure performance (Wang, 2009; Kivell et al., 2015; Sajedi & Huang, 2015).

For bond strength prediction, the previous models can be categorized into two groups: empirical-based models that is developed using experimental data and mechanism-based models. The mechanism-based approach is usually complicated and computationally intensive (Abasi et al., 2020). As an example, the corrosion effect modeling developed by Choi and Lee (2002) requires the value of confining pressure on the rebar due to corrosion, and finite element analyses are needed to determine such confining pressure. In addition, many of the numerical models require experimental data to obtain and/or update the model parameters (Abasi et al., 2021; Vu et al., 2016). On the other hand, empirical-based models (such as regression models), extract information directly from data and usually can be

easily implemented in practice and also in various probabilistic analyses (Amini et al., 2021a, 2021b; Zamanian et al., 2020). However, the validation of such empirical models heavily depends on the ranges of variables in the training dataset for the model development; they cannot be directly applied when the variables are beyond the ranges in the training dataset.

To account for the corrosion effect in the prediction, many past studies adopted empirical reduction factors over the bond strength of intact rebar, and the reduction factors were usually evaluated using a regression analysis with the experimental bond data of corroded specimens (Rodriguez et al., 1994; Maaddawy & Topper, 2005; Bhargava et al., 2007; Kivell et al., 2015). However, this approach requires that the bond strength for the intact rebar must be first predicted. This means that there are two model errors involved in the prediction of bond strength of a corroded case, one model error is from the reduction factor model, and the other one is from the bond strength model for the corresponding intact case. To overcome such limitations, some researchers attempted to develop more comprehensive models that incorporate all structural parameters. For example, Prieto et al. (2016) developed an empirical model using multiple linear regression analyses that considers corroded and uncorroded specimens as one corrosion level parameter along with other important structural parameters. Similarly, Sajedi and Huang (2015) developed an empirical probabilistic model using multivariate nonlinear regression, which can directly predict bond strength given a corrosion level including the intact case. However, as the bond data used in the model development in Sajedi and Huang's study are all identified as

splitting bond failure, their model will not be suitable for predicting bond strength in pull-out. In addition, bond strength in the pull-out has not been studied well previously.

3.1.2. Peak slip

For peak slip prediction, while Murcia-Delso (2013) suggested that the estimation of s_1 is better to be achieved by experimental testing, a practical solution is to use empirical formulas. [Table 3.1](#) summarizes the findings of the literature for the prediction of peak slip s_1 under splitting or pull-out. The first two studies (Feng et al., 2016; Kivell et al., 2015) proposed s_1 to be a constant for either splitting or pull-out, suggesting that s_1 is independent of other structural properties and corrosion; while other studies found that s_1 is impacted by various parameters such as concrete strength, cover size, transverse confinement, and rib pattern. However, the findings from those studies are not consistent.

Table 3.1. Summary of existing studies for peak slip, s_1 .

Bond failure mode	Reference	Influencing parameter	Formulation of s_1
Either splitting or pull-out	Kivell et al. (2015)	-	$s_1(Q) = 0.3 \text{ mm}$
	Feng et al. (2016)	-	$s_1(Q) = 0.175 \text{ mm}$
Splitting	Guizani and Chaallal (2011)	Transverse confinement	s_1 is proportionate transverse reinforcement confinement,
	Xu (1990)	d	$s_1 = 0.0368d$
	Khalaf and Huang (2016)	c/d	$s_1 = 0.5 + 0.1c/d$ (for $1.0 < c/d < 5.0$)
	Coccia et al. (2015)	c, d	$s_1 = 0.0035(c - 0.2d)$
	CEB (2013)	$f'_c, \tau_{\max, \text{splitting}}$	$s_1 = \left(\frac{\tau_{\max, \text{splitting}}}{2.5(f'_c)^{0.5}} \right)^{2.5}$
	Wu and Zhao (2013)	Transverse confinement quantity, $K(c/d, A_{st}, n_d, d, s_{st})$	$s_1 = (0.7315 + K)/(5.176 + 0.33K)$, $K = c/d + 33 \left(\frac{A_{st}}{n_d \cdot d \cdot s_{st}} \right)$
	Lin et al. (2017, 2019)	s_r, Q , a transverse confinement quantity, $K'(c/d, c, A_{st}, s_{st})$	$s_1(Q=0) = 0.12s_r / (1 + 85.8 \exp(-1.4K'))$, $K' = c/d + 82.7 \left(\frac{A_{st}}{c \cdot s_{st}} \right)$ $s_1(Q) = [(5.89Q + 0.12)] / [(216.84Q + 1)(1 + 85.8 \exp(-1.4K'))]$
	Harajli et al. (2004)	$(\tau_{\max, \text{splitting}} / \tau_{\max, \text{pull-out}})$	$s_1 = \exp \left(3.3 \ln \left(\frac{\tau_{\max, \text{splitting}}}{\tau_{\max, \text{pull-out}}} \right) \right) s_{1, \text{pull-out}} + s_0 \ln \left(\frac{\tau_{\max, \text{pull-out}}}{\tau_{\max, \text{splitting}}} \right)$ $s_0 = 0.15 \text{ mm}$ for unconfined concrete, $s_0 = 0.4 \text{ mm}$ for confined concrete with stirrups
	CEB (2013)	-	$s_1 = 1.0 \text{ mm}$
	Pull-out	Alsawat et al. (1992)	f'_c
Harajli et al. (2004) and Lin et al. (2019)		s_r	$s_1 = 0.2s_r$
Murcia-Delso et al. (2013)		d	$s_1 = 0.07d$ (for $36 \text{ mm} < d < 57 \text{ mm}$)
Zhao and Zhu (2018)		d, s_r	$s_1 = 0.07442d - 0.00093d^2 \approx 0.1s_r$

f'_c : concrete compressive strength
 s_r : rib spacing
 d : main rebar diameter
 c : cover size
 n_d : number of the main bar
 s_{st} : stirrups spacing
 Q : corrosion level

For s_1 under splitting bond failure mode, the findings from various studies are quite different. While CEB (2013) indicated that s_1 depends on f'_c and τ_{\max} , some studies found that s_1 is a linear function of c , d , or c/d (e.g., Coccia et al., 2015; Khalaf & Huang, 2016); some studies suggested that structural properties (such as s_r and transverse confinement) should be included in the prediction (e.g., Guizani & Chaallal, 2011; Wu & Zhao, 2013). Harajli et al. (2004) on the other hand used the ratio of $\tau_{\max, \text{pull-out}}/\tau_{\max, \text{splitting}}$, and the peak slip in the pull-out to obtain the peak slip in splitting.

For s_1 under pull-out failure mode, while CEB (2013) suggests a constant value for s_1 , Alsiwat and Saatcioglu (1992) found that s_1 is only influenced by f'_c . Other four studies (Harajli et al., 2004; Lin et al., 2019; Murcia-Delso et al., 2013; Zhao & Zhu, 2018) all showed that s_1 depends on rib spacing (s_r) or rebar diameter (d) or both.

Quantifying the impact of structural properties on s_1 is not an easy task. For example, Wu and Zhao (2013) adopted a mathematical differential equation for the peak slip in an exponential form considering the combination confinement from cover and transverse stirrups through a trial and error process and then attempted to solve and determine the necessary coefficients through a regression analysis based on experimental data. A similar approach is adopted by Lin et al. (2019); but in Lin et al.'s study, the total confinement quantity is accounted using an exponential function form, which allows the bond failure mode to have a smooth transition from splitting to pull-out.

Lastly, as shown in [Table 3.1](#), very few researchers studied the impact of corrosion level on s_1 . Amongst the three studies shown in [Table 3.1](#), Kivell et al. (2015) and Feng et al. (2016) concluded that there is no apparent corrosion impact on peak slip, while Lin et

al. (2017, 2019) developed an empirical relation of corrosion level Q and s_1 based on a limited dataset.

3.1.3. Failure mode identification

When collecting the experimental data from the literature, one needs to identify if the bond data failed in pull-out or splitting. However, determining the bond failure mode on the experimental specimens can be challenging.

As splitting bond failure is mostly due to the longitudinal splitting of the surrounding concrete of the main bar (Tang, 2007), many previous studies used the formation of the longitudinal cracking along the main rebar to determine the bond failure mode (e.g., Law & Molyneaux, 2017; Lin et al., 2017, 2019). For example, Lin et al. (2017) identified all 16 beam-end specimens failed in splitting as they observed the splitting of concrete along with the rebar in the anchorage zone on the top longitudinal side of the specimens (shown in [Figure 3.3 \(a\)](#)). In the study by Tang (2007) where the main bar was placed at the corners of the beam-end specimen as shown in [Figure 3.3 \(b\)](#), the formation of the longitudinal cracking on the lateral corner side of the specimen was used to determine the bond failure mode. Hanjari et al. (2011) also determined the bond failure mode based on the observed cracking patterns but on the lateral side of the specimens: [Figure 3.4 \(a\)](#) shows the pull-out failure where the cracks start along with the rebar and became parallel to the inclined side of the beam-end specimen, and [Figure 3.4 \(b\)](#) shows the splitting failure where the cracks are parallel to the rebar.

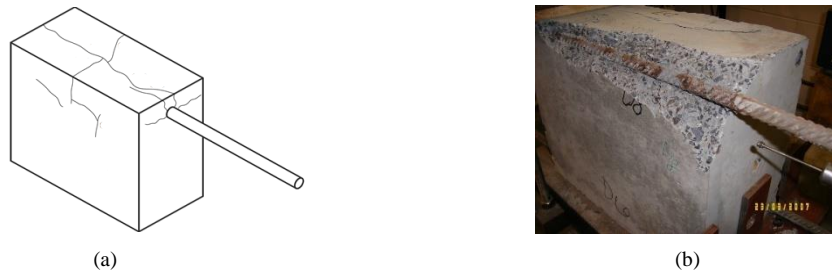


Figure 3.3 Longitudinal cracking observed by (a) Lin et al. (2017) and (b) Tang (2007).



Figure 3.4 Different failure modes observed by Hanjari et al. (2011): (a) pull-out failure, (b) splitting failure

However, Darwin and Graham (1993) detected splitting bond failure in all their studied specimens with large cover sizes or transverse stirrups without always observing longitudinal cracking: Figure 3.5 (a) shows a specimen without showing longitudinal cracking on the top side of the specimen, while Figure 3.5 (b) shows a specimen with severe longitudinal cracking.

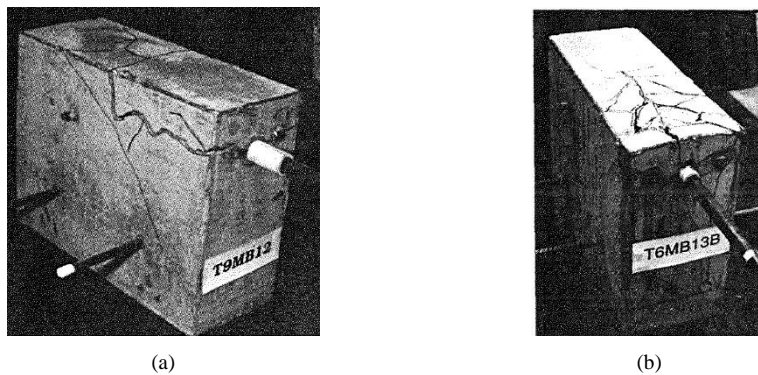


Figure 3.5 Specimens fail in splitting (a) without longitudinal crack and (b) with longitudinal crack (Darwin & Graham, 1993)

Soraghi et al. (2019) identified the cracking patterns on the perpendicular surface of the test bar in their beam-end specimens for the two failure modes; as shown in Figure 3.6, the specimens with no cracking connected to the test bar failed in pull-out, and specimens with cracking connected to the test bar failed in splitting.

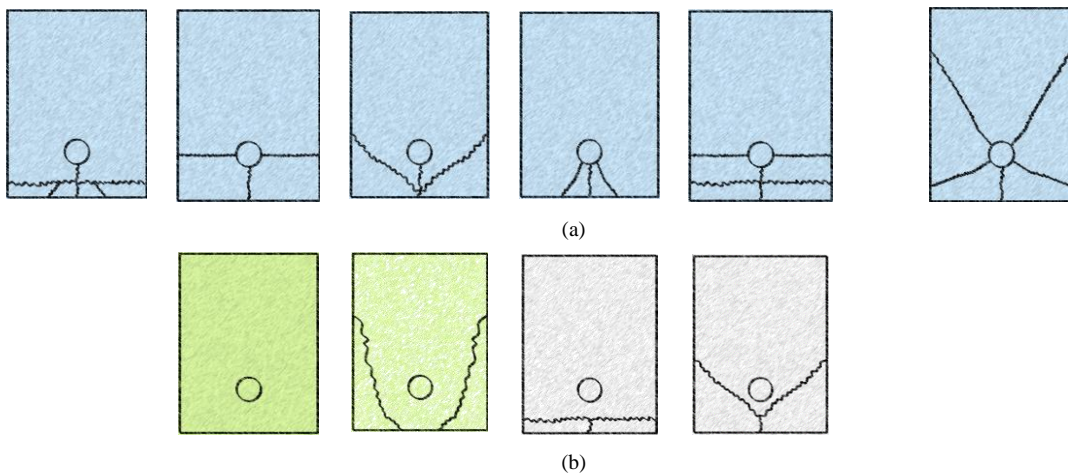


Figure 3.6 Schematic view of crack patterns formed on the test specimens after failure under (a) splitting failure mode and (b) pull-out failure mode (Soraghi et al., 2019)

In summary, previous studies relied mostly on the formation of cracking in order to specify the bond failure mode, however, as is discussed the next Section, bond failure mode should be better determined based on the behavior of the specimen upon failure.

3.2. Experimental Data

In this study, experimental data for corroded and intact rebar where bond fails either in pull-out or splitting are first collected from literature for the model development.

3.2.1. Various types of bond test setups

In the literature, there are three common test setups to study bond behavior: pull-out test, beam-end test, and beam test. The pull-out test is the simplest, and most economical testing for bond study; it is useful to investigate factors that may impact bond. However, it cannot reflect the real stress state in flexural structural components, and the setup produces large resistance to splitting due to the friction stresses at the bearing end. Thus, the results from the pull-out test are not suitable for developing prediction models for bond. Beam tests are ideal, but it needs to overcome the challenges in the beam design such as avoiding failure modes other than bond failure (e.g., shear failure, concrete crushing, and yielding of bars) (Karin Lundgren et al., 2019). In contrast, beam-end tests are much simpler than beam tests and can simulate the stress state in the flexural members. Thus, since the bond behavior obtained from beam and beam-end tests are more realistic and reliable, only beam and beam-end testing data are collected and used for the model development in this study. Note that in this study, all the collected data with corrosion are obtained from experiments where the corrosion are generalized corrosion attained through an accelerated corrosion process.

3.2.2. Proposed criteria for bond failure mode

As discussed in previous Section, there are different criteria to judge bond failure mode and it is necessary to have one consent criterion for consistency. Using a cracking pattern alone to determine the bond failure mode may not be reliable, particularly when the

corrosion-induced cracking is present. Interestingly, both studies by Kivell (2011) and Soraghi et al. (2019) showed that specimens with high corrosion levels tend to exhibit pull-out bond behavior.

Instead of relying on the cracking pattern, one can directly use the ductility observed in the recorded bond stress-slip curve to determine the bond failure mode. In a previous study by the authors (Ahmad Soraghi & Huang, 2021), 132 beam-end specimens with various levels of corrosion were tested to study bond behavior under either monotonic or cyclic loading, and [Figure 3.7](#) shows the typical bond stress-slip curves for the pull-out and splitting bond failure. When comparing the pull-out cases shown in [Figures 3.7 \(a\) and 7\(c\)](#) with the splitting cases shown in [Figures 3.7 \(b\) and \(d\)](#), it is found that splitting bond failure is mostly followed by a sudden jump in the amount of bond stress or slip, and/or the imbalance on the testing machine. The imbalance right after the jump usually occurs, an indication of the brittle failure and a sudden change in the bond. On contrary, the pull-out bond failure is gradual and continuous, and the bond stress-slip is ductile.

It is worthy to note that typically the slip measured by LVDT (Linear Variable Differential Transformer) is recorded through a data acquisition system and the applied force to calculate the bond stress is recorded by an actuator. Consequently, the slip and force are not necessarily recorded simultaneously, and the time difference is in a split second, particularly when the splitting bond failure causes the sudden drop in the actuator force. Therefore, when splitting bond failure occurs, one may observe three different scenarios shown in [Figure 3.7 \(b\)](#): (1) if slip and force are recorded simultaneously, a sudden drop of stress is captured correctly, shown as the vertical solid line; (2) if force

recording is slightly delayed, a straight plateau can be observed, shown as the dashed line; and (3) if slip recording is slightly delayed, an inclined line can be observed, shown as the dotted line. Note that scenarios 2 and 3 could be deceiving, as the stress-slip diagrams seem to have a ductile behavior. Regardless of the three different looks of the stress-slip relationships in Figure 3.7 (b), these three scenarios all suggest that there is a sudden drop in force; thus, they all indicate splitting failure. Therefore, when using the recorded bond stress-slip relationship, attention needs to discern the three scenarios described here. Note that the sudden jump in slip described in scenarios 2 and 3 is also reported in Al-Sulaimani et al. (1990).

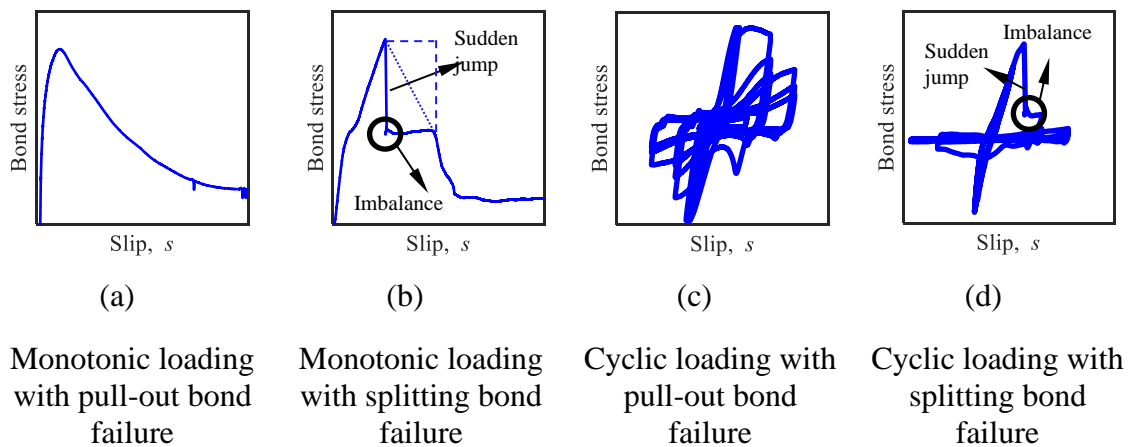
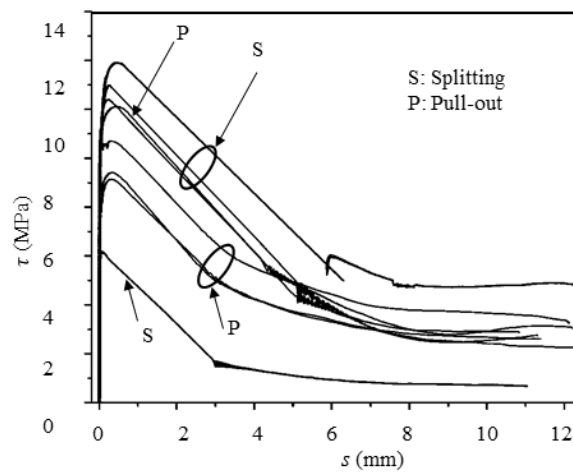


Figure 3.7. Typical bond stress-slip behavior from the study by the authors (Soraghi et al., 2019).

All the testing specimens (a total of 32) in Lin et al. (2019) and additional 9 specimens in Lin et al. (2017) were identified as splitting bond failure based on the observation of longitudinal cracking. However, based on the proposed criteria, while all of the stress-slip curves show the ductile manner (indicating pull-out), some of them are actually splitting bond failure due to a detected imbalance or the sudden jump in slip shown

as a straight line (which is the Scenario 2 described above). Therefore, the failure modes of all the specimens are re-evaluated: among the 32 specimens in (Lin et al., 2019) that were identified as splitting bond failure originally, 19 of them are re-identified as pull-out. [Figure 3.8](#) shows the corrected identification of the failure modes for eight of the specimens. Similarly, all the 9 specimens in Lin et al. (2017) are re-identified as pull-out based on the proposed criteria.



[Figure 3.8](#). Monotonic test results of Lin et al. (2019) with corrected failure mode identification

3.2.3. Data collection

A total of 557 data points is extracted from the literature and the overview of those data is summarized in [Table 3.2](#), in which about 20% fail in pull-out and the other 80% fail in splitting. The complete information of the dataset can be found in (Soaghi 2021). The corrosion degree is measured using percentage rebar mass loss Q ($= \Delta m/m_0$ where Δm refers to mass reduction and m_0 is initial mass), and it is considered as a continuous parameter ($Q \geq 0$). The collected dataset includes the database used by Sajedi & Huang (2015) for

developing a bond strength prediction model considering corrosion. Note that all the testing data report the bond strength, but not all of them report peak slip, as indicated in [Table 3.2](#).

As aforementioned, the size and ranges of the dataset are critical for developing empirical models (Esteghamati et al., 2020). Therefore, it is worth comparing the distribution of the dataset (a total of 240 data) used by Sajedi and Huang (2015) and the newly added dataset collected in this study. Note that since the dataset in Sajedi and Huang (2015) only includes splitting bond failure mode, only the splitting data in the newly added dataset (a total of 226 data) is used for the comparison.

[Figure 3.9](#) compares the histograms of four parameters in these two groups: corrosion level Q , cover to rebar diameter ratio, c/d , concrete compressive strength, f'_c , and transverse confinement index, K_{tr} , which is also defined in [Table 3.4](#). While the newly collected dataset provides similar coverage in terms of f'_c and K_{tr} as the dataset used in Sajedi and Huang, the newly collected dataset provides a good complement for Q and c/d . For example, [Figure 3.9](#) (a) shows that the majority of data in Sajedi and Huang covers $Q < 5\%$ with no coverage of $Q > 15\%$, while newly added covers a wider range of Q . With the combination of the existing and newly added data, the whole dataset provides comprehensive ranges of key parameters for the model development. It is also worthy to note that empirical models are accurate mostly on the range that the models are developed, thus, the range is application is also imposed by the collected dataset. However, since the collected data are from a wide range of parameters, it is expected that the proposed model performs well in most of the cases yet can be easily updated when more data become available.

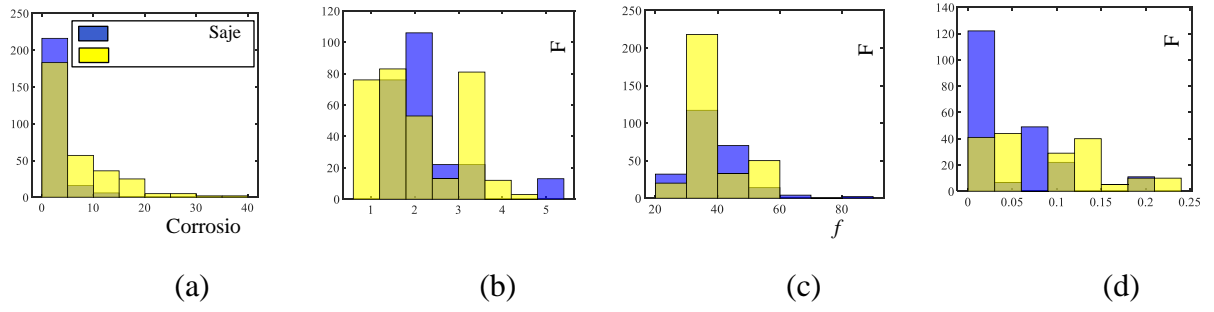


Figure 3.9. Histogram comparison of the existing dataset from Sajedi and Huang (2015) and the newly collected dataset

Table 3.2. Summary of the collected data for model development.

Reference	τ_{avg} in MPa		s_1 in mm		c (mm)	b_c (mm)	d (mm)	R_r^*	f'_c (MPa)	l_d	Q (%)
	(No. of specimens)		(No. of specimens)								
	Pull-out	Splitting	Pull-out	Splitting							
Darwin and Graham (1993)	- (0)	4.8~13.1 (110)	- (0)	- (0)	49.2~82.6	228.6~247.7	25.4	0.05~0.2	31.2~41.3	215.9, 304.4	0
Bilal† (1995)	- (0)	4.3~8.8 (56)	- (0)	- (0)	25.4	228.6	20.6	0.08~0.2	22.4, 43.1	254	0
Al-Sulaimani et al. (1990)	- (0)	5.6~9.3 (22)	- (0)	- (0)	29	150	12	0.1*	40	144~300	0~4.5
Used by Sajedi & Ghoddoussi (1996)	- (0)	6.4~7.5 (11)	- (0)	- (0)	25	75	12	0.1*	47.9~64	190	0~7.8
Huang (2015)	- (0)	3.8~5.4 (12)	- (0)	- (0)	15~40	150	16	0.12	53.6~86.2	130, 208	0~14.2
Almusallam et al. (1996)	- (0)	3.1~18.5 (14)	- (0)	- (0)	63.5	190.5	12	0.1*	30	102	0~15.65
Stanish et al. (1999)	- (0)	2.2~5.1 (8)	- (0)	- (0)	20	112.5	11.3	0.1*	36.4, 42.6	250	0~14.4
Mangat and Elgarf (1999)	- (0)	4~10 (7)	- (0)	0.01~0.36 (7)	19	57	10	0.1*	45	100	0~5
Total	- (0)	2.2~18.5 (240)	- (0)	0.01~0.36 (7)	15~82.6	57~247.7	10~25.4	0.05~0.2	22.4~86.2	100~304.4	0~15.65

	Soraghi and Huang (2021)	2.9~18.7 (48)	3.6~10.8 (84)	0.1~2.5 (48)	0.02~0.7 (84)	24.4~101.6	190.5~304.8	15.87~25.4	0.2~0.5	27~43	88.9~203.2	0~25.8
	Harajli et al. (2004)	- (0)	3.2~9.9 (8)	- (0)	0.03~0.7 (8)	18~50	150	16~32	0.2~0.3**	27.9, 32.9	80~160	0
	Lin et al. (2019a)	- (0)	4.5~9.5 (16)	- (0)	0.1~0.8 (16)	25~70	75~210	20	0.1*	30	150	0
Newly added data	Lin et al. (2019b)	7~13 (19)	- (13)	0.1~0.7 (19)	0.1~0.5 (13)	25, 35	150	20	0.1*	50	200	0~12.89
	Tang (2007)	- (0)	0.4~8.4 (64)	- (0)	- (0)	12~48	108~200	12, 16	0.1*	34~50.5	300	0~30.02
	Lin and Zhao (2016)	- (0)	3.2~9.6 (36)	- (0)	- (0)	40	150	20	0.1*	30	150	0~20.86
	Lin et al. (2017)	12~17.7 (9)	- (0)	0.2~0.9 (9)	- (0)	35	150	20	0.1*	50	100	0~16
	Hanjari et al. (2011)	2.3~8.1 (15)	- (5)	0.04~0.4 (15)	0.02~0.7 (5)	30	135	20	0.1*	30	210	0~16.7
	Total	2.2~18.7 (91)	0.4~10.8 (226)	0.04~2.5 (91)	0.02~0.8 (126)	12~101.6	75~304.8	12~32	0.1~0.5	27~50.5	80~203.2	0~30.02

* The value of R_r is assumed as is not reported in the corresponding reference.

** The value of rib spacing is reported, but not the rib height, thus a rib height of 2 mm is assumed.

3.3. Average bond strength and peak slip model development

In this section, the probabilistic prediction models for average bond strength τ_{avg} and peak slip s_1 are developed for the two bond failure modes with the comprehensive database collected. For τ_{avg} , the multivariate regression approach is used. For s_1 , the genetic programming technique is adopted, as the relationship between s_1 and the influential factors is not well studied.

To better understand how much accuracy a prediction model should have, first, one could examine the impact of the variations of τ_{avg} and s_1 on the flexural behavior of an RC beam. In this study, the analytical procedure proposed by Sajedi and Huang (2017) is used to incorporate the stress–slip bond behavior (using maximum and minimum of τ_{avg} or s_1 in the database) to obtain the nonlinear load–deflection behavior of an RC beam. The two RC beams (i.e., B4 with splitting bond failure and B6 with pull-out bond failure) studied by Abdel-Kareem et al. (2014) are adopted and the beam configuration is shown in [Figure 3.10](#). [Table 3.3](#) provides the structural parameters of the two beams.

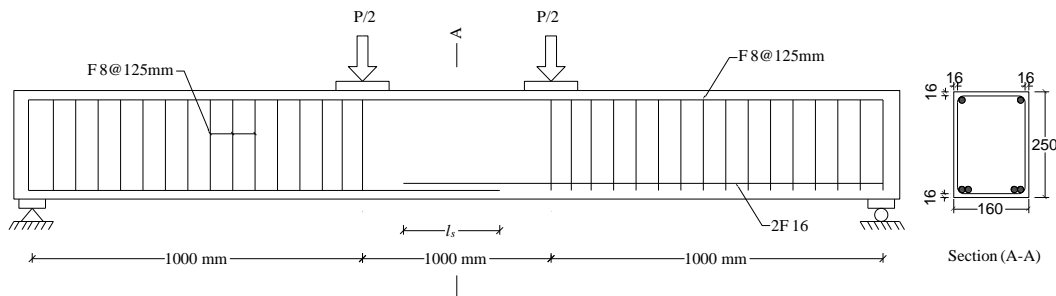


Figure 3.10. Cross-section and longitudinal detailing of RC beams studied by Abdel-Kareem et al. (2014) (dimensions are in mm)

Table 3.3. Details of experimental RC beams studied by Abdel-Kareem (2014)

Specimen	Bond failure mode	Lap splice (mm)	Stirrups spacing (mm)	Concrete strength (MPa)	Yield strength (MPa)	Ultimate strength (MPa)
B4	Splitting	420	150	58.7	440	551
B5	Splitting	420	150	80.7	440	551
B7	Splitting	320	150	104.3	440	551
B6	Pull-out	420	150	102.5	440	551
B8	Pull-out	320	125	99.6	440	551

As shown in **Figures 3.11** (a), (c), and (d), the variations in τ_{avg} for either bond failure mode and s_1 for pull-out bond failure significantly alter the load-deflection behavior of the RC beam, while s_1 for splitting bond failure does not result in a considerable difference (as shown in **Figure 3.11** (b)). This result indicates that the prediction model of s_1 in splitting can tolerate a large model error. In addition, the variations in τ_{avg} and s_1 for pull-out result in different beam failure modes (beam fails in bond or concrete crush), beam stiffness, and load-carrying capacities (expect s_1 for the pull-out), as shown in **Figure 3.11**. This indicates the accuracy of the prediction models of τ_{avg} for splitting or pull-out and s_1 for pull-out is critical for the structural performance evaluation.

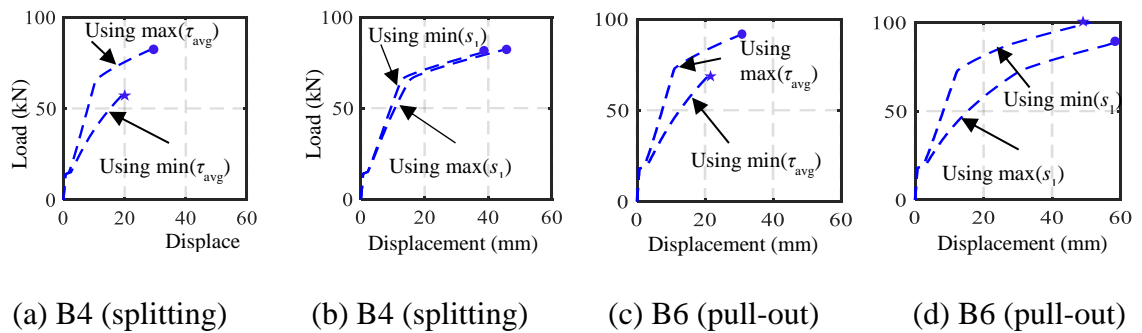


Figure 3.11. The impact of the variations in τ_{avg} and s_1 on load-deflection of RC beams

3.3.1. Probabilistic model for average bond strength, τ_{avg}

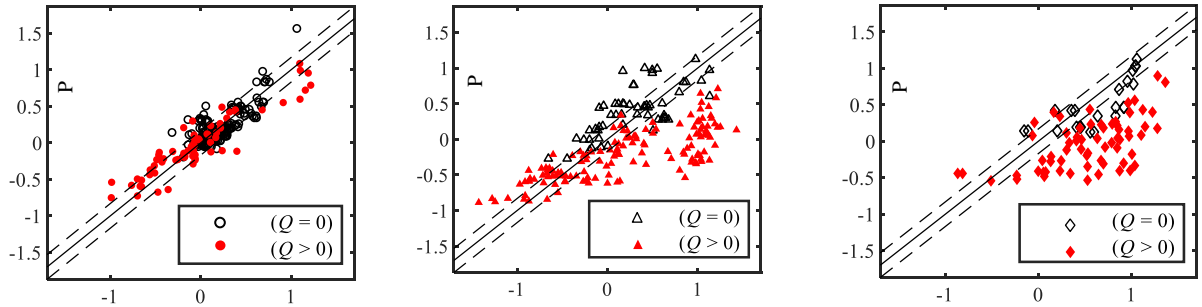
Note that the maximum bond strength τ_{max} cannot be measured directly from testing; instead, the average bond strength τ_{avg} is usually calculated based on the maximum applied force divided by the concrete-rebar interface area. Given a distribution of the bond stress along with the rebar, one can calculate τ_{max} using τ_{avg} . Some discussion on the distribution of bond stress can be found in the literature (Jiang et al., 1984; Main, 1951; Somayaji & Shah, 1981; Thompson, 1966). According to the suggestion by Thompson (1966), one could assume $\tau_{max} = 1.5 \tau_{avg}$.

3.3.1.1. Performance of Sajedi and Huang model

In this subsection, the previous prediction model developed by Sajedi and Huang (2015) is used to check the model performance on the collected data from this study. [Figures 3.12](#) (a)-(c) show the prediction of the Sajedi and Huang model (2015) compared with the experimental data used for their model development, the newly added experimental data with splitting bond failure, and the newly added experimental data with pull-out bond failure, respectively. In [Figure 3.12](#), the solid line refers to the equality line, and the dashed lines refer to the ± 1 standard deviation of model error.

As expected, Sajedi and Huang's model provides unbiased and good accuracy predictions for their database used for the model development, shown in [Figure 3.12](#) (a). However, when applying this model to the newly added data either splitting or pull-out, this model loses its accuracy and unbiasedness, as shown in [Figures 3.12](#) (b) and (c),

particularly for the corroded cases (shown in solid marks). Since Sajedi and Huang developed their model based on data with only splitting bond failure mode, it is not surprising that its prediction performance fails for the newly data with pull-out in Figure 3.12 (c). On the other hand, Figure 3.9 shows the differences in the distributions of structural parameters in Sajedi and Huang’s database and the newly added data with splitting. Those distribution differences (particularly for corrosion level, Q) may be the reason that this model also fails to provide good predictions for the newly added data with splitting in Figure 3.12 (b).



(a) Splitting data from Sajedi & Huang (Sajedi & Huang, 2015)

(b) Newly added splitting data

(c) Newly added pull-out data

Figure 3.12. Bond strength prediction, $\ln(\tau_{avg}/\sqrt{f'_c})$, using Sajedi and Huang model (2015) vs. experimental value

3.3.1.2. Proposed model development

In this study, the proposed model formulation for predicting τ_{avg} adopts the multivariate regression model used in Sajedi and Huang (2015), which can be expressed as:

$$y(\mathbf{x}, \mathbf{B}) = \sum_{i=0}^n \beta_i z_i(\tilde{\boldsymbol{\beta}}, \mathbf{x}) + \sigma \varepsilon \quad (3.1)$$

where y is the predicted response that is τ_{avg} or a suitable transformation of τ_{avg} , $z_i(\tilde{\boldsymbol{\beta}}, \mathbf{x})$ is the i th explanatory function; \mathbf{x} is the vector of independent variables; $\tilde{\boldsymbol{\beta}}$ is the vector of unknown parameters in the explanatory functions; β_i is the unknown model coefficient; $\mathbf{B} = \{\boldsymbol{\beta}, \tilde{\boldsymbol{\beta}}, \sigma\}$ is the vector of unknown model parameters, in which $\boldsymbol{\beta} = \{\beta_0, \beta_1, \dots, \beta_n\}$; and $\sigma \varepsilon$ is the model error in which σ is the standard deviation of the model error and ε is a random variable that follows a normal distribution. The model uses assumptions of homoscedasticity and normality in the model error, which can be satisfied by a variance stabilizing transformation of the predicted response. Thus, the prediction from the proposed model follows a normal distribution when point estimates are applied in the model parameter $\boldsymbol{\beta}$.

The explanatory functions, z_i , adopted here are the ones that have shown correlation with the bond strength in the literature (Bhargava et al., 2007; Chung et al., 2004; Lee et al., 2002; Orangun et al., 1977; Wang, 2009), and their formulations and their impact captured are listed in [Table 3.4](#). To capture the reduction in τ_{avg} due to the effect of corrosion, an exponential function of Q (i.e., $\exp(\tilde{\beta}Q)$) is multiplied to z_1 , z_2 , and z_3 , resulting in three additional explanatory functions: z_5 , z_6 , and z_7 . Note that $\exp(\tilde{\beta}Q)$ is not multiplied to z_4 , since it is been shown that corrosion of rebar is independent of transverse confinement (Rodriguez et al., 1993). Note that the explanatory functions provided in [Table 3.4](#) are unitless. Two dummy variables that could potentially contribute to the model prediction are also examined: (1) $d_{MC} = 0$ for specimens under monotonic loading and d_{MC}

= 1 for specimens under cyclic loading, and (2) $d_s = 0$ for specimens without the transverse rebar (i.e., $A_{tr} = 0$) and $d_s = 1$ when $A_{tr} > 0$. The two dummy variables are incorporated into the model by adding interaction terms of d_{MC} and d_s with z_1 to z_7 as additional explanatory functions. When including all explanatory functions, the model is a full model.

Table 3.4. Explanatory functions for multivariate nonlinear regression analysis.

Explanatory function	Impact captured	Notation
$z_0 = 1$	Correction of constant bias	c : clear concrete cover
$z_1 = \frac{c}{d} \cdot \frac{\mu + R_r}{1 - \mu R_r} \cdot \gamma$	Confinement effect due to cover (H. Wang, 2009)	d : intact rebar diameter μ : friction coefficient ¹ R_r : relative rib area (= rib height/rib spacing) ²
$z_2 = \frac{b_e}{d} \cdot \frac{\mu + R_r}{1 - \mu R_r} \cdot \gamma$	Confinement effect due to effective width (H. Wang, 2009)	$\gamma = \sqrt{8d/l_d} \leq 1$: reduction factor along development/splice length ³ l_d : development or splice length ⁴
$z_3 = d/l_d$	Embedment effect (Orangun et al., 1977)	$K_{tr} = A_{tr}/s \cdot d$
$z_4 = \frac{1}{\sqrt{f'_c}} \cdot K_{tr} \cdot f_{yt}$	Confinement effect due to the presence of transverse stirrups (Kemp & Wilhelm, 1978)	s : stirrups spacing A_{tr} : cross-section area of stirrups ⁵ f'_c : concrete compressive strength (MPa)
$z_5 = z_1 \cdot \exp(\tilde{\beta}_1 \cdot Q)$	Corrosion	f_{yt} : yield strength of stirrups b_e : effective beam width
$z_6 = z_2 \cdot \exp(\tilde{\beta}_2 \cdot Q)$	Corrosion	Q : corrosion level in terms of percentage mass loss
$z_7 = z_3 \cdot \exp(\tilde{\beta}_3 \cdot Q)$	Corrosion	

¹ Due to the unavailability in the literature μ is assumed to be 0.45 (Choi & Lee, 2002)

² R_r is assumed to be 0.1 based on (X. Wang & Liu, 2004) when it is not provided

^{3,4} Development or splice can be substituted with the bond length

⁵ Number of stirrups legs should be considered

An all-possible subset model selection technique is then applied to the full models, where all the reduced models are evaluated using Akaike's information criterion AIC and adjusted R -squared, $Adj-R-sq$. In each model size (that equals the number of explanatory functions), the model with the lowest AIC or highest $Adj-R-sq$ is the best model for that model size. The best models from all model sizes are then compared with each other using AIC to determine the final model, which should have the best compromise between the

accuracy and complexity. Noted that before conducting the model selection, the explanatory functions with a high variance inflation factor, VIF , (i.e., $VIF > 5$) are removed first to eliminate the presence of multicollinearity, which could lead to inaccurate evaluation of the model parameters.

As the result of the model selection, the proposed models of bond strength in splitting and pull-out are obtained, as shown below, respectively:

$$\ln\left(\frac{\tau_{avg}}{\sqrt{f'_c}}\right) = \beta_0 + \beta_1 \cdot \left(\frac{c}{d} \cdot \frac{\mu + R_r}{1 - \mu R_r} \cdot \gamma \cdot e^{\beta_1 \cdot \rho}\right) + \beta_2 \cdot \left(\frac{d}{l_d}\right) + \beta_3 \cdot \left(\frac{1}{\sqrt{f'_c}} \cdot \frac{A_{tr} \cdot f_{yt}}{s \cdot d}\right) + \sigma \varepsilon \quad (3.2)$$

$$\ln\left(\frac{\tau_{avg}}{\sqrt{f'_c}}\right) = \beta_0 + \beta_1 \cdot \left(\frac{c}{d} \cdot \frac{\mu + R_r}{1 - \mu R_r} \cdot \gamma \cdot e^{\beta_1 \cdot \rho}\right) + \beta_2 \cdot \left(\frac{d}{l_d}\right) + \beta_3 \cdot \left(\frac{1}{\sqrt{f'_c}} \cdot \frac{A_{tr} \cdot f_{yt}}{s \cdot d}\right) + \beta_4 \cdot \left(\frac{b_e}{d} \cdot \frac{\mu + R_r}{1 - \mu R_r} \cdot \gamma \cdot d_s\right) + \sigma \varepsilon \quad (3.3)$$

where both τ_{avg} and $\sqrt{f'_c}$ in MPa in which f'_c (MPa) is the compressive strength of concrete. The estimated model parameters in [Equations \(3.2\) and \(3.3\)](#) are summarized in [Table 3.5](#). For both models, the normality and homoscedasticity assumptions are checked using residual plots and $Q-Q$ plots. When comparing [Equations \(3.2\) and \(3.3\)](#), they both selected the same three exploratory functions, and the pull-out model (shown in [Equations \(3.3\)](#)) includes an additional exploratory function (i.e., $z_2 \cdot d_s$).

Table 3.5. Model coefficients for pull-out and splitting bond strength model.

Model	Splitting		Pull-out	
Coefficient	Mean	Standard deviation	Mean	Standard deviation
β_0	-0.955	0.07	-0.568	0.114
β_1	0.516	0.06	0.339	0.102
$\tilde{\beta}_1$	-0.101	0.01	-0.067	0.028
β_2	5.565	0.02	3.629	0.064
β_3	0.037	0.05	0.033	0.094
β_4	-	-	0.004	0.004
σ	0.250	-	0.190	-

Model formulation for splitting*	$\ln\left(\frac{\tau_{avg}}{\sqrt{f'_c}}\right) = \beta_0 + \beta_1 \cdot \left(\frac{c}{d} \cdot \frac{\mu + R_r}{1 - \mu R_r} \cdot \gamma \cdot e^{\tilde{\beta}_1 \cdot Q}\right) + \beta_2 \cdot \left(\frac{d}{l_d}\right) + \beta_3 \cdot \left(\frac{1}{\sqrt{f'_c}} \cdot \frac{A_r \cdot f_{yt}}{s \cdot d}\right) + \sigma \varepsilon$
Model formulation for pull-out*	$\ln\left(\frac{\tau_{avg}}{\sqrt{f'_c}}\right) = \beta_0 + \beta_1 \cdot \left(\frac{c}{d} \cdot \frac{\mu + R_r}{1 - \mu R_r} \cdot \gamma \cdot e^{\tilde{\beta}_1 \cdot Q}\right) + \beta_2 \cdot \left(\frac{d}{l_d}\right) + \beta_3 \cdot \left(\frac{1}{\sqrt{f'_c}} \cdot \frac{A_r \cdot f_{yt}}{s \cdot d}\right) + \beta_4 \cdot \left(\frac{b_c}{d} \cdot \frac{\mu + R_r}{1 - \mu R_r} \cdot \gamma \cdot d_s\right) + \sigma \varepsilon$

τ_{avg} , f'_c , and f_{yt} in MPa. c , d , l_d , and s in mm. A_r in mm². Q in %. μ , γ , and R_r are unitless

Figure 3.13 shows the scatter plot of the prediction of $\tau_{avg}/\sqrt{f'_c}$ by the proposed model vs. the actual experimental data, where the solid line refers to the equality line, the dashed lines refer to the ± 1 standard deviation of the model error, and the solid marks refer to the corroded cases. The data points on the three plots in Figures 3.13 (a)-(c) are scattered evenly around the equality line, and most of the data lie within the dashed lines, indicating that the predictions are unbiased with good accuracy. When comparing Figure 3.13 (a) with Figure 3.12 (a), one can see that the proposed model provides similar prediction performance as Sajedi and Huang's model (2015) for the splitting bond failure data used in their study. While the data in Figure 3.13 (a) is slightly more scattered than Figure 3.12 (a), as the proposed model is developed based on a larger dataset. In addition, when comparing Figures 3.13 (b) and (c) with Figures 3.12 (b) and (c), respectively, the proposed models show much better performance with much less bias and variance, particularly for

the corroded cases. These results show that the proposed models provide good predictions on the splitting bond failure data used previously in Sajedi and Huang (2015) and also newly added splitting and pull-out data.

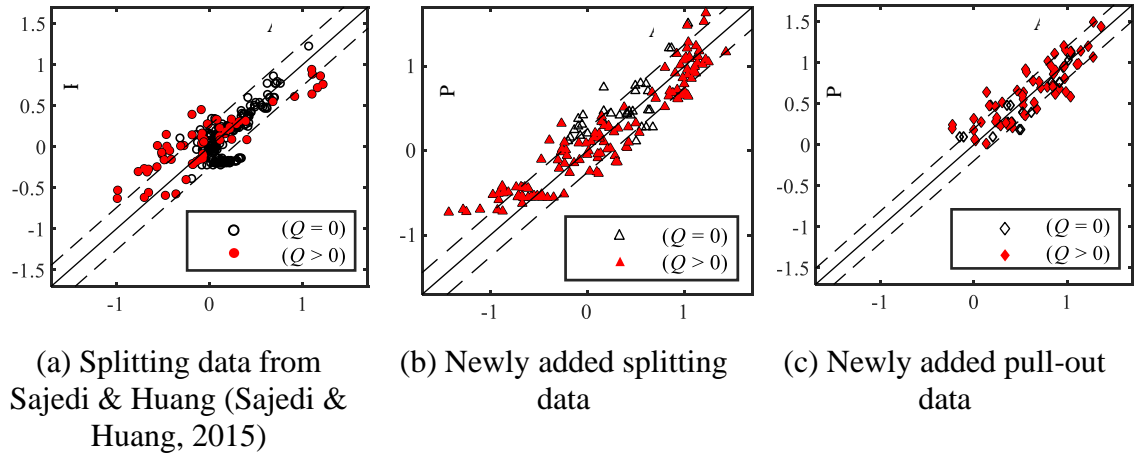


Figure 3.13. Bond strength prediction, $\ln(\tau_{avg}/\sqrt{f'_c})$, using the proposed model vs. experimental value

3.3.2. Probabilistic model for the bond peak slip s_1

As discussed in the Introduction, the findings from previous studies regarding influencing factors on s_1 are not consistent. Due to the lack of pre-existing knowledge about the relationship between s_1 and the potential influential factors, genetic programming (GP) is implemented in this study to develop the prediction formula directly from the data. GP is a machine learning technique that generates a population of random trees, also known as initial solutions, and each tree represents a gene. Then, the trees evolve and breed together to find the best-performing model (Gandomi & Atefi, 2020).

Recently, a symbolic multi-gene regression (SMGR) technique has been developed to decrease complexity and increase the accuracy and functionality of the evolution of the population of genes (Searson, 2015). In the process of SMGR, meaningful relationships from the data will be extracted in the form of symbolic equations that are “hidden” in the data. An example of symbolic multi-gene regression formulation is shown in [Figure 3.14](#), where the prediction model consists of two genes (or trees), and each gene consists of either symbol (such as multiplication ‘×’, logarithm ‘log’, subtraction ‘-’, and square root ‘√’) or input variables (such as x_1, \dots, x_n). It should be noted that even though the model structure consists of nonlinear symbols such as ‘log’ or ‘√’, the overall formulation is a linear collection of trees. A general SMGR formulation can be written as:

$$\hat{y}(\mathbf{x}, \boldsymbol{\beta}, \boldsymbol{\theta}) = \beta_0 + \sum_{j=1}^m \beta_j \cdot G_j(\boldsymbol{\theta}, \mathbf{x}) \quad (3.4)$$

where \hat{y} is the predicted response, $\mathbf{x} = [x_1, \dots, x_n]$ is the vector of input variables, $\boldsymbol{\beta} = [\beta_0, \beta_1, \dots]$ is the vector of coefficients, $G_j(\boldsymbol{\theta}, \mathbf{x})$ is the j th gene outputs, and $\boldsymbol{\theta}$ is the vector of unknown parameters for each gene. The optimal values of $\boldsymbol{\beta}$ are determined by minimizing the prediction error (e.g., root mean squared error, *RMSE* as defined in [Equation \(3.5\)](#)) over a training data set (Zamanian et al., 2020).

$$RMSE = \sqrt{\frac{\sum_{i=1}^n |\hat{y}_i - y_i|^2}{n}} \quad (3.5)$$

where \hat{y}_i and y_i are the i th predicted and actual response values, respectively, and n is the number of data points. To measure the model performance, *R*-squared, *R-sq* can be used. In this study, the genetic programming toolbox for the identification of physical

systems (GPTIPS) developed by Dominic Searson (2015), an open-source toolbox in MATLAB software, is adopted to implement SMGR.

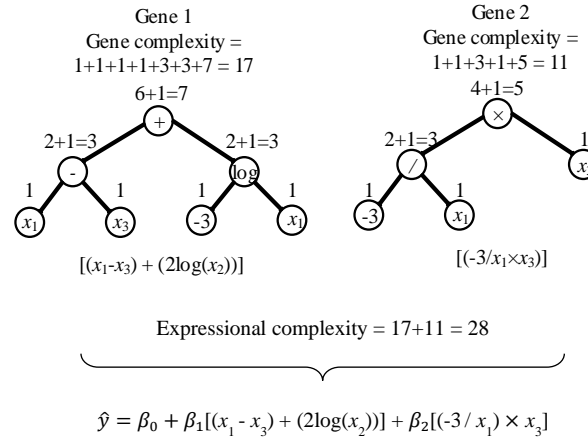


Figure 3.14. An example of the formulation of SMGR

Table 3.6 shows the values of the setting parameters used in the GPTIPS in this study. Five input variables, \mathbf{x} , are selected: c/d , f'_c (MPa), l_d (mm), K_{tr} , and $\exp(Q)$. It should be noted that, even though some literature (e.g., Harajli et al., 2004; Zhao & Zhu, 2018) suggests that the parameter rib spacing s_r has an impact on s_1 , it is not used as an input variable due to its unavailability in many of the collected testing data. It is expected that the proposed models could be improved if rib spacing information can be added as one of the input variables to the GPTIPS. In Table 3.6, the function symbols are selected to keep the final model formulation simple from an engineering practice perspective. In addition, G_{\max} and D_{\max} refer to the maximum number of genes/trees, and the number of layers in the tree, respectively, and both determine the complexity and accuracy of the final model. However, selecting the appropriate values for G_{\max} and D_{\max} is not an easy task. Setting a higher value of G_{\max} or D_{\max} leads to more accurate, yet more complicated and possibly overfitted models. A high value of G_{\max} may create “horizontal bloating” and a high value

of D_{\max} may create “vertical bloating”. Accordingly, G_{\max} and D_{\max} are determined by a trial-and-error in this study, which is elaborated later. The values for other setting parameters in [Table 3.6](#) are based on the suggestion from previous literature (Hii et al., 2011; Searson et al., 2007, 2010, 2015).

Table 3.6. GPTIPS run settings.

Parameter	Settings
Input variables, \mathbf{x}	$c/d, \tau_{\text{avg}}/\text{sqrt}(f_c), l_d/d, K_{tr}, \exp(Q)$
Function symbols	$+, -, \times, \div, \sqrt{\cdot}, (\cdot)^2, (\cdot)^3, -(\cdot)$
Maximum allowable gene (G_{\max})	3 or 4
Maximum tree depth (D_{\max})	3 or 4
Number of generations	500
Number of populations	10,000
Crossover events	0.84
Mutation events	0.14
Direct reproduction	0.02
Random constant range	[-10 10]

To determine suitable values of G_{\max} and D_{\max} , a preliminary evaluation is performed for all possible combinations of G_{\max} and D_{\max} ranging from 1 to 10, which generates 100 models. The models are then evaluated based on their accuracy (reflecting in $R\text{-sq}$) and complexity (reflecting in expressional complexity). A model with $R\text{-sq} \geq 0.6$ is considered to have acceptable accuracy. The expressional complexity is defined as the summation of node count and all its possible full sub-tree (Searson, 2015). [Figure 3.14](#) shows an example of the calculations of such complexity with two genes. As the result of the preliminary evaluation, it is found that when G_{\max} or D_{\max} is less than 3, the resulted models have very low accuracy, while when G_{\max} or D_{\max} is larger than 4, the resulted models are overly complicated. Thus, it is appropriate to use 3 or 4 for both G_{\max} and D_{\max} . [Table 3.7](#) shows the model comparison resulted from the four possible combinations of G_{\max} and D_{\max} with the values of 3 or 4.

Table 3.7. Model accuracy and complexity for various combinations of D_{\max} and G_{\max} .

		$G_{\max} = 3$		$G_{\max} = 4$	
		$R\text{-sq}$ (%)	Complexity	$R\text{-sq}$ (%)	Complexity
Splitting	$D_{\max} = 3$	16.1	40	41.7	47
	$D_{\max} = 4$	22.0	85	50.3	133
Pull-out	$D_{\max} = 3$	40.1	30	62.1	40
	$D_{\max} = 4$	42.5	63	65.0	140

As shown in [Table 3.7](#), for the pull-out, the model resulted from the case where $G_{\max} = 4$ and $D_{\max} = 3$ has the least complexity and $R\text{-sq}$ larger than 60%. Thus, this model is adopted as the final model for s_1 in pull-out and its formulation is shown as:

$$\begin{aligned} \ln(s_{1,p}) = & \beta_0 + \beta_1 \cdot (e^{-4\varrho}) + \beta_2 \cdot \left(\frac{c}{d}\right)^2 \cdot e^{3\varrho} + \beta_3 \cdot \frac{c}{d} \cdot \frac{\tau_{avg}}{\sqrt{f'_c}} + \beta_4 \cdot \frac{\tau_{avg}}{\sqrt{f'_c}} \cdot (e^{-4\varrho}) \\ & + \beta_5 \cdot \left(\frac{l_d}{d}\right)^{-1} \left(\frac{\tau_{avg}}{\sqrt{f'_c}} - K_{tr}\right)^{-1} \cdot e^{\varrho} + \sigma\varepsilon \end{aligned} \quad (3.6)$$

The estimated coefficients in [Equation \(3.6\)](#) are shown in [Table 3.8](#), and the model error $\sigma\varepsilon$ (in which σ is the standard deviation of the model error and ε is a random variable) found to follow a normal distribution, which is checked by Q-Q plot. One can notice that this model uses all of the five input variables \mathbf{x} , except c/d . This indicates that c/d does not contribute to the prediction of s_1 in the pull-out, which is also shown in previous literature (Mohamed H. Harajli et al., 2004; Murcia-Delso & Benson Shing, 2015; Saatcioglu et al., 1992; Taerwe & Matthys, 2013; W. Zhao & Zhu, 2018) in [Table 3.1](#).

Table 3.8. Statistics of model coefficients for pull-out bond peak slip model.

Coefficient	Mean	Standard deviation
β_0	-3.54	0.05
β_1	0.244	0.13
β_2	-0.631	0.07
β_3	2.52	0.11
β_4	-5.86	0.15
β_5	1.85	0.1
$\sigma\varepsilon$	-3.54	-

Model formulation for pull-out	$\ln(s_{1,p}) = \beta_0 + \beta_1 \cdot (e^{-4Q}) + \beta_2 \cdot \left(\frac{c}{d}\right)^2 \cdot e^{3Q} + \beta_3 \cdot \frac{c}{d} \cdot \frac{\tau_{avg}}{\sqrt{f'_c}} + \beta_4 \cdot \frac{\tau_{avg}}{\sqrt{f'_c}} \cdot (e^{-4Q})$ $+ \beta_5 \cdot \left(\frac{l_d}{d}\right)^{-1} \left(\frac{\tau_{avg}}{\sqrt{f'_c}} - K_{tr}\right)^{-1} \cdot e^Q + \sigma\varepsilon$	
--------------------------------	--	--

* τ_{avg}, f'_c , and f_{yt} in MPa. c, d, l_d , and s in mm. Q in %..

However, for s_1 in splitting, using SMGR fails to satisfy the R - sq criterion with reasonable complexity. As shown in Table 3.7, to achieve an R - sq of 49.1%, the complexity has reached a complexity of 133 (that is not a practical model). Based on the results in Figure 3.11, for structural performance evaluation purposes, the prediction of s_1 in splitting is not as critical as s_1 in the pull-out; thus, instead of using any model obtained from SMGR, a beta distribution is used to fit the s_1 database with splitting bond failure. Beta distribution has the advantage of imposing a boundary condition and flexibility over its shape due to the employment of shape parameters. The probability density function (PDF) of s_1 in splitting that follows a beta distribution is shown as and the coefficients are provided in Table 3.9:

$$f(s_1 | \beta_1, \beta_2) = \frac{(x - s_{1,\min})^{\beta_1 - 1} (s_{1,\max} - x)^{\beta_2 - 1}}{B(\beta_1, \beta_2) (s_{1,\max} - s_{1,\min})^{\beta_1 + \beta_2 + 1}} \quad s_{1,\min} \leq s_1 \leq s_{1,\max} \quad (3.7)$$

Figure 3.16 shows the scatter plots of the proposed model prediction of s_1 vs. experiment data, where the solid line refers to the equality line and the dashed lines refer

to the ± 1 standard deviation of the model error. In Figure 3.16, data points are evenly scattered within the dashed lines having most of the points inside, which is an indication of an unbiased prediction. Note that the prediction of s_1 in splitting is generated from the PDF of s_1 , and Figure 3.16 (a) shows the realizations sampled from the PDF. While the $\pm 1\sigma$ band is wide in Figure 3.16 (a) because no variation is reduced in the database by fitting a distribution, the proposed model prediction removes the bias. When compared with other existing models in the next section, using beta distribution shows better prediction performance.

Table 3.9. Model parameters for bond peak slip in splitting

Coefficient	Mean	Standard deviation
β_1	1.08	0.17
β_2	2.85	0.48
$\sigma\epsilon$	0.20	-
$s_{1,\min}$	0.01	-
$s_{1,\max}$	0.86	-

Model formulation*	$f(s_1 \beta_1, \beta_2) = \frac{(x - s_{1,\min})^{\beta_1 - 1} (s_{1,\max} - x)^{\beta_2 - 1}}{B(\beta_1, \beta_2) (s_{1,\max} - s_{1,\min})^{\beta_1 + \beta_2 + 1}}$	$s_{1,\min} \leq s_1 \leq s_{1,\max}$ *
--------------------	---	---

* s_1 in mm

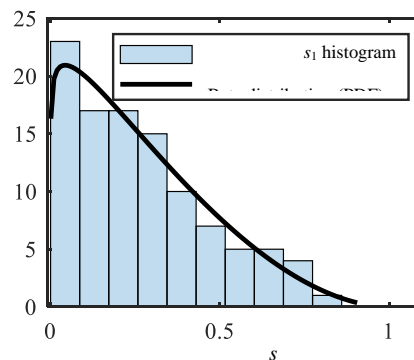


Figure 3.15. Histogram and the fitted PDF for peak slip under splitting bond failure

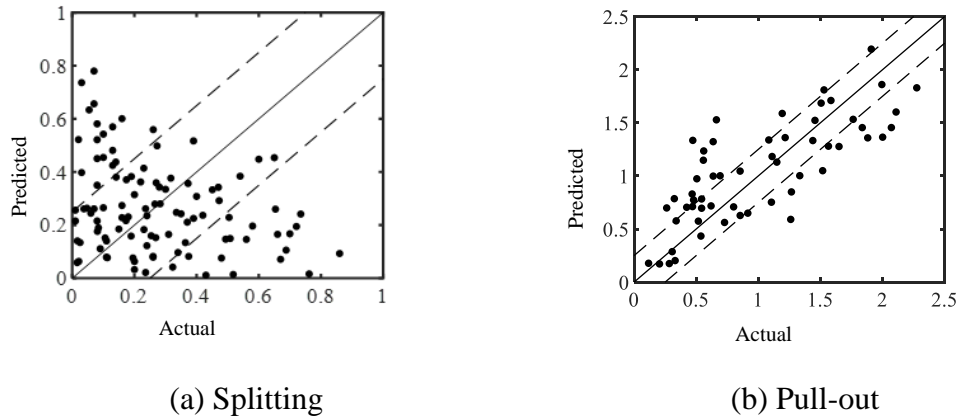


Figure 3.16. Scatter plot of developed s_1 models (in mm)

3.4. Model evaluation

In this session, the performance of the developed models is assessed by comparing with existing models in the literature based on the experimental data and applying the bond-stress relationship using the developed models in the flexural behavior evaluation of RC beams.

3.4.1. Prediction comparison of the proposed model with existing models

In this section, the predictions obtained from the proposed models and selected existing models are evaluated against experimental data. Even though those data are among the ones used for the model development, they are not used for the validation of the proposed models but for a comparison purpose

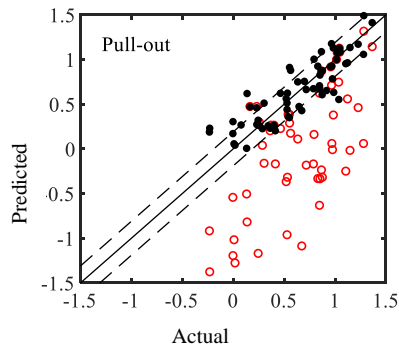
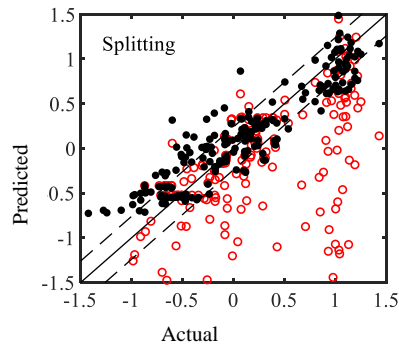
3.4.1.1. Bond strength, τ_{avg}

As mentioned before, to account for the corrosion impact, many existing prediction models for τ_{avg} are developed by applying a reduction factor to the intact bond strength, $\tau_{avg,0}$. Table 3.10 shows the formula of the four selected existing models, and $\tau_{avg,0}$ that is needed in the existing model is calculated based on the proposed models. These four models are used for both splitting and pull-out bond failure cases. In addition, only the corroded experimental data are used for this comparison.

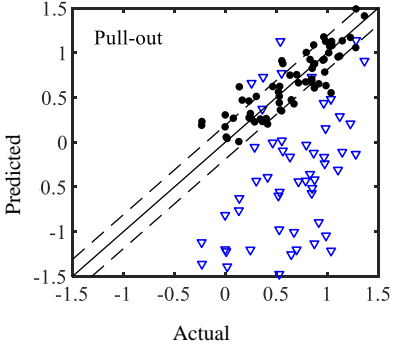
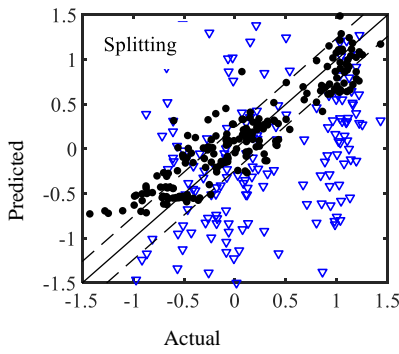
Table 3.10. Existing prediction models for bond strength.

Reference	Prediction model
Bhargava et al. (2007)	$\tau_{avg} = \tau_{avg,0} \cdot e^{-19.8(Q-1.5)} \leq \tau_{avg,0}$
Chung et al. (2004)	$\tau_{avg} = \tau_{avg,0} \cdot 0.0159Q^{-1.06} \leq \tau_{avg,0}$
Stanish et al. (1999)	$\tau_{avg} = \tau_{avg,0} \cdot (1 - 3.5Q)$
Yuan et al. (2015)	$\tau_{avg} = \tau_{avg,0} \cdot (1 - 10.544 \cdot Q + 1.586 \cdot c/d \cdot Q)$
Prieto et al. (2016)	$\tau_{avg} = f_c^{2/3} \left((1.25(d^2 + 1)^{0.052} (d/l_d)^2 + 1) \right)^{8.13} \left(\exp(-0.129f_c'/40) \left(((c+d)/2)/d \right)^4 + 1 \right)^{0.058} \left((K_{tr}^2 + K_{tr} + 1) \right)^{0.498} (\%Q^2 + 1)^{-0.016} - 1 \right)$

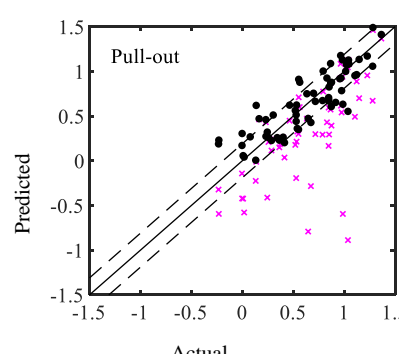
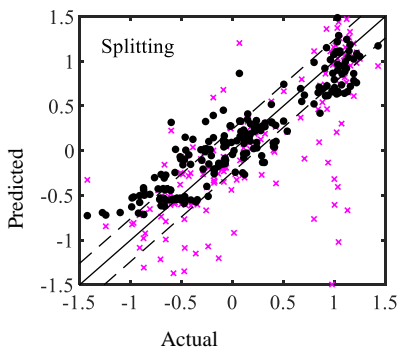
Figure 3.17 shows the prediction comparison of the normalized bond strength based on the proposed models and the existing models. Overall, all the four existing models result in a much bigger scatter than the proposed models for both splitting and pull-out, indicating the proposed models have better accuracy. Second, all the existing models underestimate the bond strength particularly for pull-out cases (shown in the right plots). Since the existing models only use Q and/or c/d to quantify the corrosion impact (as shown in Table 3.10), the results infer that using only these two quantities subsequently is insufficient.



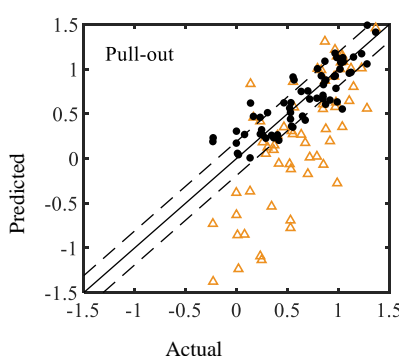
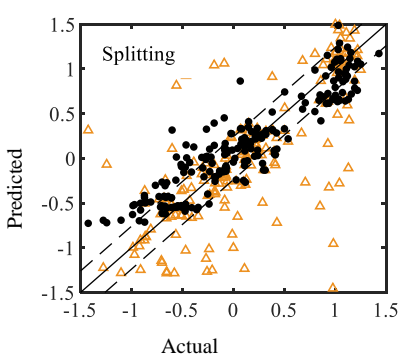
- Bhargava et al.
- Proposed model



- ▽ Chung et al.
- Proposed model



- × Stanish et al.
- Proposed model



- △ Yuan et al.
- Proposed model

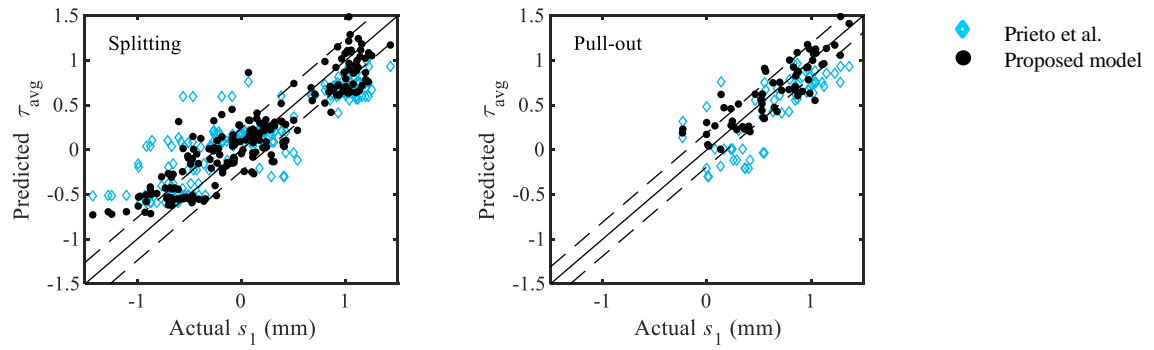


Figure 3.17. Comparison of bond strength predictions, $\ln(\tau_{\text{avg}}/\sqrt{f'_c})$, using the proposed model and four existing prediction models for bond data with corrosion

Table 3.11 further compares the prediction performance of the models in terms of R -sq and absolute error of prediction MSE that is defined as:

$$MSE = \frac{\sum_{i=1}^n (y_i - \hat{y}_i)^2}{n} \quad (3.8)$$

where \hat{y} and y_i is the predicted and actual value of $\tau_{\text{avg}}/\sqrt{f'_c}$, respectively, and n is the number of data points. **Table 3.11** shows that the proposed models have much higher R -sq values and much lower MSE values, indicating the proposed models are well-performed, consistent with the finding in **Figure 3.17**. It can also be seen that the model developed by Prieto et al. (Prieto et al., 2016) has the second highest accuracy.

Table 3.11. Comparison of proposed models and existing models for bond strength prediction.

Prediction model	R -sq (%)		MSE	
	Splitting	Pull-out	Splitting	Pull-out
Proposed model	75.5	79.0	0.22	0.15
Bhargava et al. (2007)	26.6	8.7	0.77	0.95
Chung et al. (2004)	18.8	15.3	0.91	1.15
Stanish et al. (1999)	33.8	11.5	0.49	0.65
Yuan et al. (1999)	30.7	24.2	0.51	0.56
Prieto (2016)	61.2	44.6	0.31	0.24

The contributions of the key variables in the proposed models are examined via sensitivity analysis. Figure 3.18 shows the sensitivity plots of the τ_{avg} prediction using the proposed models (i.e., Equations (3.2) and (3.3)) in terms of five variables (i.e., Q , K_{tr} , f'_c , c/d , d/l_d), where the band refers to the ± 1 standard deviation of the model error. All the cases shown in Figure 3.18 indicate that τ_{avg} in the pull-out, in general, is larger than τ_{avg} in splitting, which is consistent with CEB (2013). For both splitting and pull-out, all five variables show similar impacts on τ_{avg} : an increase in Q result in a decrease in τ_{avg} , and an increase in K_{tr} , f'_c , c/d , or d/l_d lead to an increase in τ_{avg} (consistent with previous findings (Jiang et al., 2018; Kivell et al., 2011; Yuan et al., 1999)). Also, the level of sensitivity is very similar between splitting and pull-out for K_{tr} , f'_c , and c/d , while τ_{avg} in splitting is more sensitive to Q and d/l_d .

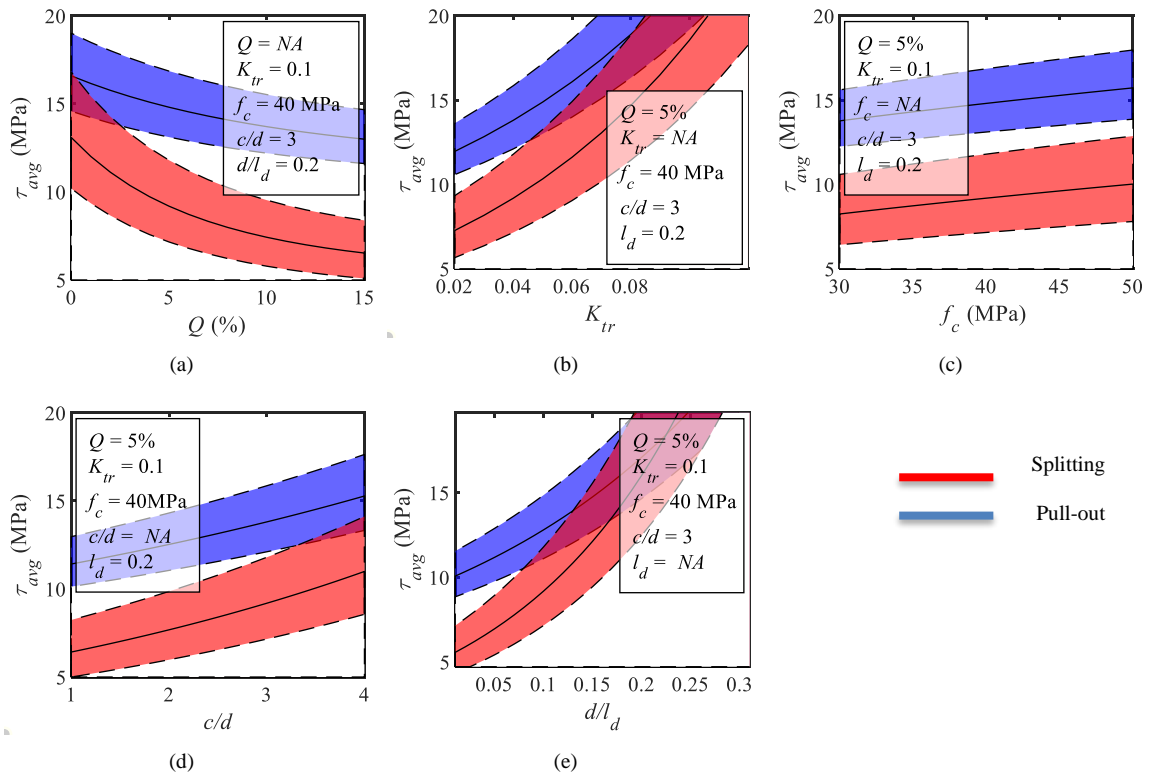


Figure 3.18. Sensitivity to proposed bond strength (τ_{avg}) prediction: (a) corrosion level Q (b) confinement from transverse stirrups K_{tr} (c) concrete strength f'_c (d) cover-to-diameter ratio c/d and (e) embedment effect d/l_d

3.4.1.2. Peak slip s_1

The performance of the proposed models for s_1 is also compared to nine selected existing models whose formulas are provided in [Table 3.1](#). The scatter plots of the prediction vs. experimental data are shown in [Figure 3.19](#). For both splitting and pull-out cases, the data points predicted by the proposed models are evenly distributed around the equality line, indicating the proposed models perform better in terms of prediction bias. In particular, the proposed model for the pull-out has much tighter scatter than the other models, indicating its better performance in terms of accuracy.

It is noticed that the prediction points obtained from the existing models are shown in [Figures 3.19](#) (a) and (c) form nearly one or multiple straight lines. This is because those models are developed based on limited variables: some of them are just constant (e.g., Kivell et al., 2015, Feng et al., 2018), and some are based on just one parameter (e.g., s_r , d , or c/d). Thus, those models ignore the potential influence of many other variables and do not provide accurate predictions, which particularly true for the pull-out. In addition, as shown in [Figure 3.19](#) (b), Wu and Zhao (2013) and Lin et al. (2017, 2019) provide better predictions compared to other existing models, this may be because their models involve more structural variables, such as transverse confinement quantity.

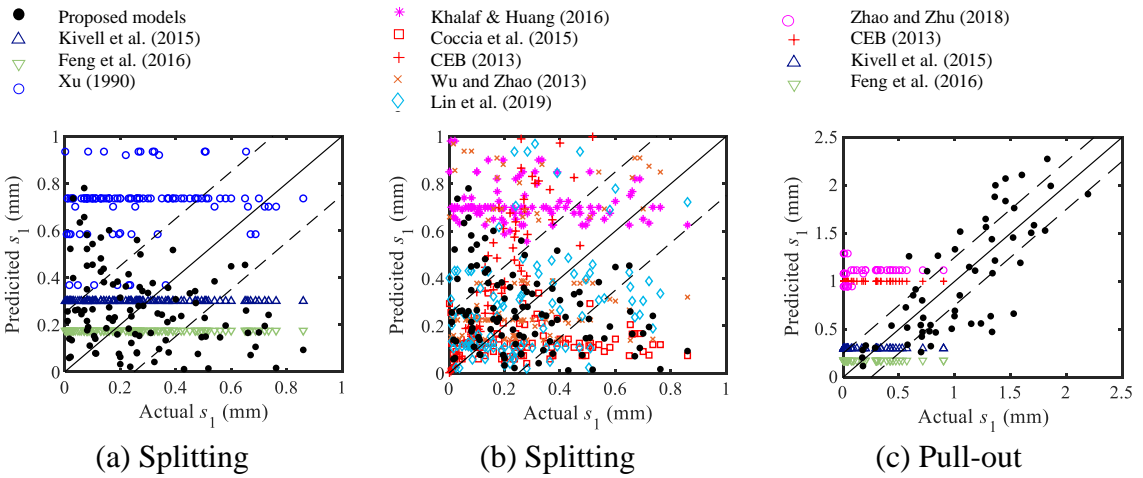


Figure 3.19. Comparison of the proposed models for s_1 and existing models in the literature

Table 3.12 shows the prediction comparison of the models in terms of R -sq and MSE . The MSE calculated here is based on the logarithm of s_1 values. For the pull-out case, the proposed model has a much higher R -sq value and lower MSE value, indicating the proposed model surpasses the existing ones. For the splitting case, all the models have rather low R -sq values, while the proposed model has the highest R -sq and the lowest MSE values. Although the proposed model using beta distribution does not reduce the data variation, it removes the bias in the prediction, and with this alone it results in a better performance compared to the existing models.

Table 3.12. Comparison of proposed models and existing models for peak slip.

Failure mode	Prediction model	$R-sq$ (%)	MSE
	Proposed model	8.15	1.00
Splitting	Kivell et al. (2015)	<1	1.24
	Feng et al. (2016)	<1	1.47
	Xu (1990)	1.53	1.61
	Khalaf and Huang (2016)	1.24	1.61
	Coccia et al. (2015)	<1	1.08
	CEB (2013)	6.1	1.36
	Wu and Zhao (2013)	5.06	1.23
	Lin et al. (2019)	3.68	1.10
	Zhao and Zhu (2018)	1.78	1.79
		Proposed model	65.22
Pull-out	Kivell et al. (2015)	18.52	0.71
	Feng et al. (2016)	10.12	0.94
	CEB (2013)	5.06	1.72
	Zhao and Zhu (2018)	4.18	1.89

3.4.1.3. Flexural behavior evaluation

In this section, the proposed models for τ_{avg} and s_1 are applied in the structural analysis of RC beams. Six beams studied by Abdel-Kareem et al. (2014) were adopted for this purpose, of which three have splitting failure and three have pull-out failure. The configuration is shown in Figure 3.10, and the structural properties (including lap splice length, stirrups spacing, and concrete compressive strength) are listed in Table 3.3. The analytical procedure proposed by Sajedi and Huang (2017) is used here to incorporate the CEB stress–slip bond model (shown in Figure 3.2) with τ_{avg} and s_1 calculated using the proposed models to obtain the nonlinear load-deflection behavior of the RC beams. To consider the prediction variation, for each beam, τ_{avg} and s_1 are predicted by the point

estimate and point estimate ± 1 standard deviation of model error; thus, a total of 9 different combinations of τ_{avg} and s_1 values are used for each beam.

Figure 3.20 compares the load-deflection predictions based on the calculated τ_{avg} and s_1 with the experimental results. For all the beams, the experimental curves are within the predicted flexural behavior, which indicates that the satisfactory prediction performance of the proposed models of τ_{avg} and s_1 for either splitting and pull-out.

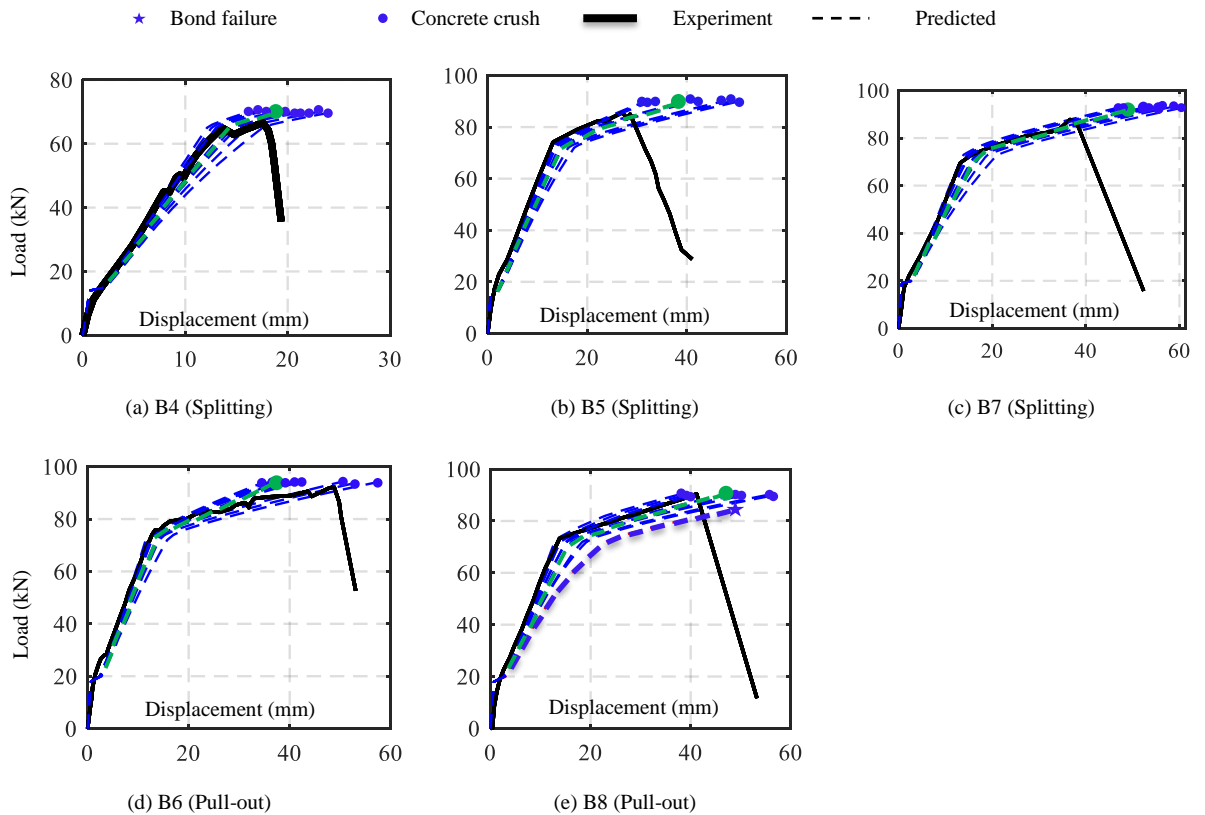


Figure 3.20. Comparison of predicted load-deflection of RC beams with experimental results from Abdel-Kareem (2014)

CHAPTER IV

SIMPLE REBAR ANCHORAGE SLIP MACROMODEL CONSIDERING CORROSION DETERIORATION EFFECT

The total lateral deformation of a reinforced concrete (RC) structural member with fixed end(s) mainly consists of two components: the flexural deformation induced by the internal bending moment over the member length and the fixed-end rotation of the member induced by the slip of the longitudinal rebar. This slip reflects the accumulation of strain along the development length of reinforcement under tensile loading due to the gradual transfer of the rebar force to the surrounding concrete; and the strain causes rebar elongation, resulting in slip at the connection interface (W. H. Pan et al., 2018). Both numerical and experimental studies have showed that this rebar slip can significantly contributes to total displacement of the RC member and consequently, affecting the static and seismic response of the structural member (W.-H. Pan et al., 2017; Schoettler et al., 2012; A. Soraghi et al., 2019; Ahmad Soraghi & Huang, 2021). Kherdmatgozar Dolati and Mehrabi ((Dolati & Mehrabi, 2021b, 2021a)) investigated the effect of debonding and bar slip in improving the seismic behavior and ductility of bar couplers in precast concrete members. Hence, in the structural analysis of RC members under either static or seismic loading, it is important to appropriately account for the slippage over the development length so that the lateral responses of the structural members can be accurately captured.

Among various approaches for calculating reinforcement slip along the development length under monotonic loading, micromodels and macromodels are often adopted. Micromodels use a bond stress-slip constitutive model to consider the rebar-concrete interface and require finite discretization process to solve their governing equations, and thus need significant computational effort (Fédération Internationale du Béton, 2000; Filippou et al., 1983; Maekawa et al., 2003; Monti et al., 1997; Monti & Spacone, 2000; SHIMA et al., 1987; S Zamanian et al., 2020). On the other hand, macromodels use a bond stress distribution function along the development length, and subsequently obtain the slip response (usually expressed as rebar stress – slip curve) by implementing the relationships of four bond fields (i.e., distributions of bond stress, rebar stress, rebar strain, and rebar slip over the rebar development length) as shown in [Figure 4.1](#). From a computational perspective, macromodels are effective and practical, and the basis used directly reflects the strain penetration mechanism (Alsiwat & Saatcioglu, 1992; Lehman, 1998; Otani, 1973; W.-H. Pan et al., 2017; Taslimi & Tehranizadeh, 2021). Hence, macromodel is found to be preferred for engineering applications (W. H. Pan et al., 2018).

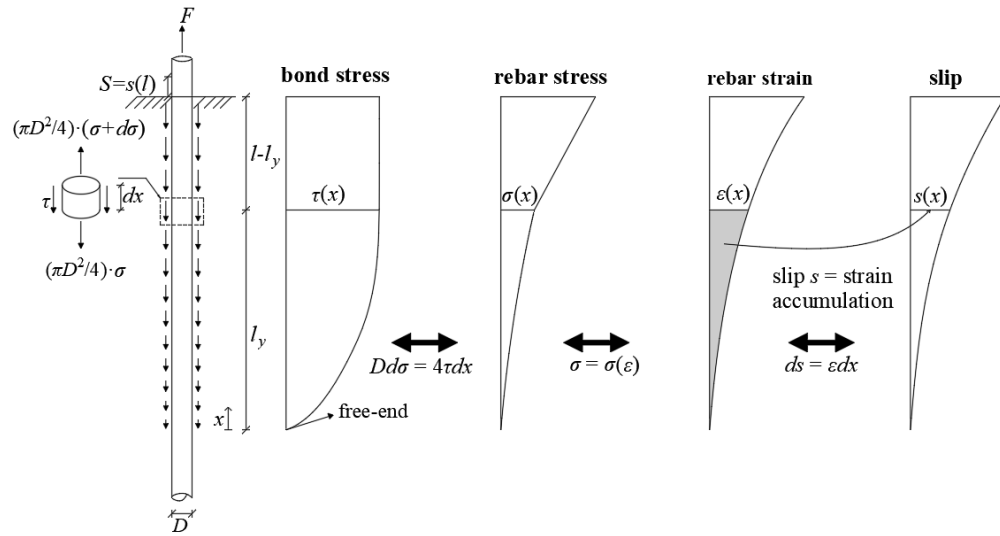


Figure 4.1. Four bond distribution fields and their relationships in rebar anchorage region

Sezen and Setzler (Sezen & Setzler, 2008) proposed a macromodel that assumes a uniform bond stress distribution along the development length to calculate the slip response of the rebar. However, this macromodel underestimate slip for smaller rebar stress values and reversed at higher rebar stress values; in addition, this macromodel is limited on prediction of the yield slip and particularly not good when the yielding strength is high, which could be an issue as in current engineering practice there is a tendency to use high-yield-strength rebars ((W. H. Pan et al., 2018; Sezen & Setzler, 2008)). Pan et al. (W. H. Pan et al., 2018) attempted to solve the issues in the Sezen and Setzler model by adopting a “real” bond stress distribution (derived from the bond-slip relationship obtained from Shima et al. (Shima et al., 1987a)) so that the model could more accurately capture the shape of the slip response before rebar yielding and predict the yield slip associated with the rebar yielding. However, the procedure developed by Pan et al. required extensive

numerical calculations and approximations, resulted in a complex rebar stress-slip model and impossible to update if more information become available. In the study by Zhang et al. (Y. Zhang et al., 2020), a nonuniform bond stress distribution is assumed to calculate the slip value, but their model is only applicable for short development length, which is often not the situation in practice (J. Zhao & Sritharan, 2007). In addition, the framework developed in Zhang et al. (Y. Zhang et al., 2020) requires a post-processing procedure in order to calculate the end rotation of the member induced by the slip of the longitudinal rebar. Lastly, as the corrosion deteriorate the bond between rebar and concrete, it is important to account for the corrosion impact on the slip calculation (Y. Zhang et al., 2020), to which very little attention have been given in the macromodels developed so far.

The proposed model utilized a simple function to approximate the “real” bond stress distribution to obtain the rebar stress-slip relationship through a macromodel approach. The model parameter is calibrated based on a set of experimental slip data with various levels of corrosion, rebar yield strength, and concrete compressive strength. The proposed model is then implemented into a conventional fiber beam-column model to simulate the lateral monotonic and cyclic behaviors of the corroded RC columns, which is compared with the experimental results. Lastly, the proposed model is implemented into a RC bridge column to investigate how the rebar slip impact seismic performance of the column based on static nonlinear analysis, probability of failure in terms of fragility curves, and time-history analysis.

4.1. Background

The basis of a macromodel consists of three governing equations that determine the relationships among four bond distribution fields over the development length, l , as shown in Fig. 1. The four bond fields are: (1) bond stress between concrete and rebar interface, $\tau(x)$, (2) rebar stress, $\sigma(x)$, (3) rebar strain, $\varepsilon(x)$, and (4) slip of rebar relative to surrounding concrete, $s(x)$. These four bond fields are variables along the rebar, which can be expressed as functions of the location of the point of interest, x (i.e., the distance from the unaffected end to the discussed point) and $0 \leq x \leq l$. The three governing equations are: (1) the equilibrium of any given segment of rebar with a length of dx , (2) the constitutive rebar stress-strain relationship, and (3) the compatibility of rebar strain-slip deformation relationship, which are shown below:

$$D \cdot d\sigma = 4\tau(x)dx \quad \text{or} \quad \sigma(x) = \int_0^x \frac{4}{D} \cdot \tau(u)du \quad (4.1)$$

$$\sigma(x) = \sigma(\varepsilon(x)) \quad \text{or} \quad \varepsilon(x) = \varepsilon(\sigma(x)) \quad (4.2)$$

$$ds = \varepsilon dx \quad \text{or} \quad s(x) = \int_0^x \varepsilon(u)du \quad (4.3)$$

Using Eqs. (4.1)-(4.3), the second order differential relationship between s and τ can be derived as:

$$\frac{d^2s}{dx^2} = 4D \cdot \tau(x) \cdot \frac{d\varepsilon}{d\sigma} \quad (4.4)$$

where $d\varepsilon/d\sigma$ can be obtained from the constitutive rebar stress-strain relationship. In the general framework of macromodel, Equation (4.4) is solved by assuming a specific bond

stress distribution function, $\tau(x)$, along the development length l , and considering the boundary conditions at the unaffected end (i.e., $x = 0$): $\tau(x = 0) = 0$, $\sigma(x = 0) = 0$, $\varepsilon(x = 0) = 0$, $s(x = 0) = 0$ for a long embedment length. Note that under the condition of long enough embedment length, the distribution of strain over l can be considered independent of the axial force magnitude, while l changes with the loading to satisfy equilibrium. Thus, for a given l and an assumed $\tau(x)$ function, one could obtain the other three bond distribution fields: $\sigma(x)$, $\varepsilon(x)$, and $s(x)$ through Eqs. (4.1)-(4.3).

Equation (4.3) shows that the slip $S = s(x = l)$ at the fixed end of a RC member is the accumulation of strain over the whole development length, l . The slip S is more useful when it is written as a function of rebar stress at the fixed end, $\sigma_b = \sigma(l)$, as σ_b can be easily calculated based on the axial loading at the fixed end, F , (that is, $\sigma_b = F/A$ where A = cross-section of the rebar). To do so, one needs to obtain l as a function of σ_b from Equation (4.1) and substitute it into Equation (4.3) by setting $x = l$.

4.1.1. Conventional macromodel method

Previous literature has simply assumed $\tau(x)$ to be a constant τ_M for the prior-to-yielding region and another constant τ'_M for the post-yield region (Maekawa et al., 2003; Sezen & Setzler, 2008; SHIMA et al., 1987), as shown in Figure 4.2. This assumption makes the sequential differentiation, integration, and inversion in Eqs. (4.1)-(4.3) to obtain S as a function of σ_b straight-forward and mathematically simple. In particular, the constants τ_M and τ'_M have been assumed to be proportional to $\sqrt{f'_c}$, where f'_c is the concrete compressive strength (in MPa). Based on existing experimental results, the

following values (in MPa) have been used (Lehman, 1998; W. H. Pan et al., 2018; Sezen & Setzler, 2008):

$$\tau = \begin{cases} \tau_M = 1.2\sqrt{f'_c} & \sigma < \sigma_y \\ \tau'_M = 0.5\sqrt{f'_c} & \sigma \geq \sigma_y \end{cases} \quad (4.5)$$

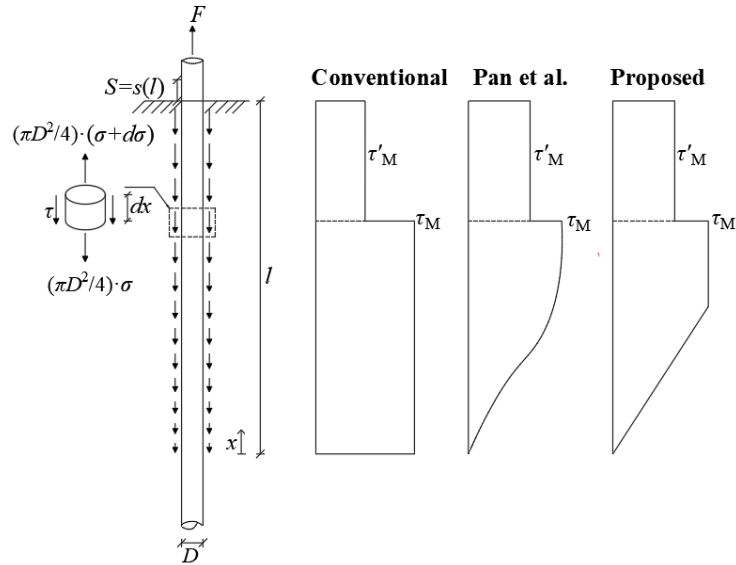


Figure 4.2. Bond stress distributions used in the conventional, Pan et al. (W. H. Pan et al., 2018), and proposed models

Assuming a uniaxial rebar stress-strain constitutive model shown as original in Figure 4.3, in which the relationship for rebar stress-strain within the strain hardening range is considered to be parabolic, the constitutive relationship can be written as:

$$\sigma = \begin{cases} E\varepsilon & 0 < \varepsilon \leq k_0\varepsilon_y \\ \sigma_y & k_0\varepsilon_y < \varepsilon \leq k_1\varepsilon_y \\ k_3\sigma_y + \frac{(1-k_3)(\varepsilon - k_2\varepsilon_y)^2 E}{(k_2 - k_1)^2 \varepsilon_y} & k_1\varepsilon_y < \varepsilon < k_2\varepsilon_y \end{cases} \quad (4.6)$$

where $k_0 = 1$, and k_1 , k_2 , and k_3 are factors used to specify the shape of the stress-strain relationship and are suggested to be 4.23, 46.9, and 1.36, respectively, by the literature (Tao & Nie, 2015). Consequently, the relationship between S and σ_b can be derived from Eqs. (4.1)-(4.3) as:

$$S(\sigma_b) = \begin{cases} \frac{\sigma_b^2 D}{8E\tau_M} & \sigma \leq \sigma_y \\ S_y + \frac{\sigma_y^2 (k_3 - 1)}{4E\tau'_M} \left[\frac{2}{3} k_1 (1 - (1 - \xi)^3) + \frac{1}{3} k_2 (1 - (1 - \xi)^2 (1 + 2\xi)) \right] \cdot D & \sigma > \sigma_y \end{cases} \quad (4.7)$$

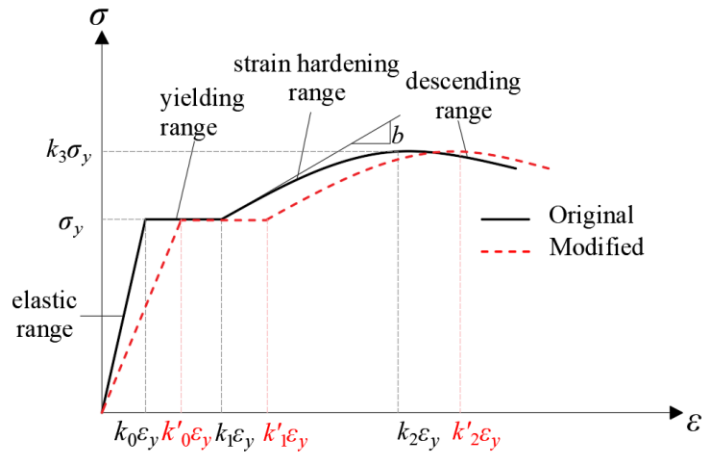


Figure 4.3. Uniaxial stress-strain constitutive model of rebar ($\sigma - \varepsilon$ relationship).

4.1.2. Pan et al. method

Pan et al. (W. H. Pan et al., 2018) pointed out assuming bond stress to be constant along the development length is oversimplified and does not accurately predict the anchorage slip prior to rebar yielding. In Pan et al. (W. H. Pan et al., 2018), they utilized the general macromodel framework but with an adoption of a much more realistic $\tau(x)$ obtained from a “real” bond-slip relationship $\tau(s)$. In particular, $\tau(s)$ used in Pan et al. (W. H. Pan et al., 2018) is developed based on a series of testing on rebar anchorage slip testing under the condition of long embedment length by Shima et al. (SHIMA et al., 1987), and is expressed as an exponential function shown below:

$$\tau(s) = \tau_M \left(1 - \exp \left[a \left(\frac{s}{D} \right)^b \right] \right) \quad (4.8)$$

where τ_M is the maximum bond stress, a ($= -40$) and b ($= 0.6$) are the model parameters whose values are calibrated by fitting the experimental data. In Equation (8), the bond stress τ gradually increases with the increase in s , until approaching the maximum bond stress τ_M . Pan et al. used Equation (8) to derive the bond stress distribution, $\tau(x)$, avoiding the oversimplification issue in the conventional method where a uniform distribution is assumed; thus, Pan et al. method is believed to have a more reliable prediction in rebar slip.

Using Eqs. (4.4) and (4.8), a second-order differential equation that relates the development length x and slip s is established for elastic range as:

$$\frac{d^2s}{dx^2} = \frac{4D}{E} \cdot \tau(s) \quad (4.9)$$

To solve Equation (4.9), it is converted into two first-order differential equations (and the details can be found in (OSU (Oregon State University), 1996; W. H. Pan et al., 2018)). As a result, the relationship between the development length x , slip S , and bond-slip $\tau(s)$ is expressed as:

$$x = \sqrt{\frac{ED}{8}} \int_0^s \frac{1}{\sqrt{T(z)}} dz = \sqrt{\frac{ED}{8}} \int_0^s \frac{1}{\int_0^z \tau(u) du} dz \quad (4.10)$$

where $T(s)$ is the primitive function of $\tau(s)$. Pan et al. numerically solved $\tau(x)$ for a given range of values of x based on Eqs. (8) and (10). Consequently, the normalized bond stress distribution $\tilde{\tau}$ ($= \tau/\tau_m$) is expressed as a function of the normalized development length $\tilde{x} = x/(aD)$ where $a = \sqrt{E/8\tau_m}$ which is plotted in Figure 4.4. Both bond stress and development length are normalized to the structural parameters (i.e., E , τ_m , and D) so the quantities become unitless for a general application.

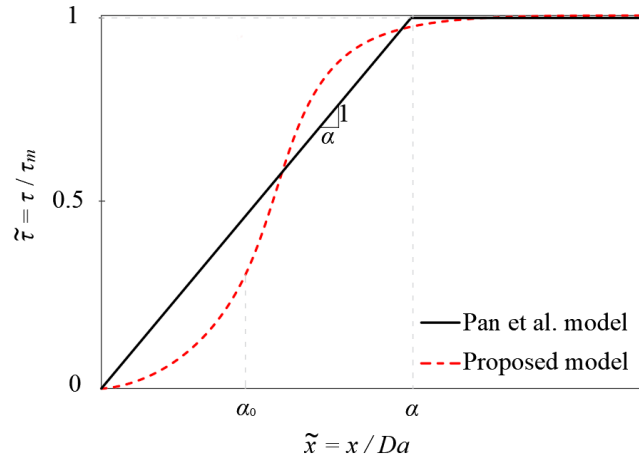


Figure 4.4. Normalized bond stress vs. normalized development length.

To obtain the relationship between slip S ($= s(l)$) as a function of rebar stress σ_b ($= \sigma(l)$), it is necessary to write an explicit function to fit the numerical results shown in Figure

4.4. Pan et al. (W. H. Pan et al., 2018) adopted two explicit functions (a polynomial function and an exponential function) to fit the two parts of the curve in Figure 4.4 by setting the separation point on the curve $\tilde{x} = \alpha_0 = 0.26$. Then through Eqs. (4.1) – (4.3) with further fittings and approximations, Pan et al. obtain the relationship between S and σ_b , shown below:

$$S = \begin{cases} \frac{4}{9} \cdot h(\tilde{\sigma}_b)^{4.5} & \sigma_b \leq \sigma_y \text{ \& } \tilde{\sigma}_b < 4\alpha_0^{3.5} \\ 0.255 \cdot h(\tilde{\sigma}_b)^2 - 0.034e^{-8.7 \cdot h(\tilde{\sigma}_b)} - 0.146h(\tilde{\sigma}_b) + 0.025 & \sigma_b \leq \sigma_y \text{ \& } \tilde{\sigma}_b \geq 4\alpha_0^{3.5} \\ S_y + \frac{\sigma_y^2(k_3 - 1)}{4E\tau'_M} \left[\frac{2}{3}k_1(1 - (1 - \xi)^3) + \frac{1}{3}k_2(1 - (1 - \xi)^2(1 + 2\xi)) \right] \cdot D & \sigma_b > \sigma_y \end{cases} \quad (4.11a)$$

$$h(\tilde{\sigma}_b) = \begin{cases} \left(\frac{\tilde{\sigma}_b}{4} \right)^{-3.5} \cdot D & \tilde{\sigma}_b < 4\alpha_0^{3.5} \\ \left[0.98(\tilde{\sigma}_b + 0.292) - 3.6e^{-12.5(\tilde{\sigma}_b + 0.292)} \right] \cdot D & \tilde{\sigma}_b \geq 4\alpha_0^{3.5} \end{cases} \quad (4.11b)$$

where $\tilde{\sigma}_b = \sigma_b / \sqrt{2\tau_M E}$, a normalized rebar stress, $\xi = (\varepsilon/\varepsilon_y)/(k_2 - k_1)$, in which should be numerically calculated from the portion where $\sigma > \sigma_y$ in Equation (4.6), S_y refers to the slip when $\sigma_b = \sigma_y$. The ultimate slip S_u associated with the ultimate rebar stress $k_3\sigma_y$ or rebar strain $k_2\varepsilon_y$ can be calculated as:

$$S_u = S_y + S_{sh} \quad (4.12)$$

where S_{sh} is the total slip within strain-hardening range and can be calculated by setting $\xi = 1$ in Equation (4.11):

$$S_{sh} = \frac{\sigma_y^2}{4E\tau'_M} (k_3 - 1) \left(\frac{2}{3}k_1 + \frac{1}{3}k_2 \right) \cdot D \quad (4.13)$$

Apparently, obtaining Equation (4.11) involves curve fittings and approximation. This means if any modification needs to be made in Equation (4.8) (e.g., updating the model parameters a or b with more bond stress-slip data), the whole process of curve fitting and approximation must be redone. This shows that the Pan et al. approach (W. H. Pan et al., 2018) is not easy to incorporate new information.

4.2. Proposed macromodel

While deriving the rebar slip model based on a real bond-slip relationship is a good idea, from a structural analysis point of view, it is more important to obtain accurate slip prediction through a simple practical approach. Thus, in this study, instead of deriving $\tau(x)$ from the bond-slip relationship (as in Pan et al. method), a bilinear function with one unknown model parameter α is implemented to directly replace the $\tilde{\tau}$ and \tilde{x} curve (shown in Figure 4.4), which is expressed as:

$$\tau(x) = \begin{cases} \tau_M \cdot \frac{x}{aD} \frac{1}{\alpha} & \text{for } \tilde{x} = \frac{x}{aD} < \alpha \\ \tau_M & \text{for } \tilde{x} = \frac{x}{aD} \geq \alpha \end{cases} \quad (4.14)$$

where the unknown parameter α can be assessed using the experimental results of the S and σ_b relationship. Using the bilinear function in Figure 4.4 provides explicit solutions to obtain the S and σ_b relationship; thus, it does not need any curve fitting and approximation as Pan et al. used, and it reduces computational complexity significantly.

Using Equation (4.1), one can obtain the rebar stress $\sigma(x)$ explicitly as:

$$\sigma(x) = \begin{cases} \frac{2}{\alpha \cdot a} \cdot \left(\frac{x}{D}\right)^2 \cdot \tau_M & \text{for } \frac{x}{aD} < \alpha \\ \sigma(x) = 2 \cdot \left(2\frac{x}{D} - \alpha \cdot a\right) \cdot \tau_M & \text{for } \frac{x}{aD} \geq \alpha \end{cases} \quad (4.15)$$

By letting $x = l$ and $\sigma_b = \sigma(l)$ one can inverse Equation (4.15) and find l in terms of σ_b as:

$$l = \begin{cases} \sqrt{\frac{\sigma_b}{2\tau_M}} \alpha \cdot a \cdot D & \text{for } \frac{\sigma_b}{\sqrt{2\tau_M E}} < \frac{\alpha}{2} \\ \frac{1}{2} \left(\frac{\sigma_b}{2\tau_M} + \alpha \cdot a \right) \cdot D & \text{for } \frac{\sigma_b}{\sqrt{2\tau_M E}} \geq \frac{\alpha}{2} \end{cases} \quad (4.16)$$

With the adopted steel constitutive law shown in Equation (4.6) and Equation (4.16), one can derive the explicit expression of the S and σ_b relationship, as shown below:

$$S(\sigma_b) = \begin{cases} \frac{\sigma_b}{3E} \cdot \sqrt{\frac{\sigma_b}{2\tau_M}} \alpha \cdot a \cdot D & \sigma_b \leq \sigma_y \ \& \ \frac{\sigma_b}{\sqrt{2\tau_M E}} < \frac{\alpha}{2} \\ \frac{2\tau_M}{E} \cdot \left[\left(\frac{\sigma_b}{4\tau_M} \right)^2 - (\alpha \cdot a)^2 \right] \cdot D & \sigma_b \leq \sigma_y \ \& \ \frac{\sigma_b}{\sqrt{2\tau_M E}} \geq \frac{\alpha}{2} \\ S_y + \frac{\sigma_y^2 (k_3 - 1)}{4E\tau'_M} \left[\frac{2}{3} k_1 (1 - (1 - \xi)^3) + \frac{1}{3} k_2 (1 - (1 - \xi)^2 (1 + 2\xi)) \right] \cdot D & \sigma_b > \sigma_y \end{cases} \quad (4.17)$$

To consider the corrosion impact on the bond strength, a reduction factor R is introduced and the bond stress τ_M is set as:

$$\tau_M = \begin{cases} 1.2\sqrt{f'_c} \cdot R & \sigma < \sigma_y \\ \tau'_M = 0.5\sqrt{f'_c} & \sigma \geq \sigma_y \end{cases} \quad (4.18)$$

One can set $R = 1 - 3.5Q$ (%) based on (Stanish et al., 1999) in which Q refers to corrosion mass percentage loss. The unknown parameter α is estimated by minimizing the

residual sum of squares where residual refers to the error between the predicted slip from Equation (4.17) and the actual slip from the experimental testing. In particular, a total of 19 rebar stress–slip test results (σ_b and S relations) are collected from literature, and the properties of the 19 experiment specimens are summarized in Table 3.1. Among the 19 specimens, 8 are corroded with corrosion levels varying from 1.3% to 10%. During the analysis, it is found the unknown parameter α is inversely proportional to $R \cdot \sqrt{f'_c}$; thus α is set as a function of an unknown parameter β by:

$$\alpha = \frac{1}{\beta \cdot R \cdot \sqrt{f'_c}} \quad (4.19)$$

As a result of the calibration, β is found to have a mean value of 0.5 and a standard deviation of 0.016. As shown in this session, the proposed model shown Equation (17) is an explicit macromodel solution without using curve fitting and other approximations, and the model is expressed explicitly as a function of model parameter α , meaning α is ready for updating when new experimental data becomes available.

Table 4.1. Specimen properties for collected testing results for rebar stress – slip relationship

Reference	Specimen label	Concrete strength, f'_c (MPa)	Rebar diameter, D (mm)	Rebar yield stress, σ_y (GPa)	Rebar elastic modulus, E (GPa)	Corrosion, Q (%)
Shima et al. (SHIMA et al., 1987)	SD30	19.60	19.5	0.353	190	0.0
	SD50	19.60	19.5	0.610	190	0.0
	SD70	19.60	19.5	0.820	190	0.0
Maekawa et al. (Maekawa et al., 2003)	Maekawa11	22.40	19.5	0.265	190	0.0
	Maekawa12	22.40	25.4	0.270	190	0.0
	Maekawa13	22.40	30.7	0.75	190	0.0
	Maekawa21	22.40	25.4	0.144	190	0.0
	Maekawa22	27.20	25.4	0.266	190	0.0
	Maekawa23	50.00	25.4	0.325	190	0.0
Ueda et al. (Ueda et al., 1986)	S64	28.75	25.4	0.172	200	0.0
	S101	19.92	31.8	0.520	200	0.0

Amleh (Amleh, 2000)	C5-5C	46.90	20.0	0.387	200	1.3
Jin (Wei-liang & Zhao, 2001)	D8	17.70	12.0	0.285	200	1.7
	D11	17.70	12.0	0.213	200	8.7
Zheng (Zheng, 2004)	D13	17.70	12.0	0.142	200	10.0
	S-8	29.2	20.0	0.303	200	2.5
	S-11	27.2	20.0	0.240	200	4.8
	S-12	27.2	20.0	0.255	200	5.4
	S-18	29.4	20.0	0.240	200	7.2

4.2.1. Bar slip comparison

Figure 4.5 compares rebar stress-slip curves obtained from the 19 experimental specimens collected from the literature (shown in diamond marks) with the results obtained from three prediction models (i.e., proposed model shown in solid lines, conventional method shown in dash-dotted line, and Pan et al. method (W. H. Pan et al., 2018) shown in dashed line). For some specimens (i.e., three specimens from Shima et al. (SHIMA et al., 1987): SD30, SD50, SD70, and two specimens from Ueda (Ueda et al., 1986): S64, S101), the predictions from all three models are similar and all match the experimental results well. However, for the rest of 14 specimens, the conventional model prediction is underestimated in slip and has the worst predictions compared with the other two models. This further confirms that assuming constant bond stress distribution is oversimplified, as suggested by Pan et al. (W. H. Pan et al., 2018).

When comparing the proposed model and Pan et al. model, their predictions are nearly the same for the 12 specimens shown in the first three rows of plots in Figure 4.5. The rebars in these specimens either have intact rebar (i.e., $Q = 0\%$) or very low corrosion (i.e., $Q = 1.3\%$ for specimen C5-5C). This indicates when there is no corrosion or slight

corrosion, the simplification adopted in the proposed model does not compromise accuracy. When examining the seven specimens in the last two rows of plots in [Figure 4.5](#), the difference in the prediction curves from the proposed model and Pan et al. model becomes apparent. Overall, the solid curves calculated by the proposed model are closer to the experimental data. For Specimens D11 and S-12, the proposed model still provides better yielding point prediction than Pan et al. model. Note that these seven specimens shown in the last two rows of the plot all have corrosion in rebar with Q varying from 1.7% to 10%. This result shows that the proposed model performs better for corroded specimens. This is not surprising as corrosion is incorporated in the reduction factor, R , in the model parameter α and bond strength τ_M .

In summary, one can conclude that the proposed model overperformed over the Pan et al. model, particularly when corrosion is present. In addition, the proposed model is more advantaged and preferred, as it is derived from explicit solutions by employing a simple bond stress distribution function over the development length, making the model more practical in engineering applications and ready for future updating when new experimental information becomes available. While the corrosion effect is incorporated through a reduction factor, a more sophisticated approach could be explored in the future to further improve the model prediction accuracy.

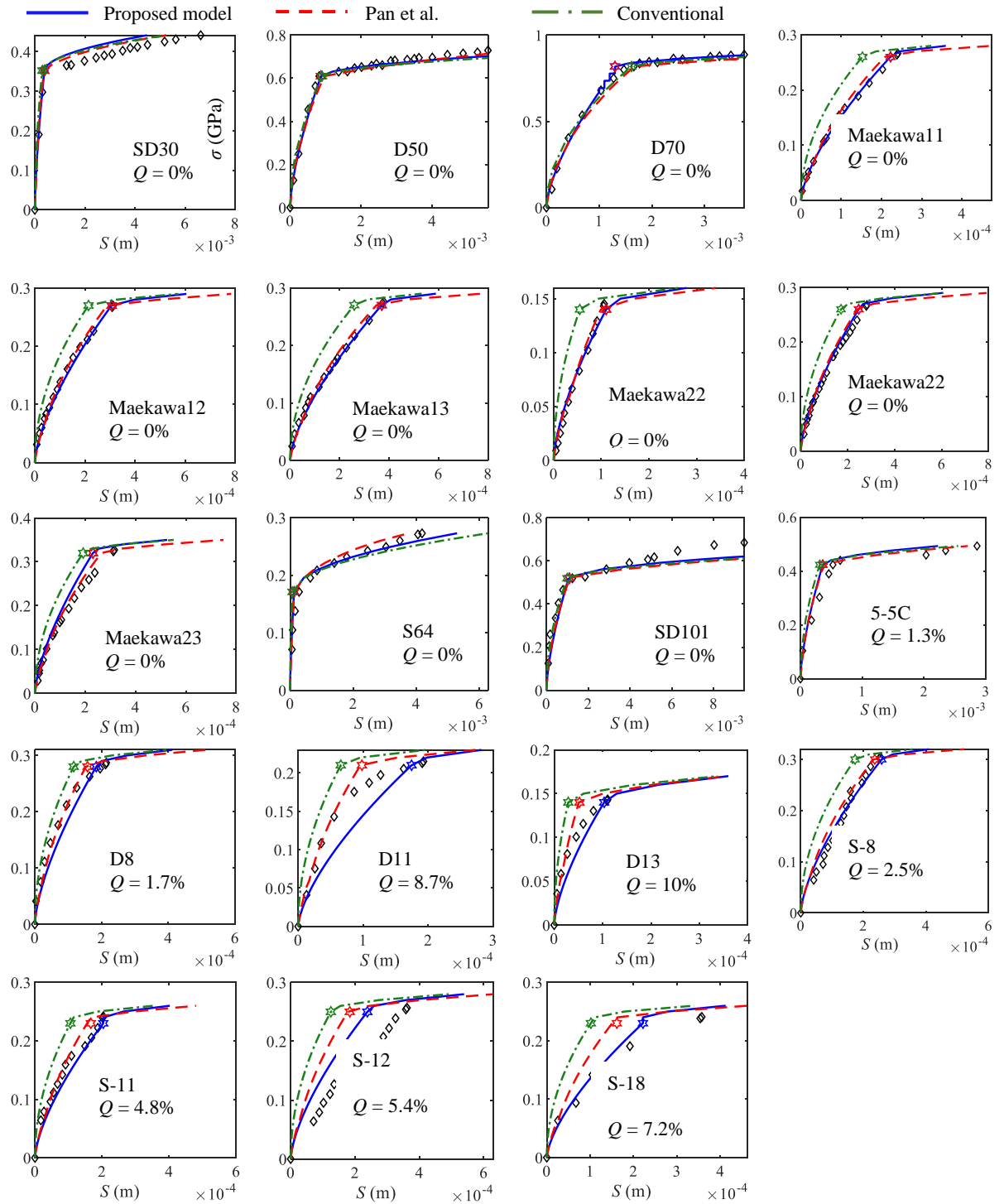


Figure 4.5. Predicted and measured stress-slip relationship for the experimental data.

4.3. Application of bar slip macromodel into the structural analysis

With the slip-rebar stress predicted from the proposed model, the uniaxial stress-strain skeleton curve of rebar can be modified to incorporate the rebar anchorage slip following Pan et al. (W.-H. Pan et al., 2017), such that the slip effect can be incorporated in the structural analysis. In this study, an open-source computer software OpenSees (GL Fenves et al., 2004) is adopted for the numerical analysis. In particular, the modified rebar constitutive model is implemented into the conventional fiber beam-column element in OpenSees. With such implementation, this section further evaluates the prediction accuracy of the proposed rebar slip macromodel and also investigates the slip effect on the flexural behavior of several RC columns and the seismic performance of a RC bridge column.

4.3.1. Modified rebar constitutive model

The reinforcement slip effect is considered in the uniaxial stress-strain skeleton curve of the rebar by adding the slip to the rebar strain. That is, the modified strain, ε' , is the summation of the original strain, ε , and the slip-induced strain, $\varepsilon_{\text{slip}}$:

$$\varepsilon' = \varepsilon + \varepsilon_{\text{slip}} \quad (4.20)$$

Note that the inelastic deformation of RC members is mostly in the plastic hinge region; thus, a slip-induced rebar fiber strain $\varepsilon_{\text{slip}}$ can be estimated by assuming the anchorage slip to be uniformly distributed over the plastic hinge length (as suggested by (Ueda et al., 1986)) as:

$$\varepsilon_{\text{slip}} = \frac{\text{slip}}{l_s} \quad (4.21)$$

where l_s is the plastic hinge length of the member that can effectually simulate the nonlinear deformation of the member end and one can set $l_s = 0.25h$, where h is the section height of the member, suggested by Bae and Bayrak (Bae & Bayrak, 2008).

For the uniaxial rebar constitutive model shown in Equation (19), the modification can be obtained by setting $k_0 = k_0'$, $k_1 = k_1'$, and $k_2 = k_2'$ in which

$$k_0' = 1 + \delta_y = 1 + \frac{S_y}{l_s \varepsilon_y} \quad (4.22)$$

$$k_1' = k_1 + \delta_y = k_1 + \frac{S_y}{l_s \varepsilon_y} \quad (4.23)$$

$$k_2' = k_2 + \delta_y + \delta_{sh} = k_2 + \frac{S_y}{l_s \varepsilon_y} + \frac{S_{sh}}{l_s \varepsilon_y} \quad (4.24)$$

where δ_y and δ_{sh} are the factors for the strain increments for the elastic and strain-hardening range of rebar, respectively. The modified rebar uniaxial stress-strain skeleton curve is compared with the original one in Figure 4.3.

4.3.2. Flexural behavior of RC columns

Flexural behavior of a total of 11 RC column specimens from literature is used to here validate the accuracy of the proposed rebar slip model. The design parameters and material properties of these 11 columns are summarized in Table 3.2, where the corrosion level, Q , varies from 0% to 20%, and the axial load ratio (i.e., vertical to lateral load ratio),

n , ranges from 0.18 to 0.6. It should be noted that the stirrups in the column experiments by Goksu (Goksu, 2012) and Meda et al. (Meda et al., 2014) are protected from corrosion, and thus, only longitudinal rebar are corroded in these experiments. Figure 4.6 shows the reinforcement and cross-section detailing for the column specimens. These columns were all tested under constant axial loading and various lateral displacements (either monotonic or cyclic) after being subjected to accelerated corrosion for $Q > 0$.

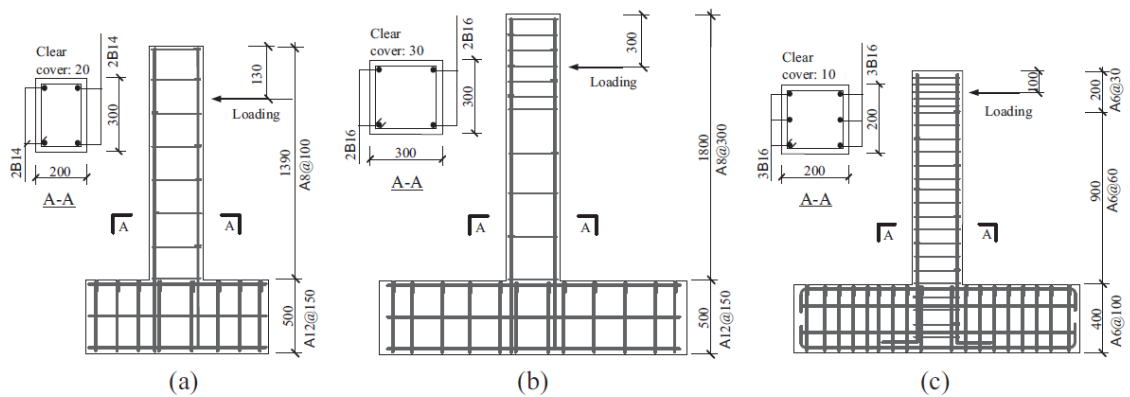


Figure 4.6. Geometry and configuration of the column specimens by (a) Goksu (Goksu, 2012), (b) Meda et al. (Meda et al., 2014), and Zheng et al. (S Zheng, L Dong, H Zuo, Q Qin, W Liu, 2018) (in mm)

Table 4.2. Properties of the test columns

Reference	Specimen	Core concrete strength, $f'_{c,core}$ (MPa)	Cover concrete strength, $f'_{c,cover}$ (MPa)	Yield strength of longitudinal rebar, f_y (MPa)	Corrosion, Q (%)	Loading type
Goksu (Goksu, 2012)	NS-X0	30.8	25.5	460	0.0	M
	NS-X9	30.8	18.2	401	9.0	M
	NS-X16	30.8	14.7	218	16.0	M
Zheng et al. (2018)	C-1	27.8	22.8	353	3.7	M
	C-2	28.1	24.6	373	0.0	M
	C-3	27.6	20.1	340	6.2	M
	C-4	28.1	24.6	373	0.0	C
	C-5	27.9	24.4	360	2.4	C
	C-6	27.6	20.1	340	6.2	C
Meda et al. (2014)	UC	21.4	20.0	353	0.0	C
	CC	21.4	10.6	353	20.0	C

Figure 4.7 shows the configuration of the OpenSees model of an RC column, where the displacement-based beam-column element with fiber section is used for modeling the cantilever column, and the modified fiber section is used between the two nodes that form the plastic hinge with length l_s . Using beam-column elements is appropriate, as the columns selected here are slender, thus, the contribution of shear effects to the displacement at top of the RC column can be neglected (Sezen & Moehle, 2006). In the modified fiber section, the constitutive relation for reinforcing steel material is constructed based on the modified stress-strain relationship shown in Figure 4.3. The confined concrete model proposed by Mander et al. (Mander et al., n.d.) and Kent-Scott-Park (B.D. Scott et al., 1982) unconfined concrete model are used for the concrete core and cover fibers, respectively. In addition, Eqs. (A.1)-(A.4) in Appendix D are also implemented in the OpenSees model to account for corrosion effect on the rebar diameter, D , rebar yielding strength, σ_y , rebar ultimate strength, σ_u , and concrete compressive strength f'_c , respectively.

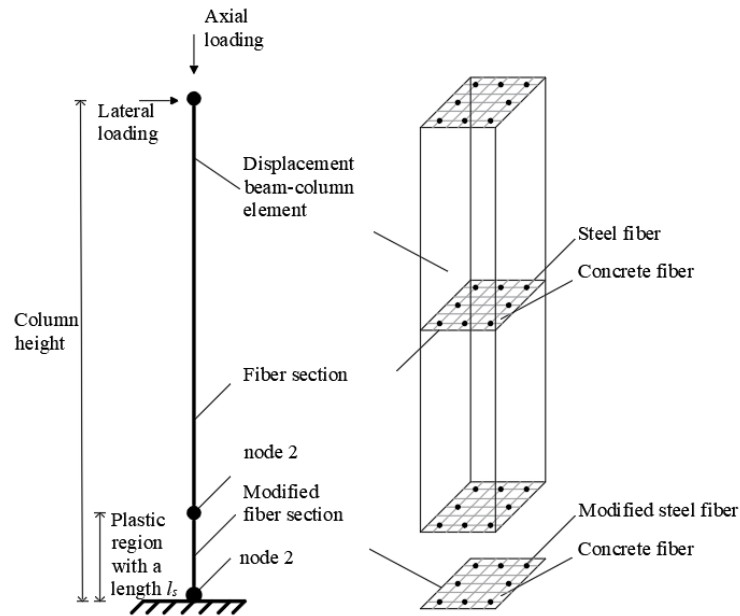


Figure 4.7. Configuration of OpenSees model of an RC column

Monotonic behavior

Figure 4.8 compares the lateral force-displacement curves of 6 RC columns under monotonic loading with the ones estimated using the OpenSees numerical models (with two modeling scenarios: considering rebar slip or not). Note that the corrosion effect on rebar size, rebar strength, and concrete strength is accounted for all OpenSees models. Apparently, the curves estimated by OpenSees models considering rebar slip (shown in dashed lines) are in a better agreement with the experimental results than the ones estimated by the OpenSees models without considering rebar slip (shown in dash-dotted lines). Without considering rebar slip leads to stiffer behavior as expected. This difference is more significant for the higher corroded specimens (i.e., $Q = 9\%$ in Figure 4.8 (b) and $Q = 16\%$

in Figure 4.8 (c)) compared with the other four specimens. In addition, the OpenSees model considering rebar slip predicts better column strength.

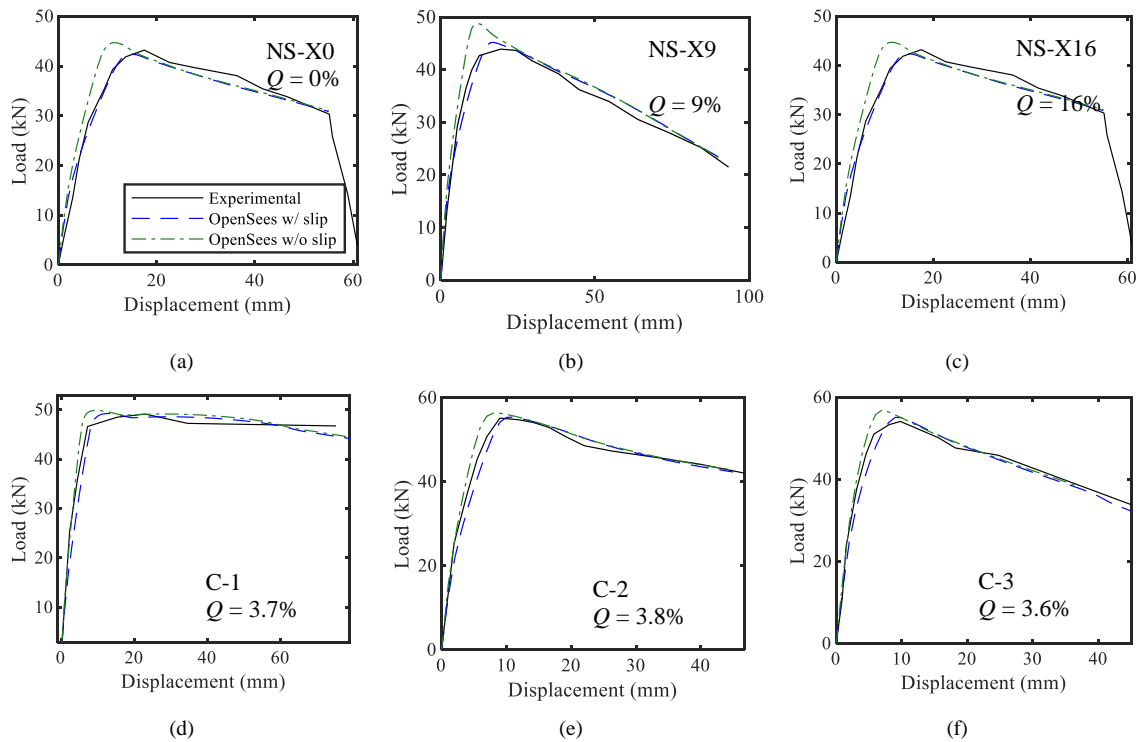


Figure 4.8. Measured and estimated lateral force-displacement response of the columns using OpenSees models

In addition, Figure 4.8 (c) shows that the initial stiffness of the experiment is slightly lower than the OpenSees model considering rebar slip, which could be due to the existence of severe cracking caused by the high level of corrosion for this specimen ($Q = 16\%$). Other slight differences between the experimental data and the calculated response in Fig. 8 could be due to some other reasons, such as OpenSees models do not consider the corrosion in stirrups and shear degradation. Furthermore, Figures 4.8 (d)-(f) show the force-displacement responses of the three corroded experiments with a similar corrosion

level but with axial load ratios of 0.2, 0.4, and 0.6, respectively. It can be seen that, by increasing the axial load ratio, the actual peak lateral load capacity increases, and the degradation portion of the curve becomes steeper. For all three cases, the OpenSees models perform well both in ascending and descending portions of the curves.

Table 3.3 shows the maximum shear strength V_{model} and the corresponding displacement, d_{model} , estimated by the OpenSees models compared with the measured shear $V_{\text{experiment}}$ and measured displacement, $d_{\text{experiment}}$. It is obvious that the proposed model with the consideration of rebar slip has a much better performance to capture the base shear and displacement of the experiments; thus, considering rebar slip in the model is necessary.

These observations from Figure 4.8 and Table 3.3 lead to the following conclusions: rebar slip needs to be considered in predicting flexural behavior of RC columns; the proposed rebar slip model is validated; and also the corrosion impact on the rebar slip cannot be ignored, which further shows the advantage of the proposed rebar slip model, as it accounts for the corrosion effect.

Table 4.3. Calculated and actual capacity of the experiment columns tested under monotonic loading.

Specimen	$V_{\text{experiment}}$ (kN)	$V_{\text{model}}/V_{\text{experiment}}$ (considering slip)	$V_{\text{model}}/V_{\text{experiment}}$ (w/o considering slip)	$d_{\text{experiment}}$ (mm)	$d_{\text{model}}/d_{\text{experiment}}$ (considering slip)	$d_{\text{model}}/d_{\text{experiment}}$ (w/o considering slip)
NS-X0	53.4	0.97	1.02	15	1.07	0.75
NS-X9	43.9	1.03	1.11	19	0.84	0.69
NS-X16	43.2	0.98	1.03	17	0.82	0.79
C-1	49.1	1.01	1.01	15	0.73	0.64
C-2	55.1	1.01	1.02	9	1.11	0.70
C-3	54.1	1.02	1.05	10	0.90	0.78

Cyclic behavior

Figure 4.9 compares the cyclic behavior of 5 experimental columns with the ones estimated from the OpenSees model (with two modeling scenarios: considering rebar slip or not). These five columns with various axial loads ratios include two without corrosion and three with corrosion (in particular, Specimen CC has $Q = 20\%$). It can be seen that the cyclic curves obtained from OpenSees model considering slip overall performs well in detecting the shape of the hysteretic loop, the lateral load resistance, and the initial stiffness. Moreover, the gradual reduction in strength, stiffness, and pinching effects with increasing cycles are demonstrated reasonably well by the OpenSees model. It is evident that the OpenSees model that uses the proposed macromodel is applicable for uncorroded and corroded specimens.

When comparing the results obtained the OpenSees model with and without slip, the differences in the cyclic behavior are noticeable and the ones based on the model with slip are closer to the experimental curves. Therefore, it can be concluded that the contribution of bar slip deformation to the lateral displacement of the member should be considered, and the proposed rebar slip macromodel that used in the OpenSees model provides accurate cyclic behavior of RC columns.

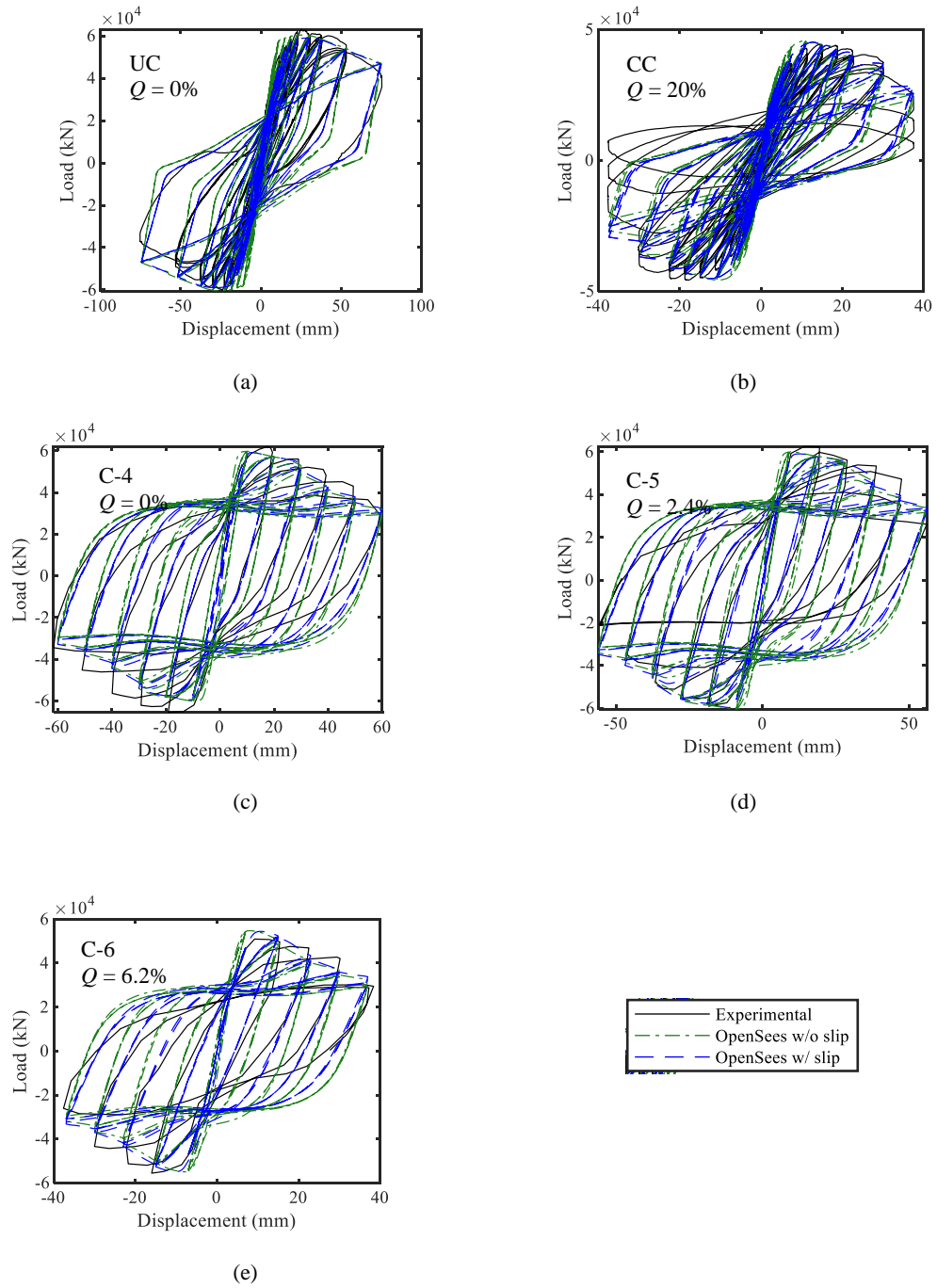


Figure 4.9. Calculated and measured cyclic response of the columns tested by Zheng et al. (S Zheng, L Dong, H Zuo, Q Qin, W Liu, 2018) and Meda et al. (Meda et al., 2014) using the proposed model

4.3.3. Seismic performance of a RC bridge column

In this section, the OpenSees model with the implementation of the proposed rebar slip macromodel is used to investigate the impact of the rebar slip on the structural performance of a highway RC bridge with single-column bent. In this study, an example bridge based on a typical construction in California used in (Huang et al., 2010b) is simulated in OpenSees. The configuration and the bridge design parameters are shown in Figure 4.10 and Table 3.4, respectively. Further details are referred to (Huang et al., 2010b).

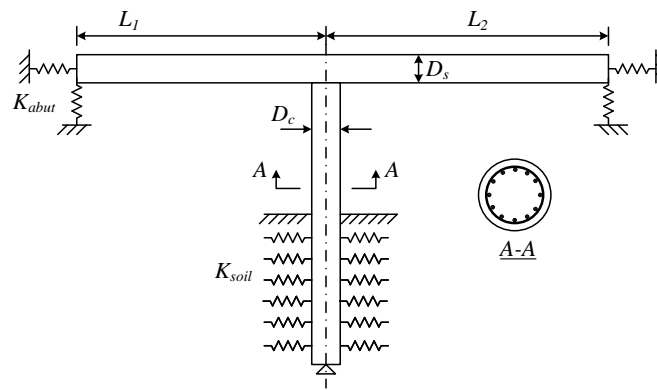


Figure 4.10. Configuration of the example RC highway bridge with single-column bent

Table 4.4. Design parameters of the example bridge with one single-column bent

Design Parameter	Value
Degree of skew, α	0°
Span (the shorter one), L_1	30.480 m
Column height, H_c	6.706 m
Column diameter-to-superstructure depth ratio, D_c	1.572 m
Reinforcement nominal yield strength, f_y	437.835 MPa
Transverse reinforcement nominal yield strength, f_{yh}	350.268 MPa
Concrete nominal strength, f'_c	35.027 MPa
Longitudinal reinforcement ratio (column), ρ_l	3.59%
Transverse reinforcement ratio (column), ρ_s	1.06%
Additional bridge dead load, w_t	45% self-weight
Pile soil stiffness, K_{soil}	(USGS) C
Abutment models, K_{abut}	C
Two-span ratio, L_2/L_1	1.25
Column concrete cover	0.038 m

In OpenSees, four scenarios are considered: two considering rebar slip in the column section by implementing the modified rebar fiber with $Q = 0$ and $Q = 20\%$, respectively, and the other two without considering rebar slip in the column section with $Q = 0$ and $Q = 20\%$, respectively. For each scenario, a nonlinear static pushover and time-history analysis of three selected ground motions are conducted.

The results of the pushover analysis are shown in [Figure 4.11](#). By comparing the pushover curves of the scenarios with and without rebar slip for the same corrosion level, it can be seen that considering slip the bridge column stiffness becomes softer and the strength is much lower, as expected. Such difference becomes smaller for $Q = 20\%$, as the corrosion impact on rebar size and material properties starts playing a role as well. The significant difference between the results based on the numerical models with and without considering

rebar slip in both [Figure 4.11](#) indicates that the rebar slip needs to be considered to accurately reflect the structural performance.

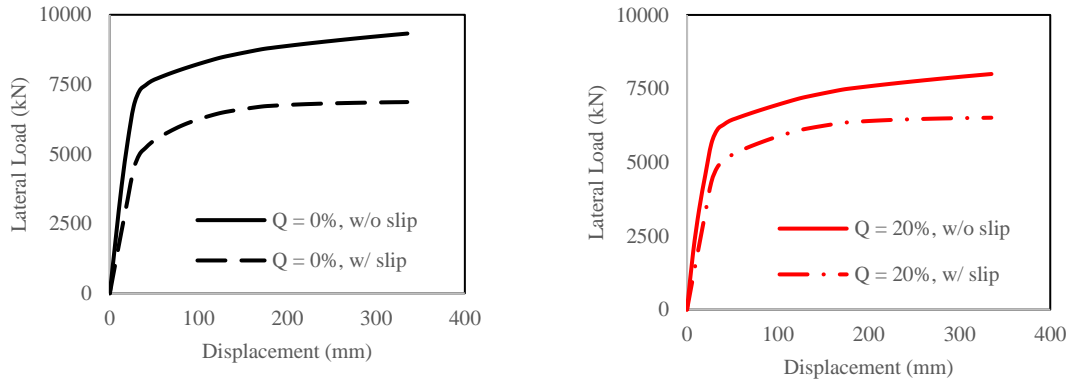


Figure 4.12. Pushover results for the bridge column under various cases based on corrosion and slip

To study the rebar slip impact on seismic performance of the example RC bridge, OpenSees models are subjected to three selected seismic excitations through nonlinear time-history analysis. The details of the three ground motions are provided in [Table 3.5](#).

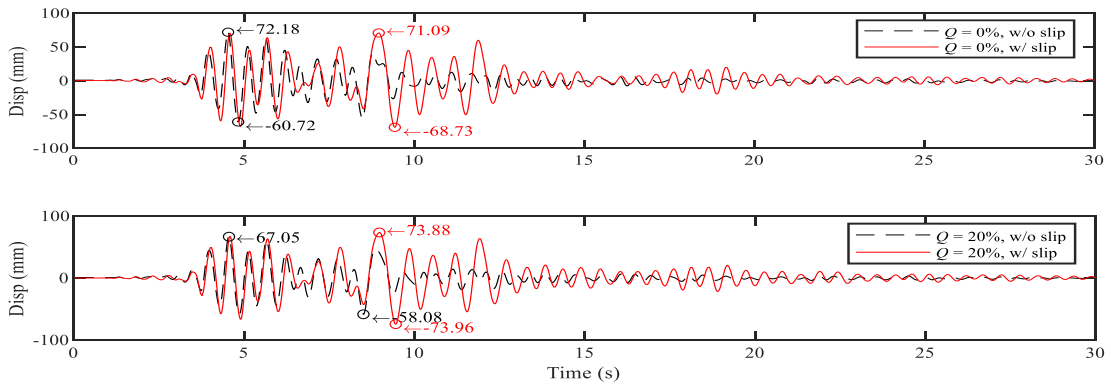
Table 4.5. Ground motion records used in the time-history analysis

Earthquake name	Year	Record series number (RSN)	Station	Magnitude
Northridge	1994	952	Beverly Hills	6.7
Tabas	1978	143	Tabas	7.35
Kobe	1995	1119	Takarazuka	6.9

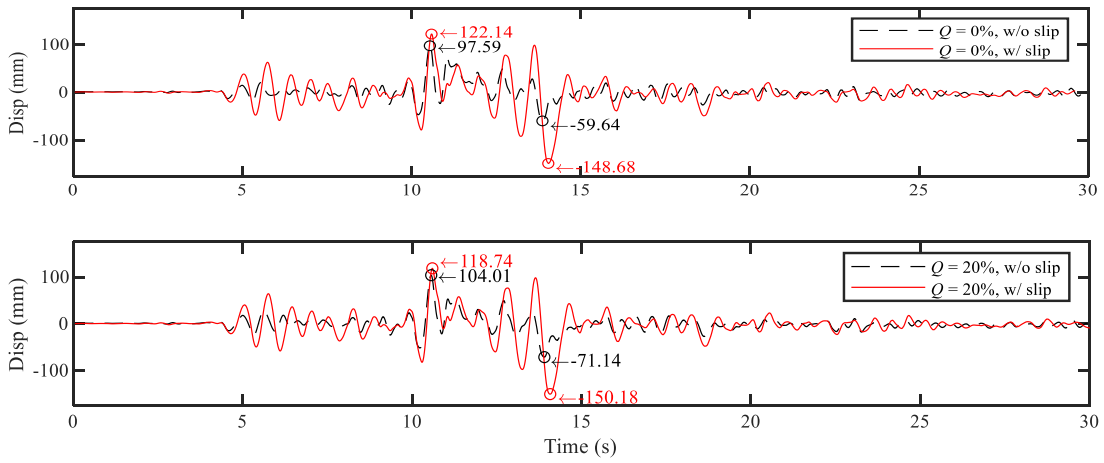
The displacement responses of the time-history analysis using OpenSees models with and without considering slip are compared in [Figure 4.13](#), where the red solid line and the black dashed line refer to the response from the model with considering slip and without considering slip, respectively. Both positive and negative peak responses are pointed out.

First, one can notice that the peaks for both models do not necessarily occur at the same time. For the same corrosion level, the responses of the model that considers slip (shown in red solid line) have larger peak values as expected (particularly true for Tabas

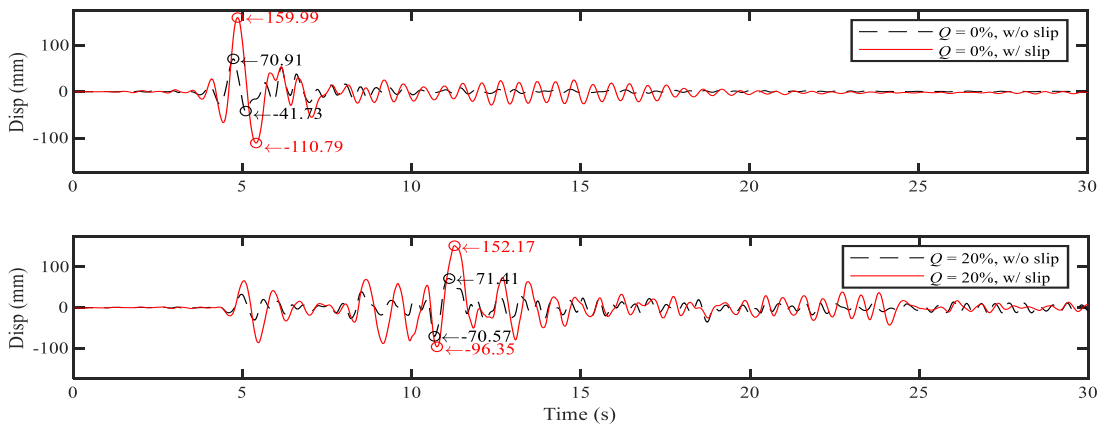
and Kobe earthquakes). This indicates the importance of incorporating slip effect in evaluating seismic behavior of a RC column. Moreover, when considering the slip, the peak responses of the model with $Q = 20\%$ are larger than the ones of the model with $Q = 0\%$. This shows that the presence of corrosion further softens the stiffness of the structure and it is another contribution to the displacement response.



(a) Northridge



(b) Tabas



(c) Kobe

Figure 4.13. Time-history response of three selected ground motions

Furthermore, seismic deformation fragility is estimated for this RC bridge column, and is defined as the condition probability that the deformation response attains or exceeds a capacity level for given earthquake intensity (e.g., pseudo acceleration spectrum of the first period, S_a). As shown in previous studies (e.g., (Dyanati et al., 2015)), the variability in the demand model error and model parameters dominates the limit state. Thus, for simplicity, the uncertainties in material and geometric properties are ignored. The deformation demand is adopted from Gardoni et al. (Gardoni et al., 2002) where the model error and statistics of the model parameters are provided. The capacity is calculated based on the yield displacement due to flexural as following:

$$\Delta f = \frac{1}{3} \phi_y (H_c + YP)^3 \quad (4.24)$$

where ϕ_y = curvature at yield, YP = depth of the yield penetration into the column base and is estimated as $YP = 0.022f_y D$ suggested by (Mander et al., n.d.).

Figure 4.13 (a) and (b) show the deformation fragility curves of the bridge column with $Q = 0$ and $Q = 20\%$, respectively. Regardless of the corrosion level, considering slip greatly reduce the probability of failure for a given S_a . This is particularly apparent for $0.5g < S_a < 1.25g$. This is expected as considering slip provides more ductility to the column. The impact of slip is significant in the seismic performance evaluation.

Kashani et al., 2013)), and some experimental studies can be found on the cyclic responses of RC structures with corroded reinforcement (e.g. (A. Guo et al., 2015; Ma et al., 2012; Meda et al., 2014; Ou et al., 2012)) only found in the past decade. Extremely limited studies have been performed on studying cyclic bond deterioration due to corrosion. Among those studies, Fang et al. (C. Fang et al., 2006; C. Q. Fang, 2006), Zhao et al. (Zhou, Lu, Xv, Dong, et al., 2015; Zhou, Lu, Xv, Zhou, et al., 2015), Kivell et al. (Kivell et al., 2011) conducted experimental testing to study on corrosion effect on bond-slip relation. In particular, Kivell et al. (ref.) is the only study that developed analytical cyclic bond models considering corrosion. Nevertheless, there are major limitations in the models proposed by Kivell et al. (ref.): *i*) the models are developed based on pullout testing that is not suggested for use in the prediction modeling of the bond response; *ii*) the modification factors used in the models only consider the confinement content and corrosion level, and these two factors are studied separately not interactively; *iii*) other key factors such as compressive strength and the ratio of cover depth to rebar diameter are not considered in model, limiting the application of the models and restraining the models to be updated by possible future experiments; and *iv*) the prevailing uncertainties, such as statistical uncertainties and model errors are not considered.

In summary, to develop a reliable constitutive bond stress-slip relationship, a large database of test results of beam-end or beam specimens is needed. Therefore, all possible important factors (namely, the size of steel bars, the ratio of concrete cover to bar diameter, the concrete compressive strength, content of confining reinforcement, and type of confinement) and all relevant uncertainties should be incorporated in the bond constitutive

law based on a probabilistic approach such that the probabilistic models can be easily updated whenever any future experimental data becomes available.

4.4.1. Probabilistic development of bond stress-slip constitutive law considering corrosion effect

The idea of developing the proposed probabilistic bond stress-slip constitutive law is to modify the available formulation by probabilistically re-assessing the bond model parameters.

4.4.1.1. Bond behavior under cyclic loading

Similar to monotonic behavior, extensively discussed in Chapter III, several researchers developed bond behavior models under cyclic loading. The general cyclic bond model that has been used for many years is developed by Eligehausen et al. (Eligehausen et al., 1982) for uncorroded bars as shown in [Figure 4.17](#).

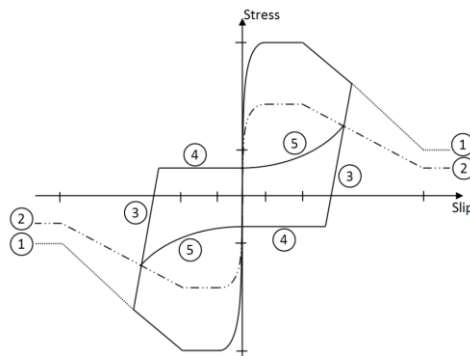


[Figure 4.17](#) General schematic of proposed cyclic bond model

Kivell et al. (Kivell et al., 2015) studied the effects of corrosion on cyclic bond behavior based on pull-out test results of corroded specimens, where they adopt the general

model of Eligehausen et al. (Eligehausen et al., 1982), modify the maximum bond strength as a function of corrosion level and accordingly, cyclic bond stresses are modified. In particular, the maximum bond strength is calculated based on the multiplication of a factor that is a function of corrosion level and the uncorroded bond strength; thus, it requires the result of the uncorroded specimen to be able to predict the bond strength of corroded specimen. Furthermore, no relationship is found for the slip corresponding to bond strength, s_1 , as well as s_2 , and s_3 to incorporate corrosion and to modify the whole cyclic behavior. It is also noted that in the experiment design of Kivell et al.'s work, the only design variable is the level of corrosion, and other parameters found to be critical to affect the cyclic behavior have been kept constant, such as rebar diameter, concrete compressive strength, cover size, confinement, etc. Recently, Lin et al. (H Lin et al., 2017) in a study on bond behavior of corroded steel bar, however under repeated loading (fatigue loading), showed that peak slippage, s_1 (or s_u) can be a function of corrosion level. However, not enough explanation is provided and the need for a further study is suggested for modeling the peak slippage.

4.4.2. Preliminary findings

Some preliminary studies are performed to identify the relation of key bond parameters with the number of cycles and as well as structural parameters. [Figure 4.18](#) shows the important parameters that found to be impacted by the cyclic behavior (Kivell et al., 2011) that are τ_{\max} , τ_s , and S_{\max} . τ_{\max} refers to the maximum stress generated in each cycle, τ_s refers to the remaining frictional stress at the end of each cycle, and S_{\max} refers to

the maximum slip achieved at the end of each cycle. Figure 4.18 (a) and (b) shows the schematic and a typical cyclic behavior, respectively.

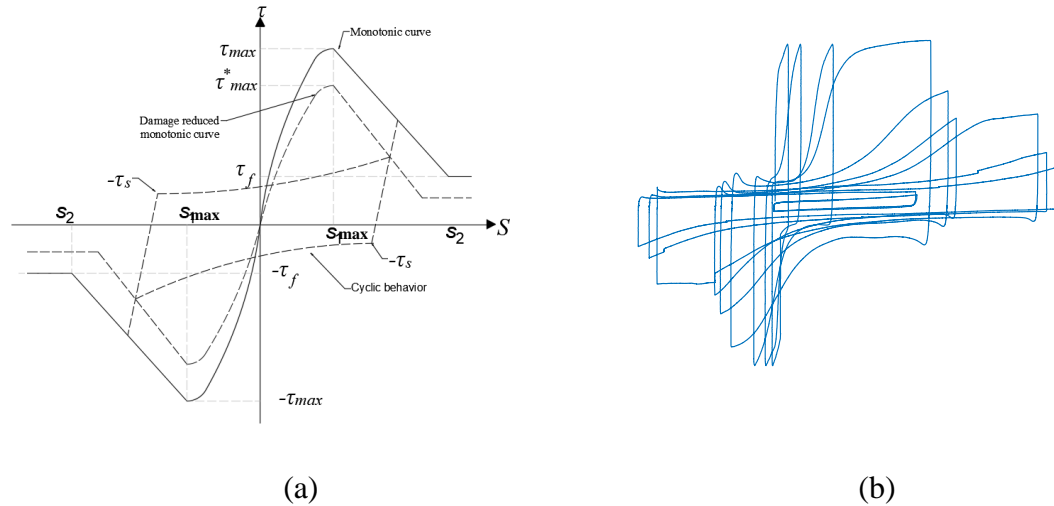


Figure 4.18. (a) Schematic and (b) a typical cyclic behavior

The relationship between three parameters, τ_{max} , τ_s , and S_{max} are compared with number of cycles and the structural parameters in order to explore possible model development for the cyclic bond-slip behavior. In particularly, the following five scatter plots are made:

- τ_{max} vs. number of cycles
- τ_s vs. number of cycles
- S_{max} vs. number of cycles
- τ_{max}/S_{max} vs. $Q, f'_c, D, C, C/d$
- τ_{max}/S_{max} vs. $Q \times f'_c$, etc.

It's worthy to note that in the scatted plots, only the first cycle of each set of cycles is used. They are Cycles #1, #4 and #7 as shown in the blue line in Figure 4.19.

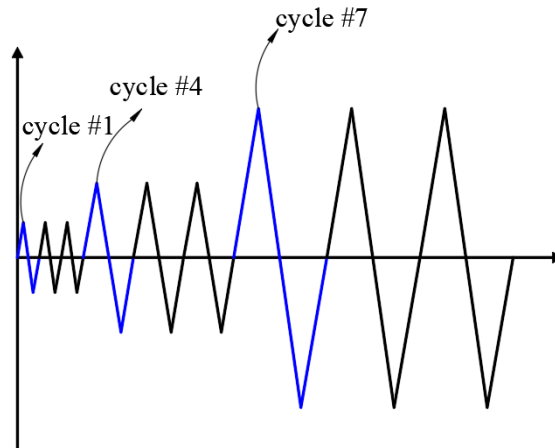


Figure 4.19. Cycles number 1, 4, and 7 used for the comparison purposes

4.4.2.1. Preliminary observations

Based on the argument presented in the previous section, Figures 4.20 - 4.22 are generated. Figures 4.20 - 4.22 provides potential relationship between τ_{\max} , τ_s , and S_{\max} with the number of cycles, structural parameters and structural parameter's interactions, respectively. Note that in Figures 4.20 - 4.22 the parameters τ_{\max} , τ_s , and S_{\max} for the vertical axes are normalized to their predicted values, based on the monotonic models, as discussed in Chapter III.

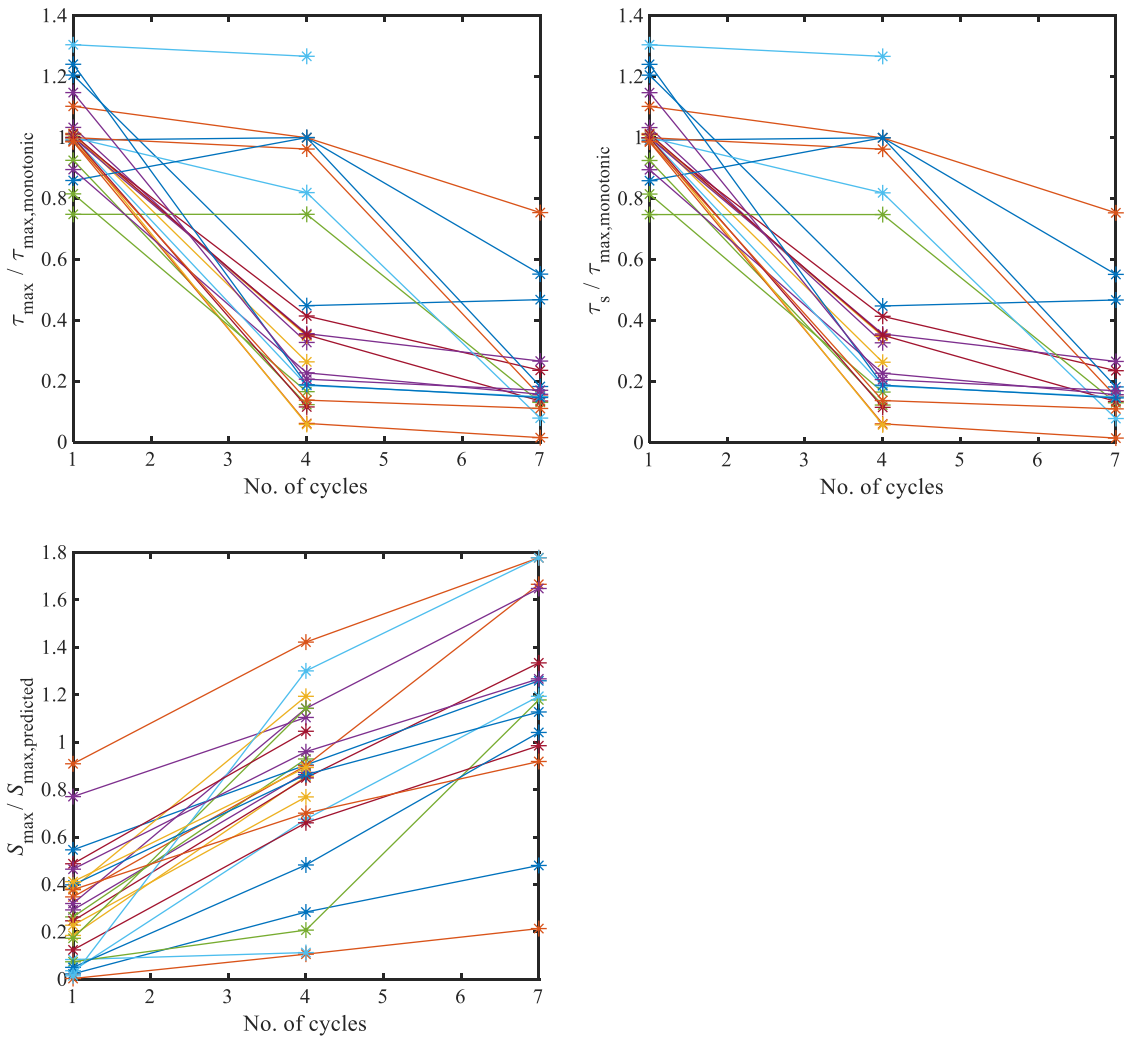


Figure 4.20. Scatter plots of τ_{\max} , τ_s , and S_{\max} vs. the number of cycles.

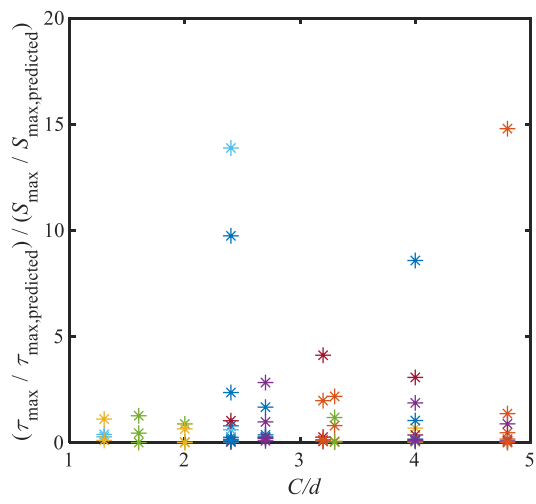
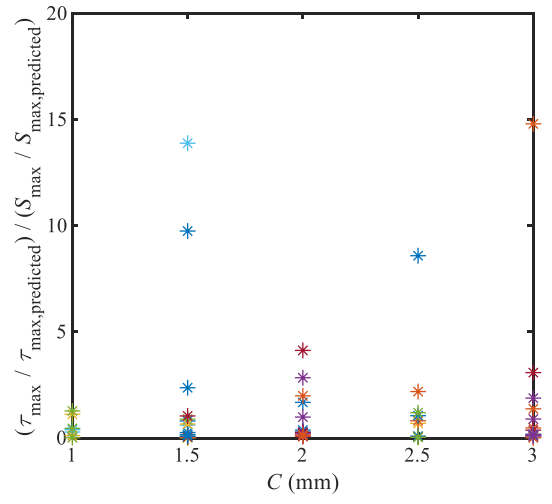
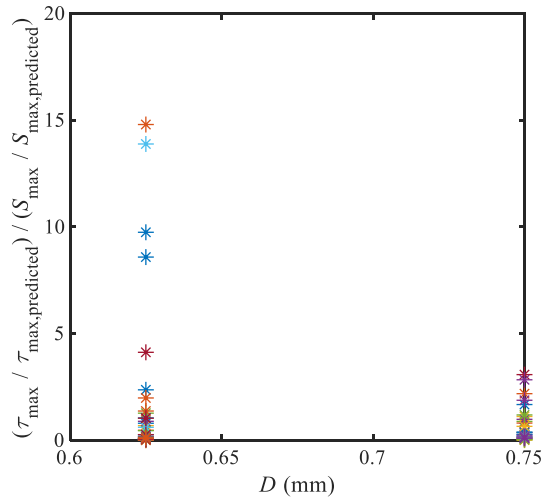
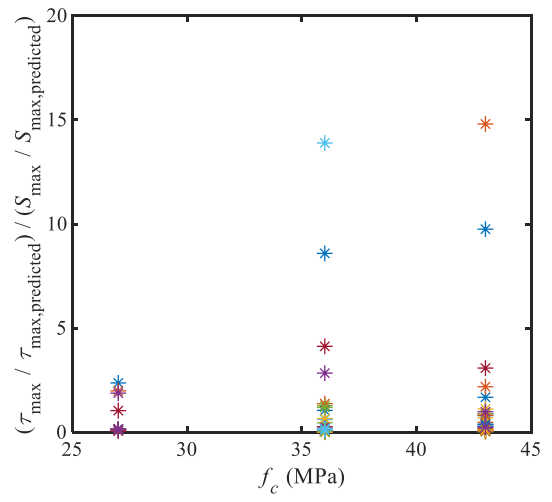
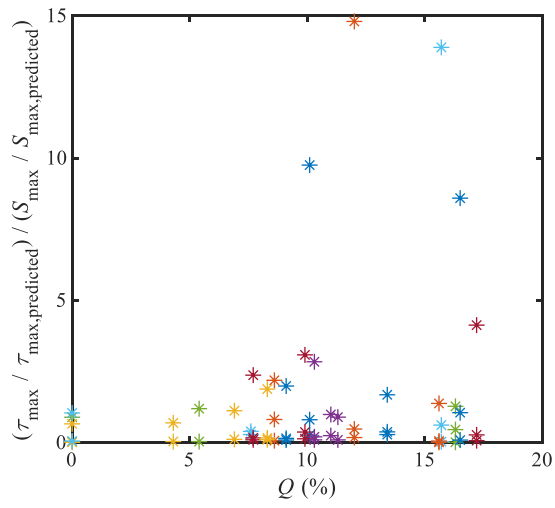
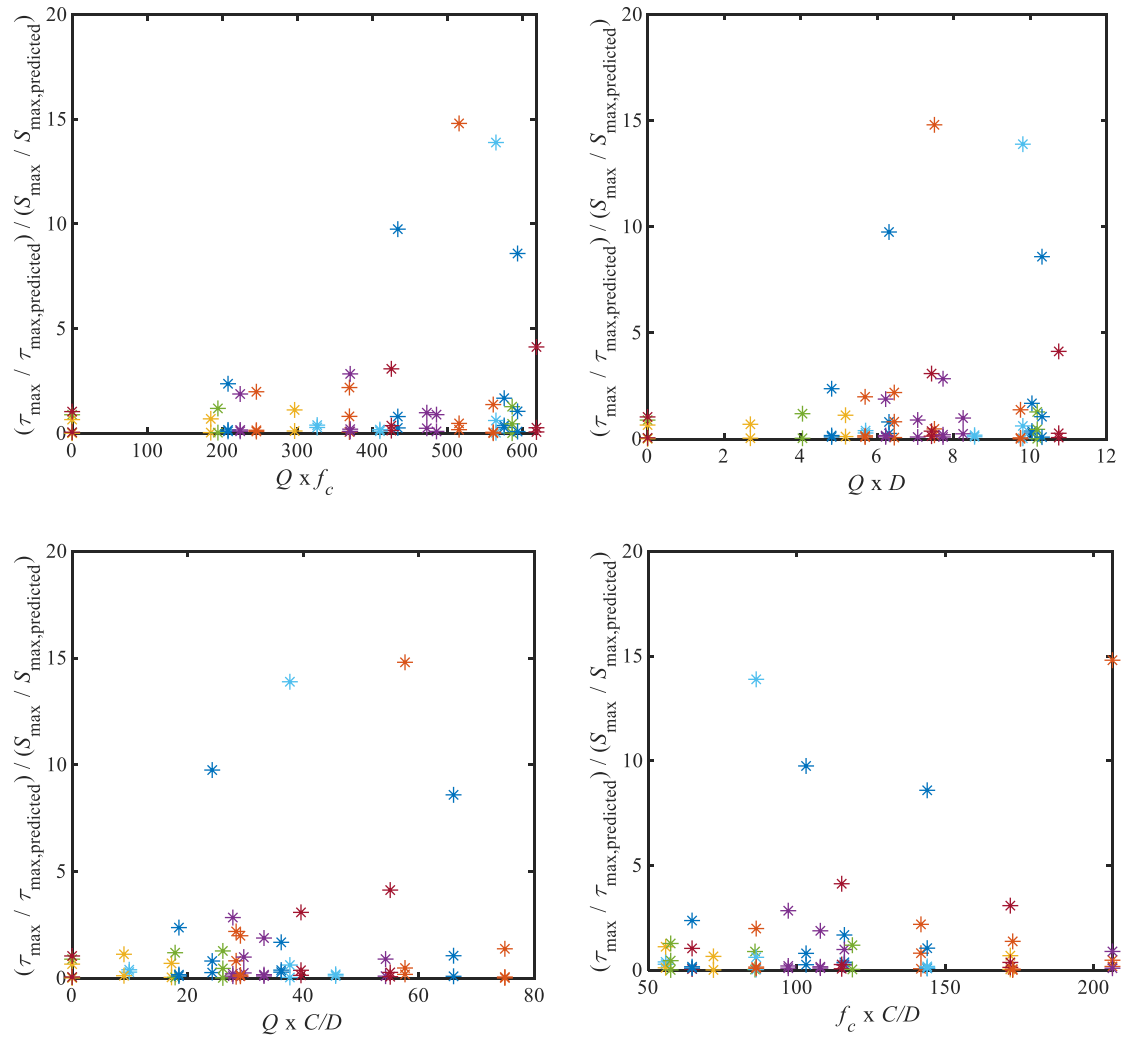


Figure 4.21. Scatter plots of τ_{\max} , τ_f , and S_{\max} (normalized to the predicted values from monotonic models) vs. the structural parameters.



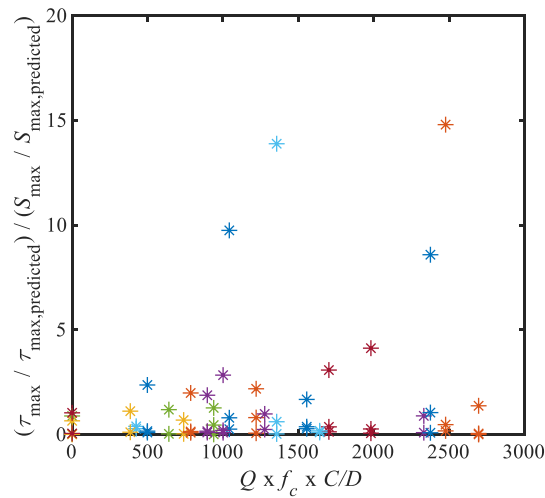


Figure 4.22. Scatter plots of τ_{\max} , τ_f , and S_{\max} (normalized to the predicted values from monotonic models) vs. structural parameter interactions.

Figure 20 shows the relationship between the normalized τ_{\max} , τ_s , and S_{\max} and the number of cycles. The following observations can be made:

- The parameter τ_{\max} and τ_s (as shown in Figure 4.20 (a) and (b), respectively) is reduced due to the cyclic loading.
- The reduction in τ_{\max} and τ_s (as shown in Figure 4.20 (a) and (b), respectively) is more significant in the first and second set of cycles, while this reduction becomes less in the last set of cycles for most of cases.
- The amount of slip that is achieved in each set of cycles increases (as shown in Figure 4.20 (c)).
- The increased slip in Figure 4.20 (c) is sometimes more significant in first sets of cycles, and sometimes greater in last set of cycles.

Figure 4.21 and 4.22 show the relationship of τ_{\max} (or $\tau_{\max} / \tau_{\max,\text{predicted}}$) normalized to S_{\max} ($S_{\max} / S_{\max,\text{predicted}}$) versus some structural parameters such as corrosion level Q , concrete strength f'_c , rebar diameter D cover C , and C/d ratio and versus the interactions of the structural parameters. No strong trend is observed from the plots. It is suggested that more analysis are needed to find a relationship between bond behavior parameters, such as τ_{\max} and S_{\max} with structural parameters in order to describe the whole cyclic behavior.

CHAPTER V

SUMMARY AND CONCLUSIONS

Sufficient bonding of rebar to concrete is crucial to ensure the reliable performance of RC structures, particularly in the corroded structures. Whilst much research has investigated the bond strength, the impact of the bond failure mode (i.e. pull-out or splitting) coupled with corrosion on bond behavior and structural performance has been given little attention. This bond behavior between the rebar and concrete plays a crucial role in the structural performance of RC structures particularly in the presence of corrosion deterioration on the rebar. Such bond behavior varies based on structural properties as well as bond failure modes. For a better RC structural evaluation, the two critical parameters to model the bond behavior, average bond strength (τ_{avg}) and peak slip (s_1), need to be predicted accurately for each bond failure mode with consideration of corrosion.

Regarding the bond failure mode, by taking advantage of machine learning classifications, a probabilistic model was developed to estimate the bond failure mode. Specifically, logistic and lasso classification techniques are found to be suitable for engineering practice, as they provide explicit formulations. The developed model is based on the results of bond tests for 132 beam-end specimens with various influencing parameters such as concrete compressive strength, rebar diameter size, cover size, corrosion level, and loading type (i.e., monotonic or cyclic). To evaluate if the bond

behavior under corrosion affects the performance of a structure, the flexural performance of an RC beam with a lap splice under various levels of corrosion is evaluated by conducting a reliability analysis.

For bond strength, the multivariate nonlinear regression approach is adopted using explanatory functions consist of structural parameters that are showed correlation with bond strength in the literature, corrosion level, as well as the loading type of the structure (i.e., monotonic or cyclic loading). The final formulations of the prediction models for bond strength under splitting and pull-out bond failure are then obtained using all-possible subset model selection. For peak slip, a symbolic multi-gene regression technique (SMGR), genetic programming (GP) approach, is adopted to find a meaningful relationship between the influencing parameters and the peak slip, where the inputs are the parameters identified in the literature that affects peak slip. Considering a good trade-off between model complexity and accuracy, an optimum model is chosen among the produced models for peak slip in the pull-out, while SMGR fails to generate a practical model for s_1 in the splitting. Consequently, a beta distribution is used for peak slip in splitting to remove the prediction bias. It is also worthy to note that the proposed models are empirical; thus, the application of those models are suitable for the cases with the variables that are within the ranges of the training dataset. However, since the collected data are comprehensive and cover a wide range of variables, it is expected that the proposed models would perform well in most of the cases, and yet can be easily updated when more data become available.

To capture the rebar anchorage slip, this study develops a simple bar stress-slip macromodel, where it uses a bilinear function to describe the bond stress distribution and

its model parameter is calibrated based on experimental bond stress-slip data. The proposed rebar slip model is then used to modify the rebar stress-strain constitutive law in order to incorporate slip in the structural analysis. In particular, a fiber beam-column element model that uses the modified rebar constitutive relations in OpenSees is applied to model RC columns to investigate the slip effect on the flexural behavior and seismic behavior of the RC columns. The proposed model has advantages over previously developed models as it is a simple model without compromising accuracy, expressed explicitly that considers structural properties such as concrete strength and corrosion level and can be updated easily when new experimental data becomes available that makes the proposed model more practical in engineering applications.

The main findings of this study are summarized as follows:

- Machine learning approaches such as logistic and lasso classification techniques provide probabilistic predictions of categorical variables such as the bond failure mode, and they provide explicit and easy-to-implement formulations for engineering practice.
- Both logistic and lasso classification methods have similar prediction performances: much better than the deterministic approaches and not worse than most of the other classification methods; however, lasso classification is found to be more accurate.
- The parameters that influence the bond failure mode prediction are concrete compressive strength, cover to the rebar diameter ratio, corrosion level, and loading type (cyclic or monotonic).
- Based on the developed probabilistic prediction models, the amount of transverse stirrup does not influence the bond failure mode.

- At the structural level, the flexural performance of the beam in the case study shows the dependence on the bond behavior, and more so at higher levels of corrosion. In addition, for high levels of corrosion where the beams exhibit splitting bond behavior, the beam fails brittlely (that is failure occurs prior to rebar yielding), which is not a desirable type of structural failure.
- The case study also shows that bond behavior has a great impact on the structural reliability index curves, and more so as the level of corrosion increases. Thus, the prediction of the bond failure mode is critical for time-dependent reliability-based analysis.
- A bond failure criterion based on the bond stress-slip relationship is proposed, and it is more reliable to specify the bond failure mode compared with the criteria that are based on cracking patterns, particularly when corrosion-induced cracking is present.
- Multivariate nonlinear regression analysis with model selection is a simple approach to develop accurate, unbiased, and practical models between the structural parameters (e.g., corrosion level, stirrups effect, loading type) and the response (i.e. bond strength), when the correlation between these parameters and the response is known.
- Due to the lack of pre-existing knowledge about the relationship between the bond-slip and the influential factors, SMGR helps extract meaningful relationships directly from data in the form of symbolic equations.
- Even though the prediction model for s_1 in splitting is developed simply by fitting a beta distribution on the data, this model provides sufficient accuracy for its application, as the impact of s_1 in splitting on the structural performance is found to be insignificant.

- The comparison result shows that the proposed models for both τ_{avg} and s_1 outperform the existing models based on the experimental data collected from the literature.
- Lastly, the proposed probabilistic models are successfully implemented into structural analysis and can predict the flexural behavior of RC beams well overall.
- The proposed model employs a bilinear bond stress distribution provides explicit solutions for slip and does not sacrifice slip prediction accuracy.
- When comparing with the experimental rebar stress-slip curves, the proposed macromodel overperforms over the Pan et al. model particular for corroded specimens.
- The proposed macromodel considers structural properties such as concrete strength, rebar yield stress, rebar diameter, and corrosion level, and the model parameter is explicitly expressed in the formula, which makes the future updating possible and easy.
- Comparing the force-displacement responses of the RC column numerical models with considering slip matches the experimental results very well, it further validates the proposed slip model used in the numerical model.
- Comparing the force-displacement responses of the numerical models with and without considering slip for various RC columns under monotonic and cyclic loading shows that the importance of incorporating rebar anchorage slip in the structural analysis.
- In the numerical analysis of an example RC bridge column, the results of pushover analysis, time-history analysis under seismic excitations, and seismic fragilities all demonstrate that the impact of slip play a significant role in the seismic performance evaluation.

- The results also show the impact of considering corrosion effect on slip prediction and on material properties.

BIBLIOGRAPHY

- Abasi, A., Harsij, V., & Soraghi, A. (2021). Damage detection of 3D structures using nearest neighbor search method. *Earthquake Engineering and Engineering Vibration*, 20(3), 705–725. <https://doi.org/10.1007/s11803-021-2048-1>
- Abasi, A., Hassanli, R., Vincent, T., & Manalo, A. (2020). Influence of prism geometry on the compressive strength of concrete masonry. *Construction and Building Materials*, 264. <https://doi.org/10.1016/j.conbuildmat.2020.120182>
- Abdel-Kareem, A. H. (2014). Shear strengthening of reinforced concrete beams with rectangular web openings by FRP Composites. *Advances in Concrete Construction*, 2(4), 281–300. <https://doi.org/10.12989/acc.2014.2.4.281>
- Abosrra, L., Ashour, A. F., & Youseffi, M. (2011). Corrosion of steel reinforcement in concrete of different compressive strengths. *Construction and Building Materials*. <https://doi.org/10.1016/j.conbuildmat.2011.04.023>
- ACI. (2003). Development of Straight Reinforcing Bars in Tension. *ACI 408R-03*.
- ACI. (2012). Report on bond of steel reinforcing bars under cyclic loads. In

American Concrete Institute - Joint ACI-ASCE Committee 408.

ACI Committee 308. (2001). Guide to Curing Concrete. *American Concrete Institute*, 1–31.

ACI Committee 318. (2014). Building Code Requirements for Structural Concrete. In *American Concrete Institute*.

Ahmed, S. F. U., Maalej, M., & Mihashi, H. (2007). Cover cracking of reinforced concrete beams due to corrosion of steel. *ACI Materials Journal*, 104(2), 153–161. <https://doi.org/10.14359/18578>

Akgül, F., & Frangopol, D. M. (2003). Rating and reliability of existing bridges in a network. *Journal of Bridge Engineering*.
[https://doi.org/10.1061/\(ASCE\)1084-0702\(2003\)8:6\(383\)](https://doi.org/10.1061/(ASCE)1084-0702(2003)8:6(383))

Al-Sulaimani, G. J., Kaleemullah, M., & Basunbul, I. A. (1990). Influence of corrosion and cracking on bond behavior and strength of reinforced concrete members. *ACI Structural Journal*, 87(2), 220–231.
<https://doi.org/10.14359/2732>

Alipour, A., Shafei, B., & Shinozuka, M. (2011). Performance evaluation of deteriorating highway bridges located in high seismic areas. *Journal of Bridge Engineering*, 16(5), 597–611. [https://doi.org/10.1061/\(ASCE\)BE.1943-5592.0000197](https://doi.org/10.1061/(ASCE)BE.1943-5592.0000197)

- Almusallam, A. A., Al-Gahtani, A. S., Aziz, A. R., & Rasheeduzzafar. (1996). Effect of reinforcement corrosion on bond strength. *Construction and Building Materials*. [https://doi.org/10.1016/0950-0618\(95\)00077-1](https://doi.org/10.1016/0950-0618(95)00077-1)
- Alsiwat, J. M., & Saatcioglu, M. (1992). Reinforcement anchorage slip under monotonic loading. *Structural Engineering*. [https://doi.org/10.1061/\(ASCE\)0733-9445\(1992\)118:9\(2421\)](https://doi.org/10.1061/(ASCE)0733-9445(1992)118:9(2421))
- Amini, A., Abdollahi, A., Hariri-Ardebili, M., & Lall, U. (2021). Copula-based reliability and sensitivity analysis of aging dams: Adaptive Kriging and polynomial chaos Kriging methods. *Applied Soft Computing*, 109, 107524. <https://doi.org/https://doi.org/10.1016/j.asoc.2021.107524>.
- Amini, A., Kia, M., & Bayat, M. (2021). Seismic vulnerability macrozonation map of SMRFs located in Tehran via reliability framework. *Structural Engineering and Mechanics*, 78, 351–368. [https://doi.org/DOI: http://dx.doi.org/10.12989/sem.2021.78.3.351](https://doi.org/DOI:http://dx.doi.org/10.12989/sem.2021.78.3.351)
- Amleh, L. (2000). *Deterioration of reinforcing steel in concrete due to corrosion*.
- Apostolopoulos, C. A. (2007). Mechanical behavior of corroded reinforcing steel bars S500s tempcore under low cycle fatigue. *Construction and Building Materials*, 21(7), 1447–1456. <https://doi.org/10.1016/j.conbuildmat.2006.07.008>

- ASTM A944-10. (2015). Standard Test Method for Comparing Bond Strength of Steel Reinforcing Bars to Concrete Using Beam-end Specimens. *ASTM International*. <https://doi.org/10.1520/A0944-10R15.2>
- B.D. Scott, Park, R., & Priestley, M. J. N. (1982). Stress-strain behavior of concrete confined by overlapping hoops at low and high strain rates. *ACI Journal Proceedings*, 79(1), 13–27.
- Bae, S., & Bayrak, O. (2008). Plastic hinge length of reinforced concrete columns. *ACI Structural Journal*, 105(3), 290–300.
- Balafas, I., & Burgoyne, C. J. (2011). Modeling the Structural Effects of Rust in Concrete Cover. *Engineering Mechanics*, 137(3), 175–185.
[https://doi.org/10.1061/\(ASCE\)EM.1943-7889.0000215](https://doi.org/10.1061/(ASCE)EM.1943-7889.0000215)
- Bamonte, P. F., & Gambarova, P. G. (2007). High-Bond Bars in NSC and HPC: Study on Size Effect and on the Local Bond Stress-Slip Law. *Journal of Structural Engineering*. [https://doi.org/10.1061/\(asce\)0733-9445\(2007\)133:2\(225\)](https://doi.org/10.1061/(asce)0733-9445(2007)133:2(225))
- Bandelt, M. J., & Billington, S. L. (2016). Bond behavior of steel reinforcement in high-performance fiber-reinforced cementitious composite flexural members. *Materials and Structures/Materiaux et Constructions*.
<https://doi.org/10.1617/s11527-014-0475-4>

- Betti, R. (2010). Aging infrastructure: issues, research, and technology. Buildings and infrastructure protection series. Infrastructure Protection and Disaster Management. *Buildings and Infrastructure Protection*.
- Bhargava, K., Ghosh, A. K., Mori, Y., & Ramanujam, S. (2007). Corrosion-induced bond strength degradation in reinforced concrete-Analytical and empirical models. *Nuclear Engineering and Design*.
<https://doi.org/10.1016/j.nucengdes.2007.01.010>
- Bilcik, J., & Holly, I. (2013). Effect of reinforcement corrosion on bond behaviour. *Procedia Engineering*, 65, 248–253.
<https://doi.org/10.1016/j.proeng.2013.09.038>
- Biondini, F., Bontempi, F., Frangopol, D. M., & Malerba, P. G. (2006). Probabilistic service life assessment and maintenance planning of concrete structures. *Journal of Structural Engineering*, 132(5), 810–825.
[https://doi.org/10.1061/\(ASCE\)0733-9445\(2006\)132:5\(810\)](https://doi.org/10.1061/(ASCE)0733-9445(2006)132:5(810))
- Cabrera, J. G. (1996). Deterioration of concrete due to reinforcement steel corrosion. *Cement and Concrete Composites*, 18(1), 47–59.
[https://doi.org/10.1016/0958-9465\(95\)00043-7](https://doi.org/10.1016/0958-9465(95)00043-7)
- Cape, M. (1999). Residual service-life assessment of existing R/C structures. *Chalmers University of Technology, Goteborg (Sweden) and Miland*

University of Technology, Italy Erasmus Program.

Castel, A., François, R., & Arliguie, G. (2000). Mechanical behaviour of corroded reinforced concrete beams - Part 1: experimental study of corroded beams.

Materials and Structures/Materiaux et Constructions, 33(9), 539–544.

<https://doi.org/10.1007/bf02480533>

Castel, Arnaud, Khan, I., François, R., & Gilbert, R. I. (2016). Modeling steel concrete bond strength reduction due to corrosion. *ACI Structural Journal*,

113(5), 973–982. <https://doi.org/10.14359/51688925>

Champiri, M. D., Hossein Mousavizadegan, S., & Moodi, F. (2012). A decision support system for diagnosis of distress cause and repair in marine concrete structures. *Computers and Concrete*, 9(2), 99–118.

<https://doi.org/10.12989/cac.2012.9.2.099>

Chang, M., Maguire, M., & Sun, Y. (2019). Stochastic modeling of bridge deterioration using classification tree and logistic regression. *Journal of Infrastructure Systems*.

[https://doi.org/10.1061/\(ASCE\)IS.1943-](https://doi.org/10.1061/(ASCE)IS.1943-555X.0000466)

555X.0000466

Choe, D. E., Gardoni, P., Rosowsky, D., & Haukaas, T. (2008). Probabilistic capacity models and seismic fragility estimates for RC columns subject to corrosion. *Reliability Engineering and System Safety*, 93(3), 383–393.

<https://doi.org/10.1016/j.res.2006.12.015>

Choi, O. C., & Lee, W. S. (2002). Interfacial bond analysis of deformed bars to concrete. *ACI Structural Journal*, 99(6), 750–756.

<https://doi.org/10.14359/12339>

Chung, L., Cho, S. H., Kim, J. H. J., & Yi, S. T. (2004). Correction factor suggestion for ACI development length provisions based on flexural testing of RC slabs with various levels of corroded reinforcing bars. *Engineering Structures*, 26(8), 1013–1026. <https://doi.org/10.1016/j.engstruct.2004.01.008>

Coccia, S., Di Maggio, E., & Rinaldi, Z. (2015). Bond slip model in cylindrical reinforced concrete elements confined with stirrups. *International Journal of Advanced Structural Engineering*. <https://doi.org/10.1007/s40091-015-0104-7>

Coronelli, D., & Gambarova, P. (2004). Structural assessment of corroded reinforced concrete beams: Modeling guidelines. *Journal of Structural Engineering*, 130(8), 1214–1224. [https://doi.org/10.1061/\(ASCE\)0733-9445\(2004\)130:8\(1214\)](https://doi.org/10.1061/(ASCE)0733-9445(2004)130:8(1214))

Corr, D. J., Monteiro, P. J. M., Kurtis, K. E., & Der Kiureghian, A. (2001). Sulfate attack of concrete: Reliability analysis. *ACI Materials Journal*, 98(2), 99–104. <https://doi.org/10.14359/10193>

Cucchiara, C., La Mendola, L., & Papia, M. (2004). Effectiveness of stirrups and

steel fibres as shear reinforcement. *Cement and Concrete Composites*.

<https://doi.org/10.1016/j.cemconcomp.2003.07.001>

Darwin, D., & Graham, E. K. (1993). Effect of deformation height and spacing on bond strength of reinforcing bars. *ACI Materials Journal*, 90(6), 646–657.

<https://doi.org/10.14359/4459>

Di Carlo, F., Meda, A., & Rinaldi, Z. (2017). Numerical evaluation of the corrosion influence on the cyclic behaviour of RC columns. *Engineering Structures*, 153, 264–278. <https://doi.org/10.1016/j.engstruct.2017.10.020>

Dolati, S., & Mehrabi, A. (2021a). Review of available systems and materials for splicing prestressed-precast concrete piles. *Structures*, 30, 850–865.

<https://doi.org/https://doi.org/10.1016/j.istruc.2021.01.029>

Dolati, S., & Mehrabi, A. (2021b). Review of Mechanical Bar Couplers for Splicing Precast Concrete Members. *Scientific Journal of Research and Reviews*, 3(1), 1–10. <https://doi.org/10.33552/SJRR.2021.03.000551>

Dyanati, M., Huang, Q., & Roke, D. (2015). Seismic demand models and performance evaluation of self-centering and conventional concentrically braced frames. *Engineering Structures*, 84, 368–381.

<https://doi.org/https://doi.org/10.1016/j.engstruct.2014.11.036>

El Maaddawy, T., Soudki, K., & Topper, T. (2005). Analytical model to predict

- nonlinear flexural behavior of corroded reinforced concrete beams. *ACI Structural Journal*. <https://doi.org/10.14359/14559>
- Eligehausen, R., Popov, E. P., & Bertero, V. V. (1982). *LOCAL BOND STRESS-SLIP RELATIONSHIPS OF DEFORMED BARS UNDER GENERALIZED EXCITATIONS*. 4, 69–80. <http://elib.uni-stuttgart.de/handle/11682/8490>
- Enright, M. P., & Frangopol, D. M. (1998a). Probabilistic analysis of resistance degradation of reinforced concrete bridge beams under corrosion. *Engineering Structures*, 20(11), 960–971. [https://doi.org/10.1016/S0141-0296\(97\)00190-9](https://doi.org/10.1016/S0141-0296(97)00190-9)
- Enright, M. P., & Frangopol, D. M. (1998b). Service-life prediction of deteriorating concrete bridges. *Journal of Structural Engineering*, 124(3), 309–317. [https://doi.org/10.1061/\(ASCE\)0733-9445\(1998\)124:3\(309\)](https://doi.org/10.1061/(ASCE)0733-9445(1998)124:3(309))
- Esteghamati, M. Z., Lee, J., Musetich, M., & Flint, M. M. (2020). INSSEPT: An open-source relational database of seismic performance estimation to aid with early design of buildings. *Earthquake Spectra*, 36(4), 2177–2197. <https://doi.org/10.1177/8755293020919857>
- Fang, C., Gylltoft, K., Lundgren, K., & Plos, M. (2006). Effect of corrosion on bond in reinforced concrete under cyclic loading. *Cement and Concrete Research*, 36(3), 548–555. <https://doi.org/10.1016/j.cemconres.2005.11.019>

- Fang, C., Lundgren, K., Chen, L., & Zhu, C. (2004). Corrosion influence on bond in reinforced concrete. *Cement and Concrete Research*, 34(11), 2159–2167.
<https://doi.org/10.1016/j.cemconres.2004.04.006>
- Fang, C. Q. (2006). Bond strength of corroded reinforcement under cyclic loading. *Magazine of Concrete Research*, 58(7), 437–446.
<https://doi.org/10.1680/macrc.2006.58.7.437>
- Fédération Internationale du Béton. (2000). Bond of reinforcement in concrete: state-of-art report. *Fib Bulletin No. 10, 112*, 434.
<https://doi.org/10.14359/51687912>
- Feng, D. C., Wu, G., & Lu, Y. (2018). Finite element modelling approach for precast reinforced concrete beam-to-column connections under cyclic loading. *Engineering Structures*. <https://doi.org/10.1016/j.engstruct.2018.07.055>
- Feng, Q., Visintin, P., & Oehlers, D. J. (2016). Deterioration of bond-slip due to corrosion of steel reinforcement in reinforced concrete. *Magazine of Concrete Research*. <https://doi.org/10.1680/jmacr.15.00217>
- fib. (2013). fib Model Code for Concrete Structures 2010. In *fib Model Code for Concrete Structures 2010*. Wiley-VCH Verlag GmbH & Co. KGaA.
<https://doi.org/10.1002/9783433604090>
- Filippou, F. C., Popov, E. P., & Bertero, V. V. (1983). Effects of Bond

Deterioration on Hysteretic Behaviour of Reinforced Concrete Joints. In *Earthquake Engineering Research Center*.

FISHER, R. A. (1936). THE USE OF MULTIPLE MEASUREMENTS IN TAXONOMIC PROBLEMS. *Annals of Eugenics*, 7(2), 179–188.

<https://doi.org/10.1111/j.1469-1809.1936.tb02137.x>

Frangopol, D. M., & Liu, M. (2007). Bridge network maintenance optimization using stochastic dynamic programming. *Journal of Structural Engineering*, 133(12), 1772–1782. [https://doi.org/10.1061/\(ASCE\)0733-9445\(2007\)133:12\(1772\)](https://doi.org/10.1061/(ASCE)0733-9445(2007)133:12(1772))

Friedman, J. H. (1989). Regularized discriminant analysis. *Journal of the American Statistical Association*.

<https://doi.org/10.1080/01621459.1989.10478752>

Fu, X., & Chung, D. D. L. (1997). Effect of corrosion on the bond between concrete and steel rebar. *Cement and Concrete Research*, 27(12), 1811–1815.

[https://doi.org/10.1016/S0008-8846\(97\)00172-5](https://doi.org/10.1016/S0008-8846(97)00172-5)

Gandomi, A. H., & Atefi, E. (2020). Software review: the GPTIPS platform. In *Genetic Programming and Evolvable Machines*.

<https://doi.org/10.1007/s10710-019-09366-0>

Gardoni, P., Kiureghian, A. Der, & Mosalam, K. M. (2002). Probabilistic Capacity

- Models and Fragility Estimates for Reinforced Concrete Columns based on Experimental Observations. *Journal of Engineering Mechanics*, 128(10), 1024–1038. [https://doi.org/10.1061/\(ASCE\)0733-9399\(2002\)128:10\(1024\)](https://doi.org/10.1061/(ASCE)0733-9399(2002)128:10(1024))
- Ghosh, J., & Padgett, J. E. (2010). Aging considerations in the development of time-dependent seismic fragility curves. *Journal of Structural Engineering*, 136(12), 1497–1511. [https://doi.org/10.1061/\(ASCE\)ST.1943-541X.0000260](https://doi.org/10.1061/(ASCE)ST.1943-541X.0000260)
- GL Fenves, S Mazzoni, F. M., & MH Scott. (2004). Open system for earthquake engineering simulation OpenSees. *Computing in Science & Engineering*, 13(4), 58–66. <https://doi.org/10.1109/MCSE.2011.66>
- Goksu, C. (2012). *Seismic behavior of RC columns with corroded plain and deformed reinforcing bars.*
- Guizani, L., & Chaallal, O. (2011). An experimental study on bond-slip in moderately confined concrete subjected to monotonic and cyclic loading using an experimental plan. *Canadian Journal of Civil Engineering*. <https://doi.org/10.1139/L10-133>
- Guo, A., Li, H., Ba, X., Guan, X., & Li, H. (2015). Experimental investigation on the cyclic performance of reinforced concrete piers with chloride-induced corrosion in marine environment. *Engineering Structures*, 105, 1–11. <https://doi.org/10.1016/j.engstruct.2015.09.031>

- Guo, Z.-H., & Shi, X.-D. (2003). Reinforced concrete theory and analyse. *Press of Tsinghua University: Beijing, China.*
- Hamad, B. S. (1995). Comparative bond strength of coated and uncoated bars with different rib geometries. *ACI Materials Journal.*
<https://doi.org/10.14359/9776>
- Hanjari, K. Z., Coronelli, D., & Lundgren, K. (2011). Bond capacity of severely corroded bars with corroded stirrups. *Magazine of Concrete Research.*
<https://doi.org/10.1680/mac.10.00200>
- Harajli, M. H. (2004). Comparison of bond strength of steel bars in normal- and high-strength concrete. *Journal of Materials in Civil Engineering.*
[https://doi.org/10.1061/\(ASCE\)0899-1561\(2004\)16:4\(365\)](https://doi.org/10.1061/(ASCE)0899-1561(2004)16:4(365))
- Harajli, M. H. (2009). Bond Stress–Slip Model for Steel Bars in Unconfined or Steel, FRC, or FRP Confined Concrete under Cyclic Loading. *Structural Engineering.* [https://doi.org/10.1061/\(asce\)0733-9445\(2009\)135:5\(509\)](https://doi.org/10.1061/(asce)0733-9445(2009)135:5(509))
- Harajli, M., Hamad, B., & Karam, K. (2002). Bond-slip Response of Reinforcing Bars Embedded in Plain and Fiber Concrete. *Journal of Materials in Civil Engineering.* [https://doi.org/10.1061/\(asce\)0899-1561\(2002\)14:6\(503\)](https://doi.org/10.1061/(asce)0899-1561(2002)14:6(503))
- Harajli, Mohamed H., Hamad, B. S., & Rteil, A. A. (2004). Effect of confinement of bond strength between steel bars and concrete. *ACI Structural Journal,*

101(5), 595–603. <https://doi.org/10.14359/13381>

Hariri-Ardebili, M. A., & Saouma, V. E. (2016). Seismic fragility analysis of concrete dams: A state-of-the-art review. *Engineering Structures*.
<https://doi.org/10.1016/j.engstruct.2016.09.034>

Harrington, P. (2012). Machine Learning in Action. In *Machine Learning*.
<https://doi.org/10.1007/s10994-011-5249-4>

Hawileh, R. A., Abdalla, J. A., Al Tamimi, A., Abdelrahman, K., & Oudah, F. (2011). Behavior of corroded steel reinforcing bars under monotonic and cyclic loadings. *Mechanics of Advanced Materials and Structures*, 18(3), 218–224. <https://doi.org/10.1080/15376494.2010.499023>

Herrmann, A. W. (2015). ASCE 2013 Report Card for America's Infrastructure. *IABSE Symposium Report*, 99(33), 9–10.
<https://doi.org/10.2749/222137813806368343>

Hii, C., Searson, D. P., & Willis, M. J. (2011). Evolving Toxicity Models using MultigeneSymbolic Regression and Multiple Objectives. *International Journal of Machine Learning and Computing*.
<https://doi.org/10.7763/ijmlc.2011.v1.5>

Hong, Sung-nam. (2008). Bond Stress-Slip Relationship in Reinforced Concrete: New Relationship and Comparative Study. *33rd Conferebce on Our World in*

Concrete & Structure, 7. <http://cipremier.com/100033019>

Hong, Sunnam, & Park, S. K. (2012). Uniaxial bond stress-slip relationship of reinforcing bars in concrete. *Advances in Materials Science and Engineering*, 2012. <https://doi.org/10.1155/2012/328570>

Huang, Q., Gardoni, P., & Hurlbaas, S. (2010a). Probabilistic seismic demand models and fragility estimates for reinforced concrete highway bridges with one single-column bent. *Journal of Engineering Mechanics*. [https://doi.org/10.1061/\(ASCE\)EM.1943-7889.0000186](https://doi.org/10.1061/(ASCE)EM.1943-7889.0000186)

Huang, Q., Gardoni, P., & Hurlbaas, S. (2010b). Probabilistic Seismic Demand Models and Fragility Estimates for Reinforced Concrete Highway Bridges with One Single-Column Bent. *Journal of Engineering Mechanics*, 136(11), 1340–1353. [https://doi.org/10.1061/\(ASCE\)EM.1943-7889.0000186](https://doi.org/10.1061/(ASCE)EM.1943-7889.0000186)

Huang, Q., Gardoni, P., & Hurlbaas, S. (2015). Adaptive Reliability Analysis of Reinforced Concrete Bridges Subject to Seismic Loading Using Nondestructive Testing. *ASCE-ASME Journal of Risk and Uncertainty in Engineering Systems, Part A: Civil Engineering*. <https://doi.org/10.1061/ajrua6.0000835>

Hussain, S., Al-Musallam, A., & Al-Gahtani, A. (1995). Factors affecting threshold chloride for reinforcement corrosion in concrete. *Cement and*

Concrete, 1543–1555.

Ikki, N., & Kiyomiya, O. (1996). Effect of axial concrete stress on bond strength of deformed bar. *Proceedings of Japan Concrete Institute*, 21(3), 373–378.

Imperatore, S., Rinaldi, Z., & Drago, C. (2017). Degradation relationships for the mechanical properties of corroded steel rebars. *Construction and Building Materials*. <https://doi.org/10.1016/j.conbuildmat.2017.04.209>

James, G., Witten, D., Hastie, T., & Tibshirani, R. (2013). An Introduction to Statistical Learning with Applications in R. In *Springer*.

<https://doi.org/10.1016/j.peva.2007.06.006>

Jiang, C., Wu, Y.-F., & Dai, M.-J. (2018). Degradation of steel-to-concrete bond due to corrosion. *Construction and Building Materials*, 158, 1073–1080.

<https://doi.org/https://doi.org/10.1016/j.conbuildmat.2017.09.142>

Jiang, D. H., Shah, S. P., & Andonian, A. T. (1984). Study of the Transfer of Tensile Forces by Bond. *Journal of the American Concrete Institute*, 81(3),

251–259. <https://doi.org/10.14359/10681>

Karbassi, A., Mohebi, B., Rezaee, S., & Lestuzzi, P. (2014). Damage prediction for regular reinforced concrete buildings using the decision tree algorithm.

Computers and Structures. <https://doi.org/10.1016/j.compstruc.2013.10.006>

- Kashani, M. M., Crewe, A. J., & Alexander, N. A. (2013). Nonlinear cyclic response of corrosion-damaged reinforcing bars with the effect of buckling. *Construction and Building Materials*, *41*, 388–400.
<https://doi.org/10.1016/j.conbuildmat.2012.12.011>
- Kemp, E. L., & Wilhelm, W. J. (1978). INVESTIGATION OF THE PARAMETERS INFLUENCING BOND CRACKING. *J Am Concr Inst*, *76*(1). <https://doi.org/10.14359/6936>
- Khalaf, J., & Huang, Z. (2016). Analysis of the bond behaviour between prestressed strands and concrete in fire. *Construction and Building Materials*.
<https://doi.org/10.1016/j.conbuildmat.2016.10.016>
- Kivell, A., Palermo, A., & Scott, A. (2011). Effects of bond deterioration due to corrosion in reinforced concrete. *Ninth Pacific Conference on Earthquake Engineering-Building and Earthquake Resilient Society*.
- Kivell, A., Palermo, A., & Scott, A. (2015). Complete model of corrosion-degraded cyclic bond performance in reinforced concrete. *Journal of Structural Engineering*, *141*(9). [https://doi.org/10.1061/\(ASCE\)ST.1943-541X.0001195](https://doi.org/10.1061/(ASCE)ST.1943-541X.0001195)
- Law, D. W., & Molyneaux, T. C. K. (2017). Impact of corrosion on bond in uncracked concrete with confined and unconfined rebar. *Construction and*

Building Materials. <https://doi.org/10.1016/j.conbuildmat.2017.08.112>

Lee, H. S., Kage, T., Noguchi, T., & Tomosawa, F. (2003). An experimental study on the retrofitting effects of reinforced concrete columns damaged by rebar corrosion strengthened with carbon fiber sheets. *Cement and Concrete Research*, 33(4), 563–570. [https://doi.org/10.1016/S0008-8846\(02\)01004-9](https://doi.org/10.1016/S0008-8846(02)01004-9)

Lee, H. S., Noguchi, T., & Tomosawa, F. (2002). Evaluation of the bond properties between concrete and reinforcement as a function of the degree of reinforcement corrosion. *Cement and Concrete Research*. [https://doi.org/10.1016/S0008-8846\(02\)00783-4](https://doi.org/10.1016/S0008-8846(02)00783-4)

Lehman, D. (1998). *Seismic performance of well-confined concrete bridge columns*. <https://search.proquest.com/openview/2803027153c8d741d903aa1b491b1518/1?pq-origsite=gscholar&cbl=18750&diss=y>

Lin, H, Zhao, Y., & Ožbolt, J. (2017). The bond behavior between concrete and corroded steel bar under repeated loading. *Engineering Structures*2. https://www.sciencedirect.com/science/article/pii/S0141029616307829?casa_token=6yrA32pOLMAAAAAA:aSc00MC_vvSqmy5gNDeNDfP4y6t_2nxd8LuXi3DYtp9HX9w9Qp6jDCjteK3_Sx8r9GaB6oJ2Mps

Lin, Hongwei, & Zhao, Y. (2016). Effects of confinements on the bond strength

- between concrete and corroded steel bars. *Construction and Building Materials*. <https://doi.org/10.1016/j.conbuildmat.2016.05.040>
- Lin, Hongwei, Zhao, Y., Ozbolt, J., Feng, P., Jiang, C., & Eligehausen, R. (2019). Analytical model for the bond stress-slip relationship of deformed bars in normal strength concrete. *Construction and Building Materials*. <https://doi.org/10.1016/j.conbuildmat.2018.11.258>
- Lin, Hongwei, Zhao, Y., Ozbolt, J., & Hans-Wolf, R. (2017). The bond behavior between concrete and corroded steel bar under repeated loading. *Engineering Structures*. <https://doi.org/10.1016/j.engstruct.2017.02.067>
- Lin, Hongwei, Zhao, Y., Ozbolt, J., & Reinhardt, H. W. (2017). Bond strength evaluation of corroded steel bars via the surface crack width induced by reinforcement corrosion. *Engineering Structures*. <https://doi.org/10.1016/j.engstruct.2017.08.051>
- Lin, Hongwei, Zhao, Y., Yang, J. Q., Feng, P., Ozbolt, J., & Ye, H. (2019). Effects of the corrosion of main bar and stirrups on the bond behavior of reinforcing steel bar. *Construction and Building Materials*. <https://doi.org/10.1016/j.conbuildmat.2019.07.156>
- Lindsey, C., & Sheather, S. (2010). Variable selection in linear regression. *Stata Journal*, 10(4), 650–669. <https://doi.org/10.1177/1536867x1101000407>

- Liu, Y., & Weyers, R. E. (1999). Modeling time-to-corrosion cracking in chloride contaminated reinforced concrete structures. In *ACI Materials Journal* (Vol. 96, Issue 5, pp. 611–613). <https://trid.trb.org/view/514367>
- Lu, R., Luo, Y., & Conte, J. P. (1994). Reliability evaluation of reinforced concrete beams. *Structural Safety*, 14(4), 277–298. [https://doi.org/10.1016/0167-4730\(94\)90016-7](https://doi.org/10.1016/0167-4730(94)90016-7)
- Lundgren, K. (2005). Bond between ribbed bars and concrete. Part 2: The effect of corrosion. *Magazine of Concrete Research*. <https://doi.org/10.1680/mac.2005.57.7.383>
- Lundgren, Karin, Robuschi, S., & Zandi, K. (2019). Methodology for Testing Rebar-Concrete Bond in Specimens from Decommissioned Structures. *International Journal of Concrete Structures and Materials*. <https://doi.org/10.1186/s40069-019-0350-3>
- Ma, Y., Che, Y., & Gong, J. (2012). Behavior of corrosion damaged circular reinforced concrete columns under cyclic loading. *Construction and Building Materials*, 29, 548–556. <https://doi.org/10.1016/j.conbuildmat.2011.11.002>
- Maaddawy, T. El, & Topper, T. (2005). Long-Term Performance of Corrosion-Damaged Reinforced Concrete Beams. In *ACI Structural Journal* (Vol. 102, Issue 5). <https://doi.org/10.14359/14660>

Maekawa, K., Okamura, H., & Pimanmas, A. (2003). *Non-linear mechanics of reinforced concrete*.

https://books.google.com/books?hl=en&lr=&id=9UpZDwAAQBAJ&oi=fnd&pg=PP1&dq=Nonlinear+mechanics+of+reinforced+concrete.+London,+UK:+Spon&ots=Dz9GgPkoNx&sig=s2_P1sMw4owG1DA0_kUok6J0Duc

Main, R. M. (1951). Measurement of the Distribution of Tensile and Bond Stresses Along Reinforcing Bars. *ACI Journal Proceedings*, 48(11).

<https://doi.org/10.14359/11882>

Mander, J. B., Priestley, M. J. N., & Park, R. (n.d.). *Theoretical Stress-Strain Model for Confined Concrete*. [https://doi.org/10.1061/\(ASCE\)0733-9445\(1988\)114](https://doi.org/10.1061/(ASCE)0733-9445(1988)114)

Mangat, P. S., & Elgarf, M. S. (1999). Bond characteristics of corroding reinforcement in concrete beams. *Materials and Structures/Materiaux et Constructions*. <https://doi.org/10.1007/bf02479434>

Meda, A., Mostosi, S., Rinaldi, Z., & Riva, P. (2014). Experimental evaluation of the corrosion influence on the cyclic behaviour of RC columns. *Engineering Structures*. <https://doi.org/10.1016/j.engstruct.2014.06.043>

Mehr, S., Research, M. G.-J. of C. S., & 2017, undefined. (n.d.). Seismic performance of retrofitted WFP connections joined to box column using ribs.

Elsevier. Retrieved November 25, 2021, from

https://www.sciencedirect.com/science/article/pii/S0143974X17306843?casa_token=QzfViDU9SO4AAAAA:E2n91CisQ4deIYUpjawoKx1emFJmdWw6SHCTNtR_-iA5Z_2YUfjyswZGcD3lPi2Ct4Vf3vq6pV8

Mirza, S. M., & Houde, J. (1978). STUDY OF BOND STRESS-SLIP RELATIONSHIPS IN REINFORCED CONCRETE. *J Am Concr Inst*, 76(1).
<https://doi.org/10.14359/6935>

Molina, F. J., Alonso, C., & Andrade, C. (1993). Cover cracking as a function of rebar corrosion: Part 2-Numerical model. *Materials and Structures*, 26(9), 532–548. <https://doi.org/10.1007/BF02472864>

Monti, G., Filippou, F. C., & Spacone, E. (1997). Finite element for anchored bars under cyclic load reversals. *Journal of Structural Engineering*, 123(5), 614–623. [https://doi.org/10.1061/\(ASCE\)0733-9445\(1997\)123:5\(614\)](https://doi.org/10.1061/(ASCE)0733-9445(1997)123:5(614))

Monti, G., & Spacone, E. (2000). Reinforced Concrete Fiber Beam Element with Bond-Slip. *Journal of Structural Engineering*, 126(6), 654–661.
[https://doi.org/10.1061/\(asce\)0733-9445\(2000\)126:6\(654\)](https://doi.org/10.1061/(asce)0733-9445(2000)126:6(654))

MUGURUMA, H., & MORITA, S. (1967). FUNDAMENTAL STUDY ON BOND BETWEEN STEEL AND CONCRETE : Part III. On the Pull-Out Test. *Transactions of the Architectural Institute of Japan*, 139, 1-10,77.

https://doi.org/10.3130/aijsaxx.139.0_1

Murcia-Delso, J., & Benson Shing, P. (2015). Bond-slip model for detailed finite-element analysis of reinforced concrete structures. *Journal of Structural Engineering (United States)*. [https://doi.org/10.1061/\(ASCE\)ST.1943-541X.0001070](https://doi.org/10.1061/(ASCE)ST.1943-541X.0001070)

Murcia-Delso, J., Stavridis, A., & Shing, P. B. (2013). Bond strength and cyclic bond deterioration of large-diameter bars. *ACI Structural Journal*.
<https://doi.org/10.14359/51685751>

Nakamura, H., Srisoros, W., Yashiro, R., & Kunieda, M. (2006). Time-dependent structural analysis considering mass transfer to evaluate deterioration process of RC structures. *Journal of Advanced Concrete Technology*.
<https://doi.org/10.3151/jact.4.147>

Nilson, A. (1972). Internal Measurement of Bond Slip. *ACI Journal Proceedings*, 69(7). <https://doi.org/10.14359/7170>

Orangun, C. O., Jirsa, J. O., & Breen, J. E. (1977). A Reevaluation of Test Data on Development Length and Splices. *ACI Journal Proceedings Proceedings*, 74(3). <https://doi.org/10.14359/10993>

OSU (Oregon State University). (1996).

<http://math.oregonstate.edu/home/programs/undergrad/CalculusQuestStudyG>

uides/ode/second/reduc1/reduc1.html

- Otani, S. (1973). *Behavior of multistory reinforced concrete frames during earthquakes*.
- Ou, Y. C., Susanto, Y. T. T., & Roh, H. (2016). Tensile behavior of naturally and artificially corroded steel bars. *Construction and Building Materials*.
<https://doi.org/10.1016/j.conbuildmat.2015.10.075>
- Ou, Y. C., Tsai, L. L., & Chen, H. H. (2012). Cyclic performance of large-scale corroded reinforced concrete beams. *Earthquake Engineering and Structural Dynamics*, *41*(4), 593–604. <https://doi.org/10.1002/eqe.1145>
- Pan, W.-H., Tao, M.-X., & Nie, J.-G. (2017). Fiber beam-column element model considering reinforcement anchorage slip in the footing. *Bulletin of Earthquake Engineering*, *15*, 991–1018. <https://doi.org/10.1007/s10518-016-9987-3>
- Pan, W. H., Tao, M. X., Nie, X., & Fan, J. S. (2018). Rebar Anchorage Slip Macromodel Considering Bond Stress Distribution: Monotonic Loading and Model Application. *Journal of Structural Engineering (United States)*, *144*(8). [https://doi.org/10.1061/\(ASCE\)ST.1943-541X.0002096](https://doi.org/10.1061/(ASCE)ST.1943-541X.0002096)
- Petcherdchoo, A., Neves, L. A. C., & Frangopol, D. M. (2008). Optimizing lifetime condition and reliability of deteriorating structures with emphasis on

bridges. *Journal of Structural Engineering*, 134(4), 544–552.

[https://doi.org/10.1061/\(ASCE\)0733-9445\(2008\)134:4\(544\)](https://doi.org/10.1061/(ASCE)0733-9445(2008)134:4(544))

Prieto, M., Tanner, P., & Andrade, C. (2016). Multiple linear regression model for the assessment of bond strength in corroded and non-corroded steel bars in structural concrete. *Materials and Structures*, 49(11), 4749–4763.

<https://doi.org/10.1617/s11527-016-0822-8>

Rahai, A., & Abasi, A. (2018). Seismic Performance and Long-Term Behavior of Balanced Cantilever Light-Weight Concrete Bridges. *16th European Conference on Earthquake Engineering (16ECEE)*.

Rehm, G. (1957). The fundamental law of bond. *Symposium on Bond and Crack Formation in Reinforced Concrete*, 491–498.

http://slubdd.de/katalog?libero_mab214578913

Rodriguez, J, Ortega, L., & Gracia, A. (1993). Corrosion of reinforcing bars and service life of R/C structures: corrosion and bond deterioration. In “Concrete Across Borders.” *Proceeding of an International Conference*, 22–25.

Rodriguez, Jesus, Ortega, L. M., & Casal, J. (1994). Corrosion of reinforcing bars and service life of reinforced concrete structures-corrosion and bond deterioration. *International Conference on Concrete across Borders, Odense, Denmark*.

- S Zheng, L Dong, H Zuo, Q Qin, W Liu, Q. L. (2018). Experimental investigation on seismic behaviors of corroded RC frame columns in artificial climate. *J. Build. Struct.*
<https://doi.org/https://doi.org/10.1016/j.conbuildmat.2020.118014>
- Saatcioglu, M., Alsiwat, J. M., & Ozcebe, G. (1992). Hysteretic behavior of anchorage slip in R/C members. *Structural Engineering*, 118(9), 2439–2548.
[https://doi.org/10.1061/\(ASCE\)0733-9445\(1992\)118:9\(2439\)](https://doi.org/10.1061/(ASCE)0733-9445(1992)118:9(2439))
- Sabzi, J., Esfahani, M., Ozbakkaloglu, T., & Farahi, B. (2020). Effect of concrete strength and longitudinal reinforcement arrangement on the performance of reinforced concrete beams strengthened using EBR and EBROG methods. *Engineering Structures*, 205, 110072.
<https://doi.org/https://doi.org/10.1016/j.engstruct.2019.110072>
- Sajedi, S., & Huang, Q. (2015). Probabilistic prediction model for average bond strength at steel-concrete interface considering corrosion effect. *Engineering Structures*, 99, 120–131. <https://doi.org/10.1016/j.engstruct.2015.04.036>
- Sajedi, S., & Huang, Q. (2017). Load-deflection behavior prediction of intact and corroded RC bridge beams with or without lap splices considering bond stress-slip effect. *Journal of Bridge Engineering*.
[https://doi.org/10.1061/\(ASCE\)BE.1943-5592.0000981](https://doi.org/10.1061/(ASCE)BE.1943-5592.0000981)

Sajedi, S., Huang, Q., Gandomi, A. H., & Kiani, B. (2017). Reliability-Based Multiobjective Design Optimization of Reinforced Concrete Bridges Considering Corrosion Effect. *ASCE-ASME Journal of Risk and Uncertainty in Engineering Systems, Part A: Civil Engineering*, 3(3).

<https://doi.org/10.1061/AJRUA6.0000896>

Schoettler, M., Restrepo, J., Guerrini, G., & Duck, D. (2012). *A full-scale, single-column bridge bent tested by shake-table excitation*.

Searson, D. P. (2015). GPTIPS 2: An open-source software platform for symbolic data mining. In *Handbook of Genetic Programming Applications*.

https://doi.org/10.1007/978-3-319-20883-1_22

Searson, D. P., Leahy, D. E., & Willis, M. J. (2010). GPTIPS: An open source genetic programming toolbox for multigene symbolic regression. *Proceedings of the International MultiConference of Engineers and Computer Scientists 2010, IMECS 2010*.

Searson, D., Willis, M., & Montague, G. (2007). Co-evolution of non-linear PLS model components. *Journal of Chemometrics*.

<https://doi.org/10.1002/cem.1084>

Sezen, H., & Moehle, J. P. (2006). Seismic tests of concrete columns with light transverse reinforcement. *ACI Structural Journal*, 103(6), 842–849.

<https://doi.org/10.14359/18236>

Sezen, H., & Setzler, E. J. (2008). Reinforcement slip in reinforced concrete columns. *ACI Structural Journal*, *105*(3), 280–289.

<https://doi.org/10.14359/19787>

Shima, H., Chou, L.-L., & Okamura, H. (1987a). Bond characteristics in post-yield range of deformed bars. *CONCRETE LIBRARY OF JSCE*, *6*.

https://doi.org/https://doi.org/10.2208/jscej.1987.378_213

SHIMA, H., Chou, L.-L., & Okamura, H. (1987). Bond-Slip-Strain Relationship of Deformed Bars Embedded in Massive Concrete (in Japanese). *CONCRETE LIBRARY OF JSCE*, *6*.

https://doi.org/https://doi.org/10.2208/jscej.1987.378_165

Shima, H., Chou, L. L., & Okamura, H. (1987b). MICRO AND MACRO MODELS FOR BOND IN REINFORCED CONCRETE. *Journal of the Faculty of Engineering, University of Tokyo, Series B*, *39*(2), 133–194.

Simon, J., Bracci, J. M., & Gardoni, P. (2010). Seismic response and fragility of deteriorated reinforced concrete bridges. *Journal of Structural Engineering*, *136*(10), 1273–1281. [https://doi.org/10.1061/\(ASCE\)ST.1943-541X.0000220](https://doi.org/10.1061/(ASCE)ST.1943-541X.0000220)

Somayaji, S., & Shah, S. P. (1981). Bond Stress Versus Slip Relationship and Cracking Response of Tension Members. *American Concrete Institute*.

<https://doi.org/10.14359/6920>

Soraghi, A., Huang, Q., & Hauff, D. A. J. (2019). Probabilistic Model for Rebar-Concrete Bond Failure Mode Prediction Considering Corrosion. *Structures Congress 2019: Blast, Impact Loading, and Research and Education*.

<https://doi.org/10.1061/9780784482247.033>

Soraghi, Ahmad, & Huang, Q. (2021). Probabilistic prediction model for RC bond failure mode. *Engineering Structures*, 233, 111944.

<https://doi.org/https://doi.org/10.1016/j.engstruct.2021.111944>

Stanish, K., Hooton, R. D., & Pantazopoulou, S. J. (1999). Corrosion effects on bond strength in reinforced concrete. *ACI Structural Journal*, 96(6), 915–921.

<https://doi.org/10.14359/765>

Stewart, M. G., & Rosowsky, D. V. (1998). Structural safety and serviceability of concrete bridges subject to corrosion. *Journal of Infrastructure Systems*, 4(4), 146–155. [https://doi.org/10.1061/\(ASCE\)1076-0342\(1998\)4:4\(146\)](https://doi.org/10.1061/(ASCE)1076-0342(1998)4:4(146))

Taerwe, L., & Matthys, S. (2013). *Fib model code for concrete structures 2010*.

Ernst & Sohn, Wiley.

Tang, B. (2007). *Influence of chloride-induced corrosion cracks on the strength of reinforced concrete*. RMIT Research Repository.

- Tao, M. X., & Nie, J. G. (2015). Element mesh, section discretization and material hysteretic laws for fiber beam–column elements of composite structural members. *Materials and Structures/Materiaux et Constructions*, 48(8), 2521–2544. <https://doi.org/10.1617/s11527-014-0335-2>
- Tarfan, S., Banazadeh, M., & Zaker Esteghamati, M. (2019). Probabilistic seismic assessment of non-ductile RC buildings retrofitted using pre-tensioned aramid fiber reinforced polymer belts. *Composite Structures*, 208, 865–878. <https://doi.org/10.1016/j.compstruct.2018.10.048>
- Taslimi, A., & Tehranizadeh, M. (2021). Seismic fragility analysis of RC frame-core wall buildings under the combined vertical and horizontal ground motions. *Earthquake and Structures*, 20(2), 175–185. <https://doi.org/http://dx.doi.org/10.12989/eas.2021.20.2.175>
- Tassios, T. (1979). Properties of bond between concrete and steel under load cycles idealizing seismic action. *Bulletin d'information Du CEB*, 65–122. <https://pascal-francis.inist.fr/vibad/index.php?action=getRecordDetail&idt=PASCALBTP8080462407>
- Thompson, J. N., & Perry, E. S. (1966). Bond Stress Distribution on Reinforcing Steel in Beams and Pullout Specimens. *ACI Journal Proceedings*, 63(8), 865–

876. <https://doi.org/10.14359/7656>

- Tibshirani, R. (1996). Journal of the Royal Statistical Society. Series B (Methodological). *Journal of the Royal Statistical Society Series B*, 58(1), 267–288.
- Tong, S. J., Yao, W. J., Su, H. T., & Li, L. (2007). Nonlinear analysis of reinforced concrete slabs by finite element method. *Xi'an Jianzhu Keji Daxue Xuebao/Journal of Xi'an University of Architecture and Technology*, 39(3).
<https://www.concrete.org/publications/internationalconcreteabstractsportal/m/details/id/7510>
- Torre-Casanova, A., Jason, L., Davenne, L., & Pinelli, X. (2013). Confinement effects on the steel-concrete bond strength and pull-out failure. *Engineering Fracture Mechanics*, 97(1), 92–104.
<https://doi.org/10.1016/j.engfracmech.2012.10.013>
- Ueda, T., Lin, I., & Hawkins, N. M. (1986). Beam Bar Anchorage in Exterior Column-Beam Connections. *Journal of the American Concrete Institute*.
<https://doi.org/10.14359/10442>
- Valente, M. (2012). Bond Strength between Corroded Steel Rebar and Concrete. *International Journal of Engineering and Technology*, 4(5), 653–656.
<https://doi.org/10.7763/ijet.2012.v4.454>

- Vu, N. S., Yu, B., & Li, B. (2016). Prediction of strength and drift capacity of corroded reinforced concrete columns. *Construction and Building Materials*, 115, 304–318. <https://doi.org/10.1016/j.conbuildmat.2016.04.048>
- Wang, H. (2009). An analytical study of bond strength associated with splitting of concrete cover. *Engineering Structures*.
<https://doi.org/10.1016/j.engstruct.2008.12.008>
- Wang, X. H., & Liu, X. La. (2008). Modeling the flexural carrying capacity of corroded RC beam. *Journal of Shanghai Jiaotong University (Science)*, 13 E(2), 129–135. <https://doi.org/10.1007/s12204-008-0129-1>
- Wang, X., & Liu, X. (2004). Modeling bond strength of corroded reinforcement without stirrups. *Cement and Concrete Research*, 34(8), 1331–1339.
<https://doi.org/10.1016/j.cemconres.2003.12.028>
- Wei-liang, J., & Zhao, Y. (2001). Effect of Corrosion on Bond Behavior and Bending. *Journal of Zhejiang University-SCIENCE A*, 3, 298–308.
<https://doi.org/10.1007/BF02839464>
- Wu, Y.-F., & Zhao, X.-M. (2013). Unified Bond Stress–Slip Model for Reinforced Concrete. *Journal of Structural Engineering*.
[https://doi.org/10.1061/\(asce\)st.1943-541x.0000747](https://doi.org/10.1061/(asce)st.1943-541x.0000747)
- Wu, Y. F., & Zhao, X. M. (2013). Unified bond stress-slip model for reinforced

concrete. *Structural Engineering*. [https://doi.org/10.1061/\(ASCE\)ST.1943-541X.0000747](https://doi.org/10.1061/(ASCE)ST.1943-541X.0000747)

Wu, Z., Zhang, X., Zheng, J., Hu, Y., & Li, Q. (2014). Bond Behavior of Plain Round Bars Embedded in Concrete Subjected to Biaxial Lateral Tensile-Compressive Stresses. *Journal of Structural Engineering*. [https://doi.org/10.1061/\(asce\)st.1943-541x.0000872](https://doi.org/10.1061/(asce)st.1943-541x.0000872)

Xiaoming, Y., Civil, Z. H.-J. J. of, & 2012, U. (2012). Finite element investigation on load carrying capacity of corroded RC beam based on bond-slip. *Jordan Journal of Civil Engineering*, 6(1).

Xu, Y. L. (1990). *Experimental study of anchorage properties for deformed bars in concrete (In Chinese)*. Tsinghua University, Beijing, China.

Yalciner, H., Eren, O., & Sensoy, S. (2012). An experimental study on the bond strength between reinforcement bars and concrete as a function of concrete cover, strength and corrosion level. *Cement and Concrete Research*, 42(5), 643–655. <https://doi.org/10.1016/j.cemconres.2012.01.003>

Yang, S., & Chen, J. (1988). BOND SLIP AND CRACK WIDTH CALCULATIONS OF TENSION MEMBERS. *ACI Structural Journal*, 85(4), 414–422. <https://doi.org/10.14359/2693>

Yuan, J., & Graybeal, B. (2015). Bond of reinforcement in ultra-high-performance

concrete. In *ACI Structural Journal* (Vol. 112, Issue 6).

<https://doi.org/10.14359/51687912>

Yuan, Y. S., Yu, S., & Jia, F. P. (1999). Deterioration of bond behavior of corroded reinforced concrete. *Industrial Construction*, 29(11), 47–50.

Zaker Esteghamati, M., Banazadeh, M., & Huang, Q. (2018). The effect of design drift limit on the seismic performance of RC dual high-rise buildings. *Structural Design of Tall and Special Buildings*.

<https://doi.org/10.1002/tal.1464>

Zamanian, S, Terranova, B., & Shafieezadeh, A. (2020). Significant variables affecting the performance of concrete panels impacted by wind-borne projectiles: A global sensitivity analysis. *International Journal of Impact Engineering*, 144, 103650.

<https://doi.org/https://doi.org/10.1016/j.ijimpeng.2020.103650>

Zamanian, Soroush, Hur, J., & Shafieezadeh, A. (2020). Significant variables for leakage and collapse of buried concrete sewer pipes: a global sensitivity analysis via Bayesian additive regression trees and Sobol' indices. *Structure and Infrastructure Engineering*, 1–13.

<https://doi.org/10.1080/15732479.2020.1762674>

Zhang, J., Ma, G., Huang, Y., sun, J., Aslani, F., & Nener, B. (2019). Modelling

uniaxial compressive strength of lightweight self-compacting concrete using random forest regression. *Construction and Building Materials*.

<https://doi.org/10.1016/j.conbuildmat.2019.03.189>

Zhang, Y., Bici, E., Sezen, H., & Zheng, S. (2020). Reinforcement slip model considering corrosion effects. *Construction and Building Materials*, 235.

<https://doi.org/10.1016/j.conbuildmat.2019.117348>

Zhao, J., & Sritharan, S. (2007). Modeling of strain penetration effects in fiber-based analysis of reinforced concrete structures. *ACI Structural Journal*.

<https://doi.org/10.14359/18525>

Zhao, W., & Zhu, B. (2018). Theoretical model for the bond–slip relationship between ribbed steel bars and confined concrete. *Structural Concrete*.

<https://doi.org/10.1002/suco.201700008>

Zheng, X. Y. (2004). Research on dynamic bond behavior between corroded steel bar and concrete [D]. *Nanjing: Hehai University*.

Zhou, H., Lu, J., Xu, X., Dong, B., & Xing, F. (2015). Effects of stirrup corrosion on bond-slip performance of reinforcing steel in concrete: An experimental study. *Construction and Building Materials*.

<https://doi.org/10.1016/j.conbuildmat.2015.05.122>

Zhou, H., Lu, J., Xu, X., Zhou, Y., & Xing, F. (2015). Experimental study of

bond-slip performance of corroded reinforced concrete under cyclic loading.

Advances in Mechanical Engineering, 7(3), 1–10.

<https://doi.org/10.1177/1687814015573787>

APPENDICES

APPENDIX A

DESIGNED SPECIMEN SPECIFICATION

Table A.1. Specimen specifications (group 1).

Group	No.	Rebar diameter, d_b [mm]	Loading type*	f'_c [MPa]	Bond length, l_b [mm]	Cover, c [mm]	c/d	K_{tr}	Q_{target} (%)	Q_{actual} (%)	Failure Mode**
Group 1	1	15.875	M	43	88.9	50.8	3.20	0.00	0%	0.0%	S
	2					63.5	4.00	0.00	10%	4.9%	P
	3					76.2	4.80	0.00	20%	7.6%	S
	4					50.8	3.20	5.89	0%	0.0%	P
	5					63.5	4.00	5.89	10%	5.3%	P
	6					76.2	4.80	5.89	20%	9.9%	P
	7		C			50.8	3.20	0.00	0%	0.0%	S
	8					25.4	1.60	0.00	5%	10.3%	P
	9					63.5	4.00	0.00	10%	11.0%	P
	10					38.1	2.40	0.00	15%	10.1%	P
	11					76.2	4.80	0.00	20%	12.0%	P
	12					50.8	3.20	5.89	0%	0.0%	P
	13					25.4	1.60	5.89	5%	7.9%	NA
	14					63.5	4.00	5.89	10%	4.3%	P
	15					38.1	2.40	5.89	15%	8.2%	S
	16					76.2	4.80	5.89	20%	11.3%	P
Group 1	17	19.05	M	114.3	38.1	2.00	0.00	0%	0.0%	S	
	18				25.4	1.33	0.00	10%	3.6%	S	
	19				50.8	2.67	0.00	20%	15.6%	P	
	20				38.1	2.00	4.91	0%	0.0%	P	
	21				25.4	1.33	4.91	10%	3.2%	S	
	22				50.8	2.67	4.91	20%	7.1%	S	
	23		C		38.1	2.00	0.00	0%	0.0%	S	
	24				63.5	3.33	0.00	5%	8.5%	NA	
	25				25.4	1.33	0.00	10%	7.6%	P	
	26				76.2	4.00	0.00	15%	9.9%	S	
	27				50.8	2.67	0.00	20%	13.4%	P	
	28				38.1	2.00	4.91	0%	0.0%	P	
	29				63.5	3.33	4.91	5%	8.6%	P	
	30				25.4	1.33	4.91	10%	6.9%	S	
	31				76.2	4.00	4.91	15%	7.7%	P	
	32				50.8	2.67	4.91	20%	11.0%	P	
Group 1	33	25.4	M	203.2	63.5	2.50	0.00	0%	0.0%	S	
	34				50.8	2.00	0.00	10%	4.3%	S	
	35				38.1	1.50	0.00	20%	10.2%	S	
	36				63.5	2.50	3.68	0%	0.0%	S	
	37				50.8	2.00	3.68	10%	7.7%	S	
	38				38.1	1.50	3.68	20%	11.9%	P	
	39		C		63.5	2.50	3.68	0%	0.0%	S	
	40				50.8	2.00	0.00	10%	5.2%	NA	
	41				38.1	1.50	0.00	20%	13.1%	NA	
	42				63.5	2.50	3.68	0%	0.0%	NA	
	43				50.8	2.00	3.68	10%	5.7%	P	
	44				38.1	1.50	3.68	20%	13.7%	P	

Table A.2. Specimen specifications (group 2).

Group	No.	Rebar diameter, d_b [mm]	Loading type*	f'_c [MPa]	Bond length, l_b [mm]	Cover, c [mm]	c/d	K_{tr}	Q_{target} (%)	Q_{actual} (%)	Failure Mode**
Group 2	1	15.875	M	36	88.9	25.4	1.60	11.73	5%	13.1%	P
	2					38.1	2.40	11.73	0%	0.0%	P
	3					38.1	2.40	11.73	10%	16.3%	S
	4					50.8	3.20	11.73	10%	14.9%	P
	5					50.8	3.20	11.73	15%	18.4%	S
	6					63.5	4.00	11.73	5%	13.0%	S
	7					63.5	4.00	11.73	15%	15.9%	S
	8					76.2	4.80	11.73	15%	18.8%	P
	9		C			25.4	1.60	11.73	5%	16.3%	P
	10					38.1	2.40	11.73	0%	0.0%	S
	11					38.1	2.40	11.73	10%	15.7%	S
	12					50.8	3.20	11.73	10%	15.4%	S
	13					50.8	3.20	11.73	15%	17.2%	P
	14					63.5	4.00	11.73	5%	19.1%	P
	15					63.5	4.00	11.73	15%	16.5%	S
	16					76.2	4.80	11.73	15%	15.6%	S
	17	19.05	M	114.3	25.4	1.33	9.78	5%	6.3%	P	
	18				38.1	2.00	9.78	0%	0.0%	P	
	19				38.1	2.00	9.78	10%	11.2%	P	
	20				50.8	2.67	9.78	10%	12.6%	P	
	21				50.8	2.67	9.78	15%	25.8%	S	
	22				63.5	3.33	9.78	5%	7.1%	P	
	23				63.5	3.33	9.78	15%	10.5%	S	
	24				76.2	4.00	9.78	15%	10.8%	P	
	25		C		25.4	1.33	9.78	5%	6.5%	S	
	26				38.1	2.00	9.78	0%	0.0%	S	
	27				38.1	2.00	9.78	10%	13.3%	S	
	28				50.8	2.67	9.78	10%	12.8%	S	
	29				50.8	2.67	9.78	15%	10.3%	S	
	30				63.5	3.33	9.78	5%	5.4%	S	
	31				63.5	3.33	9.78	15%	12.1%	S	
	32				76.2	4.00	9.78	15%	11.4%	S	
	33	25.4	M	152.4	76.2	3.00	7.33	5%	6.0%	P	
	34				76.2	3.00	7.33	0%	0.0%	P	
	35				88.9	3.50	7.33	5%	10.7%	P	
	36				88.9	3.50	7.33	10%	7.4%	S	
	37				101.6	4.00	7.33	5%	4.9%	P	
	38				101.6	4.00	7.33	10%	7.7%	S	
	39				C	76.2	3.00	7.33	5%	5.7%	S
	40					76.2	3.00	7.33	0%	0.0%	NA
	41		88.9			3.50	7.33	5%	5.1%	S	
	42		88.9			3.50	7.33	10%	7.5%	NA	
	43		101.6			4.00	7.33	5%	5.4%	NA	
	44		101.6			4.00	7.33	10%	8.1%	S	

Table A.3. Specimen specifications (group 3).

Group	No.	Rebar diameter, d_b [mm]	Loading type*	f'_c [MPa]	Bond length, l_b [mm]	Cover, c [mm]	c/d	K_{lr}	Q_{target} (%)	Q_{actual} (%)	Failure Mode**
Group 3	1	15.875	M	27	88.9	25.4	1.60	11.73	5%	7.9%	P
	2					38.1	2.40	11.73	0%	0.0%	P
	3					38.1	2.40	11.73	10%	10.3%	S
	4					50.8	3.20	11.73	10%	11.2%	S
	5					50.8	3.20	11.73	15%	6.5%	P
	6					63.5	4.00	11.73	5%	4.8%	S
	7					63.5	4.00	11.73	15%	4.0%	P
	8					76.2	4.80	11.73	15%	7.8%	S
	9	19.05	M	114.3	88.9	25.4	1.60	11.73	5%	6.2%	P
	10					38.1	2.40	11.73	0%	0.0%	P
	11					38.1	2.40	11.73	10%	7.7%	P
	12					50.8	3.20	11.73	10%	9.8%	NA
	13					50.8	3.20	11.73	15%	9.1%	P
	14					63.5	4.00	11.73	5%	3.4%	P
	15					63.5	4.00	11.73	15%	11.9%	NA
	16					76.2	4.80	11.73	15%	16.9%	P
	17	25.4	M	152.4	88.9	25.4	1.33	9.78	5%	5.2%	P
	18					38.1	2.00	9.78	0%	0.0%	P
	19					38.1	2.00	9.78	10%	6.2%	S
	20					50.8	2.67	9.78	10%	7.1%	NA
	21					50.8	2.67	9.78	15%	9.0%	P
	22					63.5	3.33	9.78	5%	5.4%	P
	23					63.5	3.33	9.78	15%	9.5%	P
	24					76.2	4.00	9.78	15%	7.2%	P
	25	25.4	C	152.4	88.9	25.4	1.33	9.78	5%	6.1%	S
	26					38.1	2.00	9.78	0%	0.0%	NA
	27					38.1	2.00	9.78	10%	6.8%	P
	28					50.8	2.67	9.78	10%	6.6%	S
	29					50.8	2.67	9.78	15%	5.8%	P
	30					63.5	3.33	9.78	5%	8.0%	S
	31					63.5	3.33	9.78	15%	8.2%	S
	32					76.2	4.00	9.78	15%	8.3%	S
	33	25.4	M	152.4	88.9	76.2	3.00	7.33	5%	5.0%	S
	34					76.2	3.00	7.33	0%	0.0%	P
	35					88.9	3.50	7.33	5%	3.7%	S
	36					88.9	3.50	7.33	10%	7.4%	S
	37					101.6	4.00	7.33	5%	4.7%	P
	38					101.6	4.00	7.33	10%	6.7%	S
	39					76.2	3.00	7.33	5%	4.7%	P
	40					76.2	3.00	7.33	0%	0.0%	P
	41	25.4	C	152.4	88.9	88.9	3.50	7.33	5%	4.6%	P
	42					88.9	3.50	7.33	10%	5.9%	P
	43					101.6	4.00	7.33	5%	5.6%	P
	44					101.6	4.00	7.33	10%	5.8%	P

* M (monotonic), and C (cyclic)

** P (pull-out), S (splitting), and NA (not assigned)

APPENDIX B

CLASSIFICATION ALGORITHMS

Decision tree

A decision tree is a decision support, non-parametric method that uses a tree-like model constructed from the training data and includes a sequence of yes/no questions to classify all observations. Hence, the response is predicted using the tree graph. The decision tree consists of nodes and branches in which the nodes belong to the test condition and the branches represent the outcome of the test. By following the nodes and branches of the tree, a decision can be made (Karbassi et al., 2014).

Discriminant analysis

In discriminant classification, different classes are assumed to generate data following various Gaussian distributions (FISHER, 1936). Linear discriminant analysis (LDA) and quadratic discriminant analysis (QDA) are two types of discriminant analysis. In LDA Bayes theorem is used to predict the probabilities of the output category, k , into the k th category given the input vector of \mathbf{x} that can be written as:

$$\Pr(Y = k | \mathbf{x}) = \frac{\pi_k f_k(\mathbf{x})}{\sum_{l=1} \pi_l f_l(\mathbf{x})} \quad (\text{B.1})$$

where π_k is the prior probability (in this study $\pi_k = 0.5$) and $f_k(\mathbf{x})$ refers to the density function of \mathbf{x} . In this study, $f_k(\mathbf{x})$ is considered to have a joint normal or Gaussian

distribution, and π_k is the prior probability of an observation belonging to the k th class. QDA is similar to LDA in that it assigns inputs to the k th category, but QDA considers each category as having a unique covariance matrix. Accordingly, classes in LDA have a linear boundary and quadratic boundary in QDA. This study adopts QDA for the class boundary due to its better prediction accuracy (Friedman, 1989).

K-nearest neighbors classification

K-nearest neighbors (KNN) classification is a non-parametric classification method (James et al., 2013). Having a test observation of y_0 and K as a positive integer, the KNN determines K observations in the training data nearest to y_0 that are denoted as N_0 . It then predicts the conditional probability for class k as the fraction of data points in N_0 as follows:

$$\Pr(Y = k | \mathbf{x}) = \frac{1}{K} \sum_{i \in N_0} I(y_i = k) \quad (\text{B.2})$$

where $I(\cdot)$ refers to the indicator variable. The main drawback of using the KNN method is that the chosen value of K is sensitive to the prediction performance. To deal with this issue, the approach of cross-validation is adopted in this study for different values of K , and the best model is selected.

Naïve Bayes classification

Naïve Bayes classification uses the Bayes theorem for classifying data by assigning an observation to a class when the probability belongs to that observation is larger than 50%. By assuming that the input vector \mathbf{x} is independent for a given class, k , the probability of an observation pertains to that class can be formulated as (James et al., 2013):

$$\begin{aligned}
\Pr(Y = k | \mathbf{x}) &= \frac{\Pr(Y = k) \Pr(\mathbf{x} | Y = k)}{\Pr(\mathbf{x})} \\
&= \frac{\Pr(Y = k) \prod_{i=1}^N \Pr(\mathbf{x}_i | Y = k)}{\Pr(\mathbf{x})}
\end{aligned} \tag{B.3}$$

Random forest

A random forest includes a group of decision trees in a way that each tree predictor produces a response based on a set of input variables (J. Zhang et al., 2019). A random forest creates many learning models (i.e., decision trees) that increase the classification accuracy. This process, also known as *bagging*, works by averaging noisy and unbiased models to create a model with low variance. The prediction of each observation is obtained from average of all decision trees and can be formulated using the following equation:

$$\Pr(Y = k | \mathbf{x}) = \frac{1}{B} \sum_{b=1}^B f_b(\mathbf{x}) \tag{B.4}$$

where B is the number of decision trees and f_b is the decision tree prediction.

Support vector machine

A support vector machine (SVM) is a simple classifier generalization known as a maximal margin classifier for categorization (James et al., 2013). This model builds a hyper-plane (e.g. a linear or polynomial equation of \mathbf{x}) that has the maximum distance from the nearest point of each category based on the training data. SVM is a non-probabilistic classification that constructs a classifier as follows:

$$\Pr(Y = k | \mathbf{x}) = \text{sign} \left[\sum_{i=1}^N \alpha_i y_i \Psi(\mathbf{x}, \mathbf{x}_i) + b \right] \tag{B.5}$$

in which N is the number of training data, α_i is a positive real factor, and b is a real constant. The parameter $\Psi(\cdot)$ is a defined function: for a linear SVM, $\Psi(\mathbf{x}, \mathbf{x}_i) = \mathbf{x}_i^T \mathbf{x}$ and for a

polynomial SVM, $\Psi(\mathbf{x}, \mathbf{x}_i) = (\mathbf{x}_i^T \mathbf{x} + 1)^d$, in which d is an a priori value specified by the user.

This study adopted a polynomial SVM to achieve the best accuracy.

APPENDIX C

LAP SPLICE LENGTH

The designed lap splice length for the adopted beam from Abdel-Kareem (Abdel-Kareem, 2014) is from ACI 318-11 design code provisions (ACI Committee 318, 2014), in which l_d can be calculated as:

$$l_d = \frac{0.9 f_y \min(\Psi_t \Psi_e, 1.7) \Psi_s \lambda}{\sqrt{f'_c} \min(\frac{c + k_{tr}}{d}, 2.5)} d_b \quad (\text{C.1})$$

where Ψ_t , Ψ_e , and Ψ_s are modification coefficients to consider the location of reinforcement effects, coating, and size of reinforcement, respectively; λ is an aggregate concrete factor, and c is the smaller of the distance from the half of center-to-center spacing of the developed bars and the distance from the nearest concrete surface to the center of the rebar (units are based on SI units). K_{tr} is the calculated based on:

$$K_{tr} = \frac{A_{tr} \cdot f_{yt}}{10.34 s \cdot n} \quad (\text{C.2})$$

where n is the number of rebars developed within the splitting plane. For the calculation of l_d in Equation C.1, the values for the modification factors are $\Psi_t = \Psi_e = \Psi_s = \lambda = 1.0$. Note that to obtain the minimum splice length, l_d can be replaced with l_s (Sajedi & Huang, 2017).

APPENDIX D

ANALYTICAL PROCEDURE

As mentioned in [Equation \(2.18\)](#), it is necessary to calculate the capacity of the structure. The following procedure is used to obtain the capacity, $C(\mathbf{x}_r)$. In this process, the beam is modeled as a series of elements having the length of crack sizes. The RC beam is assumed to be purely under a constant bending moment. The beam is assumed to have a single crack at its midpoint and, as the bending moments increase, the crack expands toward the supports. The rebar-concrete bonding transfers some portion of the tensile forces created by the bending moment and, thus, reduces the steel elongation and strain within each element, allowing the deflection and rotation be lowered. The midspan deflection, Δ , can be calculated as (El Maaddawy et al., 2005):

$$\Delta = \sum_{i=1}^{i=n} \frac{e_i}{d - c_c} x_i \quad (\text{D.1})$$

where n is the number of cracks, e_i is the elongation of each individual crack, d is the height of the center of the tensile rebar to the top of the concrete section, and c is the difference between the height of the top of the section and the top of the crack in a crack element, as shown in [Figure D.1](#).

This procedure uses compatibility and equilibrium requirements, and interested readers could refer to the authors' other publications (El Maaddawy et al., 2005; Sajedi & Huang, 2017) for further details. The probabilistic model developed by Sajedi & Huang

(Sajedi & Huang, 2015) is implemented to estimate the average bond strength, τ_m , that is a function of corrosion for intact and corroded specimens as:

$$\ln\left(\frac{\tau_m}{\sqrt{f'_c}}\right) = \theta_0 + \theta_1 \cdot \exp(\tilde{\theta}_1 \cdot Q) \cdot \frac{c}{d_{b0}} \cdot \frac{\mu + R_r}{1 - \mu R_r} \cdot \gamma + \theta_2 \cdot \exp(\tilde{\theta}_2 \cdot Q) \cdot \frac{b_e}{d_{b0}} \cdot \frac{\mu + R_r}{1 - \mu R_r} \cdot \gamma + \theta_3 \cdot \frac{1}{\sqrt{f'_c}} \cdot \frac{A_{st} f_{y,st}}{s d_{b0}} + \sigma \varepsilon \quad (D.2)$$

where the predicted coefficients are: $\theta_0 = -0.90$, $\theta_1 = 0.48$, $\theta_2 = 0.12$, $\theta_3 = 0.024$, $\tilde{\theta}_1 = -0.08$, and $\tilde{\theta}_2 = -0.148$; $\mu = 0.45$ (Choi & Lee, 2002) is the rebar friction coefficient; $R_r = 0.1$ (X. Wang & Liu, 2004) is the relative lug area of the intact bar; b_e is the effective beam width (mm) ($3c \leq b_e \leq 9c$); $\gamma = [8 \cdot d_{b0}/(l_d \text{ or } l_s)]^{0.5}$ (≤ 1) is a reduction factor to long development length (l_d) or splice length (l_s); A_{st} is the area of two legs of the transverse reinforcement in the cross-section (mm²); s = transverse reinforcement spacing (mm); and $\sigma \varepsilon$ is the model error where $\sigma = 0.169$ and ε = standard normal random variable (Sajedi & Huang, 2015).

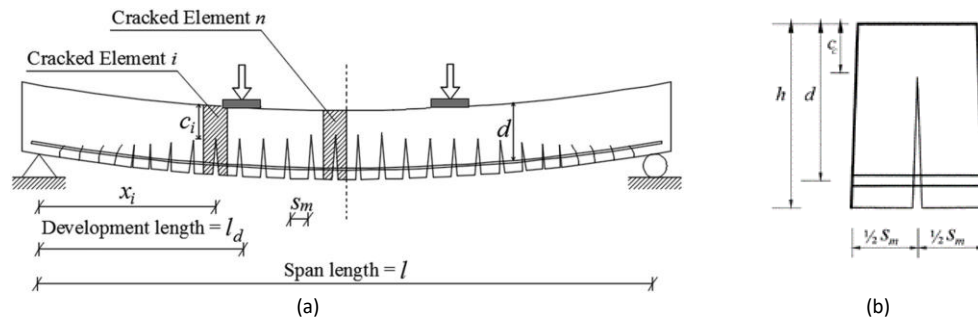


Figure. D.1 (a) Typical cracked beam under flexural loading (Maaddawy & Topper, 2005), and (b) typical crack element (El Maaddawy et al., 2005).

APPENDIX E

CORROSIN EFFECT ON MATERIAL PROPERTIES

Researches have shown that the formation of steel rust as a result of the corrosion would result in rebar section reduction, volumetric expansion, and a strong reduction in the concrete and rebar material (Coronelli & Gambarova, 2004). It is also found that the reduction in ductility and strength is significantly greater than the reduction in cross-section area (Imperatore et al., 2017; Ou et al., 2016). Thus, in the numerical analysis of a corroded RC structure, the strength of rebar and concrete (either core or cover) materials needs to be modified. Based on (Imperatore et al., 2017; Xiaoming et al., 2012), thus, the rebar yielding strength σ_y rebar ultimate strength σ_u and core or cover concrete compressive strength f'_c can be calculated as follows:

$$D = \sqrt{1 - 0.01Q} \cdot D_{\text{intact}} \quad (\text{E.1})$$

$$\sigma_y = (1 - 1.435Q) \cdot \sigma_{y,\text{intact}} \quad (\text{E.2})$$

$$\sigma_u = (1 - 1.253Q) \cdot \sigma_{u,\text{intact}} \quad (\text{E.3})$$

$$f'_c = \left[1 + 0.1\pi \frac{(D - D_c)/b_0}{\varepsilon_{co}} \right]^{-1} \cdot f'_{c,\text{intact}} \quad (\text{E.4})$$

where σ_y and σ_u are the yield and ultimate strength of corroded rebar, respectively. D and D_c are the intact and corroded rebar diameter, respectively, b_0 is the circumference of the

cross-section, and ε_{co} is the strain at the peak compressive stress (Cape, 1999; Fédération Internationale du Béton, 2000; Molina et al., 1993) and can be calculated as $\varepsilon_{co} = 2f_c'/E$ (Figure 4.7).

APPENDIX F

COLLECTED DATA FOR BOND STRENGTH AND PEAK SLIP MODEL DEVELOPMENT

#	Q (%)	c (mm)	d (mm)	R_r (mm ²)	b_e (mm)	f'_c (Mpa)	A_{tr} (mm ²)	f_{yt} (Mpa)	s (mm)	l_b [mm]	$\ln(\tau/\text{sqrt}(f'_c))$	MC	FM	Group	s_1
1	0.0	50.8	15.875	0.075	190.5	43	0	414	76.2	88.9	0.84	0	0	Batch 1	NA
2	4.9	63.5	15.875	0.075	190.5	43	0	414	76.2	88.9	-0.04	0	1	Batch 1	0.18
3	7.6	76.2	15.875	0.075	228.6	43	0	414	76.2	88.9	0.07	0	0	Batch 1	NA
4	0.0	50.8	15.875	0.075	190.5	43	258	414	76.2	88.9	1.06	0	1	Batch 1	2.02
5	5.3	63.5	15.875	0.075	190.5	43	258	414	76.2	88.9	0.97	0	1	Batch 1	4.59
6	9.9	76.2	15.875	0.075	228.6	43	258	414	76.2	88.9	0.83	0	1	Batch 1	0.14
7	0.0	50.8	15.875	0.075	190.5	43	0	414	76.2	88.9	0.87	1	0	Batch 1	NA
8	10.3	25.4	15.875	0.075	190.5	43	0	414	76.2	88.9	-0.23	1	1	Batch 1	0.87
9	11.0	63.5	15.875	0.075	190.5	43	0	414	76.2	88.9	0.67	1	1	Batch 1	0.97
10	10.1	38.1	15.875	0.075	190.5	43	0	414	76.2	88.9	0.00	1	1	Batch 1	0.33
11	12.0	76.2	15.875	0.075	228.6	43	0	414	76.2	88.9	0.14	1	1	Batch 1	0.15
12	0.0	50.8	15.875	0.075	190.5	43	258	414	76.2	88.9	0.98	1	0	Batch 1	NA
13	7.9	25.4	15.875	0.075	190.5	43	258	414	76.2	88.9	0.71	1	FALSE	Batch 1	NA
14	4.3	63.5	15.875	0.075	190.5	43	258	414	76.2	88.9	1.03	1	0	Batch 1	NA
15	8.2	38.1	15.875	0.075	190.5	43	258	414	76.2	88.9	0.91	1	0	Batch 1	NA
16	11.3	76.2	15.875	0.075	228.6	43	258	414	76.2	88.9	0.87	1	1	Batch 1	0.13
17	0.0	38.1	19.05	0.075	190.5	43	0	414	76.2	114.3	0.63	0	0	Batch 1	NA
18	3.6	25.4	19.05	0.075	190.5	43	0	414	76.2	114.3	-0.60	0	0	Batch 1	NA

19	15.6	50.8	19.05	0.075	190.5	43	0	414	76.2	114.3	-2.21	0	1	Batch 1	0.76
20	0.0	38.1	19.05	0.075	190.5	43	258	414	76.2	114.3	0.81	0	FALSE	Batch 1	NA
21	3.2	25.4	19.05	0.075	190.5	43	258	414	76.2	114.3	0.50	0	0	Batch 1	NA
22	7.1	50.8	19.05	0.075	190.5	43	258	414	76.2	114.3	0.53	0	FALSE	Batch 1	NA
23	0.0	38.1	19.05	0.075	190.5	43	0	414	76.2	114.3	0.45	1	0	Batch 1	NA
24	8.5	63.5	19.05	0.075	190.5	43	0	414	76.2	114.3	-0.58	1	FALSE	Batch 1	NA
25	7.6	25.4	19.05	0.075	190.5	43	0	414	76.2	114.3	-0.23	1	1	Batch 1	1.06
26	9.9	76.2	19.05	0.075	228.6	43	0	414	76.2	114.3	0.38	1	0	Batch 1	NA
27	13.4	50.8	19.05	0.075	190.5	43	0	414	76.2	114.3	-0.51	1	1	Batch 1	0.12
28	0.0	38.1	19.05	0.075	190.5	43	258	414	76.2	114.3	1.13	1	0	Batch 1	NA
29	8.6	63.5	19.05	0.075	190.5	43	258	414	76.2	114.3	1.03	1	0	Batch 1	NA
30	6.9	25.4	19.05	0.075	190.5	43	258	414	76.2	114.3	0.53	1	1	Batch 1	0.41
31	7.7	76.2	19.05	0.075	228.6	43	258	414	76.2	114.3	0.79	1	1	Batch 1	0.36
32	11.0	50.8	19.05	0.075	190.5	43	258	414	76.2	114.3	1.01	1	1	Batch 1	0.17
33	0.0	63.5	25.4	0.075	190.5	43	0	414	76.2	203.2	0.63	0	0	Batch 1	NA
34	4.3	50.8	25.4	0.075	190.5	43	0	414	76.2	203.2	-0.39	0	0	Batch 1	NA
35	10.2	38.1	25.4	0.075	190.5	43	0	414	76.2	203.2	-0.47	0	0	Batch 1	NA
36	0.0	63.5	25.4	0.075	190.5	43	258	414	76.2	203.2	0.61	0	0	Batch 1	NA
37	7.7	50.8	25.4	0.075	190.5	43	258	414	76.2	203.2	-0.26	0	0	Batch 1	NA
38	11.9	38.1	25.4	0.075	190.5	43	258	414	76.2	203.2	-0.82	0	1	Batch 1	0.09
39	0.0	63.5	25.4	0.075	190.5	43	0	414	76.2	203.2	0.65	1	0	Batch 1	NA
40	5.2	50.8	25.4	0.075	190.5	43	0	414	76.2	203.2	0.43	1	FALSE	Batch 1	NA
41	13.1	38.1	25.4	0.075	190.5	43	0	414	76.2	203.2	0.02	1	FALSE	Batch 1	NA
42	0.0	63.5	25.4	0.075	190.5	43	258	414	76.2	203.2	0.83	1	FALSE	Batch 1	NA
43	5.7	50.8	25.4	0.075	190.5	43	258	414	76.2	203.2	0.30	1	1	Batch 1	0.5
44	13.7	38.1	25.4	0.075	190.5	43	258	414	76.2	203.2	-0.16	1	FALSE	Batch 1	NA
45	13.1	25.4	15.875	0.075	190.5	36	142	414	38.1	88.9	1.00	0	0	Batch 2	NA
46	0.0	38.1	15.875	0.075	190.5	36	142	414	38.1	88.9	1.01	0	1	Batch 2	0.39
47	16.3	38.1	15.875	0.075	190.5	36	142	414	50.8	88.9	0.98	0	0	Batch 2	NA
48	14.9	50.8	15.875	0.075	190.5	36	142	414	63.5	88.9	1.13	0	0	Batch 2	NA
49	18.4	50.8	15.875	0.075	190.5	36	142	414	76.2	88.9	0.80	0	0	Batch 2	NA

50	13.0	63.5	15.875	0.075	190.5	36	142	414	76.2	88.9	1.07	0	0	Batch 2	NA
51	15.9	63.5	15.875	0.075	190.5	36	142	414	76.2	88.9	0.92	0	1	Batch 2	0.34
52	18.8	76.2	15.875	0.075	228.6	36	142	414	76.2	88.9	1.04	0	1	Batch 2	0.1
53	16.3	25.4	15.875	0.075	190.5	36	142	414	38.1	88.9	0.70	1	1	Batch 2	0.17
54	0.0	38.1	15.875	0.075	190.5	36	142	414	38.1	88.9	1.13	1	0	Batch 2	NA
55	15.7	38.1	15.875	0.075	190.5	36	142	414	50.8	88.9	0.98	1	0	Batch 2	NA
56	15.4	50.8	15.875	0.075	190.5	36	142	414	63.5	88.9	1.04	1	0	Batch 2	NA
57	17.2	50.8	15.875	0.075	190.5	36	142	414	76.2	88.9	0.87	1	1	Batch 2	0.71
58	19.1	63.5	15.875	0.075	190.5	36	142	414	76.2	88.9	0.99	1	1	Batch 2	0.42
59	16.5	63.5	15.875	0.075	190.5	36	142	414	76.2	88.9	0.93	1	0	Batch 2	NA
60	15.6	76.2	15.875	0.075	228.6	36	142	414	76.2	88.9	1.00	1	0	Batch 2	NA
61	6.3	25.4	19.05	0.075	190.5	36	142	414	38.1	114.3	0.72	0	1	Batch 2	0.3
62	0.0	38.1	19.05	0.075	190.5	36	142	414	38.1	114.3	0.83	0	FALSE	Batch 2	NA
63	11.2	38.1	19.05	0.075	190.5	36	142	414	38.1	114.3	0.85	0	0	Batch 2	NA
64	12.6	50.8	19.05	0.075	190.5	36	142	414	50.8	114.3	0.71	0	0	Batch 2	NA
65	25.8	50.8	19.05	0.075	190.5	36	142	414	50.8	114.3	0.86	0	0	Batch 2	NA
66	7.1	63.5	19.05	0.075	190.5	36	142	414	63.5	114.3	0.98	0	1	Batch 2	0.45
67	10.5	63.5	19.05	0.075	190.5	36	142	414	76.2	114.3	0.84	0	0	Batch 2	NA
68	10.8	76.2	19.05	0.075	228.6	36	142	414	76.2	114.3	0.85	0	1	Batch 2	0.18
69	6.5	25.4	19.05	0.075	190.5	36	142	414	38.1	114.3	0.93	1	0	Batch 2	NA
70	0.0	38.1	19.05	0.075	190.5	36	142	414	38.1	114.3	0.79	1	0	Batch 2	NA
71	13.3	38.1	19.05	0.075	190.5	36	142	414	38.1	114.3	1.03	1	0	Batch 2	NA
72	12.8	50.8	19.05	0.075	190.5	36	142	414	50.8	114.3	0.94	1	0	Batch 2	NA
73	10.3	50.8	19.05	0.075	190.5	36	142	414	50.8	114.3	0.67	1	0	Batch 2	NA
74	5.4	63.5	19.05	0.075	190.5	36	142	414	63.5	114.3	0.80	1	0	Batch 2	NA
75	12.1	63.5	19.05	0.075	190.5	36	142	414	63.5	114.3	1.02	1	0	Batch 2	NA
76	11.4	76.2	19.05	0.075	228.6	36	142	414	76.2	114.3	0.88	1	0	Batch 2	NA
77	6.0	76.2	25.4	0.075	228.6	36	142	414	38.1	152.4	1.09	0	0	Batch 2	NA
78	0.0	76.2	25.4	0.075	228.6	36	142	414	38.1	152.4	1.02	0	1	Batch 2	0.15
79	10.7	88.9	25.4	0.075	266.7	36	142	414	38.1	152.4	1.19	0	0	Batch 2	NA
80	7.4	88.9	25.4	0.075	266.7	36	142	414	50.8	152.4	0.99	0	0	Batch 2	NA

81	4.9	101.6	25.4	0.075	304.8	36	142	414	50.8	152.4	1.12	0	1	Batch 2	1
82	7.7	101.6	25.4	0.075	304.8	36	142	414	38.1	152.4	1.19	0	0	Batch 2	NA
83	5.7	76.2	25.4	0.075	228.6	36	142	414	38.1	152.4	1.03	1	0	Batch 2	NA
84	0.0	76.2	25.4	0.075	228.6	36	142	414	38.1	152.4	1.09	1	FALSE	Batch 2	NA
85	5.1	88.9	25.4	0.075	266.7	36	142	414	38.1	152.4	1.14	1	0	Batch 2	NA
86	7.5	88.9	25.4	0.075	266.7	36	142	414	50.8	152.4	1.08	1	0	Batch 2	NA
87	5.4	101.6	25.4	0.075	304.8	36	142	414	50.8	152.4	1.10	1	FALSE	Batch 2	NA
88	8.1	101.6	25.4	0.075	304.8	36	142	414	38.1	152.4	1.11	1	0	Batch 2	NA
89	7.9	25.4	15.875	0.075	190.5	27	142	414	38.1	88.9	0.85	0	1	Batch 3	0.25
90	0.0	38.1	15.875	0.075	190.5	27	142	414	38.1	88.9	1.05	0	1	Batch 3	0.22
91	10.3	38.1	15.875	0.075	190.5	27	142	414	38.1	88.9	1.14	0	0	Batch 3	NA
92	11.2	50.8	15.875	0.075	190.5	27	142	414	38.1	88.9	1.02	0	0	Batch 3	NA
93	6.5	50.8	15.875	0.075	190.5	27	142	414	38.1	88.9	1.23	0	1	Batch 3	0.12
94	4.8	63.5	15.875	0.075	190.5	27	142	414	38.1	88.9	1.22	0	0	Batch 3	NA
95	4.0	63.5	15.875	0.075	190.5	27	142	414	38.1	88.9	1.37	0	1	Batch 3	0.17
96	7.8	76.2	15.875	0.075	228.6	27	142	414	38.1	88.9	1.20	0	0	Batch 3	NA
97	6.2	25.4	15.875	0.075	190.5	27	142	414	38.1	88.9	#NUM!	1	FALSE	Batch 3	NA
98	0.0	38.1	15.875	0.075	190.5	27	142	414	38.1	88.9	1.04	1	1	Batch 3	0.17
99	7.7	38.1	15.875	0.075	190.5	27	142	414	38.1	88.9	1.28	1	1	Batch 3	0.14
100	9.8	50.8	15.875	0.075	190.5	27	142	414	38.1	88.9	#NUM!	1	1	Batch 3	0.19
101	9.1	50.8	15.875	0.075	190.5	27	142	414	38.1	88.9	1.15	1	1	Batch 3	0.09
102	3.4	63.5	15.875	0.075	190.5	27	142	414	38.1	88.9	1.28	1	1	Batch 3	0.04
103	11.9	63.5	15.875	0.075	190.5	27	142	414	38.1	88.9	1.43	1	0	Batch 3	NA
104	16.9	76.2	15.875	0.075	228.6	27	142	414	38.1	88.9	1.02	1	FALSE	Batch 3	NA
105	5.2	25.4	19.05	0.075	190.5	27	142	414	38.1	114.3	0.63	0	1	Batch 3	0.06
106	0.0	38.1	19.05	0.075	190.5	27	142	414	38.1	114.3	0.87	0	1	Batch 3	0.08
107	6.2	38.1	19.05	0.075	190.5	27	142	414	38.1	114.3	1.10	0	0	Batch 3	NA
108	7.1	50.8	19.05	0.075	190.5	27	142	414	38.1	114.3	0.97	0	1	Batch 3	0.9
109	9.0	50.8	19.05	0.075	190.5	27	142	414	38.1	114.3	0.88	0	1	Batch 3	0.5
110	5.4	63.5	19.05	0.075	190.5	27	142	414	38.1	114.3	0.99	0	FALSE	Batch 3	NA
111	9.5	63.5	19.05	0.075	190.5	27	142	414	38.1	114.3	1.11	0	1	Batch 3	0.17

112	7.2	76.2	19.05	0.075	228.6	27	142	414	38.1	114.3	0.98	0	1	Batch 3	0.39
113	6.1	25.4	19.05	0.075	190.5	27	142	414	38.1	114.3	0.79	0	1	Batch 3	0.57
114	0.0	38.1	19.05	0.075	190.5	27	142	414	38.1	114.3	0.81	1	FALSE	Batch 3	NA
115	6.8	38.1	19.05	0.075	190.5	27	142	414	38.1	114.3	1.12	1	0	Batch 3	NA
116	6.6	50.8	19.05	0.075	190.5	27	142	414	38.1	114.3	1.25	1	0	Batch 3	NA
117	5.8	50.8	19.05	0.075	190.5	27	142	414	38.1	114.3	0.56	1	1	Batch 3	0.34
118	8.0	63.5	19.05	0.075	190.5	27	142	414	38.1	114.3	1.05	1	0	Batch 3	NA
119	8.2	63.5	19.05	0.075	190.5	27	142	414	38.1	114.3	1.22	1	0	Batch 3	NA
120	8.3	76.2	19.05	0.075	228.6	27	142	414	38.1	114.3	1.15	1	0	Batch 3	NA
121	5.0	76.2	25.4	0.075	228.6	27	142	414	38.1	152.4	0.99	0	0	Batch 3	NA
122	0.0	76.2	25.4	0.075	228.6	27	142	414	38.1	152.4	0.96	0	1	Batch 3	0.47
123	3.7	88.9	25.4	0.075	266.7	27	142	414	38.1	152.4	1.04	0	0	Batch 3	NA
124	7.4	88.9	25.4	0.075	266.7	27	142	414	38.1	152.4	0.96	0	0	Batch 3	NA
125	4.7	101.6	25.4	0.075	304.8	27	142	414	38.1	152.4	1.04	0	1	Batch 3	0.07
126	6.7	101.6	25.4	0.075	304.8	27	142	414	38.1	152.4	0.92	0	0	Batch 3	NA
127	4.7	76.2	25.4	0.075	228.6	27	142	414	38.1	152.4	1.01	1	0	Batch 3	NA
128	0.0	76.2	25.4	0.075	228.6	27	142	414	38.1	152.4	1.04	1	0	Batch 3	NA
129	4.6	88.9	25.4	0.075	266.7	27	142	414	38.1	152.4	1.03	1	0	Batch 3	NA
130	5.9	88.9	25.4	0.075	266.7	27	142	414	38.1	152.4	1.05	1	0	Batch 3	NA
131	5.6	101.6	25.4	0.075	304.8	27	142	414	38.1	152.4	1.12	1	0	Batch 3	NA
132	5.8	101.6	25.4	0.075	304.8	27	142	414	38.1	152.4	0.55	1	1	Batch 3	0.45
133	0	25.4	20.6	0.12	228.6	22	0	1	1	254	0.06	0	0	Bilal	NA
134	0	25.4	20.6	0.12	228.6	22	0	1	1	254	0.06	0	0	Bilal	NA
135	0	25.4	20.6	0.12	228.6	22	0	1	1	254	0.08	0	0	Bilal	NA
136	0	25.4	20.6	0.12	228.6	22	0	1	1	254	0.12	0	0	Bilal	NA
137	0	25.4	20.6	0.12	228.6	22	0	1	1	254	0.15	0	0	Bilal	NA
138	0	25.4	20.6	0.12	228.6	22	0	1	1	254	0.10	0	0	Bilal	NA
139	0	25.4	20.6	0.12	228.6	22	0	1	1	254	0.06	0	0	Bilal	NA
140	0	25.4	20.6	0.12	228.6	22	0	1	1	254	0.06	0	0	Bilal	NA
141	0	25.4	20.6	0.2	228.6	22	0	1	1	254	0.02	0	0	Bilal	NA
142	0	25.4	20.6	0.2	228.6	22	0	1	1	254	0.02	0	0	Bilal	NA

143	0	25.4	20.6	0.17	228.6	22	0	1	1	254	0.03	0	0	Bilal	NA
144	0	25.4	20.6	0.15	228.6	22	0	1	1	254	0.17	0	0	Bilal	NA
145	0	25.4	20.6	0.15	228.6	22	0	1	1	254	0.17	0	0	Bilal	NA
146	0	25.4	20.6	0.13	228.6	22	0	1	1	254	0.09	0	0	Bilal	NA
147	0	25.4	20.6	0.12	228.6	22	0	1	1	254	0.06	0	0	Bilal	NA
148	0	25.4	20.6	0.12	228.6	22	0	1	1	254	0.08	0	0	Bilal	NA
149	0	25.4	20.6	0.08	228.6	22	0	1	1	254	-0.03	0	0	Bilal	NA
150	0	25.4	20.6	0.08	228.6	22	0	1	1	254	-0.08	0	0	Bilal	NA
151	0	25.4	20.6	0.12	228.6	22	0	1	1	254	0.13	0	0	Bilal	NA
152	0	25.4	20.6	0.12	228.6	22	0	1	1	254	0.01	0	0	Bilal	NA
153	0	25.4	20.6	0.16	228.6	22	0	1	1	254	0.20	0	0	Bilal	NA
154	0	25.4	20.6	0.16	228.6	22	0	1	1	254	0.10	0	0	Bilal	NA
155	0	25.4	20.6	0.2	228.6	22	0	1	1	254	0.10	0	0	Bilal	NA
156	0	25.4	20.6	0.2	228.6	22	0	1	1	254	0.13	0	0	Bilal	NA
157	0	25.4	20.6	0.12	228.6	43	0	1	1	254	0.11	0	0	Bilal	NA
158	0	25.4	20.6	0.12	228.6	43	0	1	1	254	0.10	0	0	Bilal	NA
159	0	25.4	20.6	0.12	228.6	43	0	1	1	254	0.12	0	0	Bilal	NA
160	0	25.4	20.6	0.12	228.6	43	0	1	1	254	0.21	0	0	Bilal	NA
161	0	25.4	20.6	0.12	228.6	43	0	1	1	254	0.22	0	0	Bilal	NA
162	0	25.4	20.6	0.12	228.6	43	0	1	1	254	0.15	0	0	Bilal	NA
163	0	25.4	20.6	0.12	228.6	43	0	1	1	254	0.14	0	0	Bilal	NA
164	0	25.4	20.6	0.12	228.6	43	0	1	1	254	0.12	0	0	Bilal	NA
165	0	25.4	20.6	0.2	228.6	43	0	1	1	254	0.08	0	0	Bilal	NA
166	0	25.4	20.6	0.2	228.6	43	0	1	1	254	0.03	0	0	Bilal	NA
167	0	25.4	20.6	0.17	228.6	43	0	1	1	254	0.13	0	0	Bilal	NA
168	0	25.4	20.6	0.15	228.6	43	0	1	1	254	0.29	0	0	Bilal	NA
169	0	25.4	20.6	0.15	228.6	43	0	1	1	254	0.28	0	0	Bilal	NA
170	0	25.4	20.6	0.13	228.6	43	0	1	1	254	0.14	0	0	Bilal	NA
171	0	25.4	20.6	0.12	228.6	43	0	1	1	254	0.19	0	0	Bilal	NA
172	0	25.4	20.6	0.12	228.6	43	0	1	1	254	0.07	0	0	Bilal	NA
173	0	25.4	20.6	0.08	228.6	43	0	1	1	254	0.12	0	0	Bilal	NA

174	0	25.4	20.6	0.08	228.6	43	0	1	1	254	0.04	0	0	Bilal	NA
175	0	25.4	20.6	0.12	228.6	43	0	1	1	254	0.15	0	0	Bilal	NA
176	0	25.4	20.6	0.12	228.6	43	0	1	1	254	0.17	0	0	Bilal	NA
177	0	25.4	20.6	0.16	228.6	43	0	1	1	254	0.23	0	0	Bilal	NA
178	0	25.4	20.6	0.16	228.6	43	0	1	1	254	0.29	0	0	Bilal	NA
179	0	25.4	20.6	0.2	228.6	43	0	1	1	254	-0.01	0	0	Bilal	NA
180	0	25.4	20.6	0.2	228.6	43	0	1	1	254	0.08	0	0	Bilal	NA
181	0	25.4	20.6	0.15	228.6	22	0	1	1	254	0.12	0	0	Bilal	NA
182	0	25.4	20.6	0.15	228.6	22	0	1	1	254	0.15	0	0	Bilal	NA
183	0	25.4	20.6	0.2	228.6	22	0	1	1	254	0.31	0	0	Bilal	NA
184	0	25.4	20.6	0.2	228.6	22	0	1	1	254	0.32	0	0	Bilal	NA
185	0	25.4	20.6	0.15	228.6	22	0	1	1	254	0.27	0	0	Bilal	NA
186	0	25.4	20.6	0.15	228.6	22	0	1	1	254	0.22	0	0	Bilal	NA
187	0	25.4	20.6	0.2	228.6	22	0	1	1	254	0.34	0	0	Bilal	NA
188	0	25.4	20.6	0.2	228.6	22	0	1	1	254	0.33	0	0	Bilal	NA
189	0	53.975	25.4	0.2	228.6	31	0	1	1	304.4	-0.01	0	0	Darwin	NA
190	0	53.975	25.4	0.2	228.6	32	0	1	1	304.4	0.01	0	0	Darwin	NA
191	0	52.3875	25.4	0.2	228.6	32	0	1	1	304.4	-0.03	0	0	Darwin	NA
192	0	52.3875	25.4	0.1	228.6	32	0	1	1	304.4	0.06	0	0	Darwin	NA
193	0	53.975	25.4	0.1	228.6	32	0	1	1	304.4	0.14	0	0	Darwin	NA
194	0	53.975	25.4	0.1	228.6	31	0	1	1	304.4	0.02	0	0	Darwin	NA
195	0	53.975	25.4	0.05	228.6	32	0	1	1	304.4	0.00	0	0	Darwin	NA
196	0	55.5625	25.4	0.05	228.6	32	0	1	1	304.4	-0.05	0	0	Darwin	NA
197	0	55.5625	25.4	0.05	228.6	31	0	1	1	304.4	0.06	0	0	Darwin	NA
198	0	60.325	25.4	0.2	228.6	32	0	1	1	304.4	0.03	0	0	Darwin	NA
199	0	53.975	25.4	0.2	228.6	31	0	1	1	304.4	-0.14	0	0	Darwin	NA
200	0	53.975	25.4	0.2	228.6	32	0	1	1	304.4	0.06	0	0	Darwin	NA
201	0	50.8	25.4	0.1	228.6	32	0	1	1	304.4	0.06	0	0	Darwin	NA
202	0	53.975	25.4	0.1	228.6	31	0	1	1	304.4	0.01	0	0	Darwin	NA
203	0	57.15	25.4	0.1	228.6	32	0	1	1	304.4	-0.13	0	0	Darwin	NA
204	0	50.8	25.4	0.05	228.6	32	0	1	1	304.4	0.05	0	0	Darwin	NA

205	0	52.3875	25.4	0.05	228.6	31	0	1	1	304.4	0.05	0	0	Darwin	NA
206	0	52.3875	25.4	0.05	228.6	32	0	1	1	304.4	-0.05	0	0	Darwin	NA
207	0	52.3875	25.4	0.2	228.6	31	0	1	1	304.4	0.06	0	0	Darwin	NA
208	0	52.3875	25.4	0.2	228.6	32	0	1	1	304.4	0.01	0	0	Darwin	NA
209	0	55.5625	25.4	0.2	228.6	31	0	1	1	304.4	-0.01	0	0	Darwin	NA
210	0	49.2125	25.4	0.1	228.6	31	0	1	1	304.4	0.02	0	0	Darwin	NA
211	0	49.2125	25.4	0.1	228.6	32	0	1	1	304.4	0.02	0	0	Darwin	NA
212	0	52.3875	25.4	0.1	228.6	32	0	1	1	304.4	0.02	0	0	Darwin	NA
213	0	53.975	25.4	0.05	228.6	32	0	1	1	304.4	0.08	0	0	Darwin	NA
214	0	55.5625	25.4	0.05	228.6	32	0	1	1	304.4	-0.06	0	0	Darwin	NA
215	0	53.975	25.4	0.05	228.6	32	0	1	1	304.4	-0.14	0	0	Darwin	NA
216	0	57.15	25.4	0.07	228.6	31	0	1	1	304.4	0.03	0	0	Darwin	NA
217	0	55.5625	25.4	0.07	228.6	32	0	1	1	304.4	0.00	0	0	Darwin	NA
218	0	50.8	25.4	0.07	228.6	32	0	1	1	304.4	-0.01	0	0	Darwin	NA
219	0	53.975	25.4	0.07	228.6	31	0	1	1	304.4	-0.07	0	0	Darwin	NA
220	0	52.3875	25.4	0.07	228.6	32	0	1	1	304.4	-0.01	0	0	Darwin	NA
221	0	52.3875	25.4	0.07	228.6	32	0	1	1	304.4	0.01	0	0	Darwin	NA
222	0	52.3875	25.4	0.2	228.6	32	0	1	1	304.4	0.08	0	0	Darwin	NA
223	0	53.975	25.4	0.1	228.6	32	0	1	1	304.4	0.07	0	0	Darwin	NA
224	0	57.15	25.4	0.05	228.6	32	0	1	1	304.4	0.07	0	0	Darwin	NA
225	0	50.8	25.4	0.2	228.6	32	0	1	1	304.4	0.08	0	0	Darwin	NA
226	0	53.975	25.4	0.1	228.6	32	0	1	1	304.4	0.06	0	0	Darwin	NA
227	0	53.975	25.4	0.05	228.6	32	0	1	1	304.4	0.02	0	0	Darwin	NA
228	0	50.8	25.4	0.2	228.6	32	0	1	1	304.4	0.07	0	0	Darwin	NA
229	0	55.5625	25.4	0.1	228.6	32	0	1	1	304.4	0.11	0	0	Darwin	NA
230	0	53.975	25.4	0.05	228.6	32	0	1	1	304.4	0.05	0	0	Darwin	NA
231	0	53.975	25.4	0.07	228.6	32	0	1	1	304.4	-0.01	0	0	Darwin	NA
232	0	50.8	25.4	0.07	228.6	32	0	1	1	304.4	-0.08	0	0	Darwin	NA
233	0	76.2	25.4	0.2	228.6	41	0	1	1	215.9	0.71	0	0	Darwin	NA
234	0	82.55	25.4	0.2	247.65	35	0	1	1	215.9	0.69	0	0	Darwin	NA
235	0	79.375	25.4	0.1	238.125	41	0	1	1	215.9	0.70	0	0	Darwin	NA

236	0	82.55	25.4	0.1	247.65	35	0	1	1	215.9	0.62	0	0	Darwin	NA
237	0	76.2	25.4	0.05	228.6	41	0	1	1	215.9	0.59	0	0	Darwin	NA
238	0	76.2	25.4	0.05	228.6	35	0	1	1	215.9	0.62	0	0	Darwin	NA
239	0	76.2	25.4	0.2	228.6	41	0	1	1	215.9	0.70	0	0	Darwin	NA
240	0	76.2	25.4	0.1	228.6	41	0	1	1	215.9	0.67	0	0	Darwin	NA
241	0	77.7875	25.4	0.05	233.3625	41	0	1	1	215.9	0.57	0	0	Darwin	NA
242	0	76.2	25.4	0.2	228.6	41	0	1	1	215.9	0.62	0	0	Darwin	NA
243	0	77.7875	25.4	0.2	233.3625	35	0	1	1	215.9	0.73	0	0	Darwin	NA
244	0	76.2	25.4	0.2	228.6	35	0	1	1	215.9	0.76	0	0	Darwin	NA
245	0	79.375	25.4	0.1	238.125	41	0	1	1	215.9	0.64	0	0	Darwin	NA
246	0	79.375	25.4	0.1	238.125	35	0	1	1	215.9	0.69	0	0	Darwin	NA
247	0	79.375	25.4	0.1	238.125	35	0	1	1	215.9	0.41	0	0	Darwin	NA
248	0	77.7875	25.4	0.05	233.3625	41	0	1	1	215.9	0.49	0	0	Darwin	NA
249	0	77.7875	25.4	0.05	233.3625	35	0	1	1	215.9	0.61	0	0	Darwin	NA
250	0	79.375	25.4	0.05	238.125	35	0	1	1	215.9	0.44	0	0	Darwin	NA
251	0	76.2	25.4	0.07	228.6	41	0	1	1	215.9	0.48	0	0	Darwin	NA
252	0	76.2	25.4	0.07	228.6	35	0	1	1	215.9	0.56	0	0	Darwin	NA
253	0	79.375	25.4	0.07	238.125	41	0	1	1	215.9	0.49	0	0	Darwin	NA
254	0	79.375	25.4	0.07	238.125	35	0	1	1	215.9	0.54	0	0	Darwin	NA
255	0	53.975	25.4	0.2	228.6	32	142.5115	533	76.2	304.4	0.35	0	0	Darwin	NA
256	0	53.975	25.4	0.2	228.6	33	142.5115	533	76.2	304.4	0.42	0	0	Darwin	NA
257	0	52.3875	25.4	0.2	228.6	31	142.5115	533	76.2	304.4	0.36	0	0	Darwin	NA
258	0	53.975	25.4	0.1	228.6	32	142.5115	533	76.2	304.4	0.30	0	0	Darwin	NA
259	0	49.2125	25.4	0.1	228.6	33	142.5115	533	76.2	304.4	0.32	0	0	Darwin	NA
260	0	49.2125	25.4	0.1	228.6	31	142.5115	533	76.2	304.4	0.28	0	0	Darwin	NA
261	0	52.3875	25.4	0.05	228.6	32	142.5115	533	76.2	304.4	0.12	0	0	Darwin	NA
262	0	58.7375	25.4	0.05	228.6	33	142.5115	533	76.2	304.4	0.20	0	0	Darwin	NA
263	0	55.5625	25.4	0.05	228.6	31	142.5115	533	76.2	304.4	0.29	0	0	Darwin	NA
264	0	57.15	25.4	0.2	228.6	33	142.5115	533	76.2	304.4	0.34	0	0	Darwin	NA
265	0	55.5625	25.4	0.2	228.6	31	142.5115	533	76.2	304.4	0.44	0	0	Darwin	NA
266	0	50.8	25.4	0.2	228.6	32	142.5115	533	76.2	304.4	0.42	0	0	Darwin	NA

267	0	53.975	25.4	0.1	228.6	33	142.5115	533	76.2	304.4	0.32	0	0	Darwin	NA
268	0	55.5625	25.4	0.1	228.6	31	142.5115	533	76.2	304.4	0.34	0	0	Darwin	NA
269	0	50.8	25.4	0.1	228.6	32	142.5115	533	76.2	304.4	0.25	0	0	Darwin	NA
270	0	52.3875	25.4	0.05	228.6	33	142.5115	533	76.2	304.4	0.19	0	0	Darwin	NA
271	0	52.3875	25.4	0.05	228.6	31	142.5115	533	76.2	304.4	0.24	0	0	Darwin	NA
272	0	52.3875	25.4	0.05	228.6	32	142.5115	533	76.2	304.4	0.20	0	0	Darwin	NA
273	0	50.8	25.4	0.2	228.6	31	142.5115	533	76.2	304.4	0.34	0	0	Darwin	NA
274	0	49.2125	25.4	0.2	228.6	32	142.5115	533	76.2	304.4	0.40	0	0	Darwin	NA
275	0	52.3875	25.4	0.2	228.6	33	142.5115	533	76.2	304.4	0.41	0	0	Darwin	NA
276	0	50.8	25.4	0.1	228.6	31	142.5115	533	76.2	304.4	0.18	0	0	Darwin	NA
277	0	53.975	25.4	0.1	228.6	32	142.5115	533	76.2	304.4	0.30	0	0	Darwin	NA
278	0	53.975	25.4	0.1	228.6	33	142.5115	533	76.2	304.4	0.39	0	0	Darwin	NA
279	0	49.2125	25.4	0.05	228.6	31	142.5115	533	76.2	304.4	0.17	0	0	Darwin	NA
280	0	50.8	25.4	0.05	228.6	32	142.5115	533	76.2	304.4	0.07	0	0	Darwin	NA
281	0	52.3875	25.4	0.05	228.6	33	142.5115	533	76.2	304.4	-0.10	0	0	Darwin	NA
282	0	52.3875	25.4	0.07	228.6	32	142.5115	533	76.2	304.4	0.18	0	0	Darwin	NA
283	0	55.5625	25.4	0.07	228.6	33	142.5115	533	76.2	304.4	0.27	0	0	Darwin	NA
284	0	57.15	25.4	0.07	228.6	31	142.5115	533	76.2	304.4	0.14	0	0	Darwin	NA
285	0	53.975	25.4	0.07	228.6	32	142.5115	533	76.2	304.4	0.12	0	0	Darwin	NA
286	0	49.2125	25.4	0.07	228.6	33	142.5115	533	76.2	304.4	0.21	0	0	Darwin	NA
287	0	52.3875	25.4	0.07	228.6	31	142.5115	533	76.2	304.4	0.09	0	0	Darwin	NA
288	0	55.5625	25.4	0.2	228.6	33	142.5115	533	76.2	304.4	0.45	0	0	Darwin	NA
289	0	52.3875	25.4	0.1	228.6	33	142.5115	533	76.2	304.4	0.38	0	0	Darwin	NA
290	0	52.3875	25.4	0.05	228.6	33	142.5115	533	76.2	304.4	0.26	0	0	Darwin	NA
291	0	53.975	25.4	0.2	228.6	33	142.5115	533	76.2	304.4	0.37	0	0	Darwin	NA
292	0	55.5625	25.4	0.1	228.6	33	142.5115	533	76.2	304.4	0.42	0	0	Darwin	NA
293	0	50.8	25.4	0.05	228.6	33	142.5115	533	76.2	304.4	0.26	0	0	Darwin	NA
294	0	50.8	25.4	0.2	228.6	33	142.5115	533	76.2	304.4	0.41	0	0	Darwin	NA
295	0	50.8	25.4	0.1	228.6	33	142.5115	533	76.2	304.4	0.41	0	0	Darwin	NA
296	0	55.5625	25.4	0.05	228.6	33	142.5115	533	76.2	304.4	0.29	0	0	Darwin	NA
297	0	53.975	25.4	0.07	228.6	33	142.5115	533	76.2	304.4	0.25	0	0	Darwin	NA

298	0	52.3875	25.4	0.07	228.6	33	142.5115	533	76.2	304.4	0.20	0	0	Darwin	NA
299	0	29	12	0.1	150	40	56.548	450	50	144	0.06	0	0	Alsulaimani	NA
300	0.11	29	12	0.1	150	40	56.548	450	50	144	0.24	0	0	Alsulaimani	NA
301	0.38	29	12	0.1	150	40	56.548	450	50	144	0.38	0	0	Alsulaimani	NA
302	0.55	29	12	0.1	150	40	56.548	450	50	144	0.39	0	0	Alsulaimani	NA
303	0.59	29	12	0.1	150	40	56.548	450	50	144	0.32	0	0	Alsulaimani	NA
304	1.25	29	12	0.1	150	40	56.548	450	50	144	0.29	0	0	Alsulaimani	NA
305	1.86	29	12	0.1	150	40	56.548	450	50	144	0.21	0	0	Alsulaimani	NA
306	2.11	29	12	0.1	150	40	56.548	450	50	144	0.11	0	0	Alsulaimani	NA
307	2.41	29	12	0.1	150	40	56.548	450	50	144	0.22	0	0	Alsulaimani	NA
308	3.05	29	12	0.1	150	40	56.548	450	50	144	0.17	0	0	Alsulaimani	NA
309	3.73	29	12	0.1	150	40	56.548	450	50	144	0.17	0	0	Alsulaimani	NA
310	4.5	29	12	0.1	150	40	56.548	450	50	144	0.11	0	0	Alsulaimani	NA
311	0.17	29	12	0.1	150	40	56.548	450	50	300	-0.07	0	0	Alsulaimani	NA
312	0.72	29	12	0.1	150	40	56.548	450	50	300	-0.07	0	0	Alsulaimani	NA
313	1.5	29	12	0.1	150	40	56.548	450	50	300	-0.08	0	0	Alsulaimani	NA
314	1.75	29	12	0.1	150	40	56.548	450	50	300	-0.07	0	0	Alsulaimani	NA
315	1.86	29	12	0.1	150	40	56.548	450	50	300	-0.09	0	0	Alsulaimani	NA
316	1.96	29	12	0.1	150	40	56.548	450	50	300	-0.10	0	0	Alsulaimani	NA
317	2.75	29	12	0.1	150	40	56.548	450	50	300	-0.14	0	0	Alsulaimani	NA
318	3.75	29	12	0.1	150	40	56.548	450	50	300	-0.18	0	0	Alsulaimani	NA
319	3.89	29	12	0.1	150	40	56.548	450	50	300	-0.17	0	0	Alsulaimani	NA
320	4.1	29	12	0.1	150	40	56.548	450	50	300	-0.18	0	0	Alsulaimani	NA
321	0	63.5	12	0.1	190.5	30	0	1	1	102	1.06	0	0	Almusallam	NA
322	2.04	63.5	12	0.1	190.5	30	0	1	1	102	1.10	0	0	Almusallam	NA
323	2.51	63.5	12	0.1	190.5	30	0	1	1	102	1.10	0	0	Almusallam	NA
324	2.69	63.5	12	0.1	190.5	30	0	1	1	102	1.19	0	0	Almusallam	NA
325	3.6	63.5	12	0.1	190.5	30	0	1	1	102	1.22	0	0	Almusallam	NA
326	4	63.5	12	0.1	190.5	30	0	1	1	102	1.16	0	0	Almusallam	NA
327	4.78	63.5	12	0.1	190.5	30	0	1	1	102	1.10	0	0	Almusallam	NA
328	5.09	63.5	12	0.1	190.5	30	0	1	1	102	0.91	0	0	Almusallam	NA

329	5.79	63.5	12	0.1	190.5	30	0	1	1	102	0.68	0	0	Almusallam	NA
330	7	63.5	12	0.1	190.5	30	0	1	1	102	-0.09	0	0	Almusallam	NA
331	7.8	63.5	12	0.1	190.5	30	0	1	1	102	-0.19	0	0	Almusallam	NA
332	12.1	63.5	12	0.1	190.5	30	0	1	1	102	-0.46	0	0	Almusallam	NA
333	15.65	63.5	12	0.1	190.5	30	0	1	1	102	-0.56	0	0	Almusallam	NA
334	0	25	12	0.1	75	49	100.48	460	40	190	0.02	0	0	Cabrera	NA
335	0.3	25	12	0.1	75	49	100.48	460	40	190	0.07	0	0	Cabrera	NA
336	0.5	25	12	0.1	75	48	100.48	460	40	190	0.08	0	0	Cabrera	NA
337	1.04	25	12	0.1	75	54	100.48	460	40	190	-0.02	0	0	Cabrera	NA
338	1.34	25	12	0.1	75	52	100.48	460	40	190	-0.02	0	0	Cabrera	NA
339	3.6	25	12	0.1	75	59	100.48	460	40	190	-0.08	0	0	Cabrera	NA
340	4.3	25	12	0.1	75	59	100.48	460	40	190	-0.19	0	0	Cabrera	NA
341	5.1	25	12	0.1	75	60	100.48	460	40	190	-0.09	0	0	Cabrera	NA
342	5.8	25	12	0.1	75	62	100.48	460	40	190	-0.06	0	0	Cabrera	NA
343	6.34	25	12	0.1	75	62	100.48	460	40	190	-0.06	0	0	Cabrera	NA
344	7.8	25	12	0.1	75	64	100.48	460	40	190	-0.08	0	0	Cabrera	NA
345	0	19	10	0.1	57	45	0	1	1	100	0.18	0	0	Mangat	NA
346	0.3	19	10	0.1	57	45	0	1	1	100	0.24	0	0	Mangat	NA
347	0.4	19	10	0.1	57	45	0	1	1	100	0.40	0	0	Mangat	NA
348	0.5	19	10	0.1	57	45	0	1	1	100	0.11	0	0	Mangat	NA
349	1.0	19	10	0.1	57	45	0	1	1	100	-0.06	0	0	Mangat	NA
350	2.0	19	10	0.1	57	45	0	1	1	100	-0.27	0	0	Mangat	NA
351	5.0	19	10	0.1	57	45	0	1	1	100	-0.51	0	0	Mangat	NA
352	0	20	11.3	0.1	112.5	36	0	1	1	250	-0.19	0	0	Stanish	NA
353	0.409836066	20	11.3	0.1	112.5	43	0	1	1	250	-0.25	0	0	Stanish	NA
354	5.905365127	20	11.3	0.1	112.5	43	0	1	1	250	-0.99	0	0	Stanish	NA
355	12.85394933	20	11.3	0.1	112.5	43	0	1	1	250	-0.70	0	0	Stanish	NA
356	7.581967213	20	11.3	0.1	112.5	36	0	1	1	250	-0.65	0	0	Stanish	NA
357	8.90461997	20	11.3	0.1	112.5	36	0	1	1	250	-0.36	0	0	Stanish	NA
358	10.30178838	20	11.3	0.1	112.5	36	0	1	1	250	-0.47	0	0	Stanish	NA

359	14.38152012	20	11.3	0.1	112.5	36	0	1	1	250	-0.99	0	0	Stanish	NA
360	0	24	16	0.12	150	54	100.48	590	70	208	-0.32	0	0	Rodriguez	NA
361	2.902153846	24	16	0.12	150	59	56.52	590	100	208	-0.41	0	0	Rodriguez	NA
362	3.015384615	24	16	0.12	150	54	100.48	590	70	208	-0.31	0	0	Rodriguez	NA
363	3.074461538	24	16	0.12	150	59	56.52	590	100	208	-0.49	0	0	Rodriguez	NA
364	3.192615385	24	16	0.12	150	54	100.48	590	70	208	-0.46	0	0	Rodriguez	NA
365	5.383384615	24	16	0.12	150	54	100.48	590	70	208	-0.43	0	0	Rodriguez	NA
366	6.424615385	24	16	0.12	150	54	100.48	590	70	208	-0.51	0	0	Rodriguez	NA
367	6.683076923	24	16	0.12	150	65	56.56	590	100	208	-0.56	0	0	Rodriguez	NA
368	8.196923077	24	16	0.12	150	59	56.52	590	100	208	-0.70	0	0	Rodriguez	NA
369	8.647384615	24	16	0.12	150	59	56.52	590	100	208	-0.65	0	0	Rodriguez	NA
370	13.7	15	10	0.12	150	86	56.56	590	100	130	-0.77	0	0	Rodriguez	NA
371	14.2	15	10	0.12	150	86	56.56	590	100	130	-0.67	0	0	Rodriguez	NA
372	0	21.5	16	0.1	150	40.7	56.5	420	40	80	0.12	0	0	Harajli	NA
373	0	34	16	0.1	150	40.7	56.5	420	40	80	0.29	0	0	Harajli	NA
374	0	34	16	0.1	150	43.2	157.1	420	40	80	0.41	0	0	Harajli	NA
375	0	17.5	20	0.1	150	42.7	56.5	420	50	100	-0.11	0	0	Harajli	NA
376	0	30	20	0.1	150	39	56.5	420	50	100	0.10	0	0	Harajli	NA
377	0	30	20	0.1	150	43.2	157.1	420	50	100	0.18	0	0	Harajli	NA
378	0	50	25	0.1	150	42.7	56.5	420	62.5	125	0.33	0	0	Harajli	NA
379	0	25	25	0.1	150	40.7	56.5	420	62.5	125	-0.09	0	0	Harajli	NA
380	0	43	32	0.1	150	39	56.5	420	80	160	-0.26	0	0	Harajli	NA
381	0	18	32	0.1	150	39	56.5	420	80	160	-0.45	0	0	Harajli	NA
382	0	21.5	16	0.3	150	40.7	56.5	420	40	80	0.09	0	0	Harajli	NA
383	0	34	16	0.3	150	40.7	56.5	420	40	80	0.29	0	0	Harajli	NA
384	0	17.5	20	0.3	150	42.7	56.5	420	50	100	-0.20	0	0	Harajli	NA
385	0	30	20	0.3	150	39	56.5	420	50	100	0.04	0	0	Harajli	NA
386	0	50	25	0.2	150	42.7	56.5	420	62.5	125	0.16	0	0	Harajli	NA
387	0	25	25	0.2	150	40.7	56.5	420	62.5	125	-0.34	0	0	Harajli	NA
388	0	43	32	0.2	150	39	56.5	420	80	160	-0.20	0	0	Harajli	NA

389	0	18	32	0.2	150	39	56.5	420	80	160	-0.65	0	0	Harajli	NA
390	0	25	20	0.05	150	33	0.0	378	1	150	-0.24	0	0	Lin 2019a	NA
391	0	25	20	0.05	150	33	100.5	378	150	150	-0.22	0	0	Lin 2019a	NA
392	0	25	20	0.05	150	33	100.5	378	100	150	-0.12	0	0	Lin 2019a	NA
393	0	25	20	0.05	150	33	100.5	378	70	150	-0.04	0	0	Lin 2019a	NA
394	0	35	20	0.05	150	33	0.0	378	1	150	-0.18	0	0	Lin 2019a	NA
395	0	35	20	0.05	150	33	100.5	378	150	150	-0.14	0	0	Lin 2019a	NA
396	0	35	20	0.05	150	33	100.5	378	100	150	-0.10	0	0	Lin 2019a	NA
397	0	35	20	0.05	150	33	100.5	378	70	150	0.12	0	0	Lin 2019a	NA
398	0	45	20	0.05	150	33	0.0	378	1	150	-0.14	0	0	Lin 2019a	NA
399	0	45	20	0.05	150	33	100.5	378	150	150	-0.09	0	0	Lin 2019a	NA
400	0	45	20	0.05	150	33	100.5	378	100	150	0.20	0	0	Lin 2019a	NA
401	0	45	20	0.05	150	33	100.5	378	70	150	0.12	0	0	Lin 2019a	NA
402	0	70	20	0.05	150	33	0.0	378	1	150	0.45	0	0	Lin 2019a	NA
403	0	70	20	0.05	150	33	100.5	378	150	150	0.12	0	0	Lin 2019a	NA
404	0	70	20	0.05	150	33	100.5	378	100	150	0.45	0	0	Lin 2019a	NA
405	0	70	20	0.05	150	33	100.5	378	70	150	0.50	0	0	Lin 2019a	NA
406	0	25	20	0.2	150	50	100.5	378	100	200	0.50	0	0	Lin 2019c	NA
407	0	25	20	0.2	150	50	100.5	378	100	200	0.49	0	1	Lin 2019c	0.15
408	0	25	20	0.2	150	50	100.5	378	100	200	0.50	0	1	Lin 2019c	0.15
409	1.77	25	20	0.2	150	50	100.5	378	100	200	0.40	0	0	Lin 2019c	NA
410	5.34	25	20	0.2	150	50	100.5	378	100	200	0.29	0	0	Lin 2019c	NA
411	2.03	25	20	0.2	150	50	100.5	378	100	200	0.41	0	0	Lin 2019c	NA
412	7.53	25	20	0.2	150	50	100.5	378	100	200	0.01	0	1	Lin 2019c	0.13
413	8.84	25	20	0.2	150	50	100.5	378	100	200	0.02	0	1	Lin 2019c	0.23
414	0	25	20	0.2	150	50	100.5	378	50	200	0.41	0	1	Lin 2019c	0.15
415	0	25	20	0.2	150	50	100.5	378	50	200	0.40	0	1	Lin 2019c	0.76
416	0	25	20	0.2	150	50	100.5	378	50	200	0.36	0	1	Lin 2019c	0.23
417	0.1	25	20	0.2	150	50	100.5	378	50	200	0.40	0	1	Lin 2019c	0.14
418	1.82	25	20	0.2	150	50	100.5	378	50	200	0.36	0	1	Lin 2019c	0.2

419	1.3	25	20	0.2	150	50	100.5	378	50	200	0.37	0	1	Lin 2019c	0.25
420	2.97	25	20	0.2	150	50	100.5	378	50	200	0.17	0	0	Lin 2019c	NA
421	5.58	25	20	0.2	150	50	100.5	378	50	200	0.00	0	1	Lin 2019c	1.06
422	0	35	20	0.2	150	50	100.5	378	100	200	0.68	0	0	Lin 2019c	NA
423	0	35	20	0.2	150	50	100.5	378	100	200	0.56	0	0	Lin 2019c	NA
424	0	35	20	0.2	150	50	100.5	378	100	200	0.61	0	0	Lin 2019c	NA
425	1.15	35	20	0.2	150	50	100.5	378	100	200	0.54	0	0	Lin 2019c	NA
426	2.81	35	20	0.2	150	50	100.5	378	100	200	0.29	0	1	Lin 2019c	0.41
427	3.86	35	20	0.2	150	50	100.5	378	100	200	0.41	0	1	Lin 2019c	0.36
428	1.43	35	20	0.2	150	50	100.5	378	100	200	0.26	0	1	Lin 2019c	0.17
429	12.89	35	20	0.2	150	50	100.5	378	100	200	-0.13	0	0	Lin 2019c	NA
430	0	35	20	0.2	150	50	100.5	378	50	200	0.52	0	1	Lin 2019c	0.19
431	0	35	20	0.2	150	50	100.5	378	50	200	0.52	0	1	Lin 2019c	0.09
432	0	35	20	0.2	150	50	100.5	378	50	200	0.62	0	1	Lin 2019c	0.04
433	1.4	35	20	0.2	150	50	100.5	378	50	200	0.55	0	1	Lin 2019c	0.09
434	1	35	20	0.2	150	50	100.5	378	50	200	0.54	0	1	Lin 2019c	0.09
435	0.89	35	20	0.2	150	50	100.5	378	50	200	0.50	0	0	Lin 2019c	NA
436	1.82	35	20	0.2	150	50	100.5	378	50	200	0.42	0	0	Lin 2019c	NA
437	2.54	35	20	0.2	150	50	100.5	378	50	200	0.43	0	-	Lin 2019c	NA
438	0.52	12	12	0.2	108	36.5	0	0	1	300	-0.67	0	0	Tang & Law 2007	NA
439	0.42	12	12	0.2	108	36.5	0	0	1	300	-0.55	0	0	Tang & Law 2007	NA
440	1.47	12	12	0.2	108	36.5	0	0	1	300	-0.41	0	0	Tang & Law 2007	NA
441	1.25	12	12	0.2	108	36.5	0	0	1	300	-0.51	0	0	Tang & Law 2007	NA
442	1.35	12	12	0.2	108	36.5	0	0	1	300	-0.61	0	0	Tang & Law 2007	NA
443	1.33	12	12	0.2	108	36.5	0	0	1	300	-0.46	0	0	Tang & Law 2007	NA
444	36.95	12	12	0.2	108	36.5	0	0	1	300	-1.43	0	0	Tang & Law 2007	NA
445	18.22	12	12	0.2	108	36.5	0	0	1	300	-0.92	0	0	Tang & Law 2007	NA
446	26.72	12	12	0.2	108	36.5	0	0	1	300	-1.90	0	0	Tang & Law 2007	NA
447	19.1	12	12	0.2	108	36.5	0	0	1	300	-1.48	0	0	Tang & Law 2007	NA

448	0.33	12	12	0.2	108	36.5	0	0	1	300	-0.51	0	0	Tang & Law 2007	NA
449	0.46	12	12	0.2	108	36.5	0	0	1	300	-0.55	0	0	Tang & Law 2007	NA
450	1.29	12	12	0.2	108	36.5	0	0	1	300	-0.34	0	0	Tang & Law 2007	NA
451	1.52	12	12	0.2	108	36.5	0	0	1	300	-0.66	0	0	Tang & Law 2007	NA
452	1.19	12	12	0.2	108	36.5	0	0	1	300	-0.57	0	0	Tang & Law 2007	NA
453	1.07	12	12	0.2	108	36.5	0	0	1	300	-0.71	0	0	Tang & Law 2007	NA
454	24.27	12	12	0.2	108	36.5	0	0	1	300	-0.87	0	0	Tang & Law 2007	NA
455	16.39	12	12	0.2	108	36.5	0	0	1	300	-1.10	0	0	Tang & Law 2007	NA
456	16.7	12	12	0.2	108	36.5	0	0	1	300	-1.28	0	0	Tang & Law 2007	NA
457	28.74	12	12	0.2	108	36.5	0	0	1	300	-1.24	0	0	Tang & Law 2007	NA
458	0.41	36	12	0.2	200	38	0	0	1	300	0.31	0	0	Tang & Law 2007	NA
459	2.95	36	12	0.2	200	38	0	0	1	300	0.12	0	0	Tang & Law 2007	NA
460	2.53	36	12	0.2	200	38	0	0	1	300	0.10	0	0	Tang & Law 2007	NA
461	11.96	36	12	0.2	200	38	0	0	1	300	-0.58	0	0	Tang & Law 2007	NA
462	11.17	36	12	0.2	200	34	0	0	1	300	-0.71	0	0	Tang & Law 2007	NA
463	6.88	36	12	0.2	200	34	0	0	1	300	-2.46	0	0	Tang & Law 2007	NA
464	0.39	36	12	0.2	200	38	0	0	1	300	0.30	0	0	Tang & Law 2007	NA
465	2.73	36	12	0.2	200	38	0	0	1	300	-0.18	0	0	Tang & Law 2007	NA
466	2.4	36	12	0.2	200	38	0	0	1	300	0.03	0	0	Tang & Law 2007	NA
467	10.31	36	12	0.2	200	38	0	0	1	300	-0.24	0	0	Tang & Law 2007	NA
468	10.42	36	12	0.2	200	38	0	0	1	300	-0.47	0	0	Tang & Law 2007	NA
469	8.93	36	12	0.2	200	34	0	0	1	300	-1.13	0	0	Tang & Law 2007	NA
470	9.31	36	12	0.2	200	34	0	0	1	300	-0.86	0	0	Tang & Law 2007	NA
471	0.44	16	16	0.2	144	37.5	0	0	1	300	-0.73	0	0	Tang & Law 2007	NA
472	0.37	16	16	0.2	144	37.5	0	0	1	300	-1.24	0	0	Tang & Law 2007	NA
473	1.01	16	16	0.2	144	37.5	0	0	1	300	-0.61	0	0	Tang & Law 2007	NA
474	0.83	16	16	0.2	144	37.5	0	0	1	300	-0.66	0	0	Tang & Law 2007	NA
475	4.38	16	16	0.2	144	37.5	0	0	1	300	-0.91	0	0	Tang & Law 2007	NA
476	4.04	16	16	0.2	144	37.5	0	0	1	300	-1.45	0	0	Tang & Law 2007	NA

477	7.07	16	16	0.2	144	37.5	0	0	1	300	-1.43	0	0	Tang & Law 2007	NA
478	5.68	16	16	0.2	144	37.5	0	0	1	300	-1.03	0	0	Tang & Law 2007	NA
479	0.39	16	16	0.2	144	37.5	0	0	1	300	-0.64	0	0	Tang & Law 2007	NA
480	0.32	16	16	0.2	144	37.5	0	0	1	300	-0.68	0	0	Tang & Law 2007	NA
481	0.94	16	16	0.2	144	37.5	0	0	1	300	-0.87	0	0	Tang & Law 2007	NA
482	1.13	16	16	0.2	144	37.5	0	0	1	300	-0.61	0	0	Tang & Law 2007	NA
483	3.51	16	16	0.2	144	37.5	0	0	1	300	-0.81	0	0	Tang & Law 2007	NA
484	4.1	16	16	0.2	144	37.5	0	0	1	300	-0.87	0	0	Tang & Law 2007	NA
485	3.15	16	16	0.2	144	37.5	0	0	1	300	-1.41	0	0	Tang & Law 2007	NA
486	3.58	16	16	0.2	144	37.5	0	0	1	300	-1.37	0	0	Tang & Law 2007	NA
487	5.4	16	16	0.2	144	37.5	0	0	1	300	-0.97	0	0	Tang & Law 2007	NA
488	5.62	16	16	0.2	144	37.5	0	0	1	300	-1.04	0	0	Tang & Law 2007	NA
489	30.02	48	16	0.2	200	38	0	0	1	300	-0.67	0	0	Tang & Law 2007	NA
490	18.49	48	16	0.2	200	38	0	0	1	300	-0.55	0	0	Tang & Law 2007	NA
491	N/A	48	16	0.2	200	38	0	0	1	300	0.27	0	0	Tang & Law 2007	NA
492	0.58	48	16	0.2	200	38	0	0	1	300	0.21	0	0	Tang & Law 2007	NA
493	2.24	48	16	0.2	200	38	0	0	1	300	0.11	0	0	Tang & Law 2007	NA
494	2.69	48	16	0.2	200	38	0	0	1	300	-0.30	0	0	Tang & Law 2007	NA
495	10.8	48	16	0.2	200	38	0	0	1	300	-0.87	0	0	Tang & Law 2007	NA
496	21.94	48	16	0.2	200	38	0	0	1	300	-0.91	0	0	Tang & Law 2007	NA
497	3.46	48	16	0.2	200	38	0	0	1	300	-0.23	0	0	Tang & Law 2007	NA
498	N/A	48	16	0.2	200	38	0	0	1	300	0.20	0	0	Tang & Law 2007	NA
499	0.47	48	16	0.2	200	38	0	0	1	300	0.24	0	0	Tang & Law 2007	NA
500	2.65	48	16	0.2	200	38	0	0	1	300	-0.08	0	0	Tang & Law 2007	NA
501	4.66	48	16	0.2	200	38	0	0	1	300	-0.29	0	0	Tang & Law 2007	NA
502	0	40	20	0.2	150	30	57	318	150	150	0.45	0	0	Lin & Zhao 2016	NA
503	0	40	20	0.2	150	30	57	318	150	150	0.34	0	0	Lin & Zhao 2016	NA
504	4.52	40	20	0.2	150	30	57	318	150	150	0.12	0	0	Lin & Zhao 2016	NA

505	8	40	20	0.2	150	30	57	318	150	150	-0.09	0	0	Lin & Zhao 2016	NA
506	7.64	40	20	0.2	150	30	57	318	150	150	-0.23	0	0	Lin & Zhao 2016	NA
507	4.3	40	20	0.2	150	30	57	318	150	150	0.08	0	0	Lin & Zhao 2016	NA
508	13.6	40	20	0.2	150	30	57	318	150	150	-0.46	0	0	Lin & Zhao 2016	NA
509	12.31	40	20	0.2	150	30	57	318	150	150	0.01	0	0	Lin & Zhao 2016	NA
510	17.24	40	20	0.2	150	30	57	318	150	150	-0.52	0	0	Lin & Zhao 2016	NA
511	11.06	40	20	0.2	150	30	57	318	150	150	-0.26	0	0	Lin & Zhao 2016	NA
512	16.11	40	20	0.2	150	30	57	318	150	150	-0.21	0	0	Lin & Zhao 2016	NA
513	20.86	40	20	0.2	150	30	57	318	150	150	-0.53	0	0	Lin & Zhao 2016	NA
514	0	40	20	0.2	150	30	57	318	100	150	0.41	0	0	Lin & Zhao 2016	NA
515	0	40	20	0.2	150	30	57	318	100	150	0.41	0	0	Lin & Zhao 2016	NA
516	2.04	40	20	0.2	150	30	57	318	100	150	0.00	0	0	Lin & Zhao 2016	NA
517	2.75	40	20	0.2	150	30	57	318	100	150	0.22	0	0	Lin & Zhao 2016	NA
518	4.52	40	20	0.2	150	30	57	318	100	150	0.28	0	0	Lin & Zhao 2016	NA
519	2.71	40	20	0.2	150	30	57	318	100	150	0.18	0	0	Lin & Zhao 2016	NA
520	6.69	40	20	0.2	150	30	57	318	100	150	0.13	0	0	Lin & Zhao 2016	NA
521	8.19	40	20	0.2	150	30	57	318	100	150	-0.26	0	0	Lin & Zhao 2016	NA
522	16.77	40	20	0.2	150	30	57	318	100	150	0.00	0	0	Lin & Zhao 2016	NA
523	13.67	40	20	0.2	150	30	57	318	100	150	0.57	0	0	Lin & Zhao 2016	NA
524	16.1	40	20	0.2	150	30	57	318	100	150	0.11	0	0	Lin & Zhao 2016	NA
525	15.47	40	20	0.2	150	30	57	318	100	150	0.14	0	0	Lin & Zhao 2016	NA
526	0	40	20	0.2	150	30	57	318	70	150	0.43	0	0	Lin & Zhao 2016	NA
527	0	40	20	0.2	150	30	57	318	70	150	0.47	0	0	Lin & Zhao 2016	NA
528	1.01	40	20	0.2	150	30	57	318	70	150	0.02	0	0	Lin & Zhao 2016	NA
529	2.24	40	20	0.2	150	30	57	318	70	150	0.15	0	0	Lin & Zhao 2016	NA
530	3.86	40	20	0.2	150	30	57	318	70	150	0.23	0	0	Lin & Zhao 2016	NA
531	4.06	40	20	0.2	150	30	57	318	70	150	0.32	0	0	Lin & Zhao 2016	NA
532	9.43	40	20	0.2	150	30	57	318	70	150	0.43	0	0	Lin & Zhao 2016	NA
533	7.31	40	20	0.2	150	30	57	318	70	150	0.07	0	0	Lin & Zhao 2016	NA

534	9.14	40	20	0.2	150	30	57	318	70	150	0.04	0	0	Lin & Zhao 2016	NA
535	9.94	40	20	0.2	150	30	57	318	70	150	-0.01	0	0	Lin & Zhao 2016	NA
536	16.33	40	20	0.2	150	30	57	318	70	150	-0.27	0	0	Lin & Zhao 2016	NA
537	14.35	40	20	0.2	150	30	57	318	70	150	-0.22	0	0	Lin & Zhao 2016	NA
538	0	35	20	0.2	150	50	100.5	378	50	100	0.92	0	1	Lin 2017a	0.33
539	0	35	20	0.2	150	50	100.5	378	50	100	0.92	0	1	Lin 2017a	0.15
540	0	35	20	0.2	150	50	100.5	378	50	100	0.83	0	1	Lin 2017a	0.15
541	2	35	20	0.2	150	50	100.5	378	50	100	0.85	0	1	Lin 2017a	0.3
542	4	35	20	0.2	150	50	100.5	378	50	100	0.46	0	1	Lin 2017a	0.13
543	7	35	20	0.2	150	50	100.5	378	50	100	0.52	0	1	Lin 2017a	1
544	10	35	20	0.2	150	50	100.5	378	50	100	0.53	0	1	Lin 2017a	0.13
545	13	35	20	0.2	150	50	100.5	378	50	100	0.65	0	1	Lin 2017a	0.23
546	16	35	20	0.2	150	50	100.5	378	50	100	0.53	0	1	Lin 2017a	0.15
547	0	30	20	0.2	270	30	0	0	1	210	-0.15	0	1	Hanjari 2011	0.76
548	0	30	20	0.2	270	30	0	0	1	210	-0.11	0	1	Hanjari 2011	0.23
549	0	30	20	0.2	270	30	0	0	1	210	0.20	0	1	Hanjari 2011	0.14
550	0	30	20	0.2	270	30	100.531	510	1	210	0.35	0	1	Hanjari 2011	0.2
551	0	30	20	0.2	270	30	100.531	510	40	210	0.18	0	1	Hanjari 2011	0.25
552	0	30	20	0.2	270	30	100.531	510	40	210	0.39	0	1	Hanjari 2011	0.22
553	3.5	30	20	0.2	270	30	100.531	510	40	210	-0.06	0	1	Hanjari 2011	1.06
554	0.2	30	20	0.2	270	30	100.531	510	40	210	0.17	0	1	Hanjari 2011	0.15
555	0.7	30	20	0.2	270	30	100.531	510	40	210	0.23	0	1	Hanjari 2011	0.12
556	7.3	30	20	0.2	270	30	0	0	1	210	-0.87	0	1	Hanjari 2011	0.13
557	8.9	30	20	0.2	270	30	0	0	1	210	-0.60	0	0	Hanjari 2011	NA
558	4.5	30	20	0.2	270	30	0	0	1	210	0.13	0	1	Hanjari 2011	0.41
559	12.4	30	20	0.2	270	30	100.531	510	40	210	0.13	0	0	Hanjari 2011	NA
560	7.7	30	20	0.2	270	30	100.531	510	40	210	0.06	0	0	Hanjari 2011	NA
561	9,8 (*)	30	20	0.2	270	30	100.531	510	40	210	0.25	0	1	Hanjari 2011	0.14
562	15,5 (*)	30	20	0.2	270	30	100.531	510	40	210	0.08	0	1	Hanjari 2011	0.19

563	14.8	30	20	0.2	270	30	100.531	510	40	210	0.23	0	1	Hanjari 2011	0.09
564	15.7	30	20	0.2	270	30	100.531	510	40	210	0.26	0	0	Hanjari 2011	NA
565	9.2	30	20	0.2	270	30	100.531	510	40	210	0.09	0	0	Hanjari 2011	NA
566	16.7	30	20	0.2	270	30	100.531	510	40	210	0.34	0	1	Hanjari 2011	0.09

